

1-1-2009

Experimental study on the structural behavior of insulated sandwich foam-timber panels under combined axial compression and bending

Mahmoud Mohamed
Ryerson University

Follow this and additional works at: <http://digitalcommons.ryerson.ca/dissertations>



Part of the [Civil Engineering Commons](#)

Recommended Citation

Mohamed, Mahmoud, "Experimental study on the structural behavior of insulated sandwich foam-timber panels under combined axial compression and bending" (2009). *Theses and dissertations*. Paper 902.

6175 75000
TA
418.9
126
M64
0009

**EXPERIMENTAL STUDY ON THE STRUCTURAL BEHAVIOR
OF INSULATED SANDWICH FOAM-TIMBER PANELS UNDER
COMBINED AXIAL COMPRESSION AND BENDING**

BY

Mahmoud Mohamed, B.Sc. in Civil Engineering.

Cairo University, Egypt, 1997

A Thesis

Presented to Ryerson University

In partial fulfillment of the

Requirement for the degree of

Master of Applied Science

In the program of

Civil Engineering

Toronto, Ontario, Canada, 2009

Mahmoud Mohamed 2009 ©

AUTHOR'S DECLARATION

I hereby declare that I am the sole author of this thesis.

I authorize Ryerson University to lend this document to other institutions or individuals for the purpose of scholarly research.

Mahmoud Mohamed

I further authorize the Ryerson University to reproduce the document by photocopying or by other means, in total or part, at the request of other institutions or individuals for the purpose of scholarly research.

Mahmoud Mohamed

EXPERIMENTAL STUDY ON THE STRUCTURAL BEHAVIOR OF INSULATED SANDWICH FOAM-TIMBER PANELS UNDER COMBINED AXIAL COMPRESSION AND BENDING

By

Mahmoud Mohamed.

Master of Applied Sciences in Civil Engineering

Department of Civil Engineering

Ryerson University, Toronto

2009

ABSTRACT

Structural Insulated Panels (SIPs) can significantly reduce emissions produced by our homes and commercial buildings by reducing the amount of energy used for heating and cooling. A SIP is composed of expanded polystyrene insulation (EPS) board laminated between two oriented-strand boards (OSB). SIPs are used all over the world because of their superior strength and quality build. The objective of this thesis is to evaluate the effectiveness of the foam core in providing composite action in SIPs under axial and bending loads to meet both the strength and serviceability requirements. This thesis presents the experimental program and the results of 32 full-size panels tested to-collapse at the Structures Laboratory of Ryerson University. The data generated from this extensive experimental program can easily be used to determine the load carrying capacity of the SIP walls when subjected to axial compressive loading or combined axial compressive loading and bending moment.

Keywords: Sandwich panels, Test methods, experiments, codes and standards, serviceability and strength limit states, wall construction, combined axial and bending.

ACKNOWLEDGEMENTS

My sincere thanks and gratitude are due to his almighty ALLAH, who helped me and blessed my work during the days of my study and research.

I wish to express my deep appreciation for Seyma Pinar Uslu, my mother and my brothers for their great support and encouragement during the course of study.

I wish to express my deep appreciation to my advisor, Dr. K. Sennah, for his continuous support and valuable supervision during the development of this research. Dr. K. Sennah devoted his time and effort to make this study a success.

I am very grateful to Dr. Lamyia Amleh, Dr. Medhat Shehata and Dr. Mustafa Warith for their knowledge which they transferred to me during my study in Ryerson University.

The in-kind technical support from Thermapan Inc. of Fort Erie, Ontario, is greatly appreciated.

I wish to express my deep appreciation to Mohamed Aldardari and Nidal Jaalouk for their technical support.

I would like to thank Assem Adel Hassan for his support generally and his creative ideas for the test set up specifically.

I am also very grateful to my family for their great support and encouragement during the course of study.

TABLE OF CONTENTS

AUTHOR'S DECLARATIONS.....	i
BORROWERS PAGE.....	ii
ABSTRACT.....	iii
ACKNOWLEDGEMENTS.....	v
TABLE OF CONTENTS.....	vi
NOTATIONS.....	x
LIST OF TABLES.....	xi
LIST OF FIGURES.....	xii
CHAPTER I: INTRODUCTION.....	1
1.1 General.....	1
1.2 The problem.....	1
1.3 The Objectives.....	3
1.4 The Scope.....	4
1.5 The Contents and Arrangement of the thesis.....	4
CHAPTER II: LITERATURE REVIEW.....	5
2.1 General.....	5
2.2 History of SIPs.....	6
2.3 Types of Common Structural Insulated Sandwich Panels.....	8
2.3.1 Fiber Cement faced Structural Insulated panels.....	8
2.3.2 Precast Concrete Sandwich panel.....	9
2.3.3 Light weight steel frame panels.....	10
2.3.4 Plywood Sandwich Panels.....	11
2.4 Structural Analysis and Design of Sandwich panels.....	11
2.4.1 Historical Development of Sandwich Theory.....	14
2.4.1.1 The General Method.....	16
2.4.1.2 The Selective Method.....	17
2.4.1.3 Flexural Stresses in Sandwich Panels.....	19
2.4.1.4 Flexural and Shear Stresses in Sandwich Panels.....	20
2.4.1.5 Elastic Deflection Analysis of Sandwich Panels.....	20
2.5 Permanent wood foundation.....	22
CHAPTER III: EXPERIMENTAL STUDY.....	
3.1 General.....	24
3.2 Description of Panels.....	25
3.3 Material Properties.....	26
3.4 Test method for SIP Panels under Axial Compressive Loading.....	29
3.4.1 Axial Compressive Load Test setup.....	30
3.4.2 Instrumentation for Axial Compressive Load Test.....	31
3.4.3 Axial Compressive Load Test Procedure.....	32

3.5 Test method for SIP panels under Flexural Load.....	33
3.5.1 Flexural Load Test setup.....	33
3.5.2 Instrumentation for Flexural Load Test.....	34
3.5.3 Flexural Load Test procedure.....	34

CHAPTER IV: EXPERIMENTAL RESULTS

4.1 General.....	35
4.2 Code Requirements for the Structural Qualification of the SIPs.....	35
4.3 Group A.....	37
4.4 Group B.....	39
4.5 Group C.....	41
4.6 Group D.....	43
4.7 Group E.....	44
4.8 Group F.....	46
4.9 Group G.....	47
4.10 Group H.....	49
4.11 Group I.....	50
4.12 Group J.....	52
4.13 Design Table for SIP wall under axial compressive load.....	53
4.14 Design Table for SIP wall under combined axial compressive load and wind load.....	54
4.15 Design Table for SIP foundation wall under combined axial compressive load and soil pressure.....	55

CHAPTER V: CONCLUSIONS

5.1 General.....	56
5.2 Conclusions.....	56
5.3 Recommendations for future research.....	57

REFERENCES.....	59
-----------------	----

NOTATIONS

x, y, z	Rectangular coordinates.
D	Flexural Rigidity
b	Width of Panel
t	Thickness of panel
l	Span length
L	Live load
E_f, E_c	Moduli of face and core along axis
c	core thickness
Δ	Deflection of panel
$\tau_{zx}, \tau_{xy}, \tau_{yz}$	Shear Stress
Δ_B	Midspan sandwich deflection due to bending
Δ_S	Midspan sandwich deflection due to shear
Δ_{Total}	Immediate deflection under dead load and long term portion of live loads
K	Constant to calibrate the long term effects of dead load and live load
$\Delta_{short\ term}$	Deflections under short term portions of design load

LIST OF TABLES

Table 3.1 Thermapan SIPs Properties.....	64
Table 3.2. Panel configurations for axial compressive load tests.....	64
Table 3.3. Panel configurations for flexure.....	64
Table 3.4. Panel configurations for axial compressive load tests for basement construction.....	65
Table 3.5. Panel configurations for flexure tests for basement construction.....	65
Table 4.1 Results from axial compressive load tests.....	66
Table 4.2 Results from flexural load tests.....	67
Table 4.3 Results from axial compressive load tests for basement construction.....	67
Table 4.4 Results from flexural load tests for basement construction.....	67
Table 4.5 Design table for SIP wall under axial compressive loading.....	68
Table 4.6 Design table for SIP wall under combined axial compressive load and bending moment.....	68
Table 4.7 Design table for SIP wall under combined axial compressive load and bending moment.....	68

LIST OF FIGURES

Figure 1.1 Comparison of SIP with I-beam section.....	69
Figure 1.2 Comparison of SIP with stud wall system	69
Figure 1.3 Use of SIPs as cladding in industrial, commercial and residential buildings.....	70
Figure 1.4 Use of SIPs as preserved wood foundation in residential construction.....	71
Figure 2.1. Loading of the permanent wood foundation (CWC, 2005).....	71
Figure 3.1 Typical floor and basement wall construction using SIPs.....	72
Figure 3.2 Typical section at panel foam-spline connection before and after assembly.....	73
Figure 3.3 Typical section at panel lumber-spline connection before and after assembly.....	74
Figure 3.4 Schematic diagram of the elevation of the test setup for axial loading test.....	75
Figure 3.5 Schematic diagram of the side view of the test setup for axial loading test.....	76
Figure 3.6 Schematic diagram of loading assembly for the axial loading test.....	77
Figure 3.7 View of wall W-2 before testing.....	78
Figure 3.8 View of the top loading system for wall W2 before testing.....	78
Figure 3.9 View of the loading assembly for and POT locations for the axial load tests.....	79
Figure 3.10 Enlarged view for the loading assembly for the eccentric compression loading test.....	79
Figure 3.11 Views of the LVDTs used to measure lateral deflection at mid-height of the left and right side of wall W5, respectively.....	80
Figure 3.12 Schematic diagram of the elevation of the test setup for flexural loading test.....	80
Figure 3.13 View of Specimen WS31 before testing.....	81
Figure 3.14 View of LVDTs at mid-span location of model WB19.....	81
Figure 4.1. View of the test setup for wall W1 before testing.....	82
Figure 4.2. Axial load-axial shortening relationship for model W1.....	82
Figure 4.3. Axial load-lateral deflection relationship for model W1.....	83
Figure 4.4. Views of the failure mode due to OSB crushing near the quarter point from the top of south side of model W1 that led to lateral deformation of the wall at this location.....	84
Figure 4.5. View of the failure mode due to OSB crushing at its connection with the bottom lumber stud in the south side of model W1.....	84
Figure 4.6. View of the failure mode due to OSB crushing near its lower quarter point in the north side of model W1.....	85
Figure 4.7. Signs of OSB crushing near the top of the wall in the north side.....	85
Figure 4.8. View of OSB crushing near its upper quarter point in the south side as well as OSB crushing near the top of the north side of model W1.....	86
Figure 4.9. View of model W1 from the south-west corner showing lateral deformation of the wall near the lower quarter point as a result of OSB crushing at this location.....	86
Figure 4.10. View of the test setup for wall W2 before testing.....	87
Figure 4.11. Axial load-axial shortening relationship for model W2.....	87
Figure 4.12. Axial load-lateral deflection relationship for model W2.....	88
Figure 4.13. View of the failure mode due to OSB crushing near the top of south side of model W2	88
Figure 4.14. View of the failure mode due to OSB crushing near the top of the wall in the north	

side of model W2.....	89
Figure 4.15. View of OSB crushing near the top of west side of model W2.....	89
Figure 4.16. View of OSB crushing near the top of east side of model W2.....	90
Figure 4.17. View of the test setup for wall W3 before testing.....	91
Figure 4.18. Axial load-axial shortening relationship for model W3.....	91
Figure 4.19. Axial load-lateral deflection relationship for model W3.....	91
Figure 4.20. View of the failure mode due to OSB crushing near the top of south side of model W3.....	92
Figure 4.21. View of the failure mode due to OSB crushing near the mid-height of the wall W3.....	93
Figure 4.22. Views of the deformed shape of wall model W3 after OSB crushing near its mid-height.....	93
Figure 4.23. View of the test setup for wall W4 before testing.....	94
Figure 4.24. Axial load-axial shortening relationship for model W4.....	94
Figure 4.25. Axial load-lateral deflection relationship for model W4.....	95
Figure 4.26. View of the failure mode due to OSB crushing at the top of north side of model W4, in addition to foam-OSB separation at the top of the south side.....	95
Figure 4.27. Other view of the failure mode at the top of the north side of wall W4.....	96
Figure 4.28. Close-up views of the deformed shape of top portion of wall W4 after failure.....	96
Figure 4.29. View of the deformed shape of OSB sheets in the south side of wall W4 after crushing.....	97
Figure 4.30. View of the test setup for wall W5 before testing.....	97
Figure 4.31. Axial load-axial shortening relationship for model W5.....	98
Figure 4.32. Axial load-lateral deflection relationship for model W5.....	98
Figure 4.33. View of the failure mode due to OSB crushing near the top quarter point in the south side of wall W5.....	99
Figure 4.34. Other views of the failure mode at the south-west corner of wall W5.....	99
Figure 4.35. Views of the deformed shape of top portion of wall W5 after failure showing OSB crushing in the south side of the wall along with foam-OSB separation.....	100
Figure 4.36. Other views of the deformed shape of wall W5.....	101
Figure 4.37. View of the test setup for wall W6 before testing.....	101
Figure 4.38. Axial load-axial shortening relationship for model W6.....	102
Figure 4.39. Axial load-lateral deflection relationship for model W6.....	102
Figure 4.40. View of the failure mode due to OSB crushing at the top of south side of model W6.....	103
Figure 4.41. Other views of OSB crushing at the top of the south side of wall W6.....	103
Figure 4.42. Views of the test setup for wall W7 before testing.....	104
Figure 4.43. Axial load-axial shortening relationship for model W7.....	104
Figure 4.44. Axial load-lateral deflection relationship for model W7.....	105
Figure 4.45. Views of the deformed shape of the wall W7 after OSB crushing at its top north side.....	105
Figure 4.46. View of the side of the wall before testing and View of OSB crushing at the top of the north side of wall W7 along with OSB- foam delamination at failure.....	106
Figure 4.47. Views of the test setup for wall W8 before testing.....	106
Figure 4.48. Axial load-axial shortening relationship for model W8.....	107

Figure 4.49. Axial load-lateral deflection relationship for model W8.....	107
Figure 4.50. Views of the deformed shape of the wall W8 after OSB crushing near its top side and OSB fracture at the same location but on the south side.....	108
Figure 4.51. Views of OSB crushing near the top side of Wall W8 and OSB fracture at the same location but on the south side.....	108
Figure 4.52. Views of the test setup for wall W9 before testing.....	109
Figure 4.53. View of the top loading system showing the t/6 eccentric loading condition.....	109
Figure 4.54. Axial load-axial shortening relationship for model W9.....	110
Figure 4.55. Axial load-lateral deflection relationship for model W9.....	110
Figure 4.56. Views of the deformed shape of the east side of wall W9 showing OSB crushing near its top quarter point in addition to foam shear failure and OSB-foam delamination.....	111
Figure 4.57. Views of OSB crushing near the top of the south side of Wall W9 in addition to OSB crushing near the quarter point of the south-east side.....	111
Figure 4.58. Views of the test setup for wall W10 before testing.....	112
Figure 4.59. Axial load-axial shortening relationship for model W10.....	112
Figure 4.60. Axial load-lateral deflection relationship for model W10.....	113
Figure 4.61. Views of the deformed shape of the west side of wall W10.....	113
Figure 4.62. Views of the OSB crushing near the bottom quarter point of the north side of wall W10 in addition to OSB crushing and foam shear failure at the bottom of the south –west side.....	114
Figure 4.63. Views of the OSB crushing near the bottom quarter point of the north side of wall W10 in addition to OSB crushing and foam shear failure at the bottom of the south–east and north-east sides.....	114
Figure 4.64. Views of the test setup for wall W11 before testing.....	115
Figure 4.65. Axial load-axial shortening relationship for model W11.....	115
Figure 4.66. Axial load-lateral deflection relationship for model W11.....	116
Figure 4.67. Views of the deformed shape of the west side of wall W11 showing OSB crushing, foam shear failure and foam-OSB delamination.....	117
Figure 4.68. Views of the deformed shape of the east side of wall W11 showing OSB crushing and foam-OSB delamination.....	117
Figure 4.69. Views of the test setup for wall W12 before testing.....	118
Figure 4.70. Axial load-axial shortening relationship for model W12.....	118
Figure 4.71. Axial load-lateral deflection relationship for model W12.....	119
Figure 4.72 Views of the deformed shape of the west side of wall W12 showing OSB crushing and foam-OSB delamination.....	120
Figure 4.73. Views of the deformed shape of the east side of wall W12 showing OSB crushing and foam-OSB delamination.....	120
Figure 4.74. View of the test setup for wall W13 before testing.....	120
Figure 4.75. Axial load-axial shortening relationship for model W13.....	121
Figure 4.76. Axial load-lateral deflection relationship for model W13.....	122
Figure 4.77. View of the failure mode due to OSB crushing near its top end point in the south-west side of wall W13.....	123
Figure 4.78. Signs of OSB crushing near the top of the wall in the east side.....	123
Figure 4.79. View of the deformed shape at failure of model W13 from the east and west sides.....	124

Figure 4.80. View of the test setup for wall W14 before testing.....	124
Figure 4.81. Axial load-axial shortening relationship for model W14.....	125
Figure 4.82. Axial load-lateral deflection relationship for model W14.....	125
Figure 4.83. Views of the failure mode due to OSB crushing the bottom of the wall and OSB-foam splitting at the bottom of Wall W14	126
Figure 4.84. Views of the failure mode due to OSB crushing the bottom of the wall and OSB-foam splitting at the bottom of Wall W14.....	126
Figure 4.85. Views of wall W14 showing lateral deformation of the wall near the lower quarter point as a result of OSB crushing at this location.....	127
Figure 4.86. View of the test setup for wall W15 before testing.....	127
Figure 4.87. Axial load-axial shortening relationship for model W15.....	128
Figure 4.88. Axial load-lateral deflection relationship for model W15.....	128
Figure 4.89. View of the failure mode due to OSB-foam splitting near its lower end point and OSB crushing in the south-east side of model W15.....	129
Figure 4.90. View of the failure mode due to OSB-foam splitting near its lower end point and OSB crushing in the south-west side of model W15.....	129
Figure 4.91. View of model W15 from the south-west corner showing lateral deformation of the wall near the lower end point as a result of OSB crushing at this location.....	130
Figure 4.92. View of the test setup for wall W16 before testing.....	131
Figure 4.93. Axial load-lateral deflection relationship for model W16.....	131
Figure 4.94. View of OSB crushing near its upper quarter point in the north side of model W16.....	132
Figure 4.95. View of model W16 from the south-east corner showing lateral deformation of the wall near the top quarter point as a result of OSB crushing at this location.....	132
Figure 4.96. View of the test setup for wall W17 before testing.....	133
Figure 4.97. Axial load-axial shortening relationship for model W17.....	133
Figure 4.98. Axial load-lateral deflection relationship for model W17.....	134
Figure 4.99. Views of OSB crushing, OSB-foam splitting and foam diagonal shear failure in Wall W17.....	134
Figure 4.100. Others views of the failure pattern of wall W17.....	135
Figure 4.101. Views of OSB-foam splitting and OSB crushing at the other side of wall W17.....	135
Figure 4.102. View of the test setup for wall W18 before testing.....	136
Figure 4.103. Axial load-axial shortening relationship for model W18.....	136
Figure 4.104. Axial load-lateral deflection relationship for model W18.....	137
Figure 4.105. View of wall W18 at the north-east showing OSB crushing at and near the bottom end	137
Figure 4.106. View of wall W18 at the north-west showing OSB crushing and foam splitting near the bottom end	138
Figure 4.107. View of wall W18 from the south-east corner showing lateral deformation of the wall near the bottom quarter point as a result of OSB crushing at this location.....	138
Figure 4.108 Views of the test setup for model WS19 before testing.....	139
Figure 4.109. Jacking load-deflection relationship for model WS19.....	140
Figure 4.110. View of the deflected shape of model WS19 after failure.....	140

Figure 4.111. View of the horizontal shear failure at the interface between the foam and top OSB at one side of the support of model WS19.....	141
Figure 4.112. View of the horizontal shear failure at the interface between the foam and top OSB at the other side of the support of model WS19.....	141
Figure 4.113. Views of the test setup for model WS20 before testing.....	142
Figure 4.114. Jacking load-deflection relationship for model WS20.....	142
Figure 4.115. View of the deflected shape of model WS20 after failure.....	143
Figure 4.116. View of the horizontal shear failure at the interface between the foam and top OSB at one side of the support of model WS20.....	143
Figure 4.117. View of the horizontal shear failure at the interface between the foam and top OSB at the other side of the support of model WS20.....	144
Figure 4.118. Views of the test setup for model WS21 before testing.....	144
Figure 4.119. Jacking load-deflection relationship for model WS21.....	145
Figure 4.120. View of the deflected shape of model WS21 after failure.....	145
Figure 4.121. View of the horizontal shear failure at the interface between the foam and top OSB at one side of the support of model WS21.....	146
Figure 4.122. View of the horizontal shear failure at the interface between the foam and top OSB at the other side of the support of model WS21.....	146
Figure 4.123. Views of the test setup for model WS22 before testing.....	147
Figure 4.124. Jacking load-deflection relationship for model WS22.....	147
Figure 4.125. View of the deflected shape of model WS22 after failure.....	148
Figure 4.126. View of the horizontal shear failure at the interface between the foam and top OSB at one side of the support of model WS22.....	148
Figure 4.127. View of the horizontal shear failure at the interface between the foam and top OSB at the other side of the support of model WS22.....	149
Figure 4.128. Jacking load-deflection relationship for model WS23.....	149
Figure 4.129. View of the deflected shape of model WS23 after failure.....	150
Figure 4.130. View of the horizontal shear failure at the interface between the foam and top OSB at one side of the support of model WS23.....	150
Figure 4.131. View of the horizontal shear failure at the interface between the foam and top OSB at the other side of the support of model WS23.....	151
Figure 4.132. View of the setup of WS24 before testing.....	152
Figure 4.133. Jacking load-deflection relationship for model WS24.....	152
Figure 4.134. View of the deflected shape of model WS24 after failure.....	153
Figure 4.135. View of the diagonal shear failure at one side of the support of model WS24....	153
Figure 4.136. View of the diagonal shear failure at the other side of the support of model WS24.....	154
Figure 4.137. View of the setup of WS25 before testing.....	154
Figure 4.138. Jacking load-deflection relationship for model WS25.....	155
4.139. View of the deflected shape of model WS25 after failure.....	155
Figure 4.140. View of the diagonal shear failure at one side of the support of model WS25....	156
Figure 4.141. View of the diagonal shear failure at the other side of the support of model WS25.....	156
Figure 4.142. View of the setup of WS26 before testing.....	157
Figure 4.143. Jacking load-deflection relationship for model WS26.....	157

Figure 4.144. View of the deflected shape of model WS26 after failure.....	158
Figure 4.145. View of the combined horizontal and diagonal shear failure at one side of the support of model WS26.....	158
Figure 4.146. View of the horizontal shear failure at the other side of the support of model WS26.....	159
Figure 4.147. View of the test setup for wall W27 before testing.....	160
Figure 4.148. Axial load-lateral deflection relationship for model W27.....	160
Figure 4.149. View of crushing of the pressure-treated facing at top of the north-west side of wall W27.....	161
Figure 4.150. View of deformation of the pressure-treated facing at top of the north-east side of wall W27.....	161
Figure 4.151. View of the lateral deformation of wall W27 after failure	162
Figure 4.152. View of the test setup for wall W28 before testing.....	162
Figure 4.153. Axial load-axial shortening relationship for model W28.....	163
Figure 4.154. Axial load-lateral deflection relationship for model W28.....	163
Figure 4.155. views of the OSB and pressure treated lumber facings at the bottom south-east side of wall W28.....	164
Figure 4.156. views of the OSB and pressure treated lumber facings at the bottom south-west side of wall W28.....	165
Figure 4.157. View of the setup of wall W-29 before testing.....	166
Figure 4.158. Axial load-axial shortening relationship for wall W-29.....	166
Figure 4.159. Axial load-lateral deflection relationship for wall W-29.....	167
Figure 4.160. Splitting of Pressure treated lumber facing at the bottom south side of wall W-29.....	167
Figure 4.161. Views of OSB crushing close to the top quarter point of the north-east side of wall W-29.....	168
Figure 4.162. Views of OSB crushing at the top of the north-west side of wall W-29.....	168
Figure 4.163. Views of the test setup for model WS30 before testing.....	169
Figure 4.164. View of deformed shape of panel WS30 after failure.....	169
Figure 4.165. Jacking load-deflection relationship for model WS30.....	170
Figure 4.166. Views of the diagonal shear failure in the foam at the left and right free edges, respectively, of the right support of panel WS30.....	170
Figure 4.167. Views of the test setup for model WS31 before testing.....	171
Figure 4.168. View of deformed shape of panel WS31 after failure.....	171
Figure 4.169. Jacking load-deflection relationship for model WS31.....	172
Figure 4.170. Views of the horizontal shear failure at the interface between the top facing and foam core the left free edge of the right support of panel WS31.....	172
Figure 4.171. Views of the horizontal shear failure at the interface between the top facing and foam core the right free edge of the right support of panel WS31.....	173
Figure 4.172. Views of the test setup for model WS32 before testing.....	173
Figure 4.173. View of deformed shape of panel WS32 after failure.....	174
Figure 4.174. Jacking load-deflection relationship for model WS32.....	174
Figure 4.175. View of the combined diagonal and horizontal shear failure at the left free edge of the right support of panel WS32.....	175
Figure 4.176. Views of the horizontal shear failure at the interface between the top facing	

CHAPTER I

INTRODUCTION

1.1 General

The structural insulated panel (SIP) is an engineered composite product composed of an insulating foam core sandwiched to provide the insulation and rigidity, and two face-skin materials to provide durability and strength. The core material may take the form of oriented strand board (OSB), traded plywood, fibre-cement board, and sheet metal. The SIP can be compared, structurally, to an I-beam; the foam core acts as the web, while the facings are analogous to the I-beam's flanges as shown in Fig. 1.1. In case of flexural loading, all of the elements of a SIP are stressed; the skins are in tension and compression, while the core resists shear and buckling. Under axial concentric in-plane loading, the facings of a SIP act as slender columns, and the core stabilizes the facings and resists forces that may cause local buckling of the facings. However, in the conventional stud wall system shown in Fig. 1.2, the studs transfer the load from the roof and floor down to the foundation, while the foam is installed between studs to provide insulation. SIPs are usually available in a thickness ranging from 100 to 350 mm, depending on climate conditions. These panels can be used in industrial, commercial and residential construction as lading. However, their significant use is walls, floors and roofs in low-rise residential buildings and as basement walls, as shown in Figs. 1.4. The energy saving insulation, design capabilities, cost effectiveness, speed of construction and exceptional strength make SIPs the future material for high performance buildings.

1.2 The Problem

The developed structural insulated sandwich timber panels comprise insulated foam glued between two OSB boards. To determine the structural adequacy of the level of adhesion

between the foam and the OSB boards and the level of composite action between them, it is felt necessary to conduct experimental testing to-collapse on the developed structural insulated sandwich timber panels. Clause 8.6 of the Canadian Standard for Engineering Design of Wood, CAN/CSA-O86-01, (2001) specifies the effective stiffness, bending resistance and shear resistance of stressed skin panels. These stressed skin panels have continuous or splice longitudinal web members and continuous or spliced panel flanges on one or both panel faces, with the flanges glued to the web members. These strength equations are not applicable to SIPs since they do not address the adequacy of the foam as the main shear carrying element near the supports and the connector between the facings at the maximum moment location. Also, CAN/CSA-O86-01 specifies expressions for the effects of combined axial and bending on the timber stud walls and posts which are applicable to SIPs. However, the available CAN/CSA-O86-01 compressive resistance equations for studs and posts can not be applied to SIPs as a result of their structural performance at failure. The technical guide of Canadian Construction Materials Commission (CCMC) and National Research Council Canada (NRC) for stressed skin panels (with lumber 1200 mm o.c. and EPS core) for walls and roof, formed the basis for the experimental testing conducted in this thesis for flexure, axial eccentric and axial concentric, with the ultimate goal of providing enough technical data for strength and serviceability of the developed structural insulated sandwich timber panels. With this database, design tables can be established. CAN/CSA-S406, Construction of Preserved Wood Foundations, (1992) allows the use of permanent wood foundation (PWF) which is referred to in Part 9 of the National Building Code of Canada (2006) and in provincial building codes as applied to buildings not exceeding 557 square meter in building area and not more than two storeys high. Building that exceed these limits must be designed according to Standard CSA O86.1, Engineering Design on Wood, which

is referenced in Part 4 of the NBCC. The PWFs are load-bearing wood-frame system designed as foundation for light frame construction. They are built using lumber and plywood, pressure-treated with approved water-borne wood preservatives. Design information for PWFs made of lumber studs is available which it is as yet unavailable for SIPs. Clause 4.1.1.4 of the 2005 Ontario Building Code (Institute for Research in Construction-2005) specifies that buildings and their structural members shall be designed by one of the following methods:

(a) standard design procedures and practices provided by Part 4 of this code and any standards and specifications referred to in this code, except in cases of conflict the provisions of the building code shall govern, or

(b) one of the following three bases of design,

(i) analysis based on generally established theory,

(ii) evaluation of a given full-scale structure or a prototype by a loading tester, or

(iii) studies of model analogues,

provided the design is carried out by a person qualified in the specific method applied and provided the design ensures a level of safety and performance at least equivalent to that provided for or implicit in the design carried out by the methods referred to in Clause (a) above.

1.3 The Objectives

The main objectives of this research work are as follows as based on experimental testing:

1. Establishing the load carrying capacities of structural insulated sandwich panels when subjected to axial compressive loading;

2. Establishing design models based on experimental testing for the effects of combined axial compressive loads and bending moments on structural insulated sandwich panels for both above-ground and basement wall construction.
3. Establishing design models for SIPs as cladding in building construction.

1.4 The Scope

The scope of this study includes the following:

- 1- Perform a literature review on previous research work on the structural behavior of sandwich timber panels when subject to transversal loading. In addition, the literature review will cover related codes of practice.
- 2- Perform experiments up-to-collapse on 32 actual-size timber panels according to ASTM standards to determine their structural performance, and ultimate load carrying capacities.
- 3- Perform correlation between the experimental findings and the code test requirements at both ultimate and serviceability limit states.
- 4- Draw conclusion with respect to the structural adequacy of the tested sandwich panels for possible qualification to be used in future residential construction.

1.5 Contents and the Arrangement of the Thesis

Chapter 1 is an introduction for the thesis which includes the problem, the objective, the scope and the contents and arrangement. Chapter 2 presents the literature review of previous work. Chapter 3 provides details of the experimental program which has been conducted on selected panel sizes. Chapter 4 presents the experimental results, while Chapter 5 presents the conclusion of this research work and recommendations for future research.

CHAPTER II

LITERATURE REVIEW

2.1 General

Structural insulated panel (SIP) is a composite building material. It consists of two layers of structural board with an insulating layer of foam in between. The board is usually oriented strand board (OSB) and the foam either expanded polystyrene foam (EPS), extruded polystyrene foam (XPS) or polyurethane foam. Structural Insulated Panels (SIPs) are prefabricated insulated structural elements for use in building walls, ceilings, floors and roofs. The Environmental Protection Agency (EPA) estimates that the average U.S. home releases 22,000 lbs of carbon dioxide (CO₂) into the atmosphere each year. This is twice the amount of the average vehicle. By reducing the amount of energy used for heating and cooling, SIPs can significantly reduce emissions produced by our homes and commercial buildings. Building with SIPs is better because it is more comfortable, stronger & safer, lightweight, faster to construct, more resource efficient, healthier living environment, save money, wave of the future, greater energy savings, straighter walls and more design friendly. A basic SIPs panel is made from Orientated Strand Board (OSB) facing boards with a Polyurethane core. SIPs can be used to construct the floor, walls and roof of a building enabling uniform detailing at interfaces providing continuity of insulation and minimal air leakage.

The literature review conducted is presented in the following manner:

1. History of SIPs;
2. Types of Structural insulated sandwich panels;
3. Structural analysis and design of Sandwich panels; and
4. Experimental studies.

2.2 History of SIPs

SIPs are environmentally friendly and ecologically sound. SIPs are the innovative building construction method of the twenty first century allowing the rapid deployment of buildings for domestic and commercial use. SIPs are structural insulated panels used to construct buildings. In the past, a significant amount of research was conducted to predict the behaviour of sandwich panels. However, only very few researchers have undertaken experimental studies to investigate the accuracy of design of timber sandwich panels. Building panels come in many configurations, known variously as foam-core panels, stressed-skin panels, nail-base panels, sandwich panels, and curtain-wall panels, among others. Many of these building panels are non-structural, while some have no insulation. And the term "panelized construction" can also include prefabricated stud walls and other configurations associated with the modular industry.

The SIPs have been used extensively in the USA and Canada over the past 50 years but the historical development of the theory of sandwich panels shows that a very few papers have been published which deal with the bending and buckling of sandwich panels with cores which are rigid enough to make a significant contribution to the bending stiffness of the panel, yet flexible enough to permit significant shear deformations (Allen, 1969).

- 1935- The concept of a structural insulated panel began as the Forest Products Lab (FPL) builds the first in a series of experimental SIP houses in Madison, WI.
- 1947- FPL builds the Experimental Sandwich building, which is tested and monitored for 31 years. The structure is still in use today.
- 1952- Alden P. Dow, one of the Wright's students, builds SIP homes in Midland, MI.
- 1958- NAHB builds demonstration research homes with SIPs.

- 1959- Koppers Corp. starts SIP plant in Detroit.
- 1962- APA Lab Report # 193 on Sandwich Panels published.
- 1967- APA Lab Report # 193 first appears in the Model Building Code- UBC.
- 1969- APA Supplement Four on Sandwich Panels is released and rigid foam insulating products became readily available resulted in the production of structural insulated panels as we know them today.
- 1970- USDA Forest Service Research Paper FPL 144, Long-time Performance of Sandwich Panels in Forest Product Laboratory Experimental Unit, is published.
- 1973- Oil embargo- fuel prices soar.
- 1981- Oriented Strand Board (OSB) manufacturing begins.
- 1990- Group of SIP manufacturers form the Foam Core Panel Association (name later changed to Structural Insulated Panel Association (SIPA)).
- 1991- SIP market study published. Spotted oil habitat threat reduces old growth timber availability.
- 1994- SIPA Strategic Long Range Plan developed. OSB oversupply brings OSB prices down.
- 1995- 1997- Industry production increases by 50% per year.
- 1962- present- The American Society for testing Materials (ASTM) standard defines a testing protocol to document the strength and stiffness properties under the following load applications:
 - (1) Creep; (2) Axial Loads; (3) Racking and diaphragm Loads; (4) Uplift Loads; (5) concentrated Loading; (6) combined Loading; (7) Impact loading; and (8) Transverse Loads.

2.3 Types of Common Structural Insulated Sandwich panels

2.3.1. Fiber Cement Faced Structural Insulated Panels

SIPs are engineered laminated panels with solid foam cores and structural sheathing on each side. The most common types of sheathing or skins materials are oriented strand board (OSB) and plywood. Cement Faced Structural Insulated Panels can be used for below grade applications, as foundation or basement walls, and above grade applications, as floors. Some manufacturers produce cementitious SIPs with typically manufactured fiber cellulose reinforced cement boards for inside and outside skins. Fiber cellulose reinforced cement boards eliminate the need for gypsum drywall for fire resistance and can be taped and finished on the interior surface. The exterior surface is painted or coated with a vinyl or synthetic stucco permanent finish. OSB can be used instead of cellulose reinforced cement board for Fiber Cement Faced Structural Insulated Panels to accept brick veneer wall ties, to accept nailing of siding and for stucco applications. Cementitious SIP spans are up to 5 m, load-bearing walls up to four stories and roof panels up to 6 m spans. Cementitious SIPs are fastened together with power-driven screws through the inner and outer skins into either cement board or wood splines. Cementitious SIP is as energy efficient as OSB SIP and has similar connection details those of OSB-sheathed panels. Cementitious SIPs typically last longer and require less maintenance than other types of SIPs panels. Cementitious SIP has higher strength, higher fire rating, higher rot and vermin resistance, higher resistance to moisture absorption and lighter in weight than OSB SIP. Cementitious SIP is air tight as it has continuous air barrier with very low air leak, fully insulated with uniform insulation coverage and thermal bridge panels. Cementitious SIP has finishes as smooth finish, stucco, vinyl siding, brick or stone which can be installed.

2.3.2 Precast Concrete Sandwich Panel

Concrete panels have been in use for more than 50 years. Precast concrete sandwich panels are made with two reinforced slabs of high strength concrete. The space between concrete slabs is filled with a sound attenuating foam barrier. To make precast concrete sandwich panels, a first concrete slab is formed having embedded in it one end of connectors which extend from its surface in two directions with the path between the two containing only thermally insulative material, a layer insulative material is positioned adjacent to a central portion of said connectors to form a solid layer and a second layer of concrete is cast so as to receive the upper ends of said connectors. The connectors provide resistance to shear in at least two directions and include insulative high tensile strength members extending in more than one direction between the concrete slabs. The face shells of sandwich panel's main functions are providing protection to the insulation and meeting the immediate demands of handling and imposed loads. The face shells of sandwich panels must continue to give satisfactory performance under long time service. The structural concrete shells of the sandwich panels were reinforced with welded wire fabric should confirm to ASTM A82-62T, "*Cold Drawn Steel wire for concrete reinforcement.*" They are available with a perfectly smooth face, ready for paint. Provisions are made for electrical boxes and conduits in the panel at the factory. The conduit is stubbed out above the ceiling line for connection by the electricians in the field. There is no need to install furring strips and drywall on either side of the demising wall. The precast concrete has benefits as a cladding material. It has strength and solidity, recalling traditional concepts of enclosure, yet is a modern prefabricated product with all the advantages of quality control, 'just-in-time' site delivery, fast installation and extreme durability. In most cases, precast panels are cast using a mix that will simulate the appearance and texture of natural stone, generally known as reconstructed or cast

stone. Panels may also be faced with brick slips, natural stone or terracotta tiles. Most precast concrete cladding systems comprise single layers of factory-manufactured precast concrete that are installed on a building, providing a weather-resistant external finish. Standard sandwich panels, with two layers of precast with insulation between, are a well-established product. The insulating materials were commercially available rigid board stock or batting: one foamed polyurethane plastic, two foamed polystyrene plastics, one glass fiber, one foamed glass and one autoclaved cellular concrete. Brick clad concrete panels have a service life greater than 60 years. The two layers are connected by proprietary stainless steel connectors, typically consisting of wind and shear connectors. The latter are strategically positioned orthogonally to achieve suitable suspension of the outer leaf. The system provides structural integrity as it does not rely on insulation for load transference. Various insulation types can be used, including mineral fibre insulation materials. In order to optimise the cladding system, the inner leaf of the sandwich panel may be used as a load-bearing structural element to support floor units. This provides further efficiencies for the construction process and minimises the need to co-ordinate different trades. Exposure conditions may cause temperature and moisture differentials in sandwich construction and these conditions may have a more pronounced effect on the satisfactory long time structural behaviour than do the imposed loads.

2.3.3. Light Weight Steel Frame Panels

As “Light Weight Steel Frame Panels” are an open type of Structural Insulated Sandwich panels, insulation is located on the external side of the frame to overcome the risk of cold bridging. Protection against corrosion of the mild steel panels is provided by galvanizing.

2.3.4. Plywood Sandwich Panels

Plywood serves as an ideal facing material for the sandwich panels. Plywood Sandwich Panel has high strength and light weight. In addition, it is easily finished, dimensionally stable, and easily repaired if damaged. Polystyrene foams, and paper honey combs can be used as core material in the Plywood Sandwich Panel after considering the resistance of the core material to shearing forces, to heat and vapour transmission, to degradation by heat, age, and moisture; and compatibility with glues.

2.4 Structural Analysis and Design of Sandwich Panels

Sandwich panel is consisting of two relatively thin faces and a foamed plastic core. The structural performance of the Sandwich panels depends on the two faces and the core acting together as a composite element, and this raises unique design problems, not all of which may be fully understood by those responsible for their manufacture, design, and use. Sandwich panels have flexible cores therefore their behaviour is more complex than that of the plain plates and it is important to understand the numerous failure modes of sandwich panels so that appropriate design criteria can be developed. In addition to face buckling, the other possible modes of failure are as follows:

- Failure of fasteners
- crushing of the sandwich panel at a point of support or line load
- yielding of metal face in tension
- shear of the core, including shear bond failure
- Failure of the sandwich panel at a point of connection
- Blistering

The expected service life of all the structural panel systems is in excess of 60 years. The fully profiled sandwich panels are susceptible to local buckling effects under compression, bending, or their combinations. Extensive research has been carried out in Europe and USA to investigate the behaviour and design of sandwich panels for different failure conditions. In Canada, the choice of faces and cores is not infinite; face materials may be available in relatively few gauges or standard thicknesses; core materials are restricted in the choice of thickness and density. Since the plate elements of the profiled sandwich panels are supported by foam core, their local buckling behaviour is significantly better than that of plate elements without foam core. Buckling of the panels may occur at a stress level lower than the yield stress of steel, but the panels, particularly those with low b/t ratios, will have considerable post-buckling strength. Such local buckling and post-buckling phenomena are very important in the design of sandwich panels. The process of trial and error is often the most effective method of designing sandwich panels. Design methods should be as precise as the final analysis or check calculation and should indicate roughly where the process of trial and error should begin. The practical usage of sandwich panels as the cladding of buildings has increased dramatically in recent years. This has stimulated increased activity in research and development as a result of which most technical problems associated with this form of construction have been solved but still a lot of research needed to be done on:

- The influence of the shear flexibility of the core on the global behaviour.
- The influence of the core in restraining local buckling of the faces.
- The variability of core material properties.

- The influence of temperature-induced stresses has to be considered as structural sandwich panels have low thermal capacity, poor fire resistance with rigid plastic foam cores and it may deform when one side of faceplate is exposed to intense heat.
- Creep under sustained load with rigid foam cores.
- The influence of deflections.

The basic concept of a sandwich panel is that the faceplates carry the bending stresses and the core carries the shear stresses. As a sandwich with thick faces and a weak core is an inefficient sandwich because the faces are working as two independent elements, one short cut is to ignore completely any effects due to the thickness of the faces. For identification and comparison for core material properties, density, shear strength, shear modulus and compression modulus have to be determined by test for each panel type produced. Classical methods of analysis solutions have only been derived for a few simple cases of greatest practical significance. An early contribution to the subject was made by Chong and Hartsock and their colleagues. A useful approximate solution for panels which have either one or both faces profiled has been given by Wolfel (1978). He makes the usual assumption that the applied load is shared between two separate load-carrying systems -- namely, the sandwich part, which includes the influence of core shear; and the flange part, which merely involves bending of the flanges. He then makes the further assumption that these two systems are quite independent, except that their deflections coincide at some critical point, usually at the mid-span. This method is worth describing in a little more detail because, as well as yielding equations of practical value, it also provides a valuable insight into the way in which sandwich panels behave. If the bending stiffness of the faces is neglected, we have the 'sandwich part' of the section which carries load as

a consequence of axial forces in the flanges and a shear force, in the core. When irregular loading or support conditions arise, it becomes necessary to resort to numerical methods of analysis. Jungbluth and Berner (1986) have described a finite difference approach which appears to be the favoured method in Germany. An alternative numerical method, related to the finite element solution, has been given by Schwartz (1984). Yet another technique has been developed in the US in which thin faces are modelled by finite shell strips and relatively weak cores by finite prisms (Chong, 1986). However, for general purposes, it is believed that the conventional finite element method offers the best approach. In many applications, the finite element method is approximate and it is necessary to use a large number of elements in order to obtain accurate solutions. For three-layered sandwich beams, the solutions are exact and the minimum number of elements necessary to model the problem will give a precise solution. The general solution for the bending of panels with profiled faces was first given by the author (Davies, 1986), who then extended it to panels subject to combined axial load and bending, giving solutions for panels with both flat and profiled faces (Davies, 1987). As the former is a special case of the latter, there is little point in omitting the axial load terms when programming the method.

2.4.1 Historical Development of Sandwich Theory

In recent years, sandwich panels are increasingly used in building structures particularly as roof and wall cladding systems. They are also being used as internal walls and ceilings. Because of their good thermal properties, they have been used in cold-storage buildings. Sandwich (SW) structures are three-layer high performance lightweight structures (Wiedemann, 1996; Stamm and Witte, 1974; Plantema, 1966), consisting of a soft core which is covered by

stiff skin layers. They are characterized by both excellent bending stiffness and low weight. However, due to their comparatively high shear flexibility, the global behaviour concerning deflection and buckling is described by a shear flexible theory (Mindlin, R. 1951; Reissner, E. 1945), where only the membrane stresses in the thin skin layers are considered, whereas the in-plane stresses appearing in the core are neglected. This theory is known as the Sandwich Membrane Theory (SWMT), which has proven to be reliable for a long time. Past research (Davies and Hakmi, 1992, 1991) has investigated the local buckling behaviour and developed modified effective width rules for the plate elements in sandwich panels. For an at least approximate description of both global structural behaviour of SW and local phenomena, the SWMT must be extended. For this purpose (Kuhhorn, 1993, Kuhhorn, 1991; Kuhhorn and Schoop, 1992) presented a thickness flexible, geometrically nonlinear SW-shell theory using seven kinematic degrees of freedom. This theory is able to solve the problems mentioned above with sufficient accuracy if the local perturbations considered are characterized by wavelengths which are not too short (numerical investigations show that this theory is applicable for wrinkling problems characterized by half waves longer than 0.8-times of the core thickness). This extended theory includes the independent bending stiffness of each skin separately. Also a linear thickness stretch distribution over the height of the core is taken into account whereas the core in-plane stresses remain unconsidered. Due to the increasing interest in the use of structural sandwich panels, a good deal of research has continued in recent years (Davies, 1993). Research and development of sandwich panels with profiled faces began only in late 1960s (Chong and Hartsock, 1993). These rules can be applied successfully for plate elements with low width to thickness ratios (b/t), but their applicability to slender plates is questionable. In sandwich panel construction, the b/t ratio can be as large as 600 (Mahendran and Jeevaharan, 1999). To

investigate the applicability of current design rules for slender plates with such large b/t ratios, a detailed investigation into the local buckling behaviour of profiled sandwich panels was conducted using extensive series of laboratory experiments on 50 foam supported steel plates. The static behaviour and strength of sandwich panels is based on the composite action of the three structural layers, namely the two faces and the core (Davies, 2001). For design purposes, such local buckling and post buckling problems are treated by utilizing the concept of effective width principles.

2.4.1.1 The General Method

The general method has been investigated by Reissner (1948) in relation to isotropic panels with very thin faces. It has been concluded that the effect of core flexibility in the z -direction is less important than the effect of core shear deformation in the transverse planes. A relatively simple differential equation for the transverse displacement has been driven by neglecting the effect of direct transverse core strains. A very similar equation to Reissner's equation has been driven by Eringen (1951) where the geometrical thickness of the equal faces was neglected, and their local bending stiffnesses and also the bending stiffness of the core was included. By the assumption that the vertical and horizontal displacements in the core are directly proportional to z -direction, the inclusion of the latter is contradicted to some extent. A much more recent analysis conducted by Heath (1960) also included a very similar equation, but for a sandwich with an orthotropic core. Heath's analysis was based on earlier work by Hemp (1948) and is apparently independent of Reissner's work (1945).

Raville (1955) applied the general method to the problem of a simply-supported rectangular panel with uniform transverse load and with thin faces. The three displacements of points in the orthotropic anti-plane core are expressed as polynomials in z , but the complexity of the analysis again makes it necessary to revert to the simplifying assumption of infinite core stiffness in the z -direction. For practical purposes the general method is evidently intractable when applied to sandwich panels, but more success has been achieved in relation to sandwich struts and beams. The early works of Williams et al (1941) and Cox and Riddell (1945) fall into this category. The first of these deals with a sandwich strut with thick faces and an isotropic core (with an extension for orthotropic cores) and the analysis is used to form a link between the extreme cases of wrinkling instability (no longitudinal displacement of the faces during buckling) and of overall Euler-type instability, modified for shear deformations in the core (no direct core strains in the z -direction). A very thorough analysis of the behaviour of struts with isotropic faces and cores has been outlined by Goodier (1946) and Goodier and Neou (1951).

2.4.1.2 The Selective Method

Selective method; bending problem

Most of published work on sandwich panels refers to the selective method and, in particular, to the bending problem, in which core strains in the z -direction is neglected. The assumption that the core is weak in the xy -plane leads in any case to the conclusions that the core makes no contribution to the flexural rigidity of the sandwich, that the core shear stresses in zx and yz planes, are independent of z and that a straight line drawn in the unloaded core normal to the faces remains straight after deformation, but is no longer normal to the faces. These assumptions (core weak in xy -plane, stiff in z -direction) allow the displacements of the panel to be expressed

in terms of only three variables, one of which is the transverse displacement. The other two variables are a matter of choice.

Selective Method; wrinkling problem

The literature of the wrinkling problem is less extensive than that of the bending problem. As has been mentioned, wrinkling is characterized by its short waves involving bending of the skins and compression or elongation of the core material in the transverse direction. This type of local failure occurs when the core thickness is such that the overall buckling is not likely to happen. The problem of symmetrical wrinkling of sandwich panels was studied by many investigators with the first major paper by Gough et al. (1940). It contains an examination of the stability of a straight strut stabilized in various ways by an isotropic elastic medium. Some of the cases considered are directly applicable to the compression faces of sandwich beams and to the anti-symmetrical wrinkling of sandwich struts which it may be referred to as a "skew ripple". An analysis of the same kind is made by Hoff and Mautner (1945) for symmetrical wrinkling of sandwich struts. In all these studies, a linear distribution of the transverse displacement through the core was considered, and the faces were treated as plates on elastic foundation. The analytic solution for the symmetrical wrinkling stress can be obtained by using an elasticity approach. The assumptions commonly accepted for this type of analysis are: The in-plane stresses in the core are neglected. That is, with X-Y axes in the plane of a sandwich plate, and Z- axis perpendicular to it: in which normal, shear stresses and subscript denoting the core. Thus, the relevant deformations in the core are in the transverse direction and shear deformations in XZ and YZ planes. The wrinkling consists of a plane deformation. Thus, if a sandwich panel is compressed in X- direction, the lateral deflection is independent of y. The core can be treated as a semi-infinite medium in which the displacement decreases exponentially with maximum value

at the interface with the skin. The faces are thin in comparison with the core thickness. This implies that the deflection of each face is identified with the displacement of the core at its surface. The effect of Poisson's ratio of the core material is neglected.

2.4.1.3 Flexural Stresses in Sandwich Panels

A number of researchers have studied the failure modes of sandwich structures in flexure (Zenkert et al., 2002; Thomsen, 1995; Yoshii, 1992; Triantafillou and Gibson, 1987). Triantafillou and Gibson studied failure modes of sandwich beams with aluminum face sheets and a rigid polyurethane foam core. Failure maps for various core densities and span-to-depth ratios were constructed for face yielding face wrinkling, core yield in shear, and core yield in tension and compression. Based on similar failure equations, a weight optimum design of composite sandwich structures was proposed by Yoshii (1992). A summary of design approaches to sandwich construction may be found in a book published by Zenkert (1997) while information on cellular solids is available elsewhere (Gibson and Ashby, 1988). Under flexure a sandwich beam exhibits various failure modes depending on the state of stress and the materials used. The flexural rigidity for the sandwich panel is highly affected the failure mode. It can be defined as the sum of the flexural rigidities of the faces and the core measured about the neutral axis of the sandwich cross-section, Allen (1969). The potential failure modes together with the corresponding simplistic failure criteria are summarized below:

1. Face failure in tension or compression: $-\sigma_{fc} \leq \sigma_f \leq \sigma_{ft}$
2. Face wrinkling due to compression: $\sigma_f \leq 0.5(E_f E_c G_c)^{1/3}$
3. Core failure in shear: $\tau_c \leq \tau_{cs}$
4. Core failure in tension or compression: $-\sigma_{cc} \leq \sigma_c \leq \sigma_{ct}$

5. Face/core interface failure: $\tau_i \leq \tau_{is}$

In the above equations σ = in-plane normal stress, τ = out-of-plane shear stress, E = Young's modulus, G = shear modulus, sub f = face, sub c = core, sub i = interface, sub fc = face compressive strength, sub ft = face tensile strength, sub cs = core shear strength, and sub is = interface shear strength. In case of localized loading, face/core indentation is an additional failure mode.

2.4.1.4 Flexural and Shear Stresses in Sandwich Panels

The use of the terms long beam flexure and short beam flexure when addressing sandwich panel testing is very essential, as the former is used to determine face-sheet, i.e. the surface layers of the sandwich panel, properties and the latter to determine core shear properties. Such a distinction is logical since we know that, for a given applied loading, the flexural stresses (tensile and compressive) in the face-sheets increase as beam length increases, but the shear stresses in the core do not. That is, long beams produce high bending stresses while short span lengths do not. Most recently, Sennah et al. (2009, 2008) and Butt (2008) performed experimental studies on the static flexural and flexural-creep performance of SIPs for roofs and floors in residential construction. The experimental program included testing 52 panels of different thickness and span length under increasing static loading to-collapse. The results proved that the tested SIPs are as good as the conventional timber joist system specified in part 9 of the NBBC, with respect to strength and serviceability.

2.4.1.5 Elastic Deflection Analysis of Sandwich Panels

The plywood Design Specification Supplement, entitled "Design and Fabrication of plywood Sandwich Panels" (APA 1990) simplifies the total elastic mid-span deflection (Δ_T) for the

uniformly loaded-simply supported sandwich beam with relatively thin and stiff faces, and thick weak cores. It is simplified to the sum of bending and shear deflection as follows:

$$\Delta_T = \Delta_B + \Delta_S$$

Where: Δ_B = deflection at mid-span of the sandwich panel due to bending

Δ_S = deflection at mid-span of the sandwich panel due to shear

The form of the elastic bending deflection for a simply-supported homogeneous beam of uniform cross-section in quarter-point loading, as follow:

$$\Delta_B = \frac{11PL^3}{384EI}$$

Where: P = total applied load

L = beam span

E = modulus of elasticity of the beam material

I = moment of inertia of the uniform cross-section

EI = flexural rigidity

As per Allen (1969), by applying the boundary conditions for the simply-supported quarter point load beam ($w_2 = 0$ at $x = 0$, the maximum shear deflection (at $x = L/4$) associated with the shear deformation of the sandwich loaded at quarter points is defined by the following equation:

$$\Delta_s = w_{2\max} = \frac{PL}{8AG}$$

Where $A = bd^2 / c$ and AG is referred to as the shear stiffness

P = total applied load

L = beam span

G = core shear modulus

X = distance from the reaction in shear zone of beam

w_2 = displacement at x

Thus, the total sandwich beam deflection reflecting the bending and shear component is defined in by the following equation:

$$\Delta_s = \frac{11PL^3}{384D} + \frac{PL}{8AG}$$

2.5 Permanent wood foundation

The permanent wood foundation (PWF), shown in Fig. 2.1, is a complete wood frame foundation (load-bearing walls) for low-rise, residential, industrial, commercial and other types of buildings (CSA, 1997). All lumber and plywood in PWF is pressure treated with water-borne preservatives. Nails and straps must be corrosion resistant. The walls are designed to resist soil pressure loads in addition to the normal vertical loads from roofs, floors and top walls. Improved moisture control methods around and beneath the foundation result in comfortable, dry living space below grade. The foundation is placed on a granular drainage layer which extends 300 mm beyond the footings. Porous backfill is brought up to within 300 mm of finished grade and the remaining space filled with less permeable or native soil sloped away from the house. The porous drainage material directs ground water to below the basement, thus preventing hydrostatic pressure and leaks in the basement walls or floors. A sump is provided, in accordance with the building code, and is drained by mechanical or gravity means. No drainage (weeping) tile is needed around the footings as this may impede the flow of water. The granular drainage layer can accommodate a large influx of water during peak storm conditions. It also provides a

large surface area for water to percolate into the subsoil. Caulking between all wall panels and between the walls and the footings, and a moisture barrier applied to the outside of the walls provide additional protection against moisture. The result is a dry basement that can be easily insulated and finished for maximum comfort and energy conservation. PWF has many other advantages including (i) increased living space since drywall can be attached to the foundation wall studs, (ii) rapid construction, whether framed on site or prefabricated off-site, and (iii) buildable during winter times using minimal measures around the footings to protect them from freezing. CAN/CSA-S406, *Construction of Preserved Wood Foundations*, (CSA, 1992) allows the use of permanent wood foundation (PWF) which is referred to in Part 9 of the National Building Code of Canada (Institute for Research in Construction-2005) and in provincial building codes. It describes the required materials and methods of construction of permanent wood foundations made of lumber studs. While more design information is available in the CSA book "Permanent Wood Foundation (CSA, 1997). Design information of PWF made of SIPs is as yet unavailable.

CHAPTER III

EXPERIMENTAL STUDY

3.1 General

The SIPs which have been used in the experimental study, are produced by Thermapan Inc. in standard sizes of 1.2 m wide and lengths of 2.43, 2.72, 3.05, 3.66, 4.27 and 4.90 m. SIPs can be used in used for many different applications, such as interior and exterior walls, roofs, floors, foundations, timber frame, additions, and renovations. Thermapan SIPs are composed of thick layer of expanded polystyrene insulation (EPS) board laminated between two sheets of oriented strand board (OSB), as shown in Figure 3.1. The facing of these developed panels is made of two faces of Oriented Strand Board (OSB), 11 mm (7/16") thickness, holding a foam core for floor and wall construction. These SIPs meets building code for many residential and commercial applications based on the R-Value, as shown in Table 3.1 (Thermapan, 2007).

SIP floors and roofs are installed by placing the panels side by side as shown in Fig. 1.3. The joint between the panels in the span direction can be either foam-spline connection or lumber-spline connection. In the foam-spline connection, shown in Fig. 3.2, a recess is formed in the foam core at the long edges of the panels. A foam block, with two OSB facings glued to it, is inserted at the edge of one panel. Then, the other panel is slide over the spline. The block OSB facings are then nailed to the OSB of the connected panels which provides structural integrity to the floor or wall. Figure 3.2 shows a typical section of foam-spline connection before and after assembly. The width of the insert for the foam-spline connection is usually half the width of the solid sawn lumber. It is preferred for roof construction to assist in energy efficiency. In case of lumber-spline joint, shown in Fig. 3.3, a recess in formed along the longitudinal edges of the

foam during manufacturing. After placing the panel over the wall, a sawn lumber is inserted in the recess along the panel length. Then, the adjacent panel slides over the sawn lumber, followed by nailing the OSB facings to the solid lumber. Figure 3.3 shows a schematic diagram of the solid lumber-spline connection. The experimental research program aimed to develop a better understanding of the structural behaviour of these timber sandwich panels at service and ultimate loading conditions when they act as walls or cladding in residential construction. 32 tests were performed on different panel sizes at the structures laboratory of Ryerson University to provide experimental data that would then be evaluated for building code compliance. This chapter summarizes the geometrical and material properties of the tested panels, the different setups for the tests, and the test procedure.

3.2 Description of Panels:

The tested panels were divided into 9 groups based on the size of the panel, the connection between adjacent panels in real structure (i.e. foam-spline or lumber-spline), and the thickness of the OSB facings. This is in addition to the type of testing to be conducted on the panel group. Tables 3.2 through 3.5 summarize the geometric characteristics of the tested panels. The description of each panel group is summarized as follows.

All panels were manufactured for wall construction with 1.2 m wide and 11 mm (7/16") thick OSB boards for the side facings, except for those for basement construction. Group A consisted of 3 identical panels of 2.73 m (9') length, 165 mm (6 1/2") total depth, and foam-spline connection. It should be noted that the foam core depth is simply the difference between the total depth and the thickness of the two OSB facings. Group B is similar to Group A but with lumber-

spline connection. It should be noted that in Groups A and B, the compressive load was applied concentrically at the mid-thickness of the panel. Group C consisted of 3 panels identical to those for Group. However, the applied compressive load was eccentric to the mid-thickness of the panel. An eccentricity of $t/6$ was considered, where t is the thickness of the panel. Group D, E, and F are identical to Group A with respect to geometry and loading except that the length of the panels were 3.05 m (10'), 3.66 m (12'), and 4.90 m (16'), respectively. Table 3.2 summarizes panel geometries and loading type for Groups A to F. To examine the effect of combined axial and bending on the capacity of the tested wall panels, it was decided to conduct testing to determine the axial load carrying capacity from the axial load tests as specified in Table 3.2 for zero eccentricity and the resisting moment of the same panels as obtained from flexure tests on identical panels. Table 3.3 summarizes the geometries of panel groups G and H which are identical to Groups A and E, respectively, shown in Table 3.2. This type of combined loading is applicable to wall construction over ground. However, to study this combined effect in basement wall construction, identical panel Groups I and J were considered for axial load and flexural load tests, respectively. The size of each panel in these groups was 2.74 m (9') length, 1.20 m (4') width and 210 mm (8 1/4") total depth. To allow for the construction of preserved wood foundation the interior facing was made of 11 mm (7/16") OSB sheets, while the exterior facing exposed to soil was made of 15.5 mm (5/8") Canadian softwood plywood.

3.3 Material Properties

The exterior faces of the Thermapan SIPs, are oriented strand board (OSB) manufactured and grade stamped as per APA (1990). The OSB board fabricate panels had 1R24/EF16/W24²₅

panel mark with 11 mm thickness construction sheathing. The material properties for OSB boards are specified as follows:

Modulus of elasticity: 800,000 psi (5515 MPa) in the span direction

225,000 psi (1551 MPa) in the direction normal to the span direction

Modulus of rupture: 4200 psi (28.955 MPa) in the span direction

1800 psi (12.409 MPa) in the direction normal to the span direction

However, material characteristics as specified in the OSB Design Manual (2004) for the 1R24/EF16/W24 panel are as follows:

Bending resistance, M_r = 228 N.mm/mm

Bending stiffness, EI = 730,000 N.mm²/mm

Axial stiffness, EA = 38,000 N/mm

Axial tensile resistance, T_r = 57 N/mm

Axial compressive resistance, P_r = 67 N/mm

Shear through thickness resistance, V_r = 44 N/mm

Shear through thickness rigidity, G = 11,000 N/mm

When expanded Polystyrene exposed to steam, it creates a uniform closed cell structures highly resistant to heat flow and moisture penetration. This process called in-plant expansion process and it is fused into blocks. Blocks are cured for dimensional stability and cut into boards. The expanded polystyrene (EPS) core type 1 has been used to fabricate the panels. The priority density demonstrates a load failure of 25 psi when tested as per ASTM C297. The expanded polystyrene (EPS) core material must meet the standard CAN/ULC-S701 and demonstrate the following characteristics:

Nominal density	1.0 Ibs/ft ³ (16 kg/m ³)
Flexural strength:	25 psi (172 kPa)
Tensile strength:	15 psi (103 kPa)
Compressive strength:	10 psi (70 kPa)
Shear strength:	12 psi (83 kPa)
Shear modulus:	400 psi (2758 kPa)

The urethane adhesive must meet the following standards:

ASTM D-2294: 7 Day High Temperature Creep Test

ASTM C-297: Tension Test of Flat Sandwich Construction in a Flatwise Plane

ASTM D-1877: Resistance of Adhesive to Cyclic Laboratory Aging Conditions

ASTM D-905: Block Shear Test Using Plywood

ASTM D-1002: Strength Properties of Adhesive Bonds in Shear by Tension Loading

To allow for the construction of preserved wood foundation the panel exterior facing exposed to soil was made of 15.5 mm (5/8") Canadian softwood plywood (CSP). CSP has 5 plies and demonstrates the following characteristics:

Bending resistance = 520 N.mm/mm if the applied force is in the direction of face grain

Bending resistance = 280 N.mm/mm if the applied force is normal to the direction of face grain

Bending stiffness, EI = 2000,000 N.mm²/mm if the applied force is in the direction of face grain

Bending stiffness, EI = 630,000 N.mm²/mm if applied force is normal to direction of face grain

Axial stiffness, EA = 71,000 N/mm if the applied force is in the direction of face grain

Axial stiffness, EA = 47,000 N/mm if the applied force is normal to the direction of face grain

Axial tensile resistance, T_r = 110 N/mm if the applied force is in the direction of face grain

Axial tensile resistance, $T_r = 71$ N/mm if the applied force is normal to direction of face grain

Axial tensile resistance, $P_r = 120$ N/mm if the applied force is in the direction of face grain

Axial tensile resistance, $P_r = 79$ N/mm if the applied force is normal to direction of face grain

Shear through thickness resistance, $V_r = 38$ N/mm

Shear through thickness rigidity, $G = 7,100$ N/mm

These values are based on dry service conditions and standard-term duration of load.

For all panels, 2"x0.095" diameter, hot-dipped galvanized, gun nails at 8" spacing with 3/4" minimum edge distance to connect the OSB sheets to the foam splines and limber splines. Also, this nail arrangement was used to connect the panel facings to the lumber studs at the top and bottom of the walls.

3.4 Test method for SIP Panels under Axial Compressive Loading

The objective of this set of testing is to provide design tables of wall panels in the form of factored design resisting line load. These design tables will assist in establishing the maximum span of joists of roof/floor panels or the maximum span of SIP floor or roof served by SIP wall as based on different snow load values (i.e. 1.0, 1.5, 2.0, 2.5 and 3.0 kPa for example). For the purpose of structural qualifications of SIPs, the Canadian Construction Materials Commission (CCMC) produced a technical guide (IRC, 2007) in collaboration with the National Research Council Canada (NRC) to describe the technical requirements and performance criteria for the assessment of stressed skin panels (with lumber 1200 mm o.c. and EPS core) for walls and roofs. In this guide, The performance of the stressed skin panels for walls and roofs, have been evaluated, as an alternative solution, with respect to Part 4, Structural Design, and Part 9,

Housing and Small Buildings, of the National Building Code of Canada (NBCC, 2005). The Technical Guide focuses on structurally qualifying the stressed skin composite panels to be as good as the structural capacity of the conventional wood-frame buildings. A successful evaluation conforming to this Technical Guide will result in a published CCMC Evaluation Report. The published CCMC Evaluation Report is applicable only to products bearing the proper identification number of CCMC's evaluation number. This NRC/IRC/CCMC Technical Guide specifies test methods for SIPs which is similar to those specified in ASTM E72-02, *Standard Test Methods for Conducting Strength Tests of Panels for Building Construction*, (ASTM, 2002) as well as ICC AC04, *Acceptance Criteria for Sandwich Panels*, (2004). The ICC AC04 acceptance criteria are based on ASTM E72 standard test methods. The 2008 ANSI/APA PRS-610.1, *Standard for Performance-Rated Structural Insulated Panels in Wall Applications*, published by *APA—The Engineered Wood Association* in USA, provides similar structural qualification procedure and criteria for the performance-rated SIPs to those in ASTM E72-02 and ASTM E 1803-06, *Test Methods for Determining Structural Capacities of Insulated Panels*. ASTM E72-02 specifies at least three identical specimens for each test group. As such, Groups A, B, D, E, F and I have been selected for tests under axial compressive loading as shown in Tables 3.2 and 3.4.

3.4.1 Axial Compressive Load Test setup

AC04 specifies that load bearing wall panels shall support an axial loading applied with an eccentricity on one-sixth the panel thickness to the interior or towards the weaker facing material of an interior panel. The test setup shall be capable of accommodating rotation of the test panel at the top of the wall due to out-of-plane deflection with the load applied throughout

the duration of the test with the required eccentricity. AC04 also specifies that the test panel shall have wall sill and cap plate details with connections matching the proposed field installations. Axial loads shall be applied uniformly or at the anticipated spacing of the floor or roof framing.

To prepare for the test, the wall panel aligned vertically and supported directly over the laboratory's floor or over an elevated precast concrete slab units. A uniformly distributed line load was applied on the top side over the 1200 mm width using a loading assembly. This loading assembly was composed of a 1200×350×12 mm steel base plate resting over the top side of the panel. A 125×125×12.7 mm HSS box beam of length 1200 mm was welded to the top side of the steel base plate to transfer the applied jacking load over the panel width. Two 70×70×9 mm steel angles of 1200 mm length were welded to the steel base plate, one on each side of the wall panel to stabilize the loading assembly during the test. The weight of the loading assembly was calculated as 1.25 kN. Figure 3.4 and 3.5 show schematic diagrams of the elevation and side view of the test setup for axial loading. While Fig. 3.6 shows schematics diagram of the loading assembly for both concentric and $t/6$ eccentric compressive loading. Figure 3.7 shows view of Wall W2 before testing, while Fig. 3.8 shows view of the top loading system for Wall W2. Figure 3.9 and 3.10 show views of the top loading assembly with the concentric and eccentric HSS beam.

3.4.2 Instrumentation for Axial Compressive Load Test

Four Linear Variable Displacement Transducers, (LVDT's) were used to measure horizontal displacement at the mid-height of the panel. The four LVDTs were located at the mid-height of the wall panel, two on each side of the panel facing. Each LVDT was located at 300

mm from the vertical free edge of the wall panels. LVDTs 1 and 2 have been installed on the south side of the panel while LVDTs 3 and 4 have been installed on the north side of the panel as shown in Fig. 3.11. Four potentiometers (POTs) were installed vertically over the four corners on the top side of the panels as shown in Figs. 3.9 and 3.10 to record axial shortening of the wall panel under load. The compressive load was applied through a jacking load system with a universal flat load cell of 222 kN (50,000 lb) capacity to measure the jacking load. During testing, the process for collecting and converting data captured by the LVDT's, POTs and load cell were done using a test control software (TCS) with SYSTEM 5000 data acquisition unit which was adjusted to sample the data at rate of 10 reading per second during the test.

3.4.3 Axial Compression Load Test Procedure

ASTM E72 specifies that wall panels shall be loaded in increments to failure with deflections taken to obtain deflections and set characteristics. The tests were performed in the structures laboratory of Ryerson University. The test set-up was prepared for each test which included installing the POTs and LVDTs at the predetermined locations. For each panel, the jacking load was continuously at a slow rate. Visual inspection was continuously conducted during the test record any change in the structural integrity of the wall panel. Each test was terminated after the wall panel failure. Failure of the panel was considered when the recorded jacking load was not increasing or when the panel could not absorb more loads while recorded axial shortening was increasing by continuously pressing the pump handle. Mode of failure was recorded and test data was then used to draw the load-deflection and load-axial shortening relationships for each panel.

3.5 Test method for SIP Panels under Flexural Load

As it was mentioned earlier, the objective of this test was to establish the factored design flexural capacity of selected wall panels that would further be used with the obtained factored design axial compressive load with zero eccentricity to apply the axial load-moment interaction equation to determine either the factored axial load or factored bending moment that can safely be applied on the wall panels. Bending qualification tests on the panels were conducted as specified in the method described in the ASTM E72-02, *Transverse Load Test*. ASTM E72-02 specifies at least three identical specimens for each test group. Groups G, H and J listed in Tables 3.3 and 3.5.

3.5.1 Flexure Load Test setup

Each tested panel was supported over two 25.4 mm steel rollers at each side in the short direction. 1200×150×12 mm steel plates were inserted between the steel rollers and the supporting steel pedestal resting on the laboratory strong floor. Other similar-size steel plates were inserted between the supporting roller and the panel bottom facing. A 150×150×12.7 mm HSS beam of 2400 mm length used to transfer the applied jacking load to a 102×1020×6.4 mm HSS beam that was laid transversally over the top panel facing at the quarter points to spread the load over the panel width. Steel roller and plate assembly similar to that used to support the panel over the steel pedestals was used to support the 2400 mm length HSS beam over the two 1200 mm length HSS spread beams at the quarter points. The weight of this loading system is 2.0 kN. Figure 3.13 shows view of the test setup of WS31 wall panel.

3.5.2 Instrumentation for the Flexure Load Test

Mid-span deflection was measured using 4 Linear Variable Displacement Transducers (LVDTs). These LVDTs were positioned underneath the panel, with two LVDTs were located at 25 mm from the panel free edges and other two LVDTs located at the third points of the panel width. Figure 3.14 shows view of the LVDTs installed at mid-span location under panel WB19. The load was applied through a jacking load system with a universal flat load cell of 222 kN (50,000 lb) capacity. During each test, the process for collecting and converting data captured by the LVDTs and load cell was done using a test control software (TCS) with a SYSTEM 5000 data acquisition unit which was adjusted to sample the data at rate of 10 reading per second during the loading test.

3.5.3 Flexure Load Test Procedure

Flexural tests were performed in the structures laboratory of Ryerson University. The test set-up was prepared for each test as explained earlier. For each panel, jacking load was applied in increments so that visual inspection could be performed to record any change in structural integrity of the sandwich panel. The tests were terminated after panel failure when the jacking load was not increasing while panel deflection was increasing by continuous pressing of the pump handle. At that stage, failure mode was observed and test data was then used to draw the load-deflection relationships for each panel.

CHAPTER IV

EXPERIMENTAL RESULTS

4.1 General

This Chapter discusses the experimental results of testing to-collapse 32 actual-size timber panels according to ASTM standards to qualify them based on code requirements and test method criteria. The experimental results for all panels, in the form of load-axial shortening relationship, load-lateral deflection relationship, and failure pattern, are presented in sequence for each panel group. The structural adequacy of the tested sandwich panels for possible use in residential construction was presented at the end of the Chapter.

4.2 Code Requirements for the Structural Qualification of the SIPs

The Structural qualifications of the SIPs have been assessed based on:

- 1- The general design principles provided in CSA Standard CAN/CSA-086.1, Engineering Design of Wood;
- 2- The evaluation criteria set forth in the NRC/CCMC Technical Guide which focuses on SIPs as being "as good as" the conventional wood-frame buildings with respect to strength and serviceability; and
- 3- CSA Standard CAN/CSA-S406-92, Construction of Preserved Wood Foundations, (1992) and the National Building Code of Canada (NBCC 2005).

Based on NBCC and CAN/CSA-S406, the following loads and load factors can be used to examine the structural adequacy of the panels for serviceability and ultimate limit states design:

Dead load factor = 1.25

Live load factor = 1.50

Dead load for roofs = 0.5 kPa

Dead load for floors = 0.47 kPa

The intensity of the triangular lateral soil pressure = 4.7 kN/m^2

Live load for residential construction = 1.9 kPa

Snow load for residential construction = 1.9 kPa (for simplification of comparison)

Deflection limit for serviceability (live load effect) = $\text{span} / 360$

The deflection limit of $\text{span}/360$ is a serviceability limit condition which may be waived in case of industrial buildings, with $\text{span}/180$ as live load deflection limit when no roof ceiling is provided and with $\text{span}/240$ when ceilings other than plaster or gypsum are used (NBCC Part 9, 2005). The deflection limit of $\text{span}/360$ is intended to limit floor vibration and to avoid damage to structural elements or attached nonstructural elements. The average deflection and ultimate load carrying capacity of each panels group are basically the average of those for the three panels in each panel group as per the Acceptance criteria for SIPs set forth in ICC-ES AC04 (2004). Further, when the results of one of the tested panel vary more than 15% from the average of the three panels, one of the following two actions was chosen: (i) the lowest test value may be used; or (ii) the average result based on a minimum of five tests may be used regardless of the variations. Moreover, the results from two tests could be used when the higher value does not exceed the lower value by more than 5% and the lower value is used with the required factors of safety. Factor of safety for ultimate load carrying capacity of SIPs is dependant on the followings: (i) consistency of materials, (ii) the range of test results, and (iii) the load-

deformation characteristics of the panel. AC04 generally applies a factor of safety of 3 to the ultimate load based on the average of three tests which called in this research as panel group. However, for the case of the tested panels in this research, AC04 provides the following factors of safety applicable to uniform transverse loads:

F.S. = 3.0 for ultimate load at shear failure for all loading conditions.

F.S. = 2.5 for ultimate reaction at failure for all loading conditions

F.S. = 2.5 for ultimate load determined by bending (facing buckling) failure under allowable snow loads.

F.S. = 2 for ultimate load determined by bending (facing buckling) failure under allowable live loads up to 0.958 kPa (20 Lb per square foot).

In case of wall panel axial load tests, AC04 specifies that wall panels shall support an axial loading applied with an eccentricity of 1/6 the panel thickness. Also, AC04 specifies that the factored design resisting axial load is determined from the experimental axial load at a net axial deformation of 3.18 mm (1/8") or the ultimate load divided by a factor of safety determined in accordance with those specified for transverse load testing mentioned above, whichever is lower.

4.3 Group A

In this group, three identical panels were tested to complete collapse under uniformly distributed axial concentric compression load. Each panel was of 9 feet height, 4 feet wide and 6.5 inch thick, with foam-spline connection. Figure 4.1 shows view of panel W1 before testing, while Figs. 4.4 through 4.9 show views of the permanent deformed shape of the panel after

failure as well as close-up views of the local damage and deformation. It was observed that the failure mode in wall W1 was due to OSB facing crushing near the top quarter point on one side of the panel and near the lower quarter point on the other side of the panel that led to global permanent lateral deformation of the panel as shown in Fig. 4.9. It should be noted that local OSB crushing along its connection with the top and bottom wall studs as shown in Figs. 4.5 and 4.7. The failure was abrupt causing a sudden drop in the applied jacking load as depicted in the load-axial shortening relationship in Fig. 4.2. It was observed that linear elastic behaviour was maintained till failure.

Figure 4.10 shows view of panel W2 before testing, while Figs. 4.13 through 4.16 show views of the permanent deformed shape of the panel after failure as well as close-up views of the local damage and deformation in the OSB facing. Figure 4.11 depicts the load-axial shortening relationship for the model. It was observed that the failure mode of OSB crushing near the top part of the wall as well as at the connection with the top wall stud. Figure 4.17 shows view of panel W3 before testing, while Figs. 4.20 through 4.22 show views of the permanent deformed shape of the panel after failure as well as close-up views of the local damage and deformation in the OSB facing. Figure 4.18 depicts the load-axial shortening relationship for the model. It was observed that the failure mode of OSB crushing occurred on one side of the panel near its mid-height as well as at the connection with the top wall stud.

Figures 4.3, 4.12, and 4.19 depict the jacking load-lateral deflection relationships for walls W-1, W2 and W3, respectively. It can be observed that lateral deflection increase with increase in the applied load. This may be attributed to the lateral instability of the OSB facings

as a result of the high flexibility of the foam in between. However lateral deflection is not considered in this study as design criteria per AC04. Table 4.1 shows that the experimental ultimate jacking load was 324.97, 323.27 and 283.84 kN for walls W1, W2 and W3, respectively. As per AC-04, the ultimate factored design axial resisting compressive load is the experimental ultimate load divided by 2.5. Thus, the factored design axial resisting load is 130.00, 129.31 and 113.54 kN for walls W1, W2 and W3, respectively. Since the obtained design values for each walls is within 15% difference with the average value of the three panels, the design factored axial compressive load for Group A is 124.30. kN. This value will be farther be used to examine the axial force-moment interaction for this wall group.

4.4 Group B

In this group, three identical panels were tested to-collapse under uniformly distributed axial concentric compression load. Each panel was of 9 feet height, 4 feet wide and 6.5 inch thick, with lumber-spline connection. Figure 4.23 shows view of panel W4 before testing, while Figs. 4.26 through 4.29 show views of the permanent deformed shape of the panel after failure as well as close-up views of the local damage and deformation. It was observed that the failure mode in wall W4 was due to OSB facing crushing near the top of the panel and that led to global permanent lateral deformation of the panel as shown in Fig. 4.28. Foam-OSB facing delamination at their interface was observed at the same location at failure. The failure was abrupt causing a sudden drop in the applied jacking load as depicted in the load-axial shortening relationship in Fig. 4.24. It was observed that linear elastic behaviour was maintained till failure.

Figure 4.30 shows view of panel W5 before testing, while Figs. 4.33 through 4.36 show views of the permanent deformed shape of the panel after failure as well as close-up views of the local damage and deformation in the OSB facing. Figure 4.31 depicts the load-axial shortening relationship for the model. It was observed that the failure mode of OSB crushing near the top quarter point in addition to foam-OSB facing delamination at their interface at the same location. Figure 4.37 shows view of panel W6 before testing, while Figs. 4.40 and 4.41 show views of the permanent deformed shape of the panel after failure as well as close-up views of the local damage and deformation in the OSB facing. Figure 4.38 depicts the load-axial shortening relationship for the model. It was observed that the failure mode of OSB crushing at the top of the wall.

Figures 4.25, 4.32, and 4.39 depict the jacking load-lateral deflection relationships for walls W4, W5 and W6, respectively. It can be observed that lateral deflection increase with increase in the applied load. This may be attributed to the lateral instability of the OSB facings as a result of the high flexibility of the foam in between. However lateral deflection is not considered in this study as design criteria per AC04. Table 4.1 shows that the experimental ultimate jacking load was 286.35, 286.50 and 344.64 kN for walls W4, W5 and W6, respectively. As per AC-04, the ultimate factored design axial resisting compressive load is the experimental ultimate load divided by 2.5. Thus, the factored design axial resisting load is 114.54, 114.50 and 127.86 kN for walls W4, W5 and W6, respectively. Since the obtained design values for each walls is within 15% difference with the average value of the three panels, the design factored axial compressive load for Group B is 122.30 kN. This value will be farther be used to examine the axial force-moment interaction for this wall group. One may observe that the design resisting axial compressive load for Group B with lumber spline connection is 1.6%

less than that for Group A with foam-spline connection. Thus, it can be concluded that the presence of lumber studs at the joint between wall panels has insignificant effect of the load carrying capacity.

4.5 Group C

In this group, three identical panels were tested to complete collapse under uniformly distributed axial compression load with $t/6$ eccentricity. Each panel was of 9 feet height, 4 feet wide and 6.5 inch thick, with foam-spline connection. Figure 4.42 shows view of panel W7 before testing, while Figs. 4.45 through 4.47 show views of the permanent deformed shape of the panel after failure as well as close-up views of the local damage and deformation. It was observed that the failure mode in wall W7 was due to OSB facing crushing at one side of its top leading to global permanent lateral deformation of the panel as shown in Fig. 4.45. The failure was abrupt causing a sudden drop in the applied jacking load as depicted in the load-axial shortening relationship in Fig. 4.43. It was observed that linear elastic behaviour was maintained till failure.

Figure 4.47 shows view of panel W8 before testing, while Figs. 4.50 and 4.51 show views of the permanent deformed shape of the panel after failure as well as close-up views of the local damage and deformation in the OSB facing. Figure 4.48 depicts the load-axial shortening relationship for the model. It was observed that the failure mode of OSB crushing near the top part of the wall on one facing and tensile fracture on the other facing at the same location. Figure 4.52 shows view of panel W9 before testing, while Figs. 4.56 and 4.57 show views of the permanent deformed shape of the panel after failure as well as close-up views of the local

damage and deformation in the OSB facing. Figure 4.54 depicts the load-axial shortening relationship for the model. It was observed that the failure mode of OSB crushing occurred on one side of the panel near its top quarter point, associated with diagonal tensile fracture of the foam at the same location as shown in Fig. 4.56, as well as at the connection with the top wall stud as shown in Fig. 4.57.

Figures 4.44, 4.49, and 4.55 depict the jacking load-lateral deflection relationships for walls W7, W8 and W9, respectively. It can be observed that lateral deflection increase with increase in the applied load. This may be attributed to the lateral instability of the OSB facings as a result of the high flexibility of the foam in between. However lateral deflection is not considered in this study as design criteria per AC04. Table 4.1 shows that the experimental ultimate jacking load was 199.58, 172.36 and 268.23 kN for walls W7, W8 and W9, respectively. As per AC-04, the ultimate factored design axial resisting compressive load is the experimental ultimate load divided by 2.5. Thus, the factored design axial resisting load is 79.83, 68.94 and 107.29 kN for walls W7, W8 and W9, respectively. Since the obtained design values of two of the walls are more than 15% difference with the average value of the three panels, the design factored axial compressive load for Group A is 68.94 kN, as the least value of the three. Also, Table 4.1 shows that the jacking loads at $1/8''$ axial shortening were 91.72, 59.91 and 92.94 kN for walls W7, W8 and W9, respectively. Since the obtained design values of two of the walls are more than 15% difference with the average value of the three panels, the design factored axial compressive load per on the deflection criteria for Group C is 59.91 kN, as the least value of the three. To meet both the strength and deflection criteria, the factored resisting compressive load would be 59.91 kN for Group C. Comparing results for Group A with zero eccentricity and

Group C with $t/6$ eccentricity, it can be observed that the design resisting axial forces decreased by 52%.

4.6 Group D

In this group, three identical panels were tested to complete collapse under uniformly distributed axial concentric compression load. Each panel was of 10 feet height, 4 feet wide and 6.5 inch thick, with foam-spline connection. Figure 4.57 shows view of panel W10 before testing, while Figs. 4.60 through 4.62 show views of the permanent deformed shape of the panel after failure as well as close-up views of the local damage and deformation. It was observed that the failure mode in wall W10 was due to OSB facing crushing near the bottom end of wall on one facing in addition to OSB crushing along its connection with the bottom wall studs that led to global permanent lateral deformation of the panel as shown in Fig. 4.60. It should be noted that diagonal tensile fracture in the foam was observed at the same location of OSB failure as shown in Fig. 4.61. The failure was abrupt causing a sudden drop in the applied jacking load as depicted in the load-axial shortening relationship in Fig. 4.58. It was observed that linear elastic behaviour was maintained till failure.

Figure 4.63 shows view of panel W11 before testing, while Figs. 4.66 and 4.67 show views of the permanent deformed shape of the panel after failure as well as close-up views of the local damage and deformation in the OSB facing. Figure 4.64 depicts the load-axial shortening relationship for the model. It was observed that the failure mode of Wall W12 was identical to model W10. Figure 4.68 shows view of panel W12 before testing, while Figs. 4.71 and 4.72 show views of the permanent deformed shape of the panel after failure as well as close-up views

of the local damage and deformation in the OSB facing. Figure 4.69 depicts the load-axial shortening relationship for the model. It was observed that the failure mode was similar to that for Wall w10 expect that foam-OSB delamination occurred at the bottom of the wall, as shown in Fig. 4.72.

Figures 4.59, 4.65, and 4.70 depict the jacking load-lateral deflection relationships for walls W10, W11 and W12, respectively. It can be observed that lateral deflection increase with increase in the applied load. This may be attributed to the lateral instability of the OSB facings as a result of the high flexibility of the foam in between. However lateral deflection is not considered in this study as design criteria per AC04. Table 4.1 shows that the experimental ultimate jacking load was 221.70, 215.56 and 186.19 kN for walls W10, W11 and W12, respectively. As per AC-04, the ultimate factored design axial resisting compressive load is the experimental ultimate load divided by 2.5. Thus, the factored design axial resisting load is 88.68, 86.22 and 74.48 kN for walls W10, W11 and W12, respectively. Since the obtained design value for each wall is within 15% difference with the average value of the three panels, the design factored axial compressive load for Group D is 83.13 kN. This value will be farther be used to examine the axial force-moment interaction for this wall group.

4.7 Group E

In this group, three identical panels were tested to complete collapse under uniformly distributed axial concentric compression load. Each panel was of 12 feet height, 4 feet wide and 6.5 inch thick, with foam-spline connection. Figure 4.73 shows view of panel W13 before testing, while Figs. 4.76 through 4.78 show views of the permanent deformed shape of the panel after failure as well as close-up views of the local damage and deformation. It was observed that the failure mode in wall W13 was due to OSB facing crushing near and at the top part of the wall

panel in addition to foam-OSB splitting as shown in Fig. 4.77. The failure was abrupt causing a sudden drop in the applied jacking load as depicted in the load-axial shortening relationship in Fig. 4.74. It was observed that linear elastic behaviour was maintained till failure.

Figure 4.79 shows view of panel W14 before testing, while Figs. 4.82 through 4.84 show views of the permanent deformed shape of the panel after failure as well as close-up views of the local damage and deformation in the OSB facing. Figure 4.80 depicts the load-axial shortening relationship for the model. It was observed that the failure mode was similar to that for wall W13 but at the bottom end of the wall. Figure 4.85 shows view of panel W15 before testing, while Figs. 4.88 through 4.91 show views of the permanent deformed shape of the panel after failure as well as close-up views of the local damage and deformation in the OSB facing. Figure 4.86 depicts the load-axial shortening relationship for the model. It was observed that the failure mode of wall W15 was similar to that for wall W14. Figures 4.75, 4.81, and 4.87 depict the jacking load-lateral deflection relationships for walls W13, W14 and W15, respectively. It can be observed that lateral deflection increase with increase in the applied load. This may be attributed to the lateral instability of the OSB facings as a result of the high flexibility of the foam in between. However lateral deflection is not considered in this study as design criteria per AC04. Table 4.1 shows that the experimental ultimate jacking load was 259.35, 217.34 and 218.30 kN for walls W13, W14 and W15, respectively. As per AC-04, the ultimate factored design axial resisting compressive load is the experimental ultimate load divided by 2.5. Thus, the factored design axial resisting load is 103.74, 86.94 and 87.32 kN for walls W13, W14 and W15, respectively. Since the obtained design values for each walls is within 15% difference with the average value of the three panels, the design factored axial compressive load for Group E is

92.66. kN. This value will be further be used to examine the axial force-moment interaction for this wall group.

4.8 Group F

In this group, three identical panels were tested to complete collapse under uniformly distributed axial concentric compression load. Each panel was of 16 feet height, 4 feet wide and 6.5 inch thick, with foam-spline connection. Figure 4.92 shows view of panel W16 before testing, while Figs. 4.94 and 4.95 show views of the permanent deformed shape of the panel after failure as well as close-up views of the local damage and deformation. It was observed that the failure mode in wall W16 was due to OSB facing crushing near the top quarter point on one side of the panel and tensile fracture on the OSB on the other side of the wall at the same location. Diagonal tensile fracture in the foam between the top quarter point and the top end of the wall was observed as shown in Fig. 4.95. It should be noted that local OSB crushing along its connection with the top wall stud was observed. Figure 4.96 shows view of panel W17 before testing, while Figs. 4.99 through 4.101 show views of the permanent deformed shape of the panel after failure as well as close-up views of the local damage and deformation in the OSB facing. Figure 4.97 depicts the load-axial shortening relationship for the model. It was observed that the failure mode of OSB crushing between the mid-height and bottom quarter point of the wall, associated with OSB-foam splitting and diagonal tensile fracture on the foam as shown in Fig. 4.99. Figure 4.102 shows view of panel W18 before testing, while Figs. 4.105 through 4.107 show views of the permanent deformed shape of the panel after failure as well as close-up views of the local damage and deformation in the OSB facing. Figure 4.103 depicts the load-axial shortening relationship for the model. It was observed that the failure mode of OSB crushing

occurred on one side of the panel near its bottom end as well as at OSB connection with the bottom wall stud. This led to foam-OSB splitting on one side of the wall at the failure location as shown in Fig. 4.106.

Figures 4.93, 4.98, and 4.104 depict the jacking load-lateral deflection relationships for walls W16, W17 and W18, respectively. It can be observed that lateral deflection increase with increase in the applied load. This may be attributed to the lateral instability of the OSB facings as a result of the high flexibility of the foam in between. However lateral deflection is not considered in this study as design criteria per AC04. Table 4.1 shows that the experimental ultimate jacking load was 209.64, 145.14 and 119.91 kN for walls W16, W17 and W18, respectively. As per AC-04, the ultimate factored design axial resisting compressive load is the experimental ultimate load divided by 2.5. Thus, the factored design axial resisting load is 83.86, 58.06 and 47.97 kN for walls W16, W17 and W18, respectively. Since the obtained design values for walls are more 15% difference with the average value of the three panels, the design factored axial compressive load for Group F is 47.97 kN, as the least one of the three values. This value will be farther be used to examine the axial force-moment interaction for this wall group.

4.9 Group G

In this group, as two panels have been added two the originally three panels, five identical panels were tested to complete collapse under flexure load. Each panel was of 9 feet height, 4 feet wide and 6.5 inch thick. The thickness of the sheathing (OSB) is 7/16 inch for each of the two sides facings. Figure 4.108 shows view of panel WS19 before testing, while Fig. 4.110 shows view of the permanent deformed shape of the panel after failure. The failure mode

was due to horizontal shear failure at the interface between the foam and top OSB facing. The failure was between the top surface of the foam and the adhesive over a panel length between the support and the quarter-point line, causing top foam-OSB delamination (debonding) over the supports. Shear failure was sudden causing a sudden drop in the applied jacking load as depicted in the load-deflection history shown in Fig. 4.109. Figure 4.111 and 4.112 shows a close-up view of this type of failure. It has been noted that noise was heard when approaching failure load and the shear failure was abrupt causing a sudden drop in the applied jacking load as depicted in the load-deflection results shown in Figure 4.109. It was observed that the LVDT readings at each side of the panel correlate well. It was observed that linear elastic behaviour was maintained at the live load level (i.e. serviceability limit state) and even at the design factored load level (i.e. ultimate limit state).

Similar behavior of WS19 was observed for walls WS20 through WS23 of the same size. Figures 4.113, 4.118, 4.123 show view of panel WS20, WS21, and WS22, respectively, before testing. Figures 4.115 through 4.117 show views of the permanent deformed shape of the panel after failure and close-up views of the OSB-foam splitting, While Fig. 4.114 depicts the jacking load-deflection relationship for wall WS20. Figures 4.120 through 4.122 show views of the permanent deformed shape of the panel after failure and close-up views of the OSB-foam splitting, While Fig. 4.119 depicts the jacking load-deflection relationship for wall WS21. Figures 4.125 through 4.127 show views of the permanent deformed shape of the panel after failure and close-up views of the OSB-foam splitting, While Fig. 4.124 depicts the jacking load-deflection relationship for wall WS22. Figures 4.129 through 4.131 show views of the permanent deformed shape of the panel after failure and close-up views of the OSB-foam splitting, While Fig. 4.128 depicts the jacking load-deflection relationship for wall WS23.

Table 4.2 shows a summary of panel configurations along with the ultimate jacking load for Group G. It can be observed that the ultimate jacking load was 27.22, 27.77, 24.99, 28.77 and 26.77 kN for panels WS19, WS20, WS21, WS22 and WS23, respectively. Conservatively, the jacking load did not include the weight of the loading system of 2 kN. It is worth mentioning that the ultimate jacking load for each panel is within 15% difference from the average jacking load of the three panels. Thus, the design ultimate jacking load is taken as the average experimental ultimate jacking load divided by a factor of safety of 3 (i.e. $27.10 / 3 = 9.03$ kN). This makes the design ultimate bending moment resistance as 2.93 kN.m for 1.2 m panel width.

4.10 Group H

In this group, three identical panels were tested to complete collapse under flexure load. Each panel was a foam-spline-connected walls with 12 feet height, 4 feet wide and 6.5 inch thick. The thickness of the sheathing (OSB) is 7/16 inch for each of the two sides facings. Figure 4.132 shows view of panel WS24 before testing, while Fig. 4.134 shows view of the permanent deformed shape of the panel after failure. The failure was due to diagonal shear crack at approximately mid-length between the support and the quarter point, continued with delamination between OSB facings and the foam core towards support as well as the quarter point. Shear failure was sudden causing a sudden drop in the applied jacking load as depicted in the load-deflection history. Figures 4.135 and 4.136 show a close-up view of this type of failure. It has been noted that noise was heard when approaching failure load and the shear failure was abrupt causing a sudden drop in the applied jacking load as depicted in the load-deflection results shown in Figure 4.133. Similar behavior of WS24 was observed for walls WS25 through WS26 of the same size. Figures 4.137 and 4.142 show view of panel WS25, and WS26, respectively,

before testing. Figures 4.139 through 4.144 show views of the permanent deformed shape of the panel after failure and close-up views of the OSB-foam splitting, While Figs. 4.138 and 4.143 depict the jacking load-deflection relationship for walls WS25 and WS26, respectively. Figures 4.140 and 4.141 show views of the permanent deformed shape of the panel after failure and close-up views of the OSB-foam splitting. Figures 4.145 through 4.146 show close-up views of the OSB-foam splitting at the support locations.

Table 4.2 shows a summary of panel configurations along with the ultimate jacking load for walls Group H. It can be observed that the ultimate jacking load was 26.99, 28.55 and 27.99 kN for panels WS24, WS25 and WS26, respectively. Conservatively, the jacking load did not include the weight of the loading system of 2 kN. It is worth mentioning that the ultimate jacking load for each panel is within 15% difference from the average jacking load of the three panels. Thus, the design ultimate jacking load is taken as the average experimental ultimate jacking load divided by a factor of safety of 3 (i.e. $27.84 / 3 = 9.28$ kN). This makes the design ultimate bending moment resistance as 4.07 kN.m for 1.2 m panel width.

4.11 Group I

In this group, three identical panels were tested to complete collapse under uniformly distributed axial concentric compression load. Each panel was lumber-spline-connected foundation wall with 9 feet height, 4 feet wide and 8.25 inch thick. The interior facing was made of OSB sheet with 7/16 inch thickness, while the exterior facing was made of 5/8" thick pressure-treated plywood. Figure 4.147 shows view of wall panel W27 before testing, while Figs. 4.149 through 4.151 shows view of the permanent deformed shape of the panel after failure

as well as close-up views of local failure in the facings. It was observed that the failure mode the panels of group I, was due to plywood crushing near and at the top end of the wall. It should be noted that noise was heard when approaching failure load and the failure was abrupt causing a sudden drop in the applied jacking load as depicted in the load-lateral deflection results shown in Fig. 4.148.

Figure 4.152 shows view of wall panel W28 before testing, while Figs. 4.155 and 4.156 shows view of the permanent deformed shape of the panel after failure as well as close-up views of local failure in the facings. It was observed that the failure mode wall W28 was due to plywood as well as OSB crushing at the bottom end of the wall. It should be noted that noise was heard when approaching failure load and the failure was abrupt causing a sudden drop in the applied jacking load as depicted in the load-axial shortening relationship shown in Fig. 4.153. Figure 4.154 shows view of the jacking load-lateral deflection relationship of wall W28. Figure 4.157 shows view of wall panel W29 before testing, while Figs. 4.160, 4.161 and 4.162 shows view of the permanent deformed shape of the panel after failure as well as close-up views of local failure in the facings. It was observed that the failure mode wall W29 included crushing of plywood facing at the bottom end of the wall as shown in Fig. 4.160 and crushing of OSB facing at the top quarter point and near the top of the wall as shown in Figs. 4.161 and 4.162, respectively. It should be noted that noise was heard when approaching failure and the failure was abrupt. Figures 4.158 and 4.159 depict the load-axial shortening relationship and the load-lateral deflection relationship for wall W29.

Table 4.3 shows a summary of panel configurations along with the ultimate jacking load for walls Group I. It can be observed that the ultimate jacking load was 355.81, 317.94 and

408.26 kN for panels W27, W28 and W29, respectively. It is worth mentioning that the ultimate jacking load for each panel is within 15% difference from the average jacking load of the three panels. Thus, the design ultimate jacking load is taken as the average experimental ultimate jacking load divided by a factor of safety of 2.5 (i.e. 144.23 kN as shown in Table 4.3).

4.12 Group J

In this group, three identical panels similar to the wall foundation in Group I were tested to complete collapse under flexure load. Figure 4.163 shows view of panel WS30 before testing, while Fig. 4.164 shows view of the permanent deformed shape of the panel after failure. The failure was due to diagonal shear crack at the support as shown in Fig. 4.166. Shear failure was sudden causing a sudden drop in the applied jacking load as depicted in the load-deflection history shown in Fig. 4.165. Figure 4.167 shows view of panel WS31 before testing, while Fig. 4.168 shows view of the permanent deformed shape of the panel after failure. The failure was due to horizontal shear failure between the foam and the top plywood facing at the support as shown in Figs. 4.170 and 4.171. Shear failure was sudden causing a sudden drop in the applied jacking load as depicted in the load-deflection history shown in Fig. 4.169. Figure 4.172 shows view of panel WS32 before testing, while Fig. 4.173 shows view of the permanent deformed shape of the panel after failure. The failure was due to diagonal shear crack in the foam between the support and the quarter point on one free edge of the panel as shown in Fig. 4.175 and due to horizontal shear between the plywood top facing and the foam on the other free edge of the panel as shown in Fig. 4.176. Shear failure was sudden causing a sudden drop in the applied jacking load as depicted in the load-deflection history shown in Fig. 4.174.

Table 4.4 shows a summary of panel configurations along with the ultimate jacking load for panel Group J. It can be observed that the ultimate jacking load was 51.54, 49.77 and 51.10 kN for panels WS30, WS31 and WS32, respectively. It is worth mentioning that the ultimate jacking load for each panel is within 15% difference from the average jacking load of the three panels. Thus, the design ultimate jacking load is taken as the average experimental ultimate jacking load divided by a factor of safety of 3 (i.e. $50.80 / 3 = 16.93$ kN). This makes the design ultimate bending moment resistance as 5.48 kN.m for 1.2 m panel width.

4.13 Design Table for SIP wall under axial compressive load

As shown in Table 4.1, Wall Group C is the only group that was tested under $t/6$ eccentricity. As such, manual calculations were performed to determine the maximum served joist span by the wall. As mentioned earlier, the design factored axial compressive load obtained experimentally was 59.91 kN. By dividing this load over 1.2 m width of the tested wall, the factored uniform load over the wall would be 49.93 kN. Three building configurations are considered herein, namely: (i) a wall carrying single flat roof, (ii) a wall carrying a flat roof and a floor; and (iii) a wall carrying a flat roof and two floors. For the first case, the factored combined load would be $1.25D$ and $1.5S$, where D and S are dead load and snow load on the roof, respectively. Assuming that D is 0.5 kPa for the roof and 0.4 kPa for the wall, the served joist span is calculated as 22.9, 16.9, 13.4, 11.1 and 9.5 m for specified snow load of 1.0, 1.5, 2.0, 2.5 and 3.0 kPa. Results are listed in Table 4.5. In case of a wall carrying a roof and a floor, two load combinations were considered as follows:

Case (1): $1.25D + 0.5S$ for the roof and $1.25D + 1.5L$ for the floor, where L is the floor live load.

Case (2): $1.25D + 1.5S$ for the roof and $1.25D + 0.5L$ for the floor, where L is the floor live load.

Considering the floor live load in residential construction as 1.9 kPa, the served span for the first and second load combination cases are 10.3, 9.72, 9.3, 8.8 and 8.43 for case (1) and 12.75, 10.6, 9.1, 7.9 and 7.0 for case (2). The smaller served span for each snow load is then listed in Table 4.5. Similar procedure was performed for the wall case carrying a roof and two floors, leading to served joist spans of 5.7, 5.5, 5.3, 5.2, and 5.0 m for snow loads of 1.0, 1.5, 2.0, 2.5 and 3.0 kPa, respectively. Final results are reported in Table 4.5.

4.14 Design Table for SIP wall under combined axial compressive load and wind load

Clause 5.5.10 of CAN/CSA-O86-01 stated that members subjected to combined bending and compressive axial loads shall be designed to satisfy the following interaction equation:

$$\frac{P_f}{P_r} + \frac{M_f}{M_r} \leq 1 \quad (4.1)$$

Where P_f = factored compressive axial load; P_r = factored compressive load resistance; M_f = factored bending moment, taking into account end moments and amplified moments due to axial loads in laterally loaded members; M_r = factored bending moment resistance.

Table 4.6 provides the factored compressive axial resisting load and factored resisting moment as obtained experimentally for the 9', 10' and 12' walls. For a specified wind load in a given area in Canada, the factored applied axial compressive load can be then obtained from equation 4.1, from which the maximum roof or floor joist span served by this wall can be easily obtained. Special attention must be given to the effects of the following on the interaction equation:

- (i) The P- Δ effect since the axial load would be eccentric as a result of lateral deflection of the wall due to lateral loading.
- (ii) When the compressive axial load is not applied in the centre of the vertical axis of the wall, the eccentricity will create a bending moment on the column.

4.15 Design Table for SIP foundation wall under combined axial compressive load and soil pressure

Clause A5.5.12.6 of CAN/CSA-O86-01 stated that members subjected to combined bending and compressive axial loads shall be designed to satisfy the following interaction equation:

$$\left(\frac{M_f + P_f \Delta}{M_r} \right) + \left(\frac{P_f}{P_r} \right)^2 \leq 1 \quad (4.2)$$

Where P_f = factored compressive axial load; P_r = factored compressive load resistance; M_f = factored bending moment due to soil pressure; M_r = factored bending moment resistance.

Table 4.7 provides the factored compressive axial resisting load and factored resisting moment as obtained experimentally for the 9' PWF wall. For a specified soil pressure of 4.7 kPa, the factored applied axial compressive load can be then obtained from equation 4.2, from which the maximum floor joist span served by this wall can be easily obtained. Special attention must be given to the effects of the following on the interaction equation:

- When the compressive axial load is not applied in the centre of the vertical axis of the wall, the eccentricity will create a bending moment on the column.

CHAPTER V

CONCLUSIONS

5.1 General

A literature review was conducted in order to establish the foundation of the research program which includes an extensive experimental program to investigate the static structural behavior of insulated sandwich timber panels under axial concentric loading and axial eccentric loading. The experimental program included testing to-collapse 32 actual-size timber panels according to the ASTM standards. The structural adequacy of the tested sandwich panels for possible use in residential construction was presented, based on an assessment for the experimental results with respect to code requirements for ultimate and serviceability limit states design of such panels.

5.2 CONCLUSIONS

Based on the experimental findings, the following conclusions can be drawn:

- 1- The dominant failure mode in panels with foam-spline connection under axial concentric or eccentric uniform load is due to crushing of the panel facing at two main locations that let to lateral permanent deformation of the wall panel after failure. These locations are (i) the connection between the OSB or plywood facings with the top or bottom stud plates; (ii) the quarter point area of the wall height. In some failure cases, shear debonding between the foam and OSB facing was observed. Moreover, some panels exhibited diagonal crack in the foam associated with OSB crushing.

- 2- Panel Groups A and B showed that the presence of lumber-spline connection rather than the foam-spline connection has insignificant effect of the structural response and the load carrying capacity of the wall panels.
- 3- The dominant failure mode in panels under flexural load is due to the horizontal shear failure at one of the two areas of the panel end-quarters. When the panel span increases, The diagonal shear failure, at one of the two areas of the panel end-quarters, started to be the dominant failure mode.
- 4- Based on the data generated from testing panel group C of 9'x4'x6 1/2" size, a design table was developed to provide designers with the maximum served joist span when this wall size is used in residential building. Three types of building sizes were considered, namely: (i) wall supporting single roof, (ii) wall supporting a roof and a floor; and (iii) wall supporting a roof and two floors.
- 5- Similar design information was established for walls subjected to both axial compressive loading and wind loading as well as basement walls subjected to both axial compressive loading and soil pressure.
- 6- Testing of preserved SIPs for basement foundation showed that failure always occur at the junction between the plywood facing and the wall end that had the single timber plate with one row of nails rather than the end that had two timber plates with two rows of nails. Thus, it is recommended to use two timber plates with two rows of nails at each wall end to better transfer the axial compressive force in the facing to the end plates. This modification would certainly increase the load carrying capacity of the basement wall.

5.3 RECOMMENDATIONS FOR FUTURE RESEARCH

- 1- Study the ultimate capacity and serviceability of SIPs under impact loading.
- 2- Develop empirical expressions for the ultimate load carrying capacity for various SIP sizes based on finite-element modeling for the tested panels.
- 3- Study the structural response of SIPs under racking loading.

4- Study the flexural creep response of basement walls made of SIPs under sustained soil pressure.

CONCLUSION

5.1 INTRODUCTION

The objective of this study is to investigate the flexural creep response of basement walls made of SIPs under sustained soil pressure. The study is divided into two main parts: experimental and analytical. In the experimental part, a series of tests were conducted on SIP walls under sustained soil pressure. The results show that the walls exhibit significant flexural creep over time, which is influenced by the soil pressure and the properties of the SIP material. In the analytical part, a finite element analysis (FEA) was performed to simulate the behavior of the walls under sustained soil pressure. The FEA results show that the walls exhibit a similar flexural creep response to the experimental results, indicating that the FEA model is capable of accurately predicting the behavior of SIP walls under sustained soil pressure.

5.2 CONCLUSION

The study concludes that the flexural creep response of basement walls made of SIPs under sustained soil pressure is significantly influenced by the soil pressure and the properties of the SIP material. The FEA model is capable of accurately predicting the behavior of SIP walls under sustained soil pressure, which can be used to design and analyze SIP walls in practice. The study also highlights the need for further research on the flexural creep response of SIP walls under sustained soil pressure, particularly in the area of material properties and boundary conditions.

REFERENCES

- APA. 1993. Design and Fabrication of Plywood Sandwich Panels. APA – The Engineering Wood Association, Tacoma, WA, USA.
- Allen, H. G. 1969. Analysis and Design of Structural Sandwich Panels. Pergaman Press.
- ASTM. 2002. Standard Test Methods of Conducting Strength Tests of Panels for Building Construction, ASTM E72-02. American Society for Testing Materials, Philadelphia, PA, USA.
- ASTM. 1988. Standard Test Methods of for Flexural Creep of Sandwich Construction. ASTM C 480-62. American Society for Testing Materials, Philadelphia, PA, USA.
- Aviles, F. and Carlsson, L. 2006. Experimental Study of Debonded Sandwich Panels under Compressive loading. Journal of Sandwich Structures and Materials- 8: 7-31.
- Bau-Madsen, N. K., Svendsen, K. H. and Kildegaard, A. 1993. Large deflection of sandwich Plates – an experimental investigation- Composite Structures, Vol. 23, No.1, pp. 47-52.
- Butt, Aleem. Experimental Study on the flexural behaviour of structural insulated sandwich timber panels. M.A.SC. Thesis, Civil Engineering Department, Ryerson University, Toronto, ON, Canada.
- Canadian Standard Association. 1992. Construction of Preserved Wood Foundation, CAN/CSA-S406-92. Etobicoke, Ontario, Canada.
- Canadian Standard Association. 1997. Permanent Wood Foundation. Etobicoke, Ontario, Canada.
- Canadian Standard Association. 2001. Engineering Design of Wood. (CSA-086-01), Etobicoke, Ontario, Canada.

Canadian Wood Council-(2005). Wood Design Manual 2005. Ottawa, Canada

Chong, K. P. 1986. Sandwich panels with cold-formed thin facings. Proc. IABSE Colloquium: Thin-walled Metal Structures in Buildings. Stockholm, pp. 339-348.

Chong, K.P. and Hartsock 1993. Structural Analysis and Design of Sandwich Panels with Cold-Formed Steel Facings. Thin-Walled Structures, Vol. 16, pp.199-218.

Cox, H. and Riddell, J. 1945. Sandwich construction and core materials, Part 3. Instability of sandwich struts and beams, A.R.C., R & M 2125.

Davies, J. M. 1987. Axially loaded sandwich panels. ASCE, J. Struct. Engng. 113: (11), 2212-2230.

Davies, J. M. 1986. The analysis of sandwich panels with profiled faces. Proc. Eighth Int. Speciality Conf. on Cold-Formed Steel Struct, St Louis, November, pp. 351-369.

Davies, J. M., Hakmi, M.R. and Hassinen, P. 1991. Face Buckling Stress in Sandwich Panels. Nordic Conference Steel Colloquium, pp. 99-110.

Davies, J. M. and Hakmi 1992. Postbuckling Behaviour of Foam-Filled Thin-Walled Steel Beams. Journal of Constructional Steel Research, Vol. 20, pp.75-83.

Eringen, A. C. 1951. Bending and buckling of rectangular sandwich plates, proc. 1st U.S. Nat. Cong. App. Mech. 1951, pp. 381-90.

Goodier, J. 1946. Cylindrical buckling of sandwich plates, J. App. Mech. 13, 4, Dec., pp.253-260.

Goodier, J. and I. M. Neou, I. 1951. The evaluation of theoretical critical compression in sandwich plates, J. Aero. Sci. 18, 10, Oct. pp. 649-657.

Gibson, L. and Ashby, M. 1988. Cellular Solids Structure and Properties. , Pergaman Press.

- Gough, G., Elam, C., and De Bruyne, N. 1940. The stabilization of a thin sheet by a continuous supporting medium, *J. Roy. Aero. Soc.* 44, 349, Jan., pp. 12-43.
- Heath, W. G. 1960. Sandwich construction: Correlation and extension of existing theory of flat panels subjected to lengthwise compression, *Aircraft Engg.* 32, 377 and 378, July and Aug. 1960, pp. 186-91 and 230-5.
- Hemp, W. S. 1948. On a theory of sandwich construction, *A.R.C., R & M 2672*, Mar.
- Hoff, N. and Mautner, S. 1945. Buckling of sandwich-type panels, *J. Aero. Sci.* 121, 3, July, pp. 285-297.
- ICC AC04-(2004). Acceptance Criteria for Sandwich Panels. ICC Evaluation Service Inc., USA.
- Institute for Research in Construction-2005. National Building Code of Canada, NBCC-2005. National Research Council, Ottawa, Ontario, Canada.
- Institute for Research in Construction. 2007. Technical Guide for Stressed Skin Panels (with lumber 1200 mm o.c. and EPS Core) for Walls and Roofs. National Research Council, Ottawa, Ontario, Canada.
- Jungbluth, O. & Berner, IC, *Verbund-und Sandwichtragwerke*. (Composite and sandwich structures.) Springer-Verlag, Berlin, 1986 (in German).
- Kuhhorn, A. 1991. Geometrisch nichtlineare Theorie für Sandwichschalen unter Einbeziehung des Knitterphänomens. *VDI-Verlag*, Reihe 18, no. 100.
- Kuhhorn, A. 1993. Nichtlineare Theorie und finites Element für Sandwichtragwerke zur Beschreibung des globalen und lokalen (Knittern) Versagens. *ZAMM Z. Angew. Math. Mech.* 73 4-5, pp. T438-T443.
- Kuhhorn, A. and Schoop, H. 1992. A nonlinear theory for sandwich shells including the wrinkling phenomenon. *Arch. Appl. Mech.* 62, pp. 413-427.

Mahendran and Jeevahan (1999), Local buckling behaviour of steel plate elements supported by plastic foam material. *Structural Engineering and Mechanics*, Vol. 7, No. 5, pp. 433-445.

Mindlin, R. 1951. Influence of rotatory inertia and shear on flexural vibrations of isotropic, elastic plates. *J. Appl. Mech.* 18, pp. 31-38.

Plantema, F.J., 1966. *Sandwich Construction*. John Wiley and Sons, New York.

Raville, M.E. 1955. Deflection and stresses in a uniformly loaded, simply supported, rectangular sandwich plate, FPL Report 1847, Dec.

Reissner, E. 1948. Finite deflections of sandwich plates, *J. Aero. Sci* 15, 7, July, pp.435-440.

Reissner, E., 1945. The effect of transverse shear deformation on the bending of plates. *J. Appl. Mech.* 12, pp. 69-77.

Schwartz, IC, *Numerische Methoden zur Berechnung von Sandwichelementen*. (Numerical methods for the calculation of sandwich elements.) *Der Stahlbau*, 12 (1984) (in German).

Sennah, K. and Butt, A. 2009. Structural Behavior of Insulated Sandwich Foam-Timber Panels under Sustained Loading for Roof Construction. *Proceedings of the International Conference on Sustainable Green Building Design and Construction*, Cairo, Egypt, pp. 1-11.

Sennah, K., Butt, A., and Taraba, E. 2008. Development of Structural Insulated Sandwich Timber Panels with Foam-Core Spline Connections for Roof Construction. *Proceedings, 6th Structural Specialty Conference*, Canadian Society for Civil Engineering, Quebec, pp. 1-10.

Sennah, K., Butt, A., and Taraba, E. 2008. Qualification of Structural Insulated Sandwich Panels with Lumber-Spline Connections for Floor Construction. *Proceedings of the 2nd Canadian Conference on Effective Design of Structures*, McMaster University, Hamilton, Ontario, pp. 1-10.

- Stamm, K. and Witte, H. 1974. Sandwichkonstruktionen—Berechnung, Fertigung, Ausführung. Springer, Wien.
- Structural Board Association. (2004). OSB Performance by Design Manual: Construction Sheathing and Design Rated Oriented Strand Board. Markham, Ontario, Canada.
- Thermapan Structural Insulated Panels Inc. 2007. www.thermapan.com.
- Thomsen, O. 1995. Theoretical and experimental investigation of local bending effects in sandwich plates. *Composite Structures*, 30: pp. 85–101.
- Triantafillou, T. and Gibson, L. 1987. Failure mode maps for foam core sandwich beams. *Materials Science and Engineering*, 95: pp. 37–53.
- Williams, D., Leggett, D. and Hopkins, H. 1941. Flat sandwich panels under compressive end loads, A.R.C., R & M 1987.
- Wolfel, E., Nachgiebiger Verbund: Eine Näherungslösung und deren Anwendungsmöglichkeiten. (Elastic bond: an approximate solution and its applications.) *Stahlbau*, 6 (1978) 173-80 (in German).
- Wiedemann, J. 1986. *Leichtbau: Band 1—Elemente*. , Springer, Berlin.
- Yoshii, A. 1992. Optimum design of advanced sandwich composite using foam core. *Advanced Composite Materials*, 2 (4), 289–305.
- Zenkert D., Hallstrom S., and Shipsha, A. 2002. Design Aspects of Marine Sandwich Structures, *Composites for Marine Structures*, 6 (8): pp. 28–32.
- Zenkert, D. 1997. *The Handbook of Sandwich Construction*, EMAS Publishing.

TABLES

Table 3.1 Thermapan SIPs Properties

SIP Thickness (Timber)	4.5"	6.5"	8.25"	10.25"	12.25"
EPS Core Thickness	3-5/8"	5-5/8"	7-3/8"	9-3/8"	11-3/8"
Dimensional Lumber	2x4	2x6	2x8	2x10	2x12
Weight (lbs/sq.ft.)	3.13	3.32	3.48	3.66	3.84
R-Value	19.147	29.147	37.897	47.897	57.897

Table 3.2. Panel configurations for axial compressive load tests

Group	Test No.	Test type	Panel size Length× Width× Thick.	Thickness of facings	Connection type
A	W1	Axial loading (zero eccentricity)	4×9×6 ½"	7/16"	Foam spline connection
	W2	Axial loading (zero eccentricity)	4×9×6 ½"	7/16"	Foam spline connection
	W3	Axial loading (zero eccentricity)	4×9×6 ½"	7/16"	Foam spline connection
B	W4	Axial loading (zero eccentricity)	4×9×6 ½"	7/16"	Lumber spline connection
	W5	Axial loading (zero eccentricity)	4×9×6 ½"	7/16"	Lumber spline connection
	W6	Axial loading (zero eccentricity)	4×9×6 ½"	7/16"	Lumber spline connection
C	W7	Axial loading (at t/6)	4×9×6 ½"	7/16"	Foam spline connection
	W8	Axial loading (at t/6)	4×9×6 ½"	7/16"	Foam spline connection
	W9	Axial loading (at t/6)	4×9×6 ½"	7/16"	Foam spline connection
D	W10	Axial loading (zero eccentricity)	4×10×6 ½"	7/16"	Foam spline connection
	W11	Axial loading (zero eccentricity)	4×10×6 ½"	7/16"	Foam spline connection
	W12	Axial loading (zero eccentricity)	4×10×6 ½"	7/16"	Foam spline connection
E	W13	Axial loading (zero eccentricity)	4×12×6 ½"	7/16"	Foam spline connection
	W14	Axial loading (zero eccentricity)	4×12×6 ½"	7/16"	Foam spline connection
	W15	Axial loading (zero eccentricity)	4×12×6 ½"	7/16"	Foam spline connection
F	W16	Axial loading (zero eccentricity)	4×16×6 ½"	7/16"	Foam spline connection
	W17	Axial loading (zero eccentricity)	4×16×6 ½"	7/16"	Foam spline connection
	W18	Axial loading (zero eccentricity)	4×16×6 ½"	7/16"	Foam spline connection

Table 3.3. Panel configurations for flexure

Group	Test No.	Test type	Panel size Length× Width × Thick. of foam	Thickness of facings	Connection type
G	WS19	Flexural loading	4×9×6 ½"	7/16"	Foam spline connection
	WS20	Flexural loading	4×9×6 ½"	7/16"	Foam spline connection
	WS21	Flexural loading	4×9×6 ½"	7/16"	Foam spline connection
	WS22	Flexural loading	4×9×6 ½"	7/16"	Foam spline connection
	WS23	Flexural loading	4×9×6 ½"	7/16"	Foam spline connection
H	WS24	Flexural loading	4×12×6 ½"	7/16"	Foam spline connection
	WS25	Flexural loading	4×12×6 ½"	7/16"	Foam spline connection
	WS26	Flexural loading	4×12×6 ½"	7/16"	Foam spline connection

Table 3.4. Panel configurations for axial compressive load tests for basement construction

Group	Test No.	Test type	Panel size Length× Width× Thick.	Thickness of facings	Connection type
I	W27	Axial loading (zero eccentricity)	4×9×8 ¼"	7/16"-5/8"*	Lumber spline connection
	W28	Axial loading (zero eccentricity)	4×9×8 ¼"	7/16"-5/8"*	Lumber spline connection
	W29	Axial loading (zero eccentricity)	4×9×8 ¼"	7/16"-5/8"*	Lumber spline connection

* The 7/16" (11 mm) interior facing is made of OSB sheets and the 5/8" (15.5 mm) exterior facing is made of Canadian softwood plywood.

Table 3.5. Panel configurations for flexure tests for basement construction

Group	Test No.	Test type	Panel size Length× Width × Thick. of foam	Thickness of facings	Connection type
J	WS30	Flexural loading	4×9×8 ¼"	7/16"-5/8"*	Lumber spline connection
	WS31	Flexural loading	4×9×8 ¼"	7/16"-5/8"*	Lumber spline connection
	WS32	Flexural loading	4×9×8 ¼"	7/16"-5/8"*	Lumber spline connection

* The 7/16" (11 mm) interior facing is made of OSB sheets and the 5/8" (15.5 mm) exterior facing is made of Canadian softwood plywood.

Table 4.1 Results from axial compressive load tests

Group	Test No.	Test type	Panel size Length× Width × Thick.	Connection type	Experim. Ultimate jacking load (kN)	Design ultimate jacking load (kN)	J a s I
A	W1	Axial loading (zero eccentricity)	4×9×6 ½"	Foam spline connection	324.97	130.00	-
	W2	Axial loading (zero eccentricity)	4×9×6 ½"	Foam spline connection	323.27	129.31	-
	W3	Axial loading (zero eccentricity)	4×9×6 ½"	Foam spline connection	283.84	113.54	-
B	W4	Axial loading (zero eccentricity)	4×9×6 ½"	Lumber spline connection	286.35	114.54	-
	W5	Axial loading (zero eccentricity)	4×9×6 ½"	Lumber spline connection	286.50	114.5	-
	W6	Axial loading (zero eccentricity)	4×9×6 ½"	Lumber spline connection	344.64	137.86	-
C	W7	Axial loading (at t/6)	4×9×6 ½"	Foam spline connection	199.58	79.83	9
	W8	Axial loading (at t/6)	4×9×6 ½"	Foam spline connection	172.36	68.94	5
	W9	Axial loading (at t/6)	4×9×6 ½"	Foam spline connection	268.23	107.29	9
D	W10	Axial loading (zero eccentricity)	4×10×6 ½"	Foam spline connection	221.70	88.68	-
	W11	Axial loading (zero eccentricity)	4×10×6 ½"	Foam spline connection	215.56	86.22	-
	W12	Axial loading (zero eccentricity)	4×10×6 ½"	Foam spline connection	186.19	74.48	-
E	W13	Axial loading (zero eccentricity)	4×12×6 ½"	Foam spline connection	259.35	103.74	-
	W14	Axial loading (zero eccentricity)	4×12×6 ½"	Foam spline connection	217.34	86.94	-
	W15	Axial loading (zero eccentricity)	4×12×6 ½"	Foam spline connection	218.30	87.32	-
F	W16	Axial loading (zero eccentricity)	4×16×6 ½"	Foam spline connection	209.64	83.86	-
	W17	Axial loading (zero eccentricity)	4×16×6 ½"	Foam spline connection	145.14	58.06	-
	W18	Axial loading (zero eccentricity)	4×16×6 ½"	Foam spline connection	119.91	47.97	-

Table 4.2 Results from flexural load tests

Group	Test No.	Test type	Panel size Length× Width × Thick. of foam	Connection type	Experim. Ultimate jacking load (kN)	Design ultimate jacking load (kN)	Design Ultimate moment (kN.m)
G	WS19	Flexural loading	4×9×6 ½"	Foam spline connection	27.22	9.03	2.93
	WS20	Flexural loading	4×9×6 ½"	Foam spline connection	27.77		
	WS21	Flexural loading	4×9×6 ½"	Foam spline connection	24.99		
	WS22	Flexural loading	4×9×6 ½"	Foam spline connection	28.77		
	WS23	Flexural loading	4×9×6 ½"	Foam spline connection	26.77		
H	WS24	Flexural loading	4×12×6 ½"	Foam spline connection	26.99	9.28	4.07
	WS25	Flexural loading	4×12×6 ½"	Foam spline connection	28.55		
	WS26	Flexural loading	4×12×6 ½"	Foam spline connection	27.99		

Table 4.3 Results from axial compressive load tests for basement construction

Group	Test No.	Test type	Panel size Length× Width × Thick. of foam	Connection type	Experim. Ultimate jacking load (kN)	Design ultimate jacking load (kN)
I	W27	Axial loading (zero eccentricity)	4×9×8 ¼" OBS / press-treated	Lumber spline connection	355.81	142.32
	W28	Axial loading (zero eccentricity)	4×9×8 ¼" OBS / press-treated	Lumber spline connection	317.94	127.18
	W29	Axial loading (zero eccentricity)	4×9×8 ¼" OBS / press-treated	Lumber spline connection	408.26	163.30

Table 4.4 Results from flexural load tests for basement construction

Group	Test No.	Test type	Panel size Length× Width × Thick. of foam	Comments	Experim. Ultimate jacking load (kN)	Design ultimate jacking load (kN)	Design Ultimate moment (kN.m)
J	WS30	Flexural loading	4×9×8 ¼" OBS / press-treated	Lumber spline connection	51.54	16.93	5.48
	WS31	Flexural loading	4×9×8 ¼" OBS / press-treated	Lumber spline connection	49.77		
	WS32	Flexural loading	4×9×8 ¼" OBS / press-treated	Lumber spline connection	51.10		

Table 4.5 Design table for SIP wall under axial compressive loading

Test type	Panel size Length× Width × Thick.	Design ultimate jacking load, kN	Design ultimate uniform load capacity = design load /1.2, kN/m	Building storeys	Maximum supported joist length ^{(1), (2)} , based on ultimate strength, m				
					Specified snow load, kPa				
					1.00	1.50	2.00	2.50	3.00
Axial loading (at t/6)	4×9×6 ½"	59.91	49.93	Roof only	22.9	16.9	13.4	11.1	9.5
				Roof and floor	10.3	9.7	9.1	7.9	7.0
				Roof and 2 floors	5.7	5.5	5.3	5.2	5.0

⁽¹⁾ Supported joist length means half the sum of the joist spans on both sides of the internal wall or half the joist span of the exterior wall.

⁽²⁾ Maximum supported length of roof is based on 0.5 kPa dead load, 1.9 kPa live load for floors and a specified snow load as shown on flat roofs. Wall (with siding, stucco) weight of 0.4 kPa is considered as dead load

Table 4.6 Design table for SIP wall under combined axial compressive load and bending moment

Panel size Length× Width × Thick.	Design ultimate jacking load, P _r (kN)	Design Ultimate Moment, M _r (kN.m)
4×9×6 ½"	124.30	2.93
4×10×6 ½"	83.13	4.54
4×12×6 ½"	92.66	4.07

Table 4.7 Design table for SIP wall under combined axial compressive load and bending moment

Panel size Length× Width × Thick.	Design ultimate jacking load, P _r (kN)	Design Ultimate Moment, M _r (kN.m)
4×9×8 ¼"	144.23	5.48

FIGURES

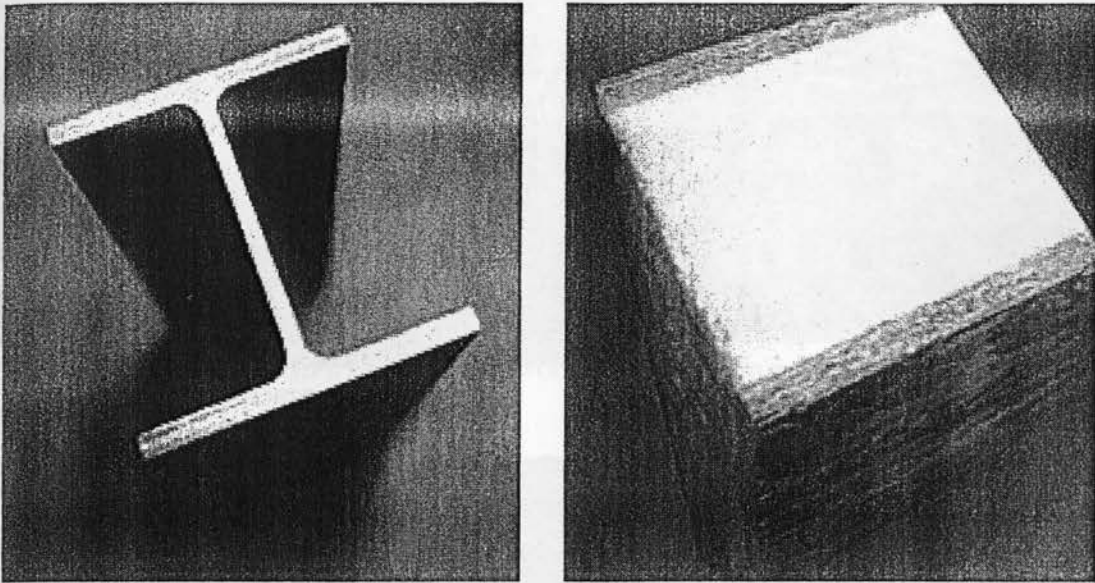


Figure 1.1. Comparison of SIP with I-beam section

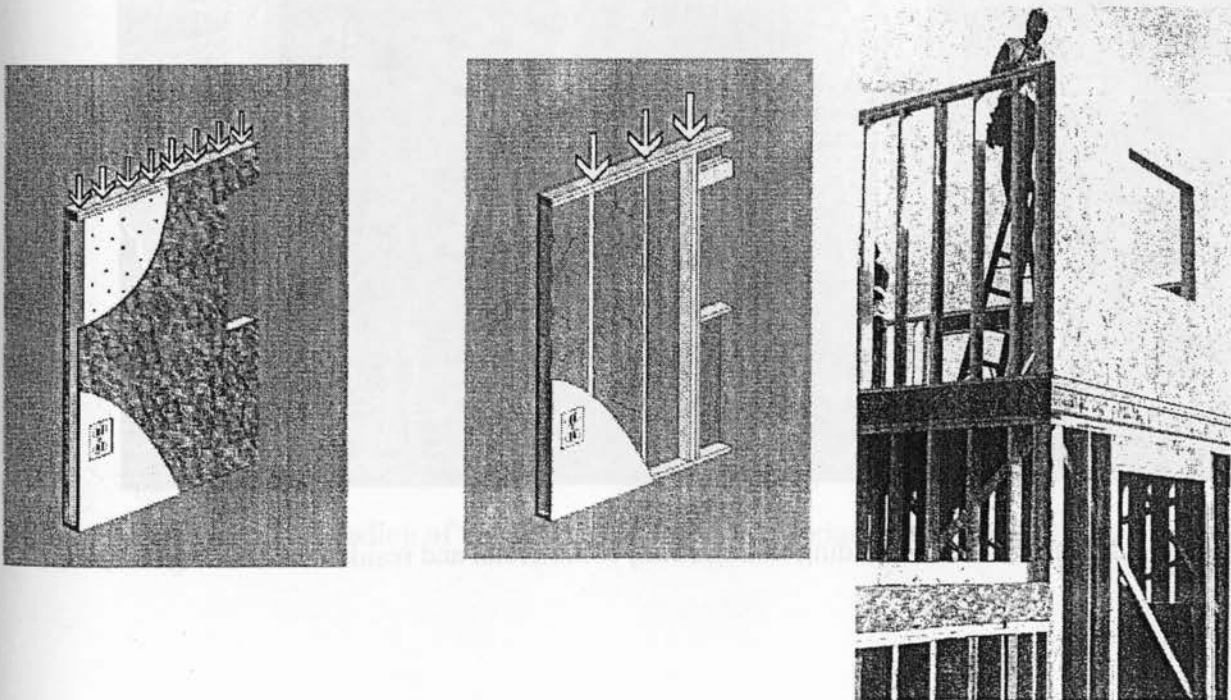
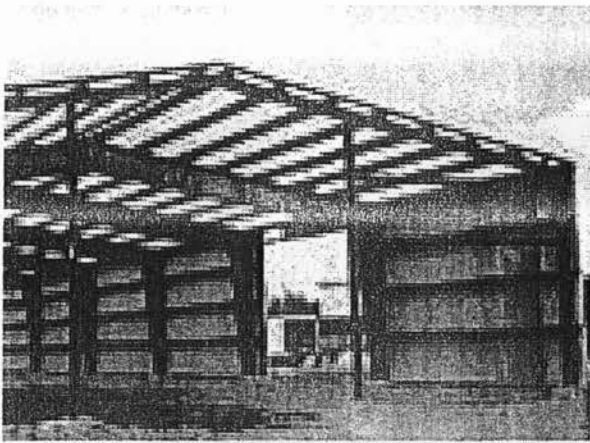


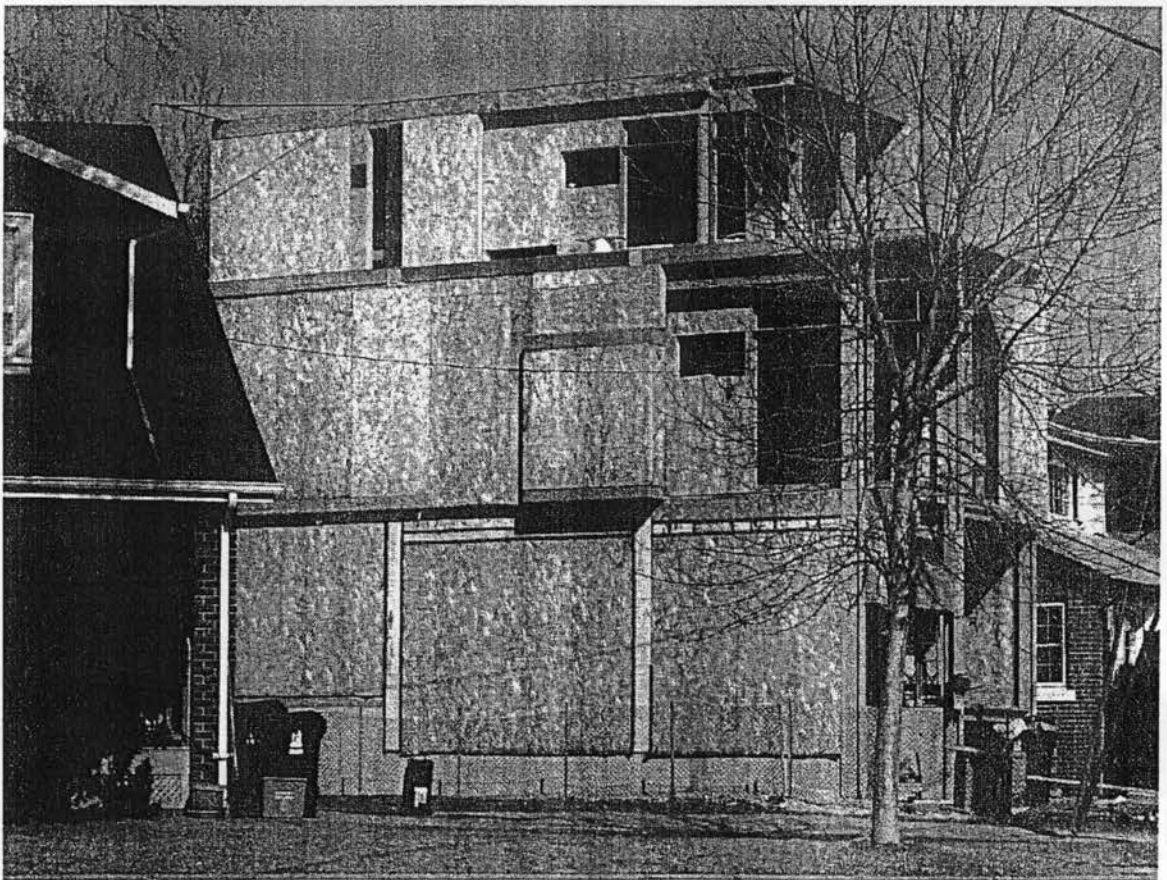
Figure 1.2. Comparison of SIP with stud wall system



(a) Industrial



(b) Commercial



(c) Residential

Figure 1.3. Use of SIPs as cladding in industrial, commercial and residential buildings

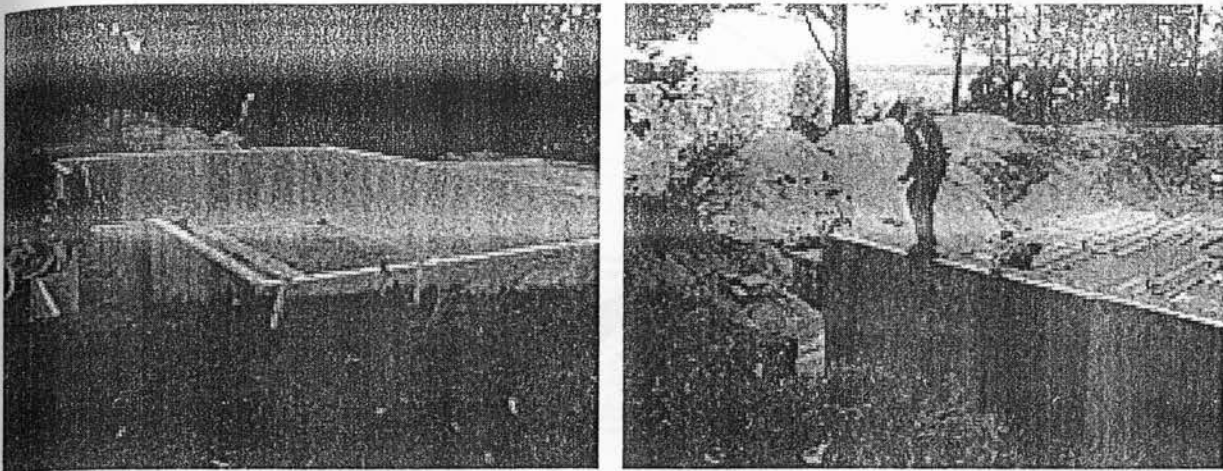


Figure 1.4. Use of SIPs as preserved wood foundation in residential construction

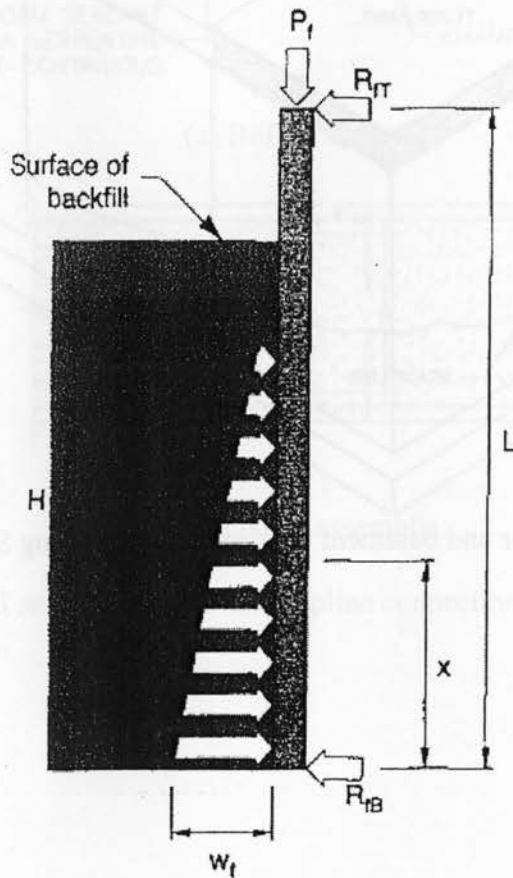


Figure 2.1 Loading of the permanent wood foundation (CWC, 2005)

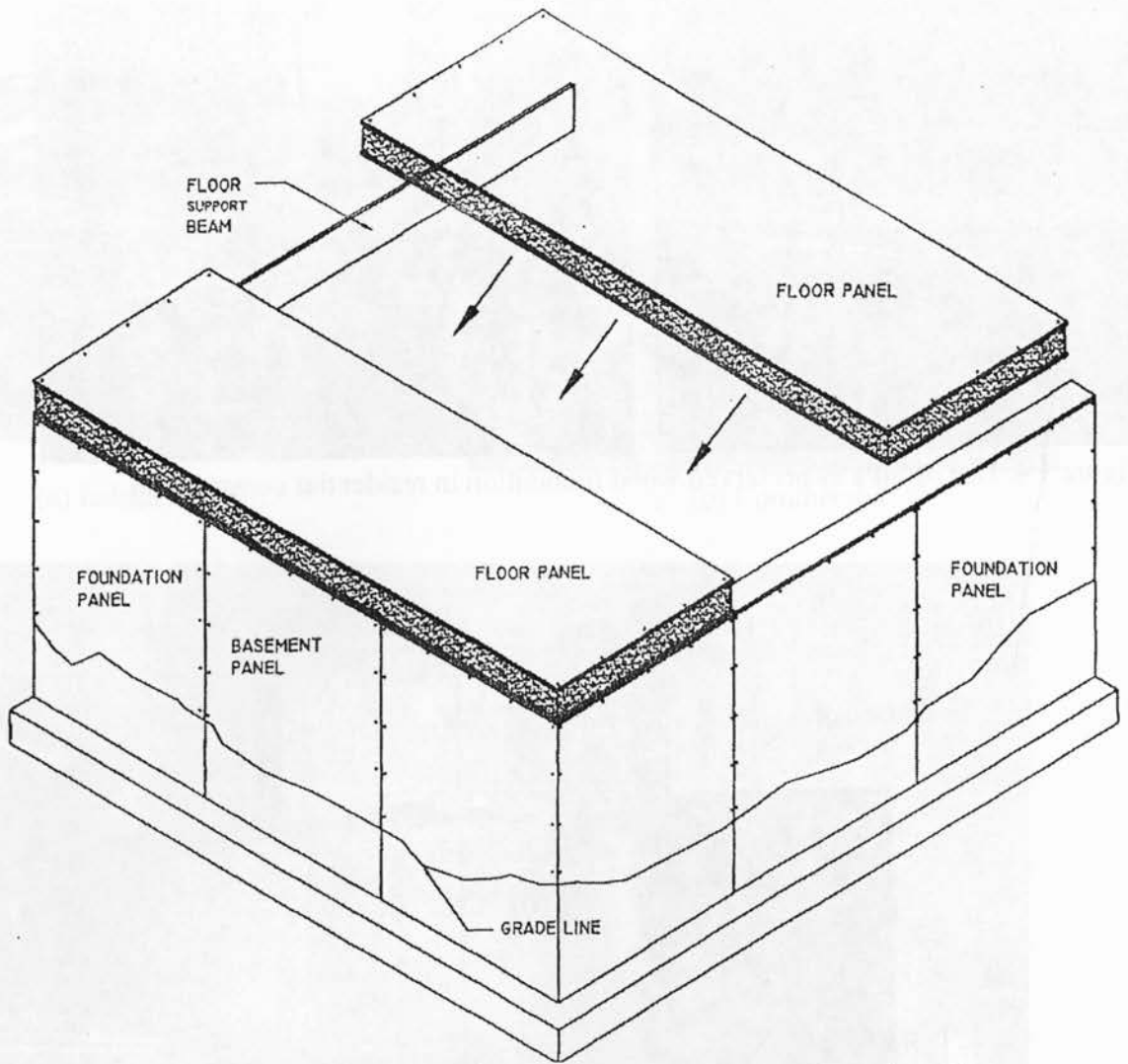
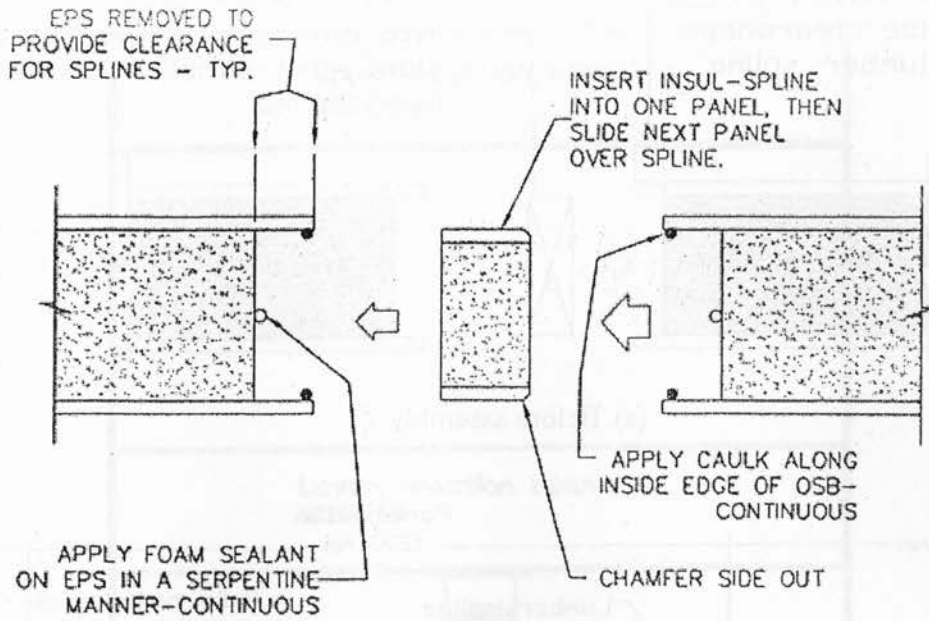
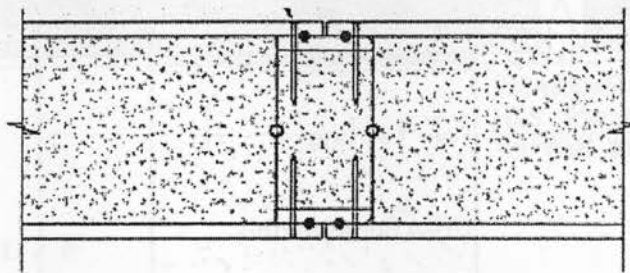


Figure 3.1. Typical floor and basement wall construction using SIPs



(a) Before assembly



(b) After assembly

Figure 3.2 Typical section at panel foam-spline connection before and after assembly

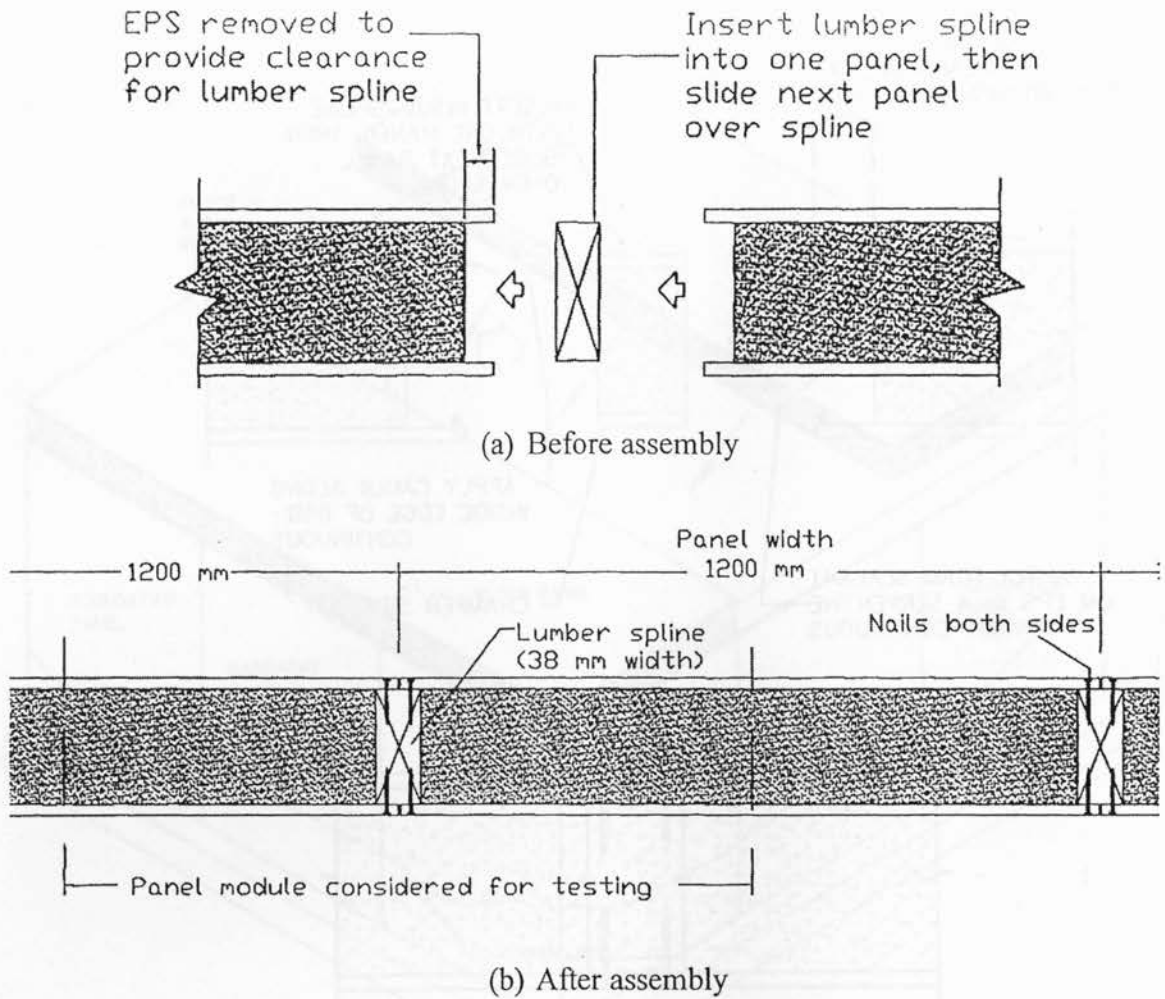


Figure 3.3 Typical section at panel lumber-spline connection before and after assembly

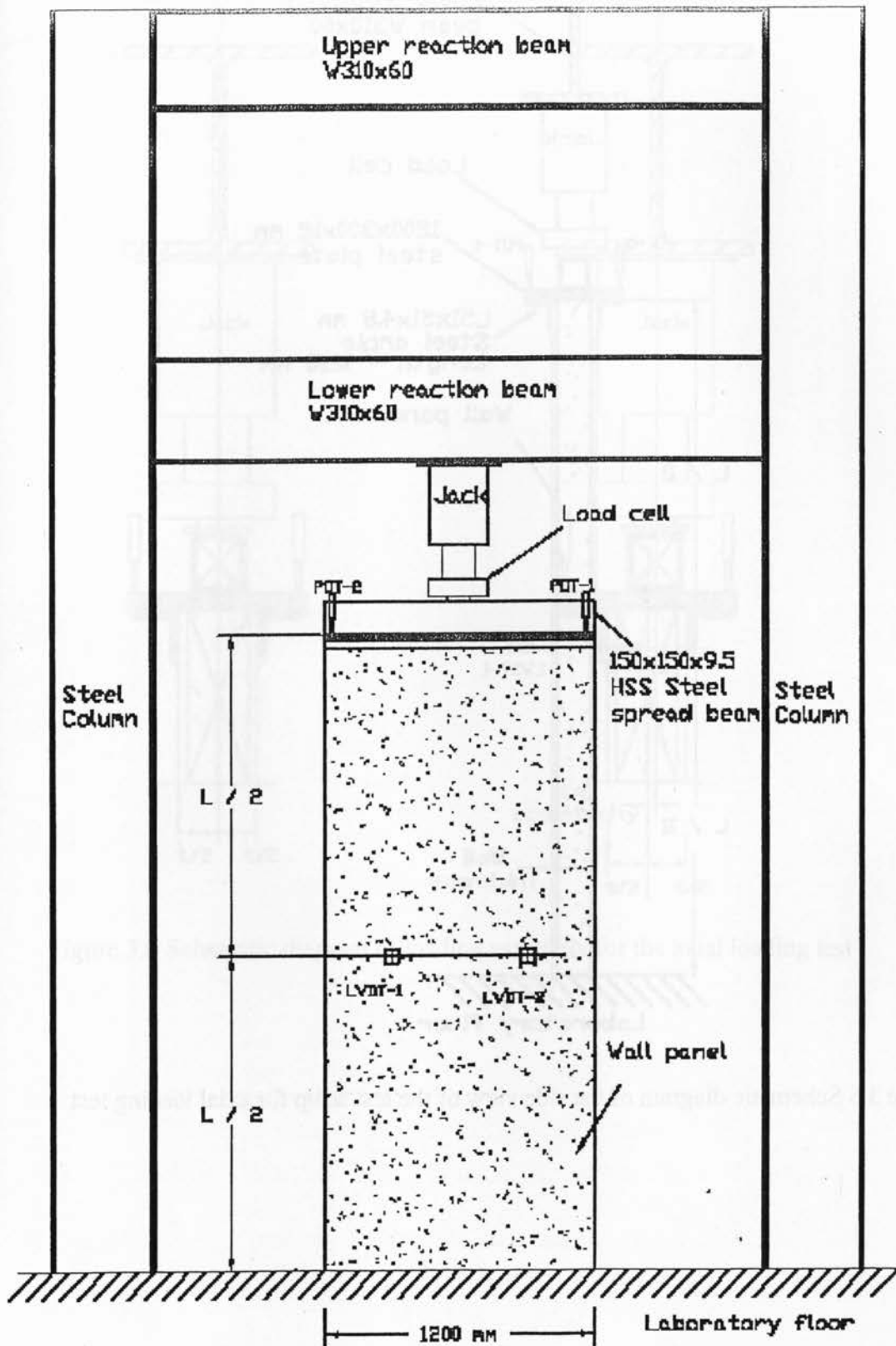


Figure 3.4 Schematic diagram of the elevation of the test setup for axial loading test

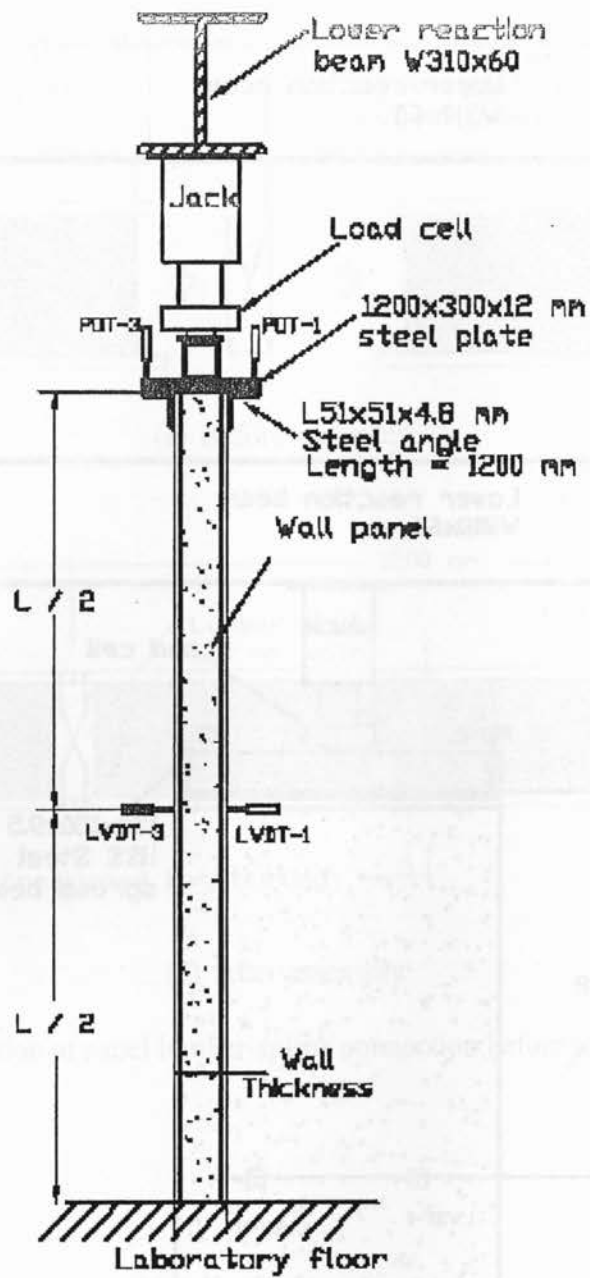


Figure 3.5 Schematic diagram of the side view of the test setup for axial loading test

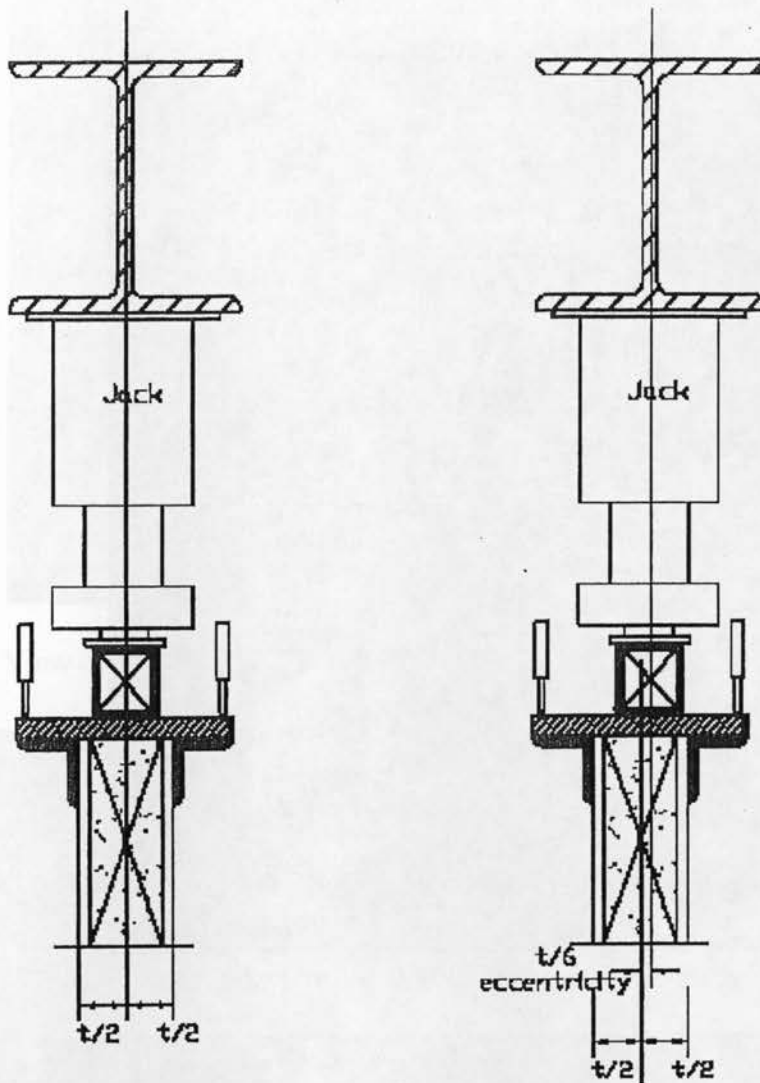


Figure 3.6 Schematic diagram of loading assembly for the axial loading test

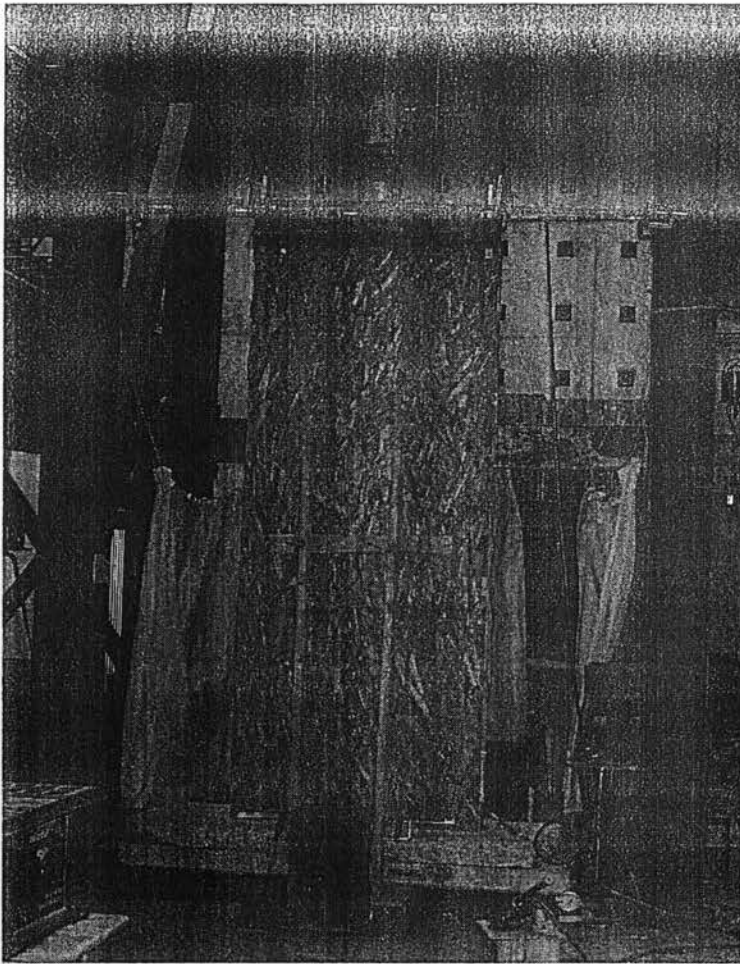


Figure 3.7. View of wall W-2 before testing

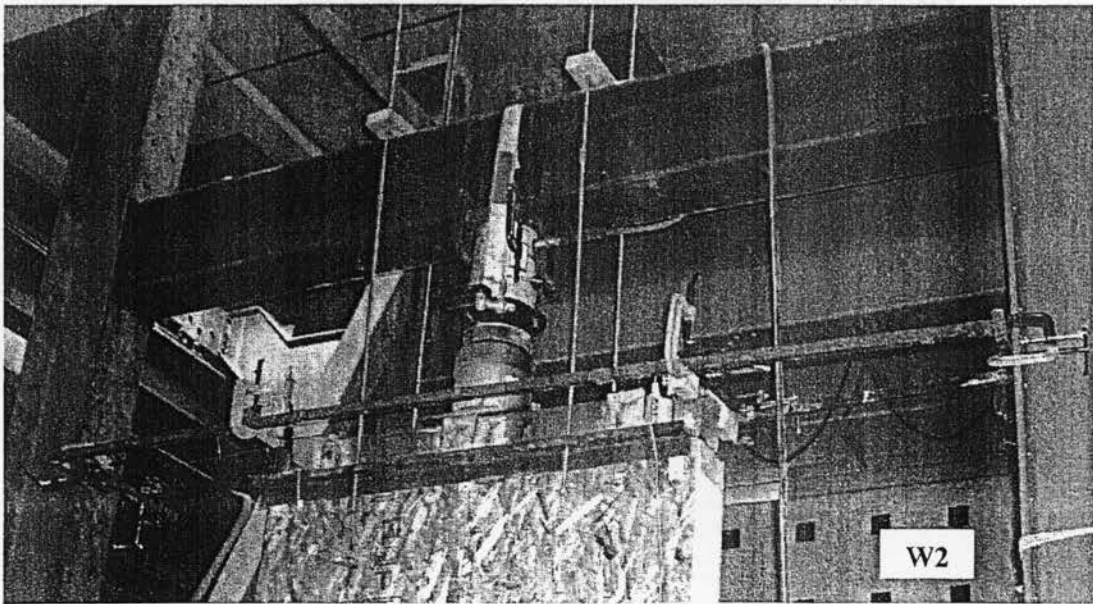


Figure 3.8. View of the top loading system for wall W2 before testing

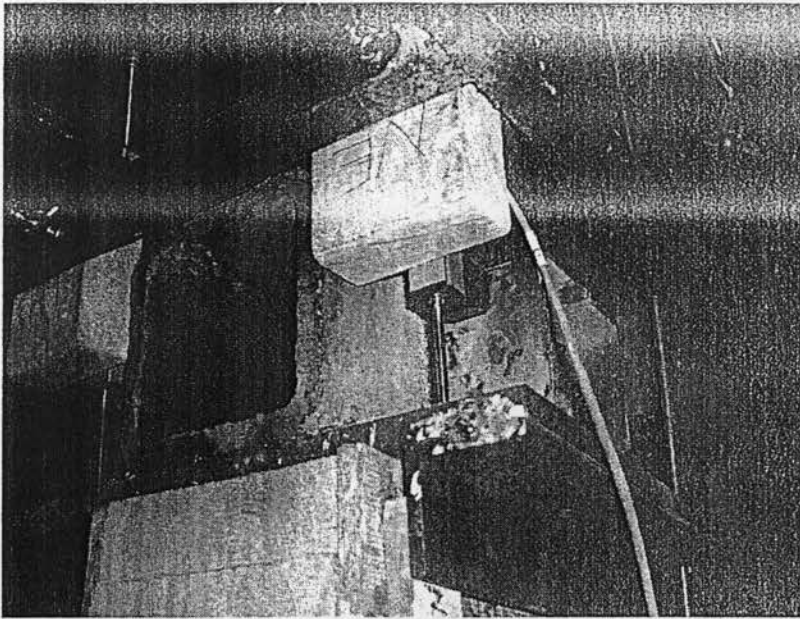


Figure 3.9. View of the loading assembly for and POT locations for the axial load tests

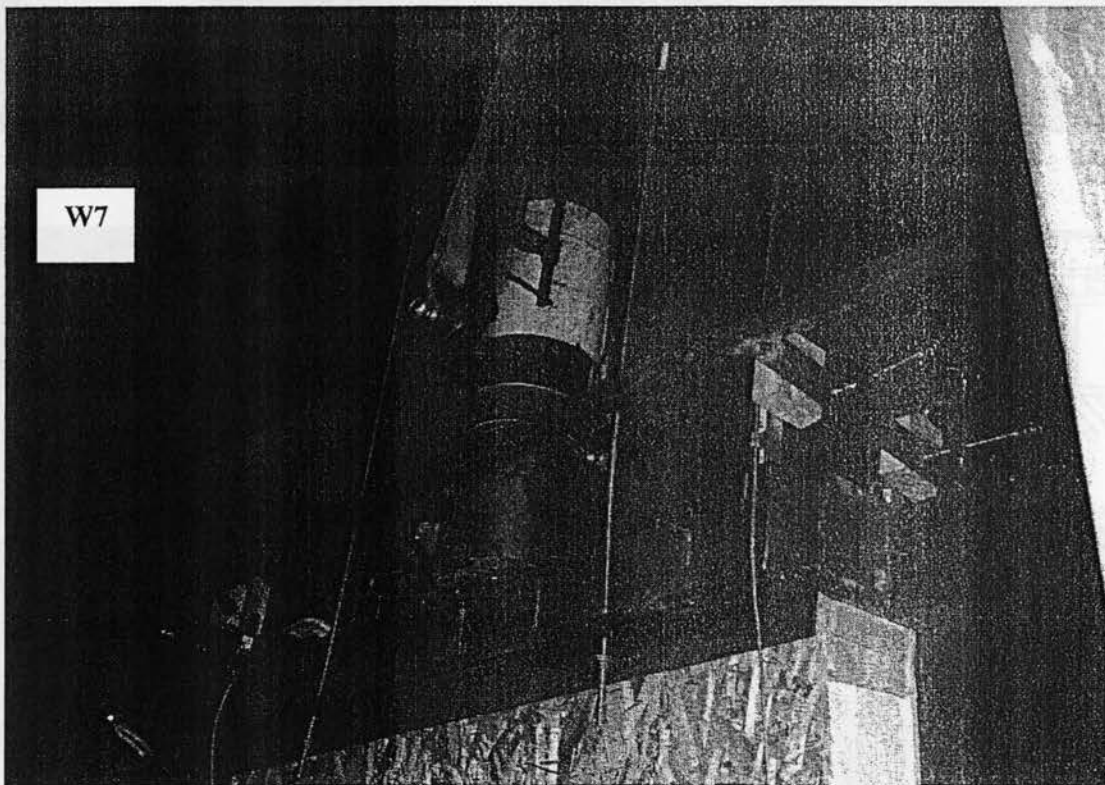


Figure 3.10. Enlarged view for the loading assembly for the eccentric compression loading test

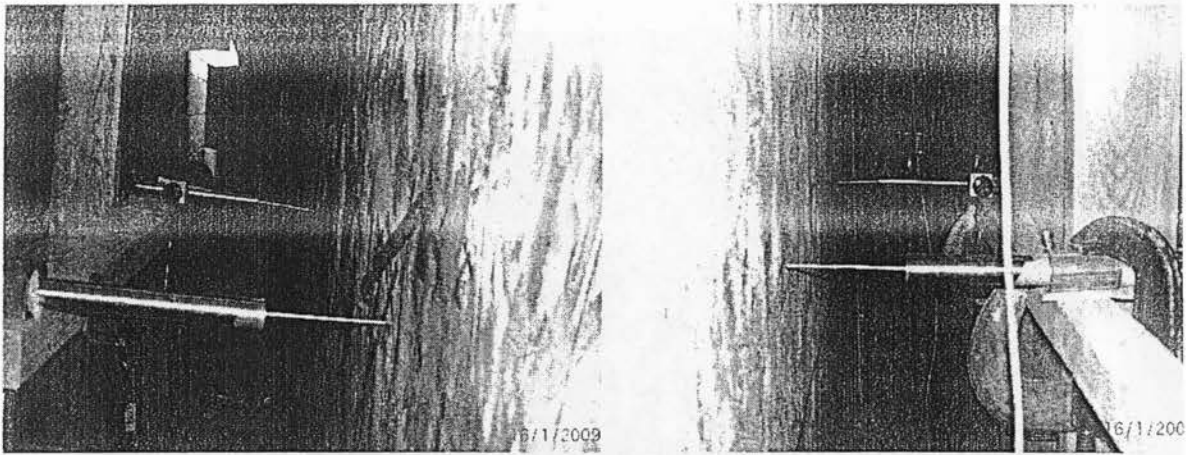


Figure 3.11. Views of the LVDTs used to measure lateral deflection at mid-height of the left and right side of wall W5, respectively.

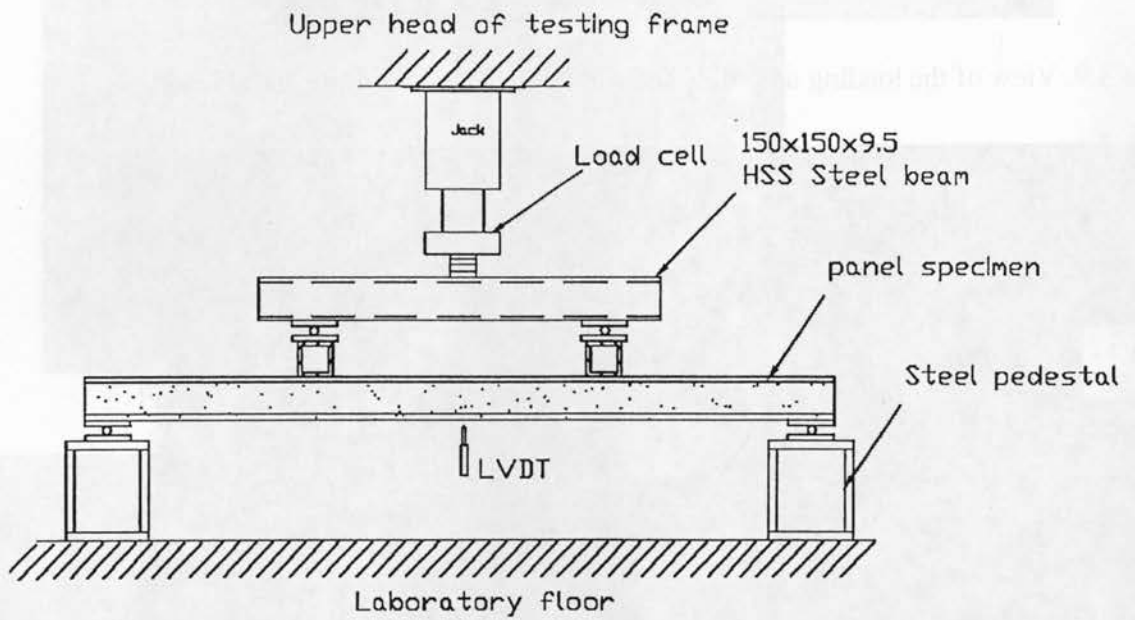


Figure 3.12. Schematic diagram of the elevation of the test setup for flexural loading test

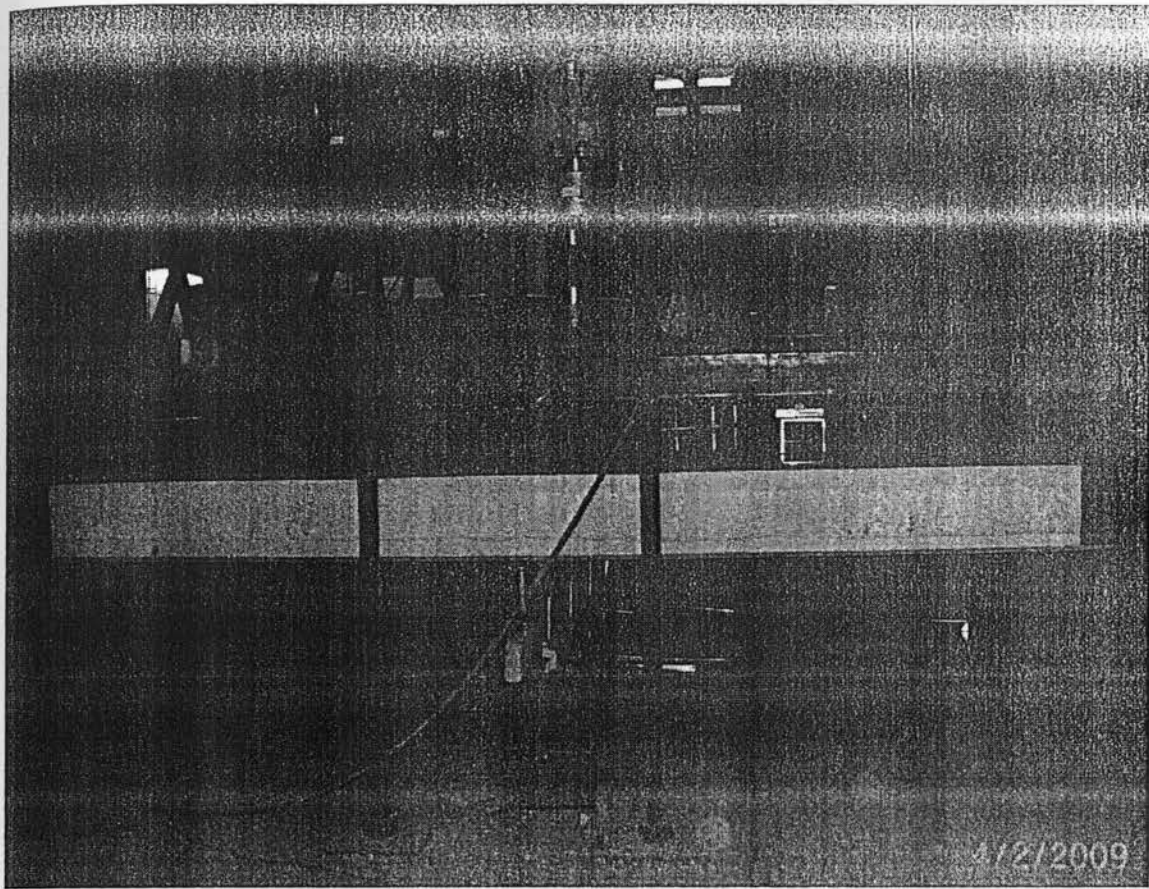


Figure 3.13. View of Specimen WS31 before testing

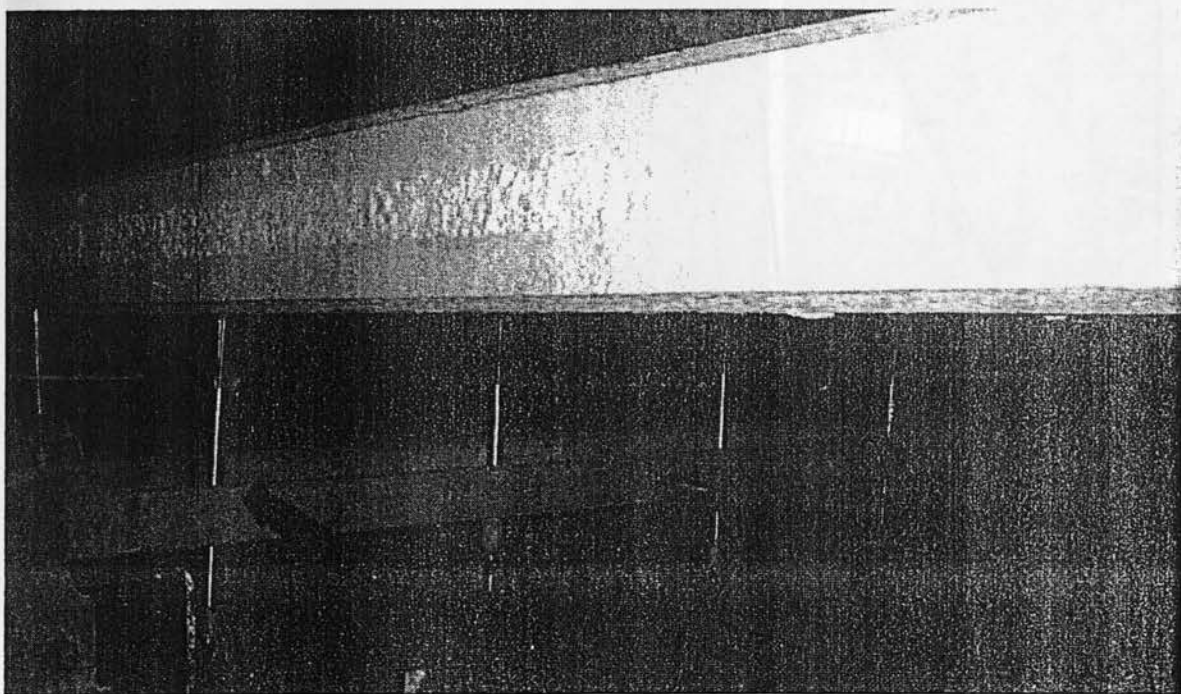


Figure 3.14. View of LVDTs at mid-span location of model WB19

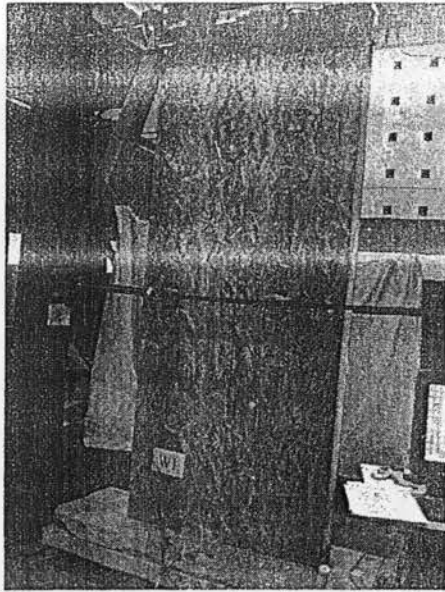


Figure 4.1. View of the test setup for wall W1 before testing

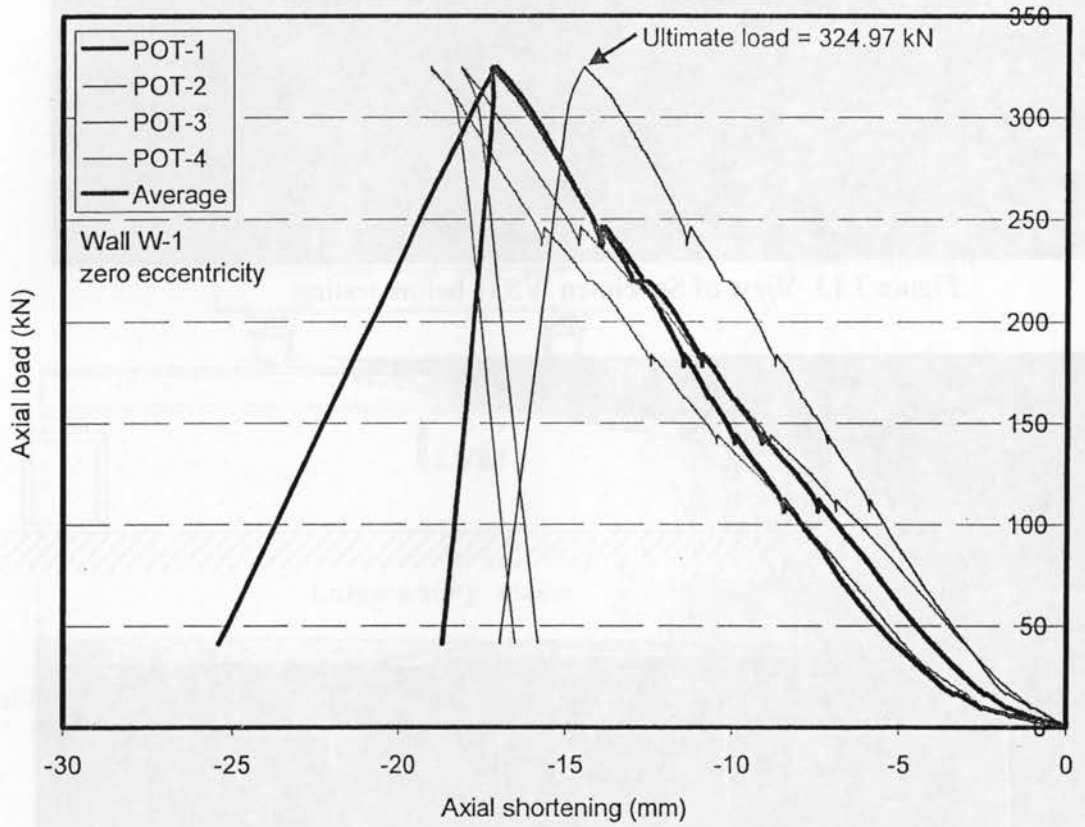


Figure 4.2. Axial load-axial shortening relationship for model W1

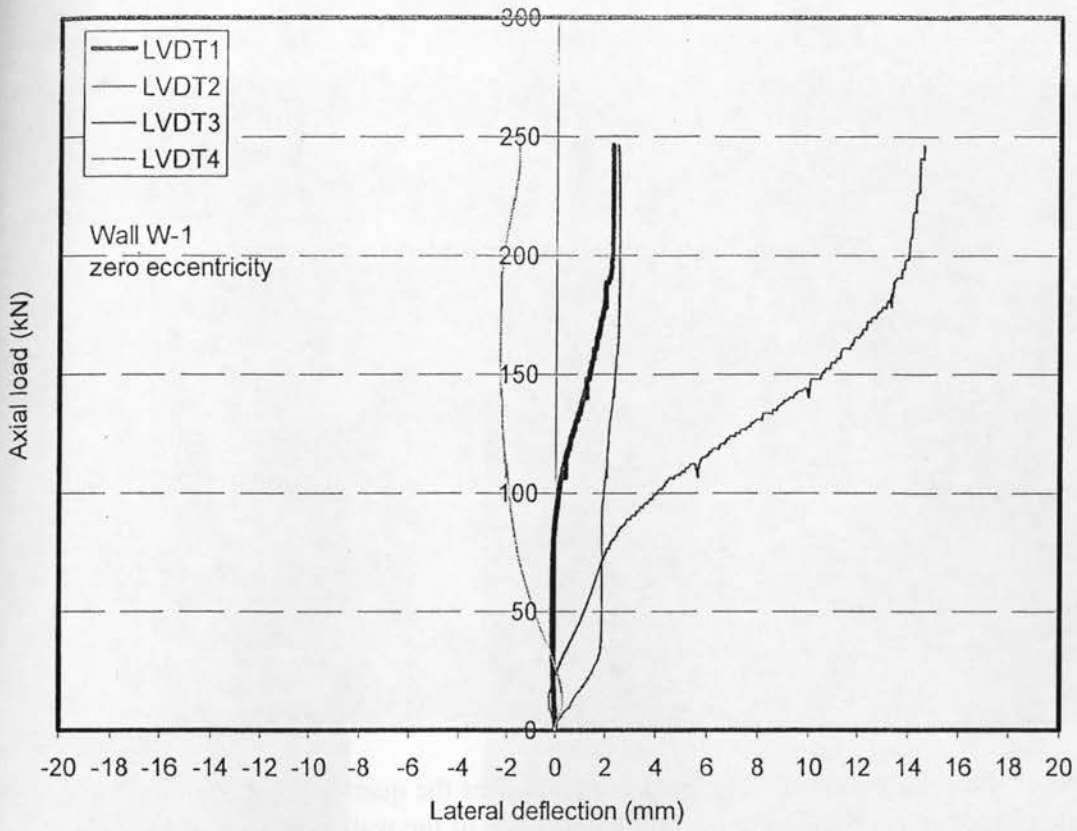
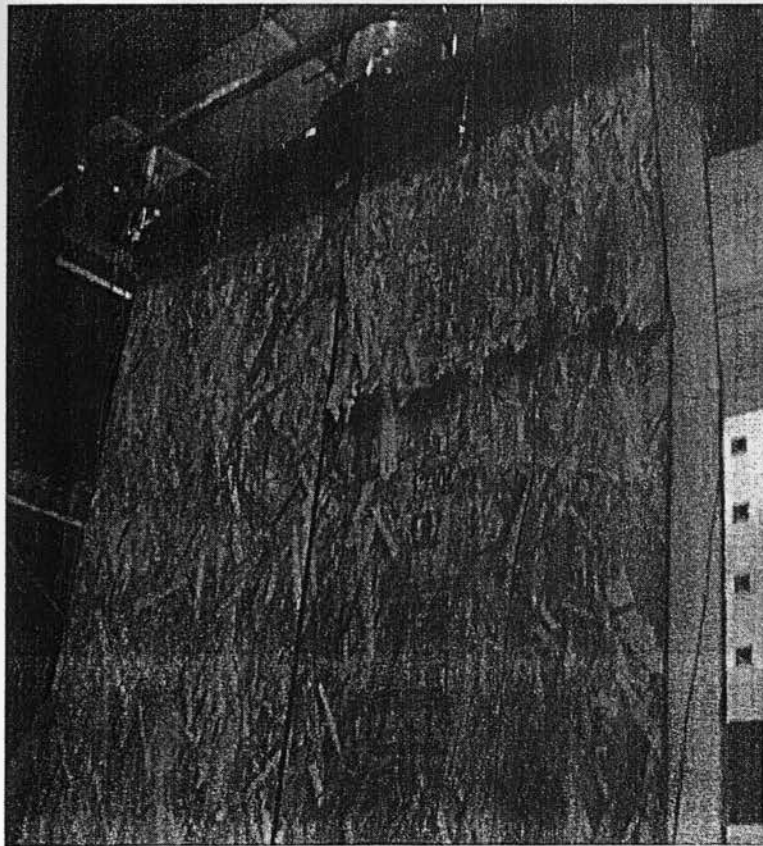


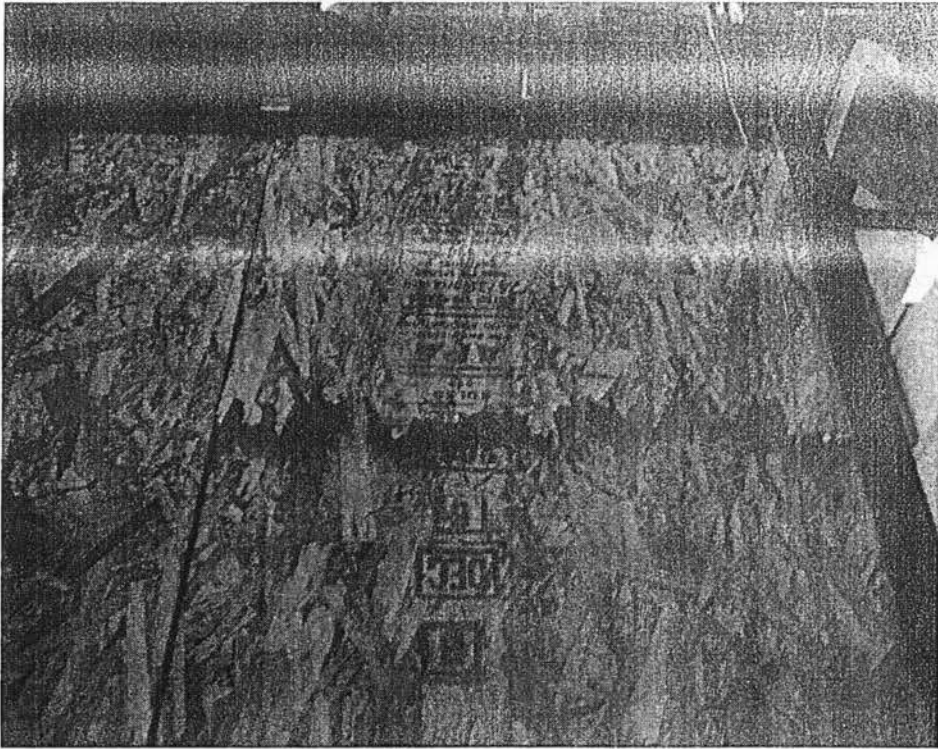
Figure 4.3. Axial load-lateral deflection relationship for model W1



(a)



(b)



(c)

Figure 4.4. Views of the failure mode due to OSB crushing near the quarter point from the top of south side of model W1 that led to lateral deformation of the wall at this location



Figure 4.5. View of the failure mode due to OSB crushing at its connection with the bottom lumber stud in the south side of model W1

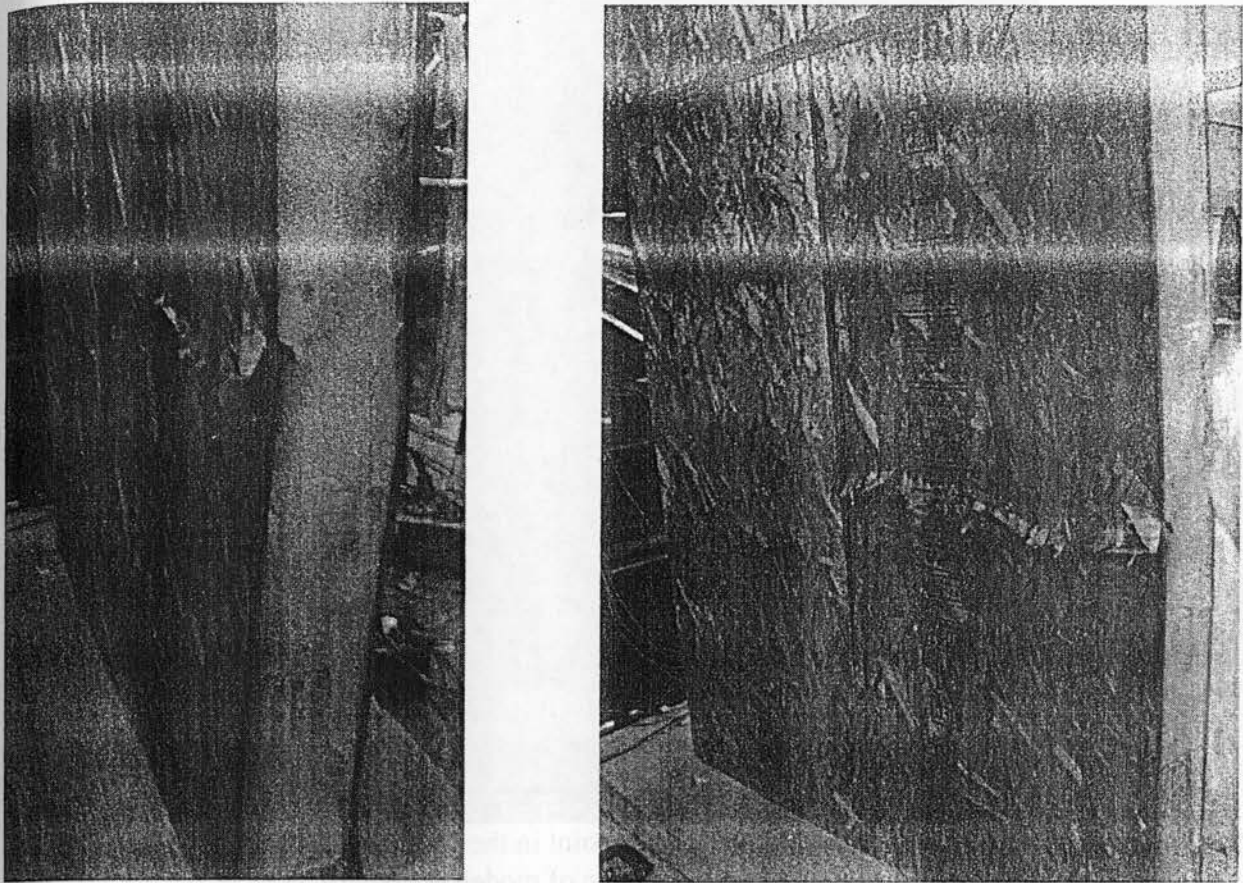


Figure 4.6. View of the failure mode due to OSB crushing near its lower quarter point in the north side of model W1

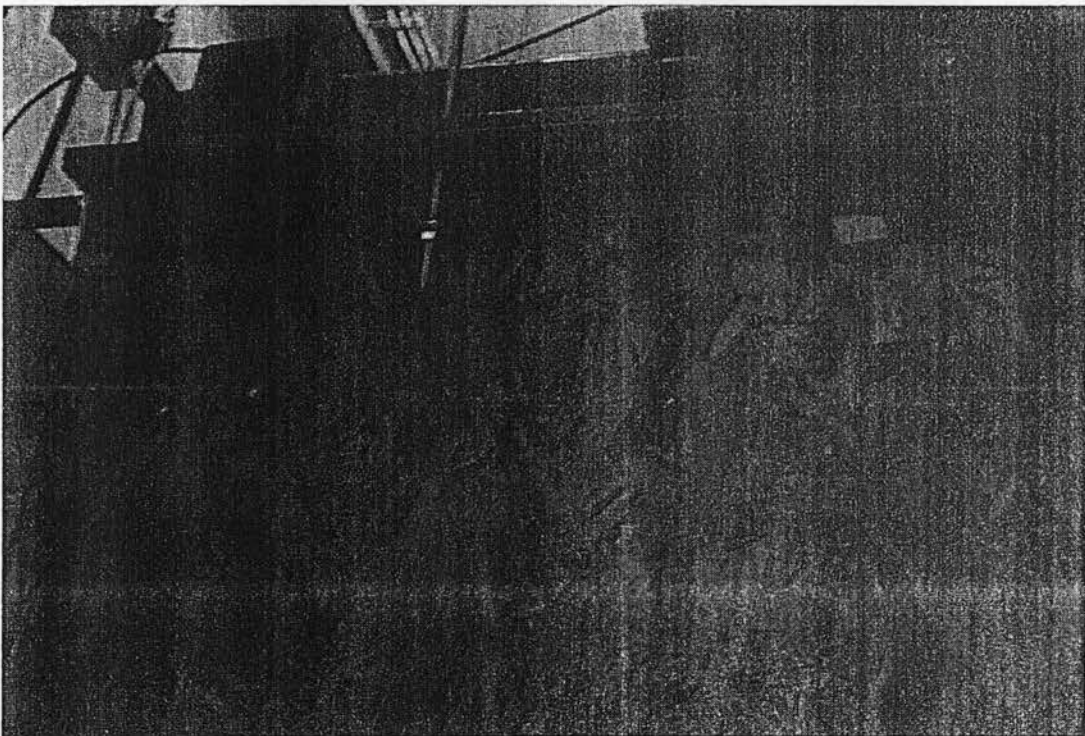


Figure 4.7. Signs of OSB crushing near the top of the wall in the north side

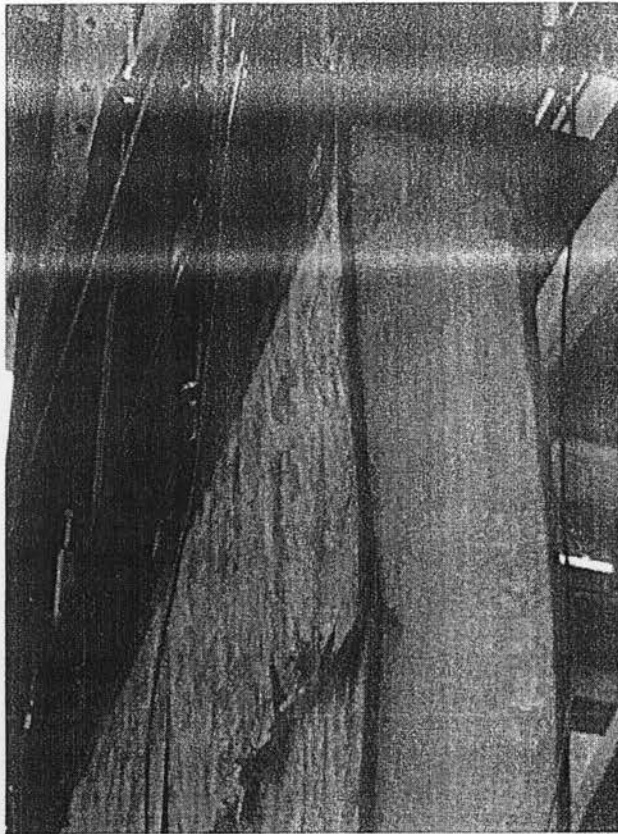


Figure 4.8. View of OSB crushing near its upper quarter point in the south side as well as OSB crushing near the top of the north side of model W1

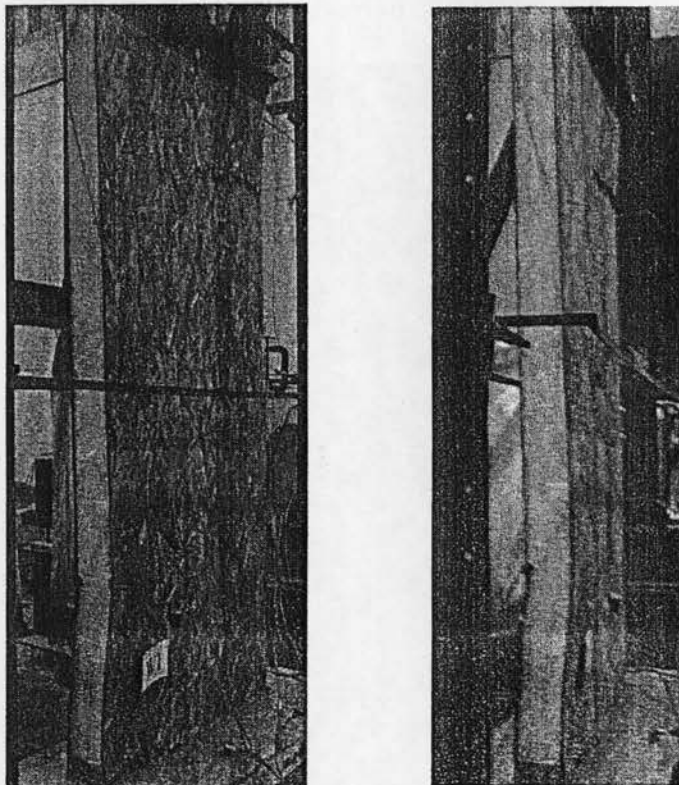


Figure 4.9. View of model W1 from the south-west corner showing lateral deformation of the wall near the lower quarter point as a result of OSB crushing at this location

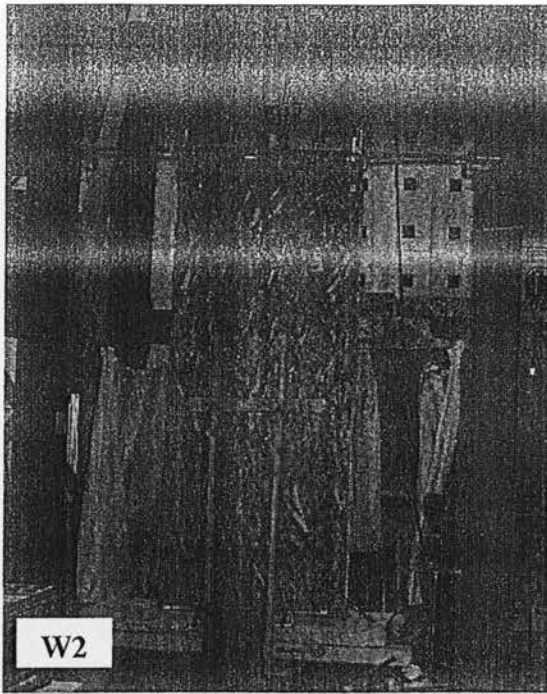


Figure 4.10. View of the test setup for wall W2 before testing

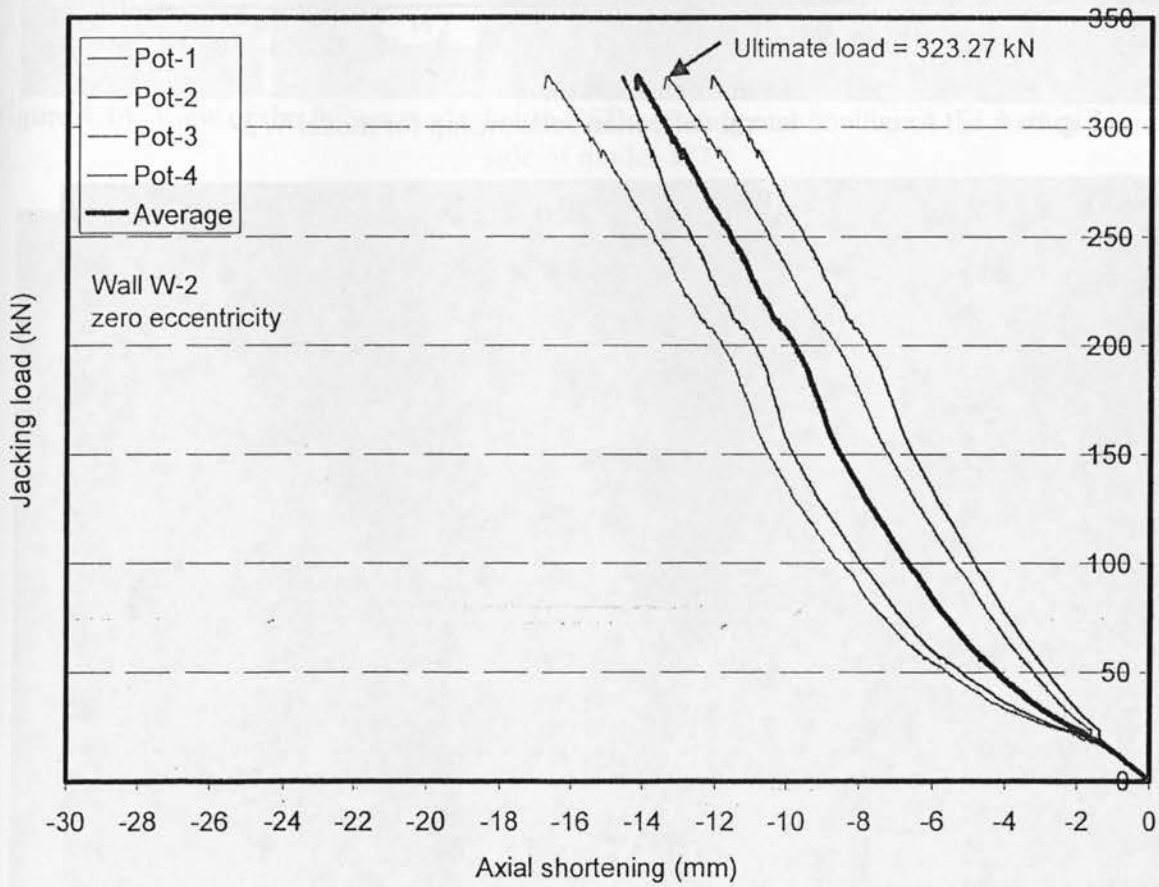


Figure 4.11. Axial load-axial shortening relationship for model W2

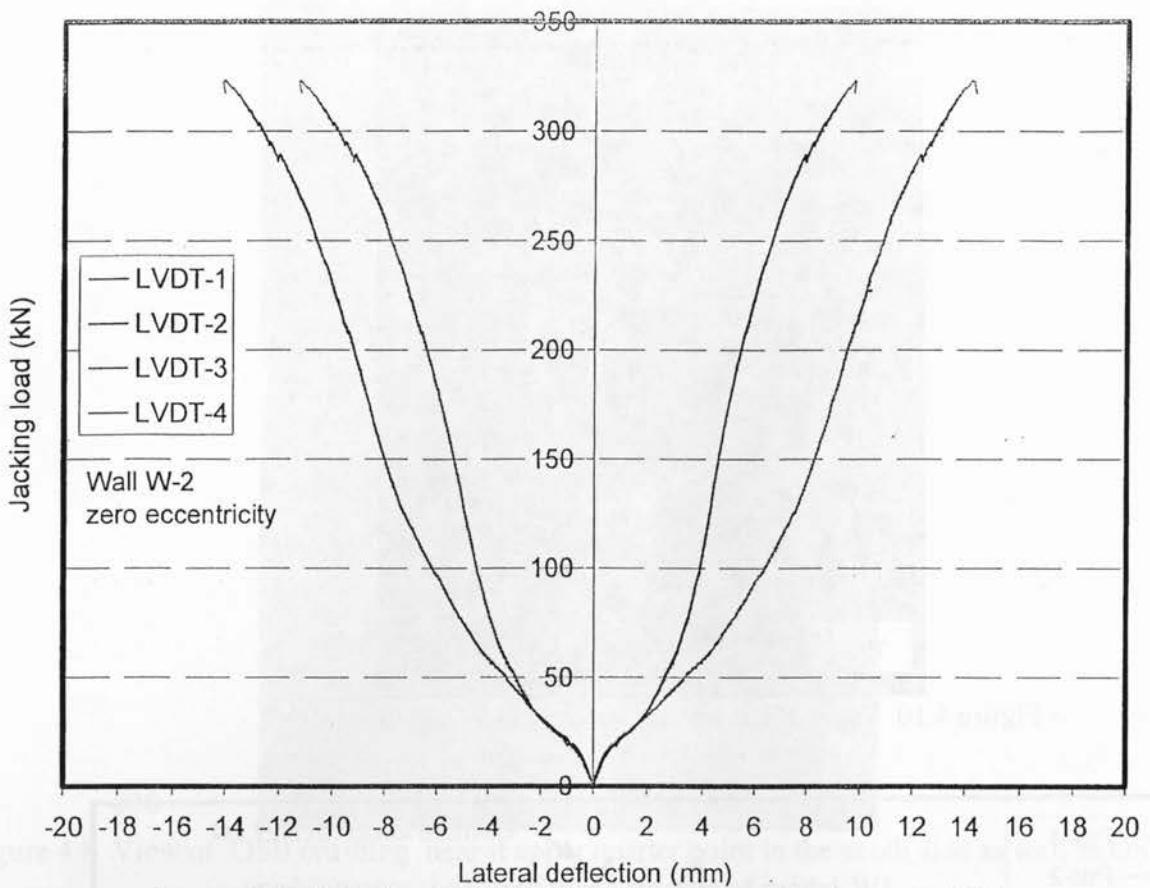


Figure 4.12. Axial load-lateral deflection relationship for model W2

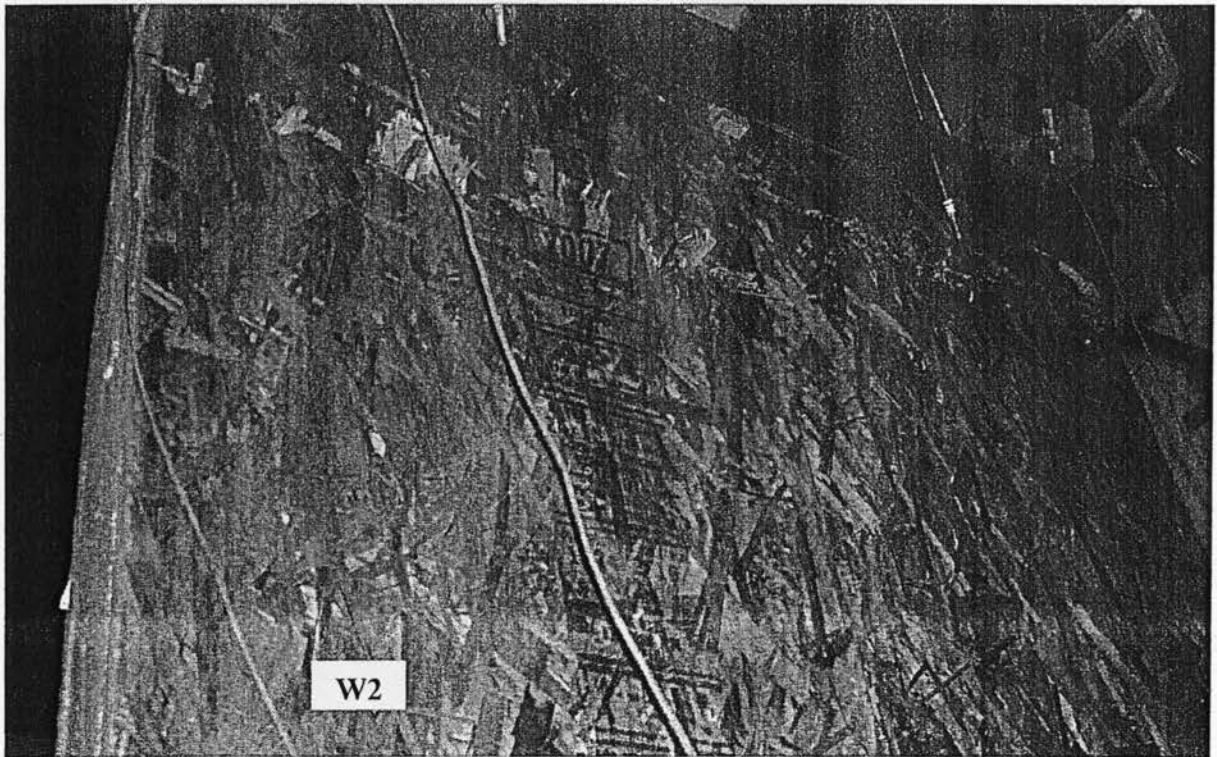


Figure 4.13. View of the failure mode due to OSB crushing near the top of south side of model W2



Figure 4.14. View of the failure mode due to OSB crushing near the top of the wall in the north side of model W2

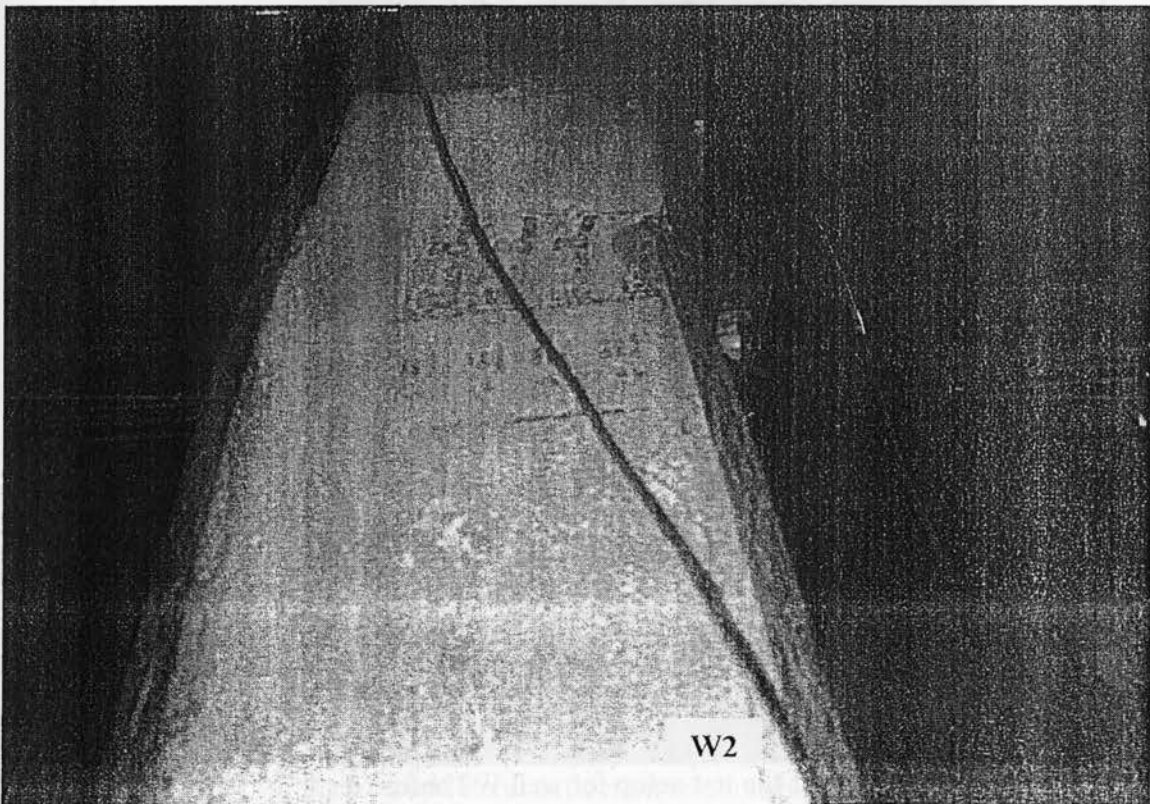


Figure 4.15. View of OSB crushing near the top of west side of model W2

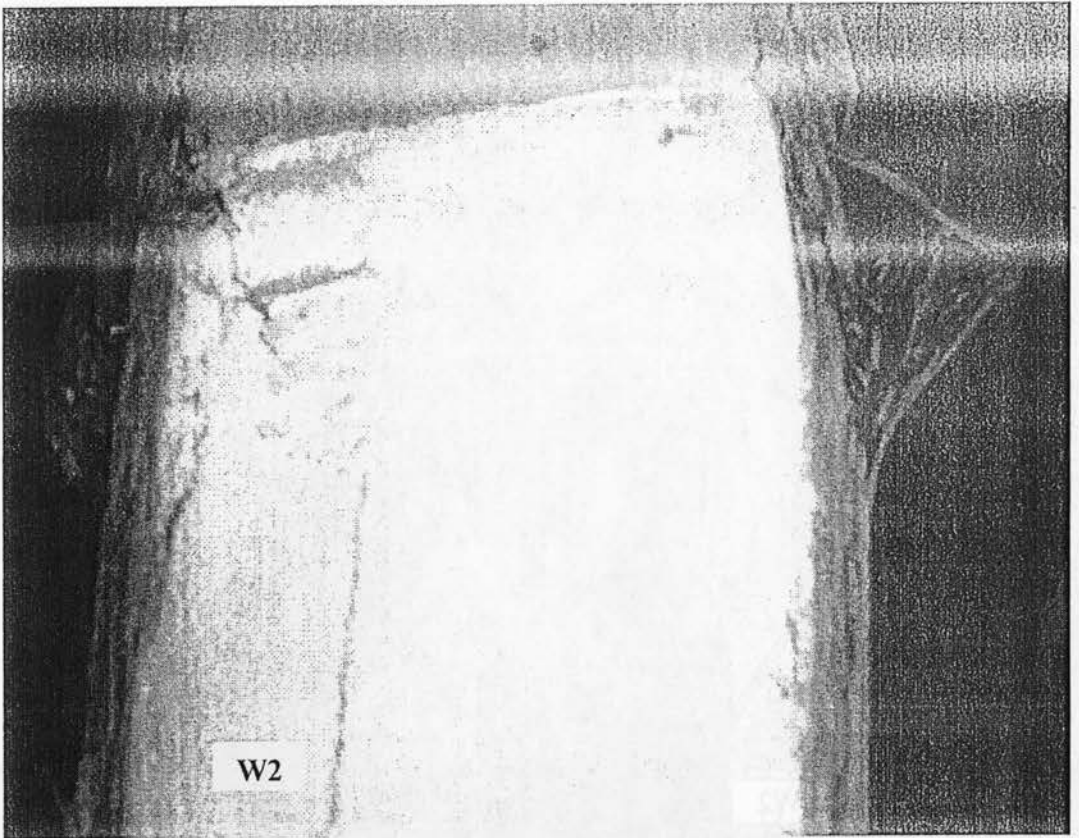


Figure 4.16. View of OSB crushing near the top of east side of model W2

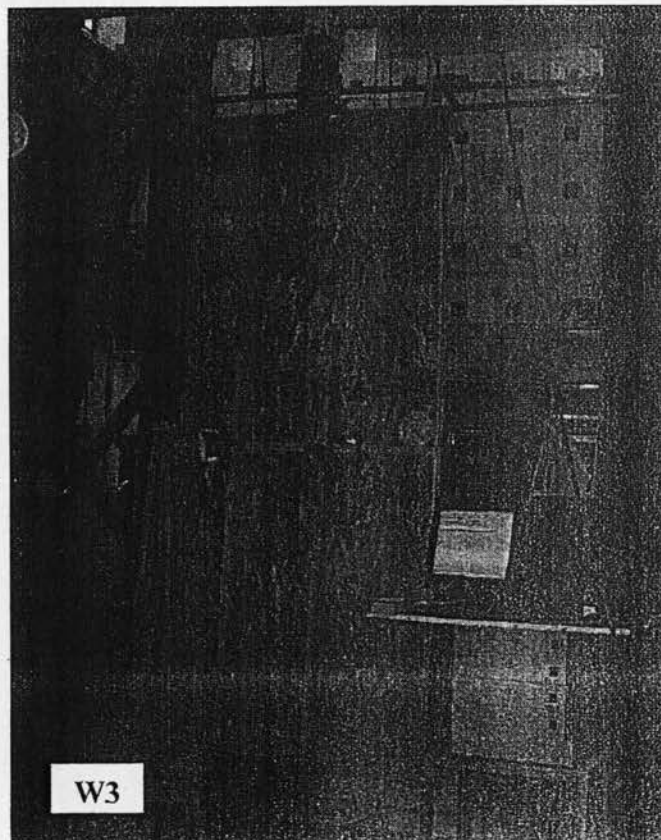


Figure 4.17. View of the test setup for wall W3 before testing

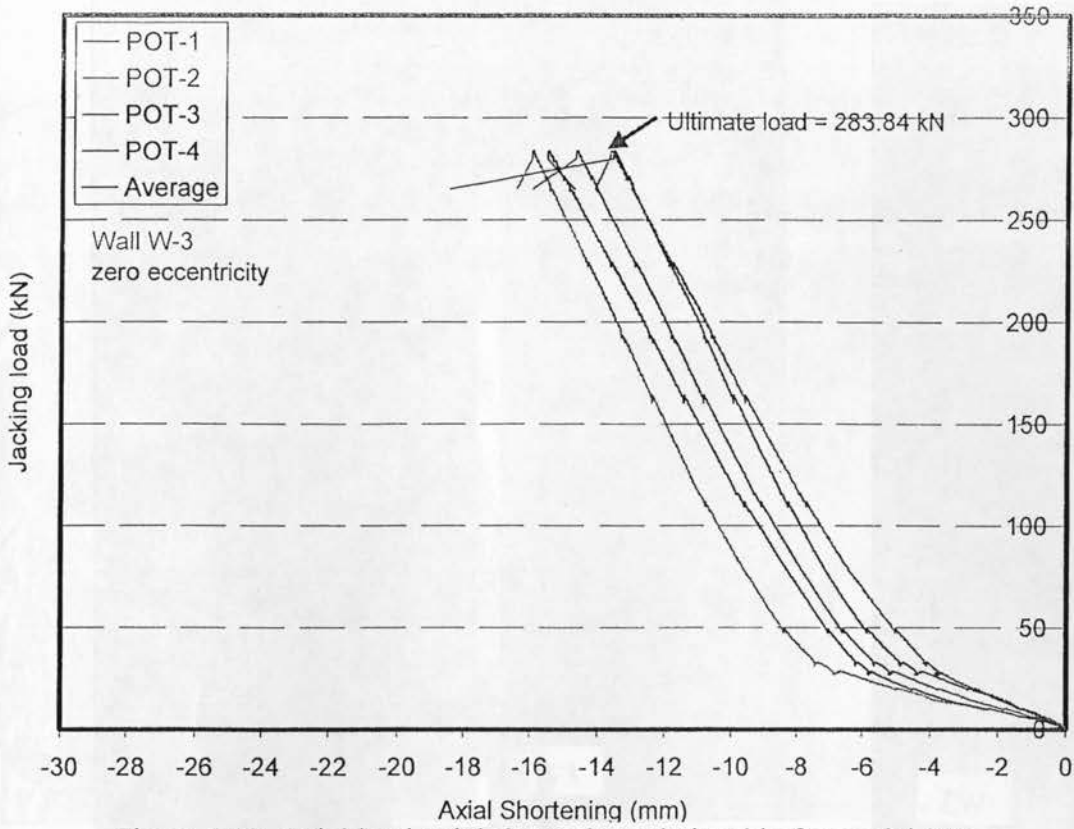


Figure 4.18. Axial load-axial shortening relationship for model W3

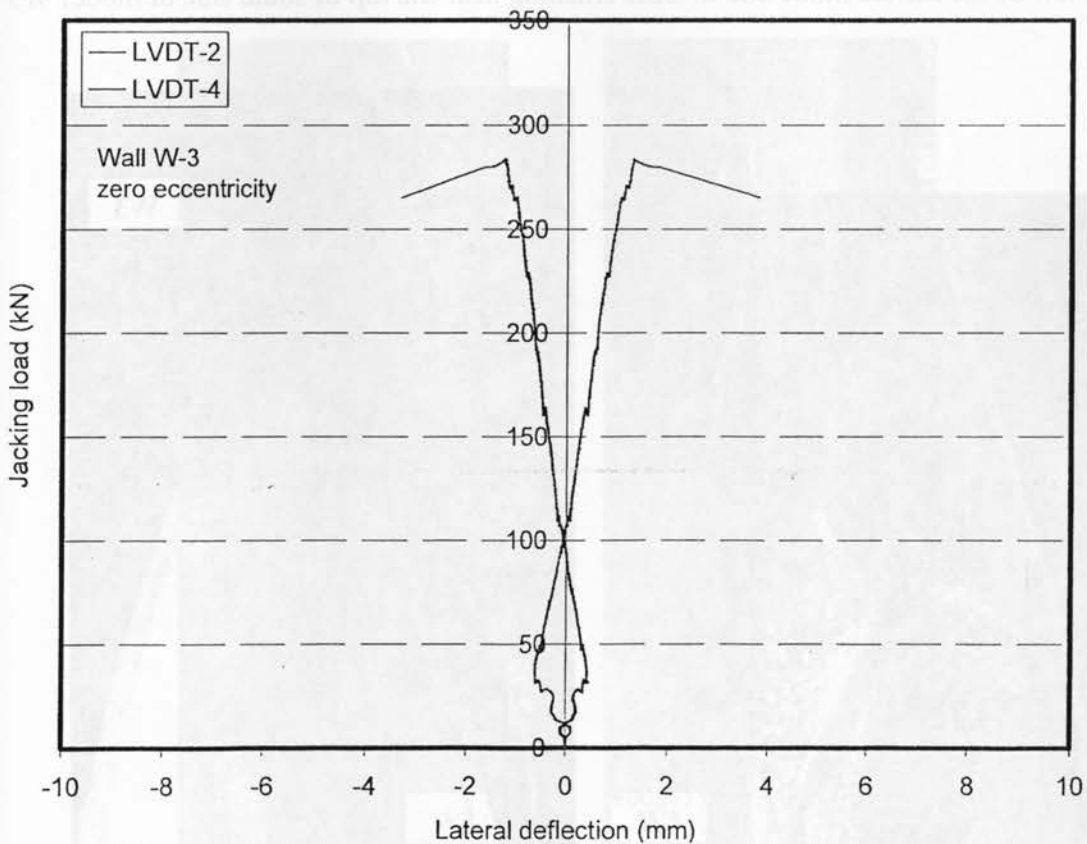


Figure 4.19. Axial load-lateral deflection relationship for model W3

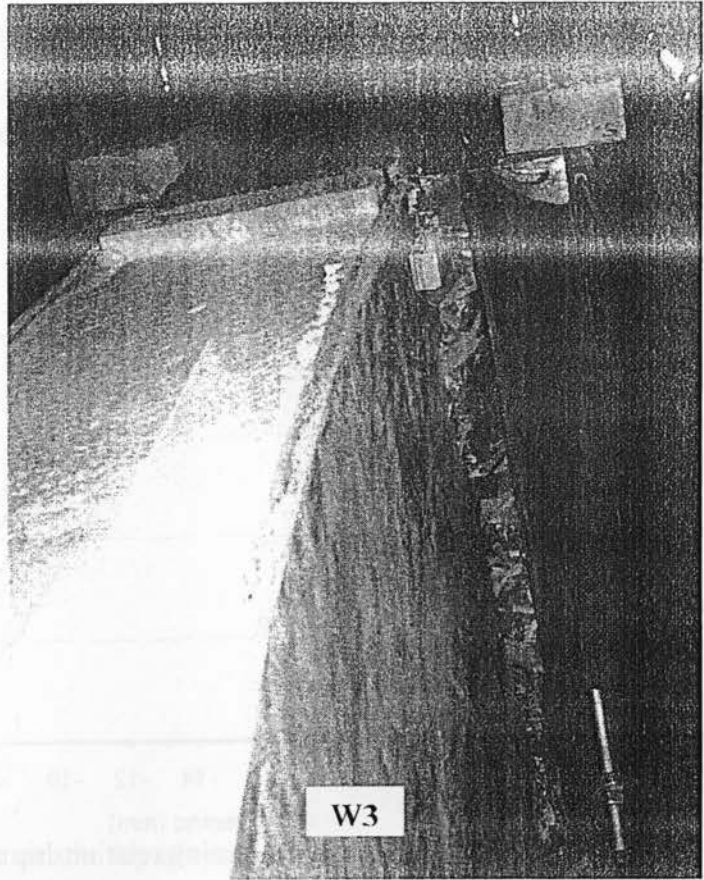
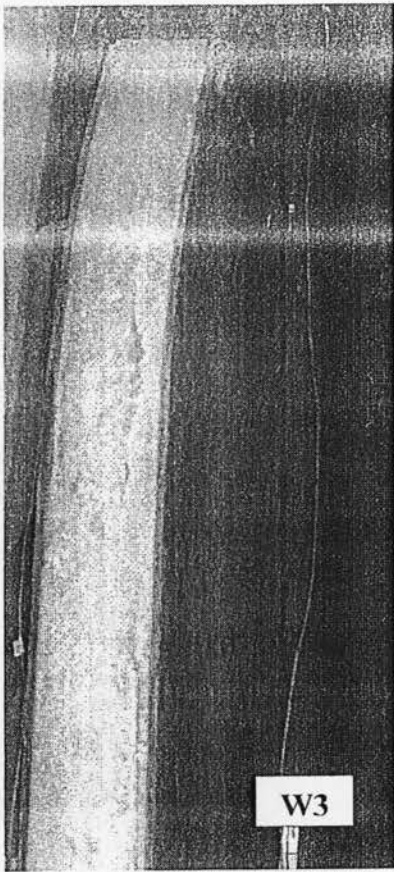
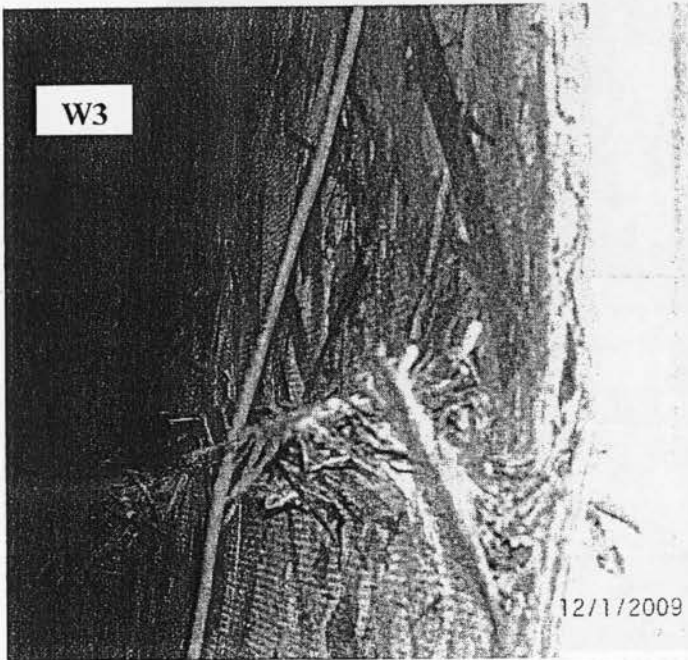


Figure 4.20. View of the failure mode due to OSB crushing near the top of south side of mo



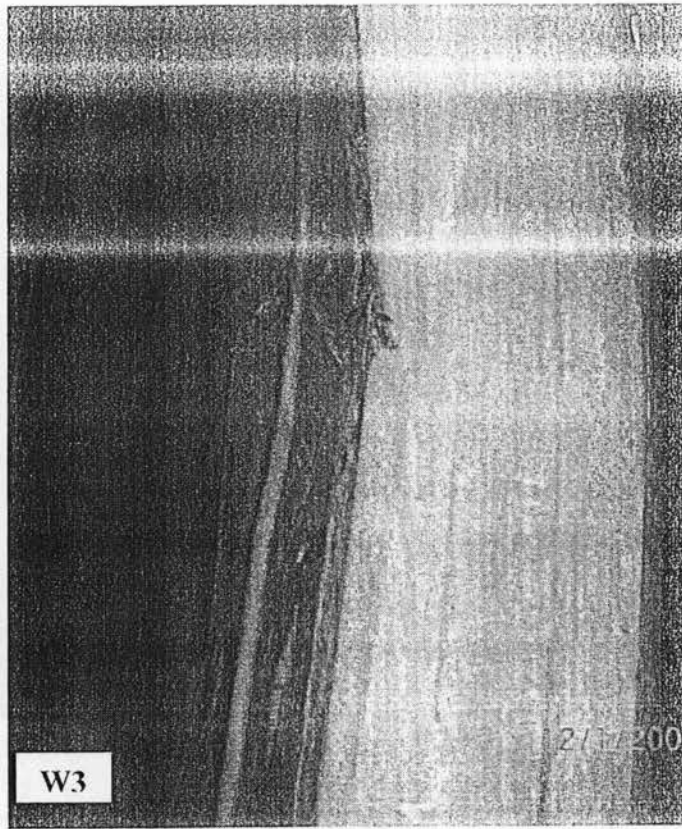
(a)



(b)



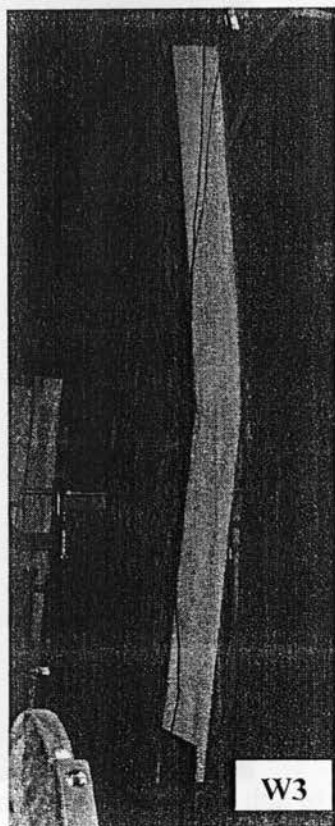
(c)



(d)

el W3

4.21. View of the failure mode due to OSB crushing near the mid-height of the wall W3



4.22. Views of the deformed shape of wall model W3 after OSB crushing near its mid-height

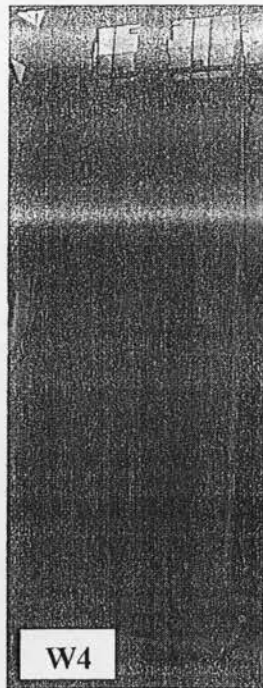


Figure 4.23. View of the test setup for wall W4 before testing

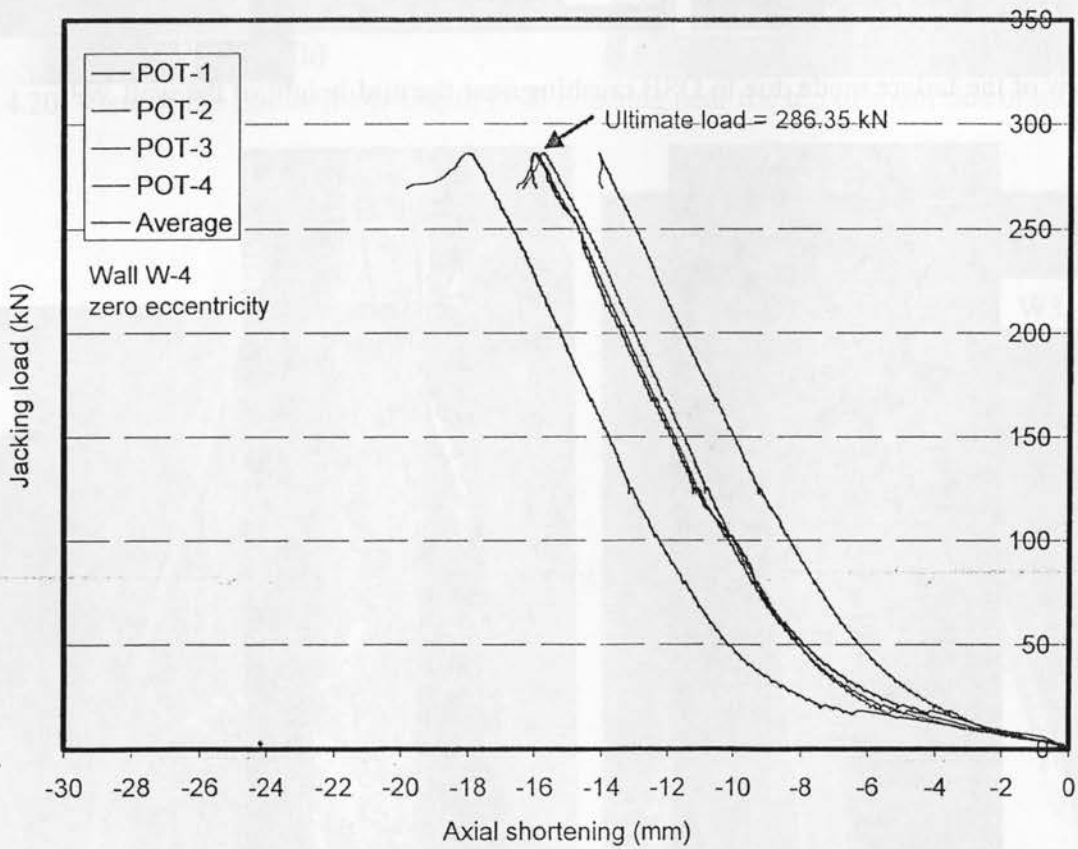


Figure 4.24. Axial load-axial shortening relationship for model W4

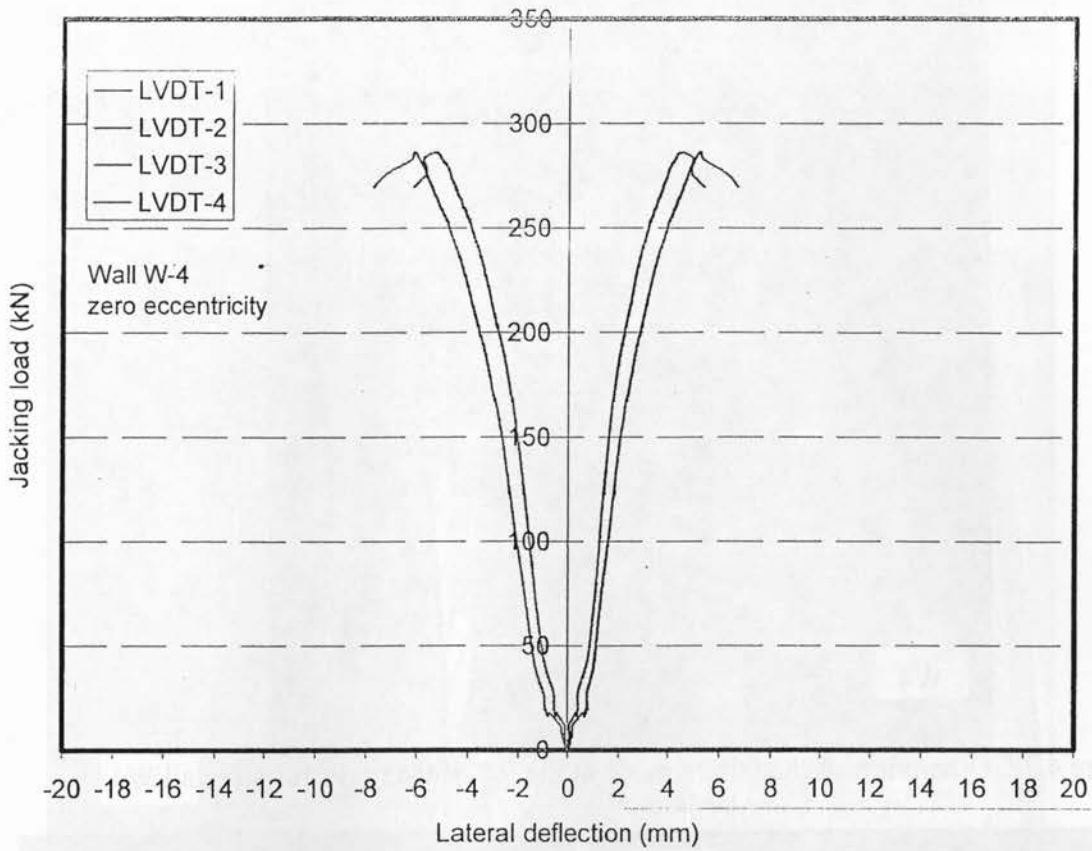


Figure 4.25. Axial load-lateral deflection relationship for model W4

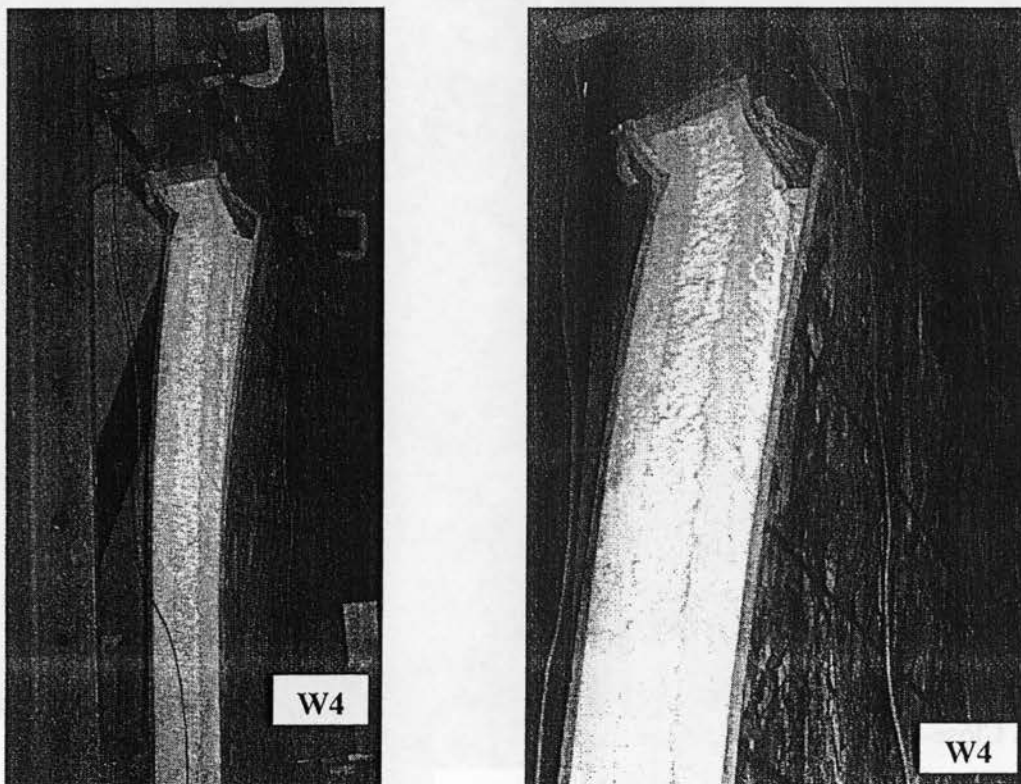


Figure 4.26. View of the failure mode due to OSB crushing at the top of north side of model W4, in addition to foam-OSB separation at the top of the south side

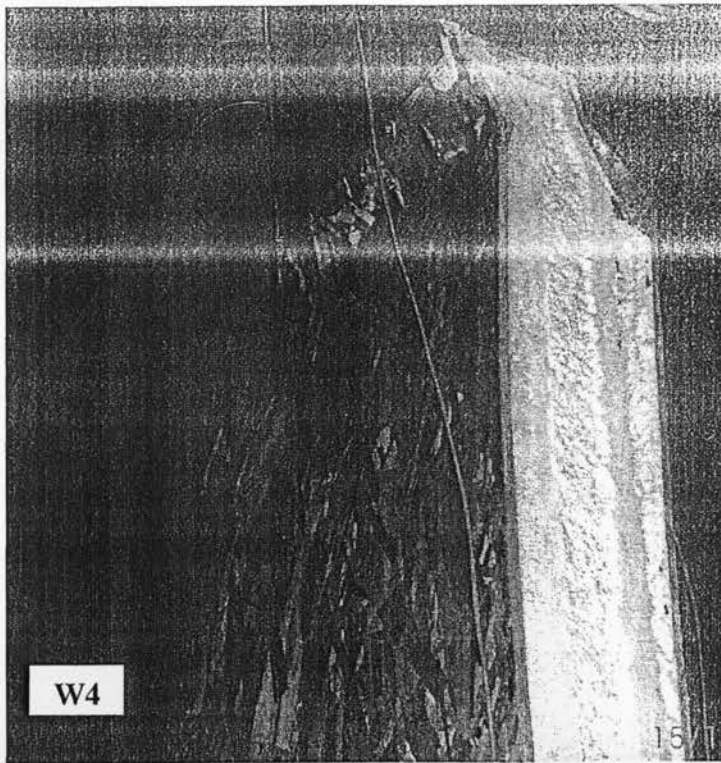


Figure 4.27. Other view of the failure mode at the top of the north side of wall W4

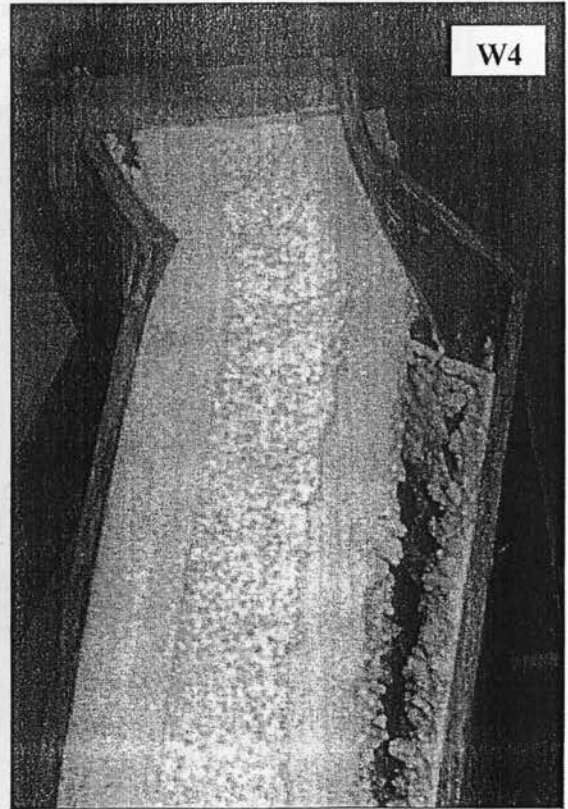
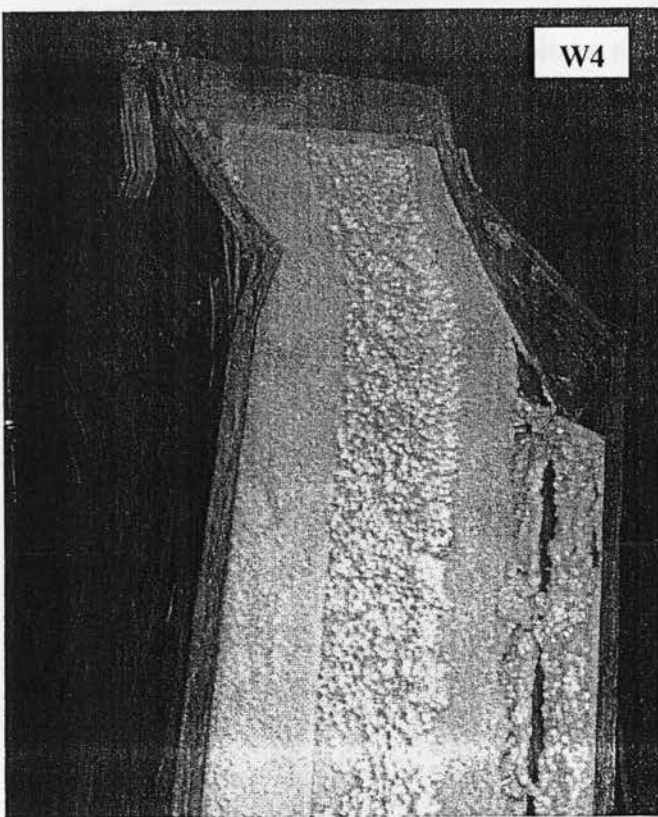


Figure 4.28. Close-up views of the deformed shape of top portion of wall W4 after failure



Figure 4.29. View of the deformed shape of OSB sheets in the south side of wall W4 after crushing

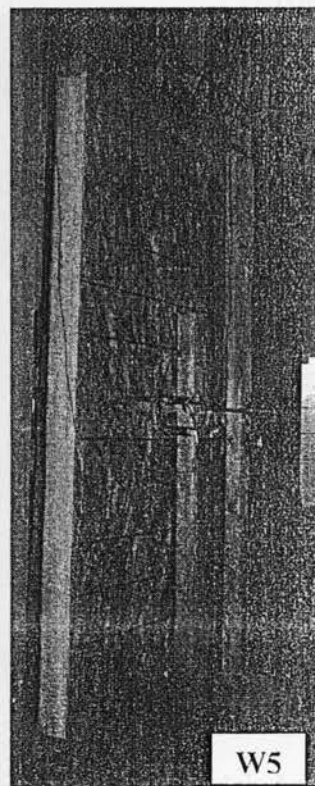
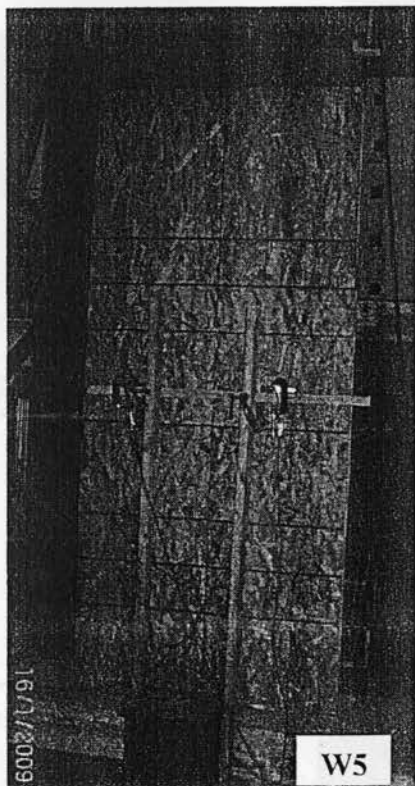


Figure 4.30. View of the test setup for wall W5 before testing

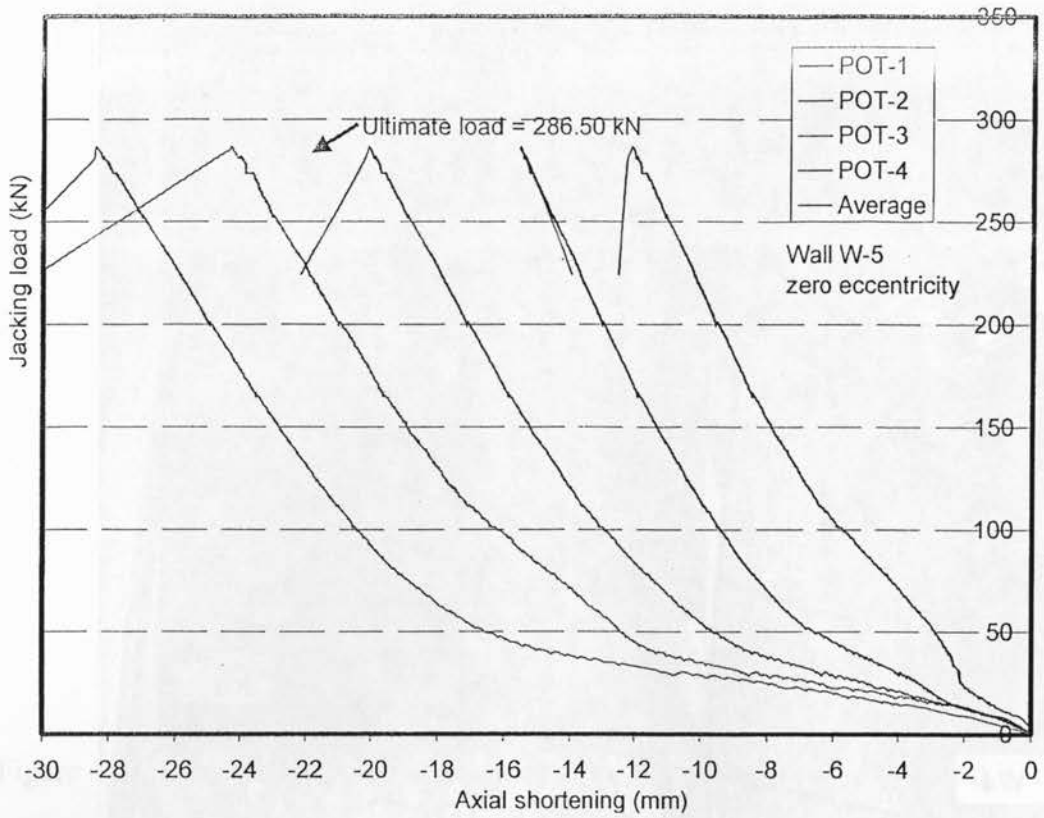


Figure 4.31. Axial load-axial shortening relationship for model W5

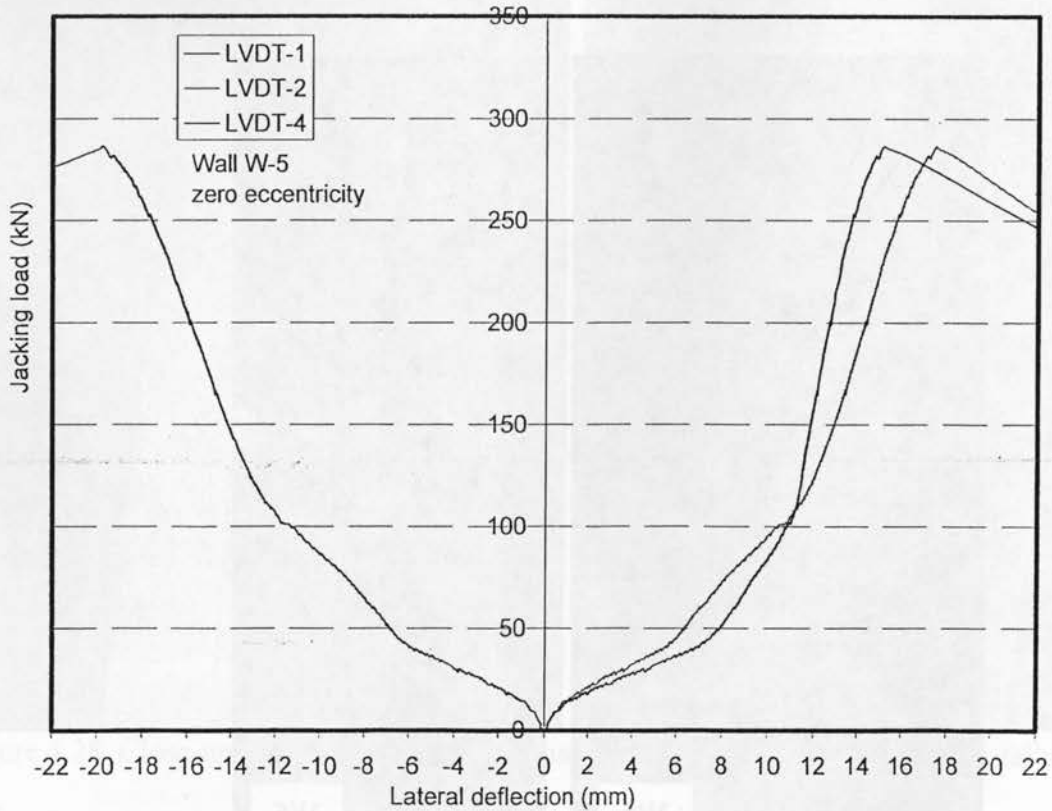


Figure 4.32. Axial load-lateral deflection relationship for model W5

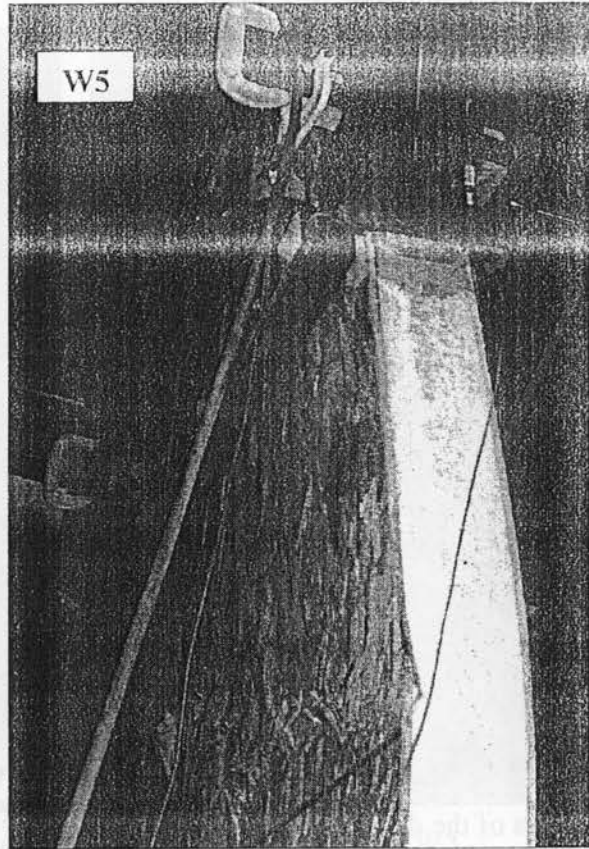
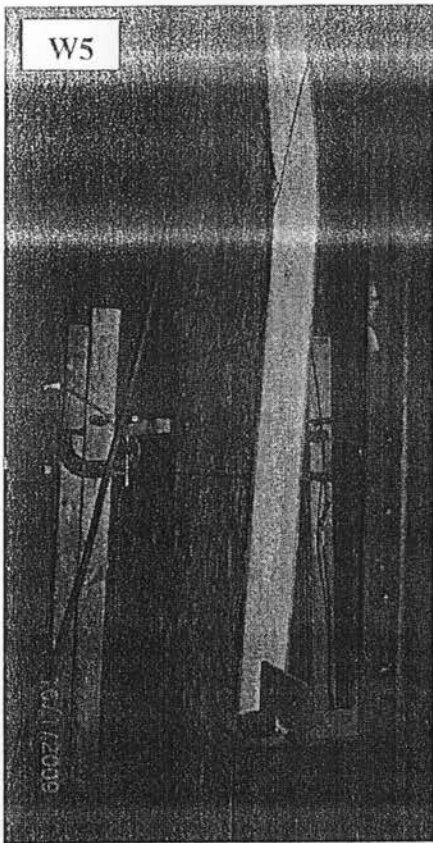


Figure 4.33. View of the failure mode due to OSB crushing near the top quarter point in the south side of wall W5

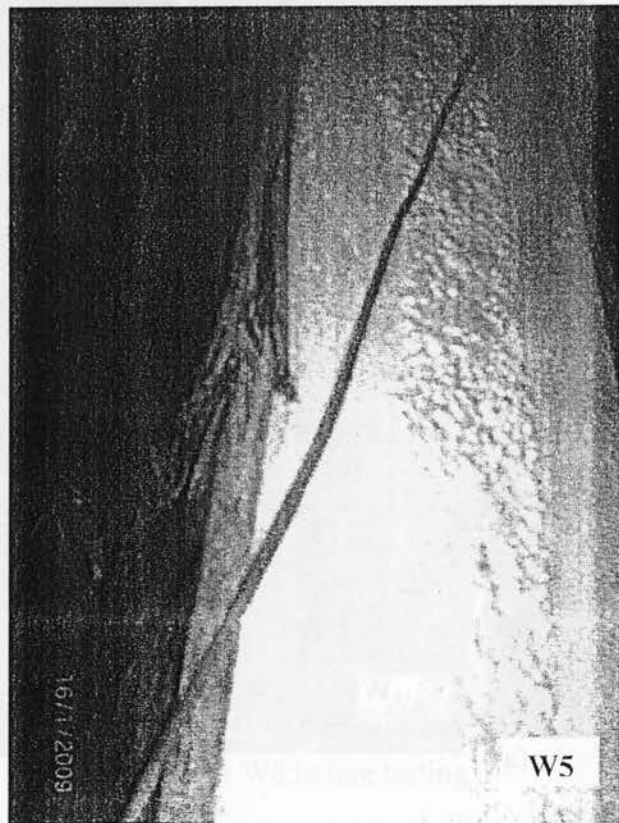
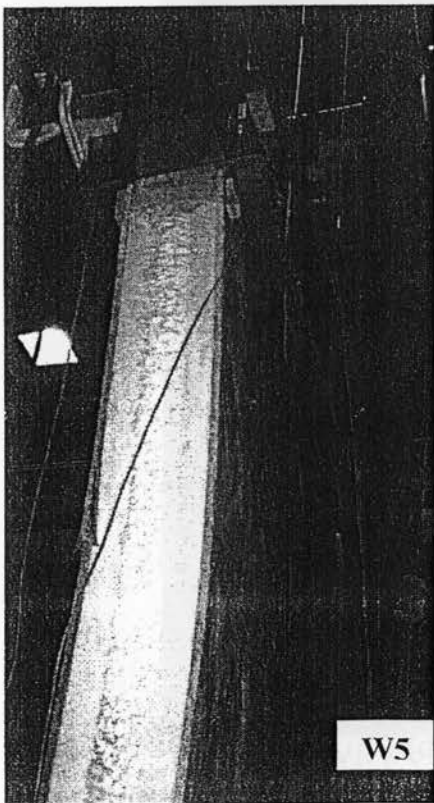


Figure 4.34. Other views of the failure mode at the south-west corner of wall W5

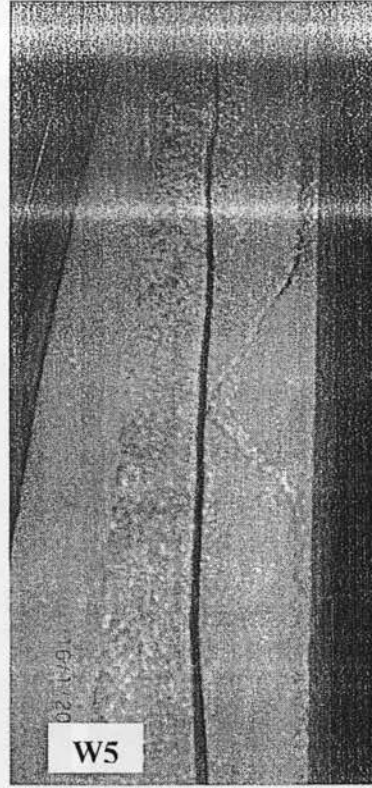
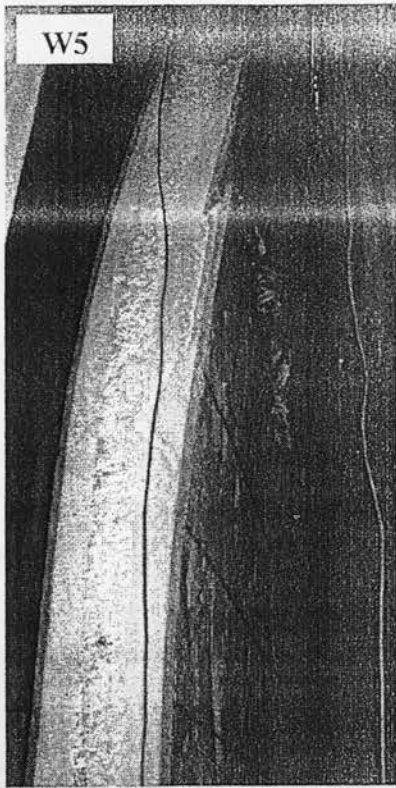
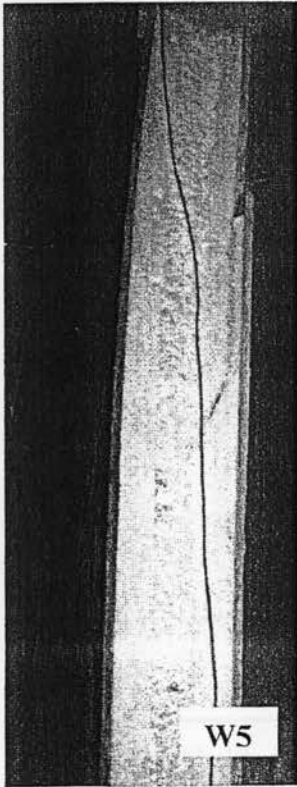
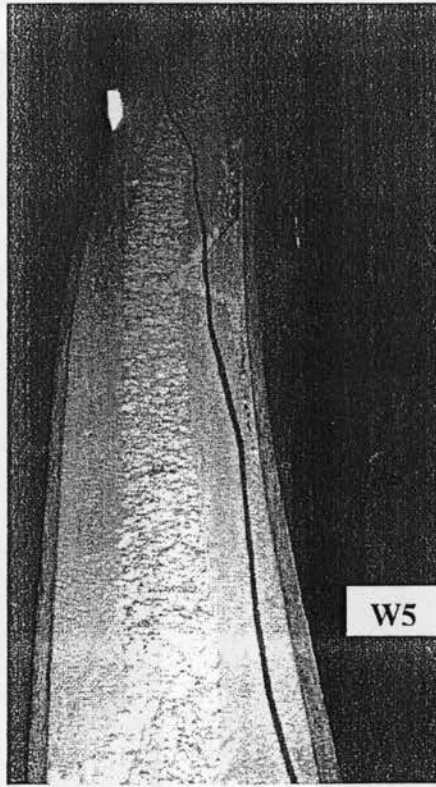


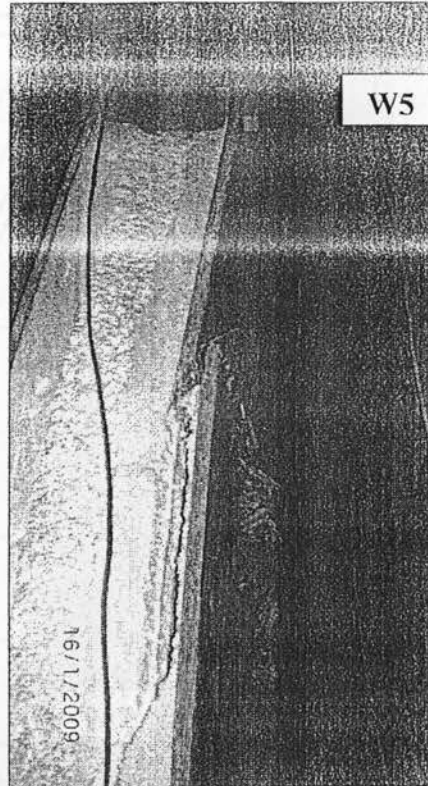
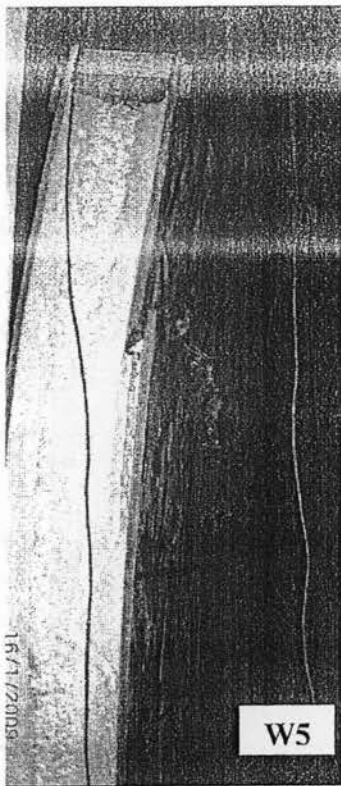
Figure 4.35. Views of the deformed shape of top portion of wall W5 after failure showing OSB crushing in the south side of the wall along with foam-OSB separation



(a)



(b)



(c) (d)
Figure 4.36. Other views of the deformed shape of wall W5

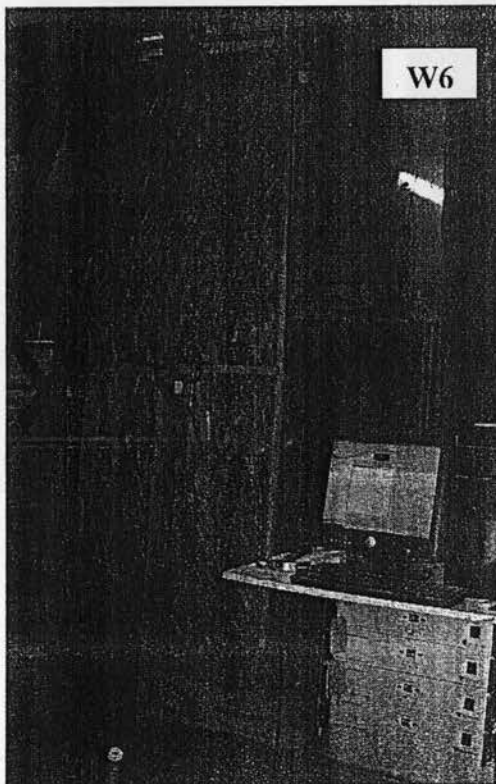


Figure 4.37. View of the test setup for wall W6 before testing

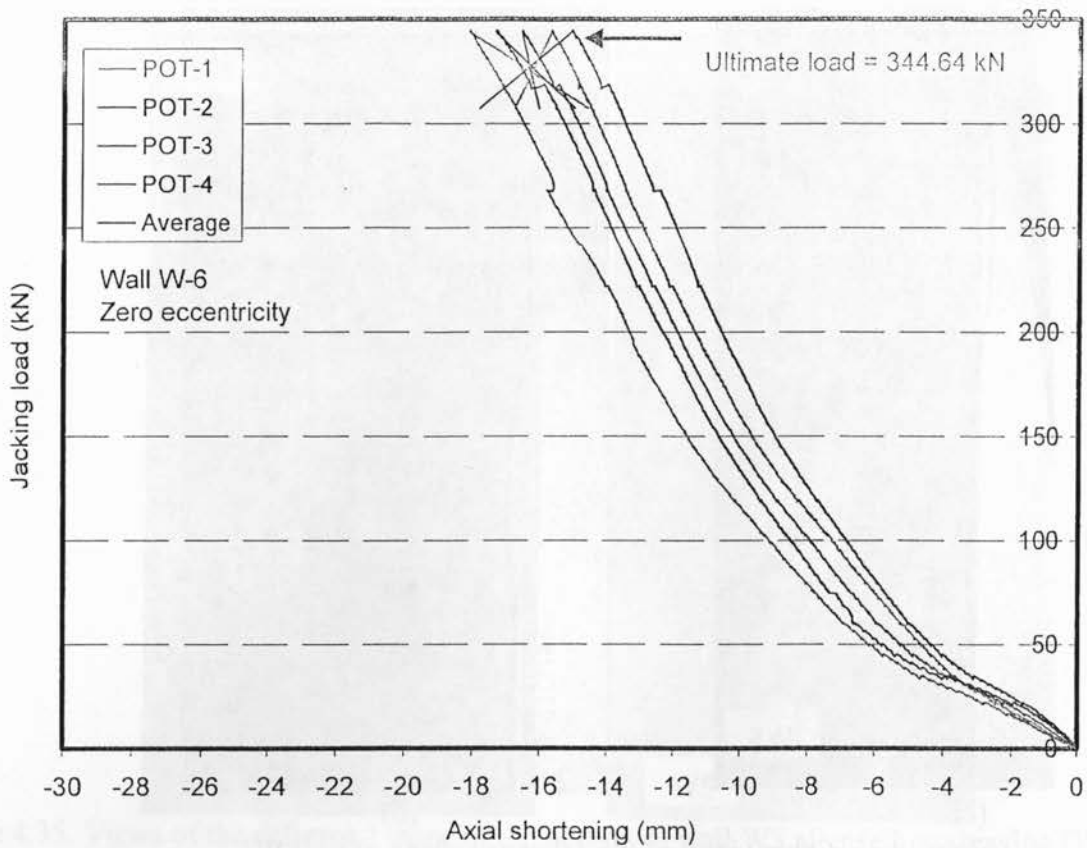


Figure 4.38. Axial load-axial shortening relationship for model W6

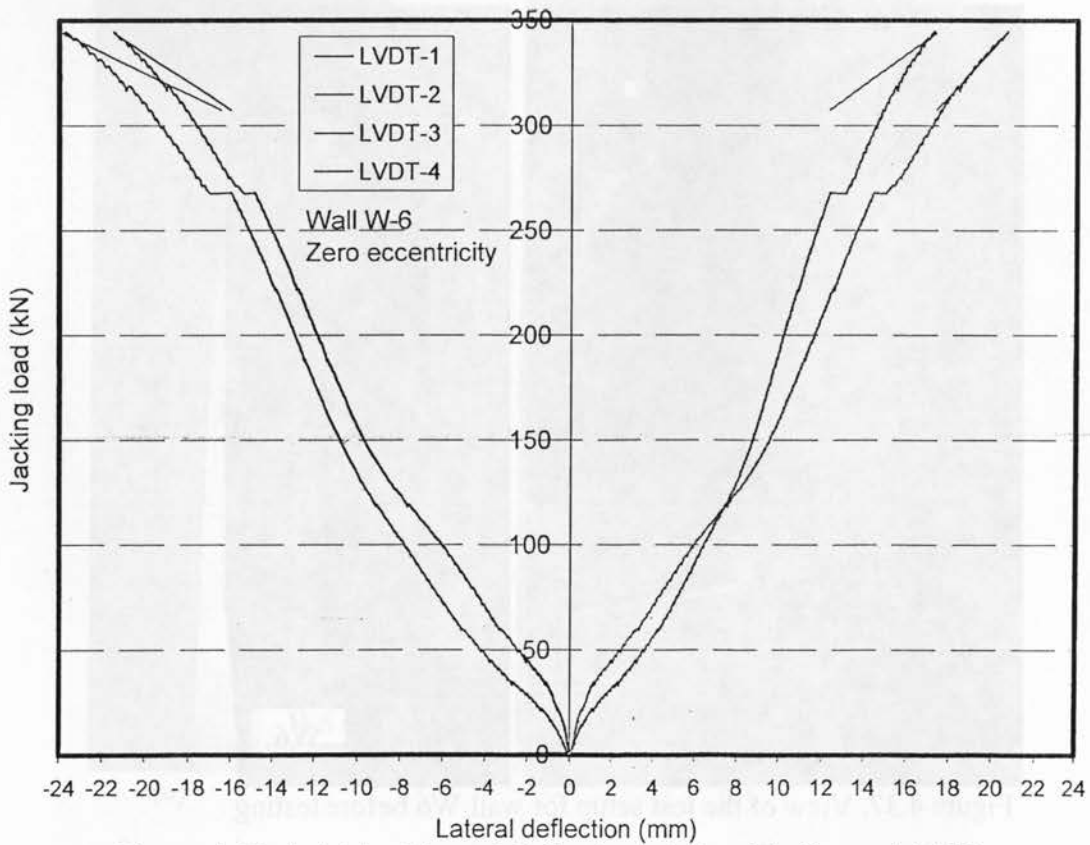


Figure 4.39. Axial load-lateral deflection relationship for model W6

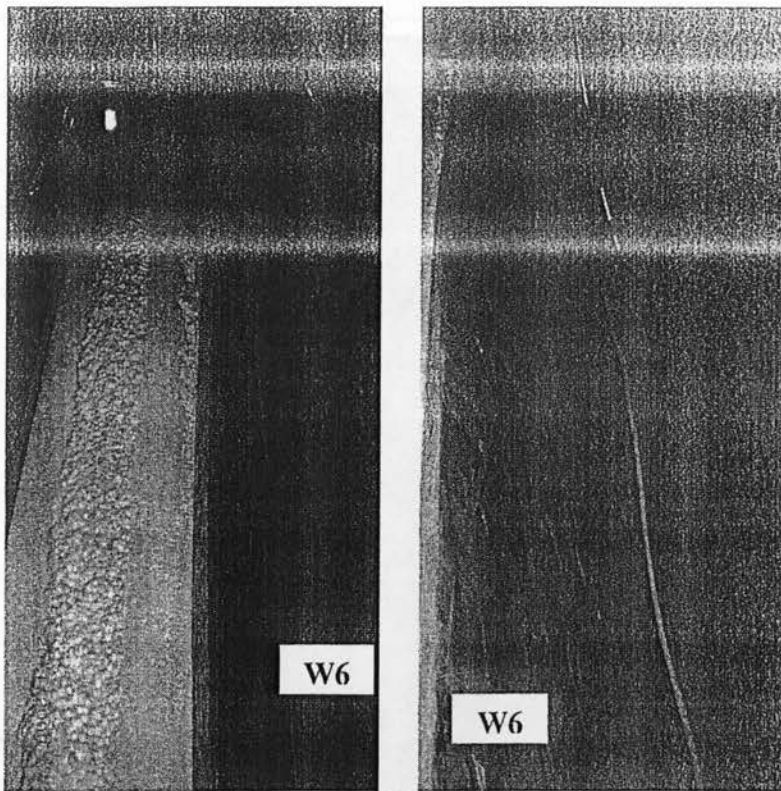


Figure 4.40. View of the failure mode due to OSB crushing at the top of south side of model W6

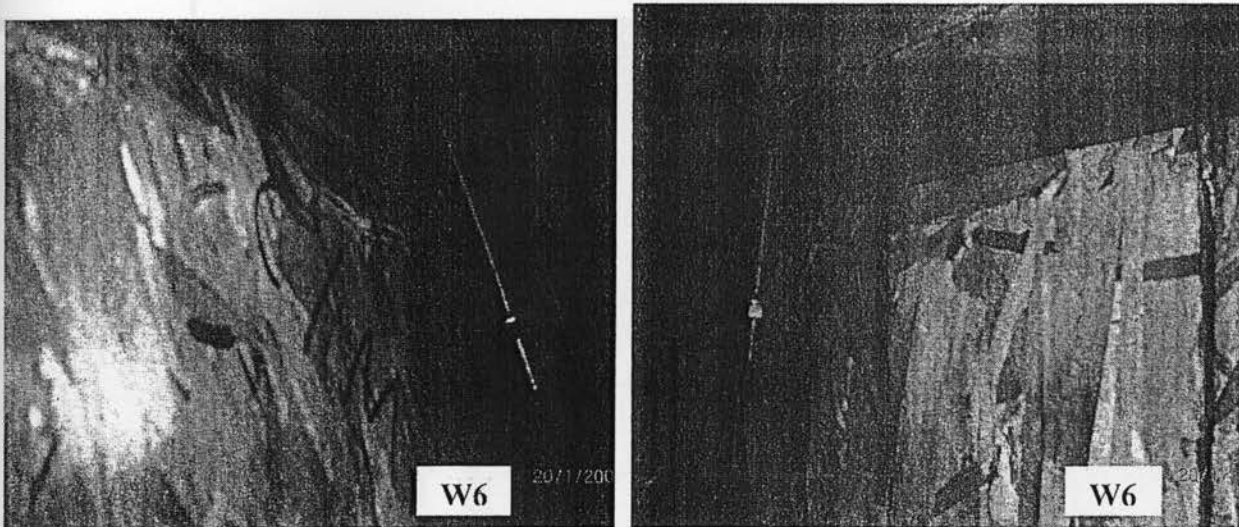


Figure 4.41. Other views of OSB crushing at the top of the south side of wall W6

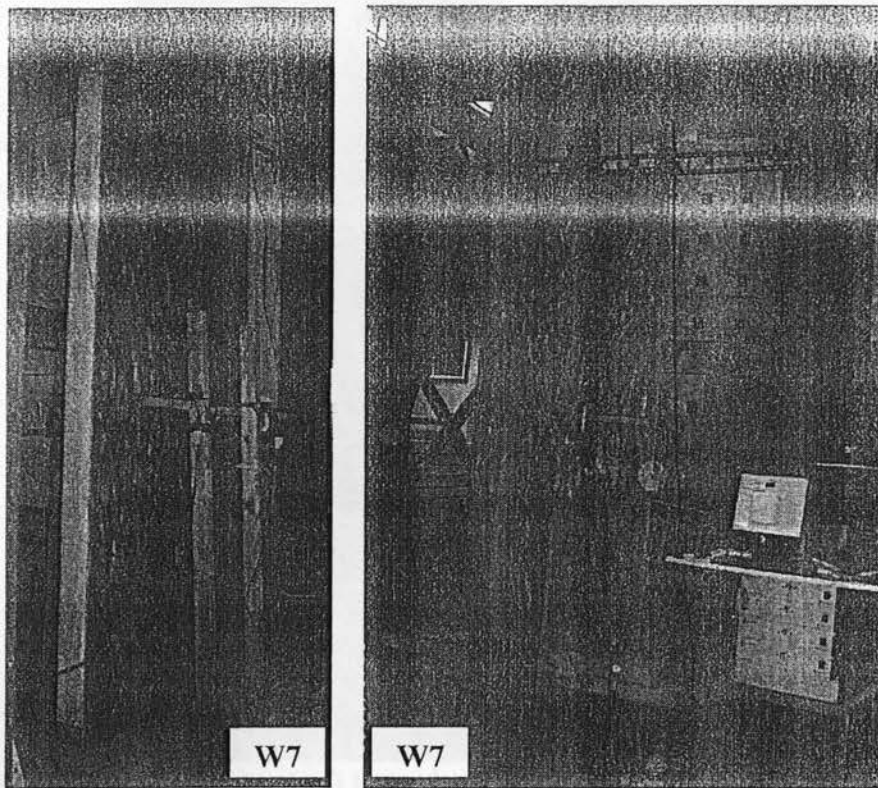


Figure 4.42. Views of the test setup for wall W7 before testing

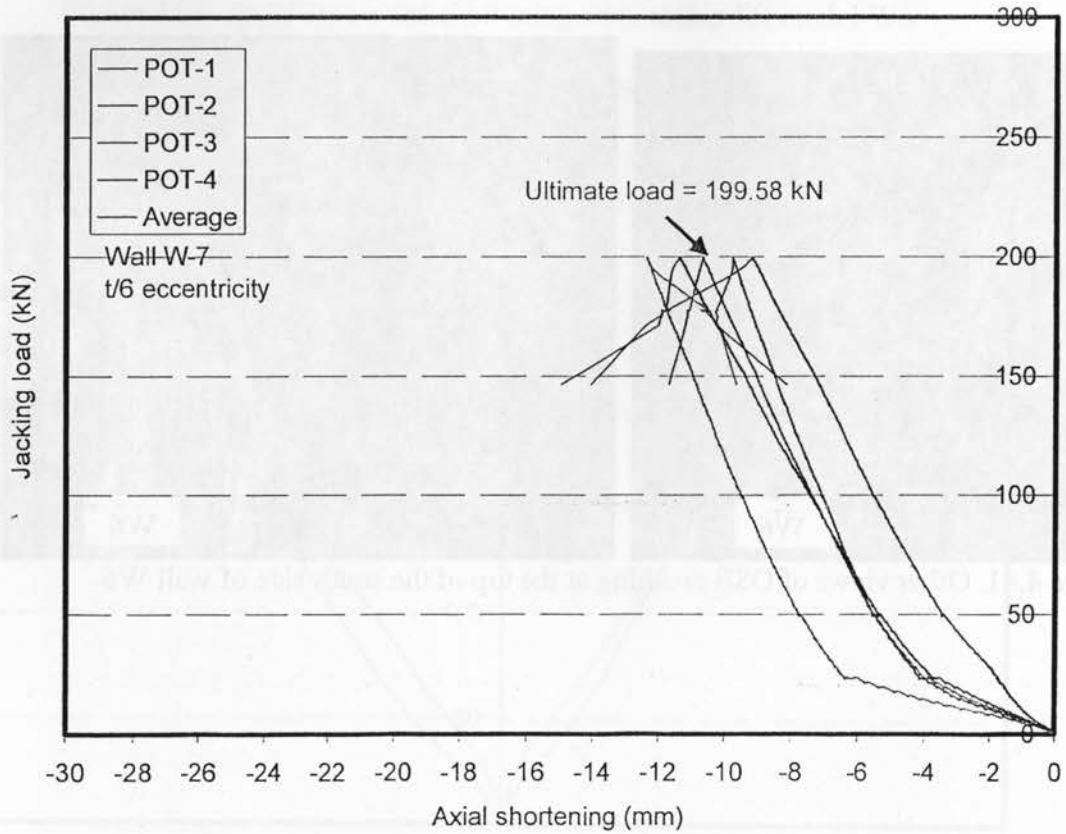


Figure 4.43. Axial load-axial shortening relationship for model W7

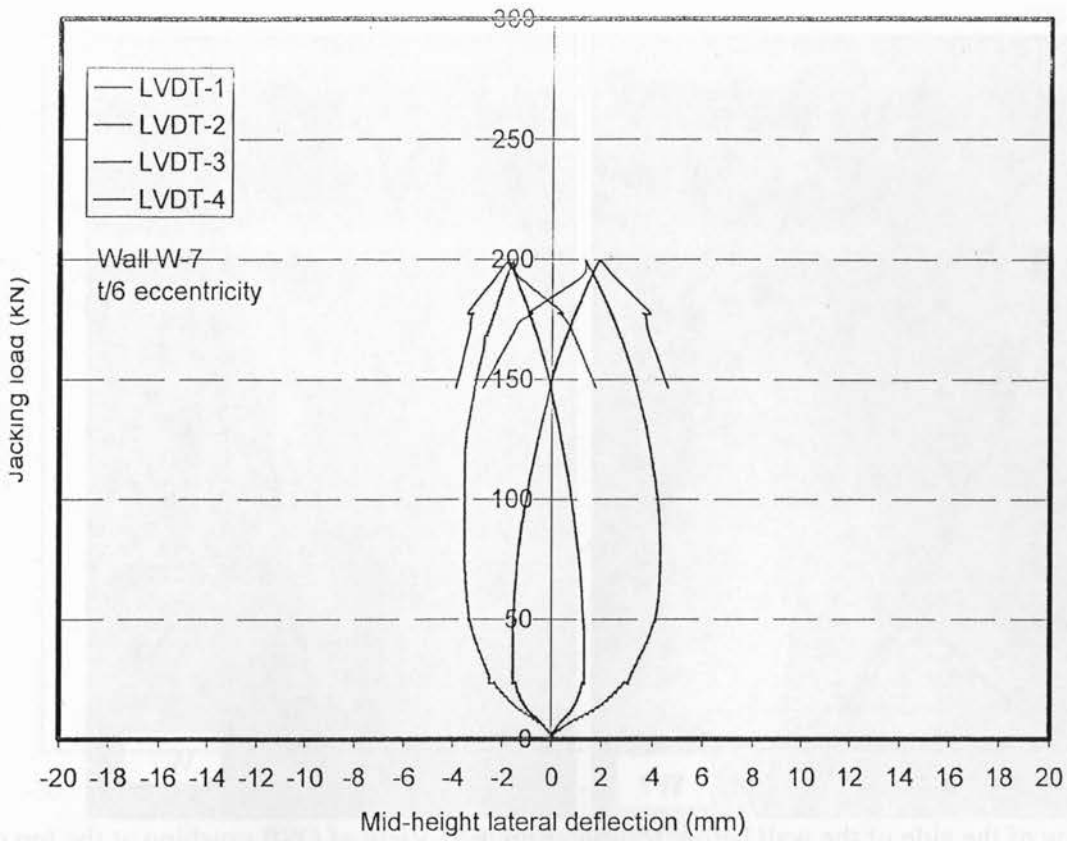


Figure 4.44. Axial load-lateral deflection relationship for model W7

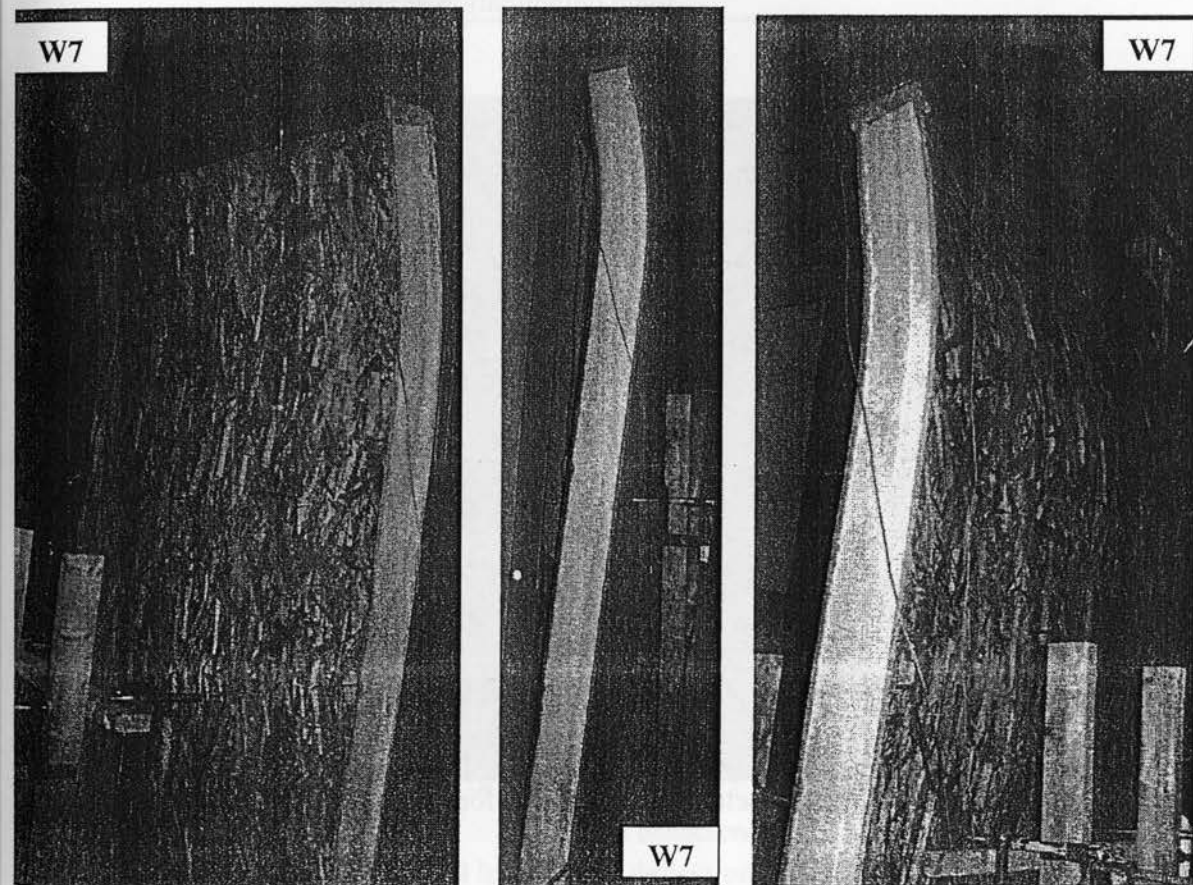


Figure 4.45. Views of the deformed shape of the wall W7 after OSB crushing at its top north side

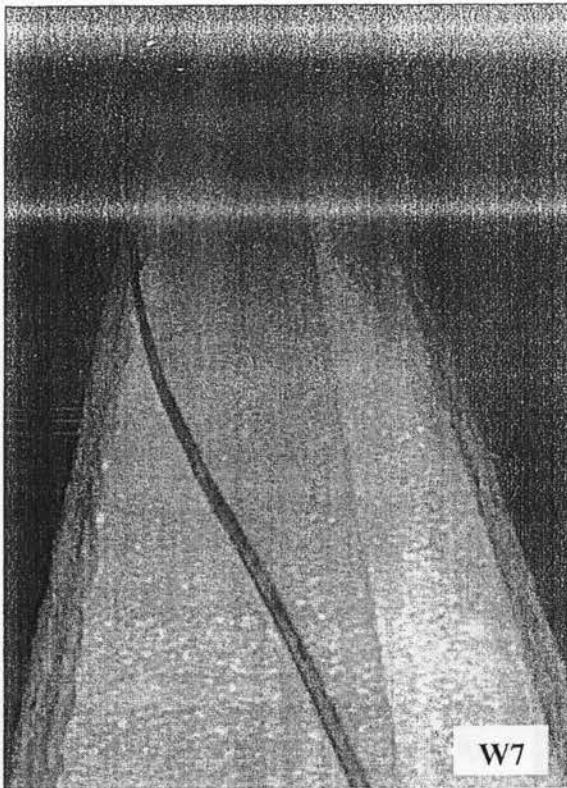


Figure 4.46. View of the side of the wall before testing

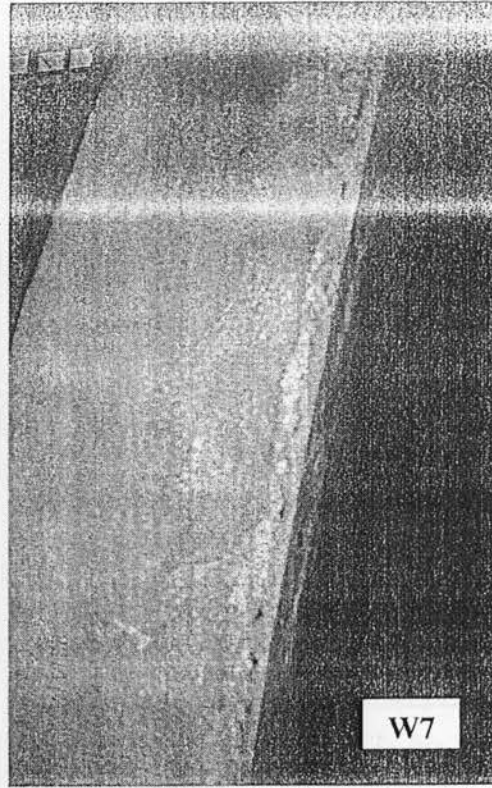


Figure 7. View of OSB crushing at the top of the north side of wall W7 along with OSB-foam delamination at failure

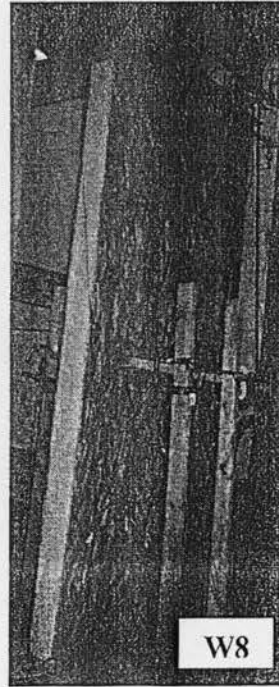
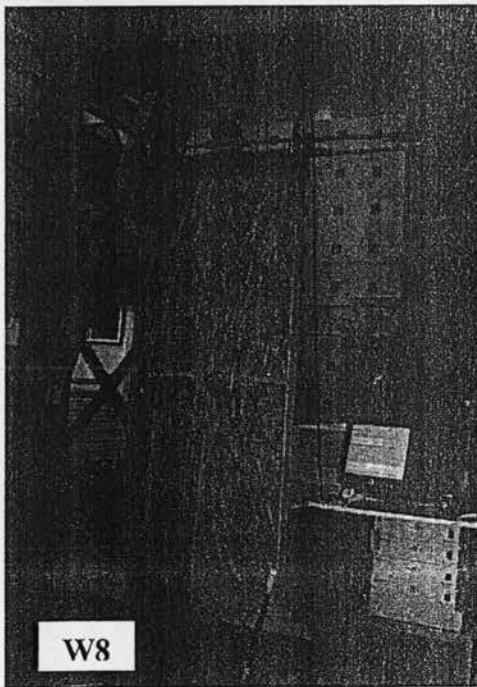


Figure 4.47. Views of the test setup for wall W8 before testing

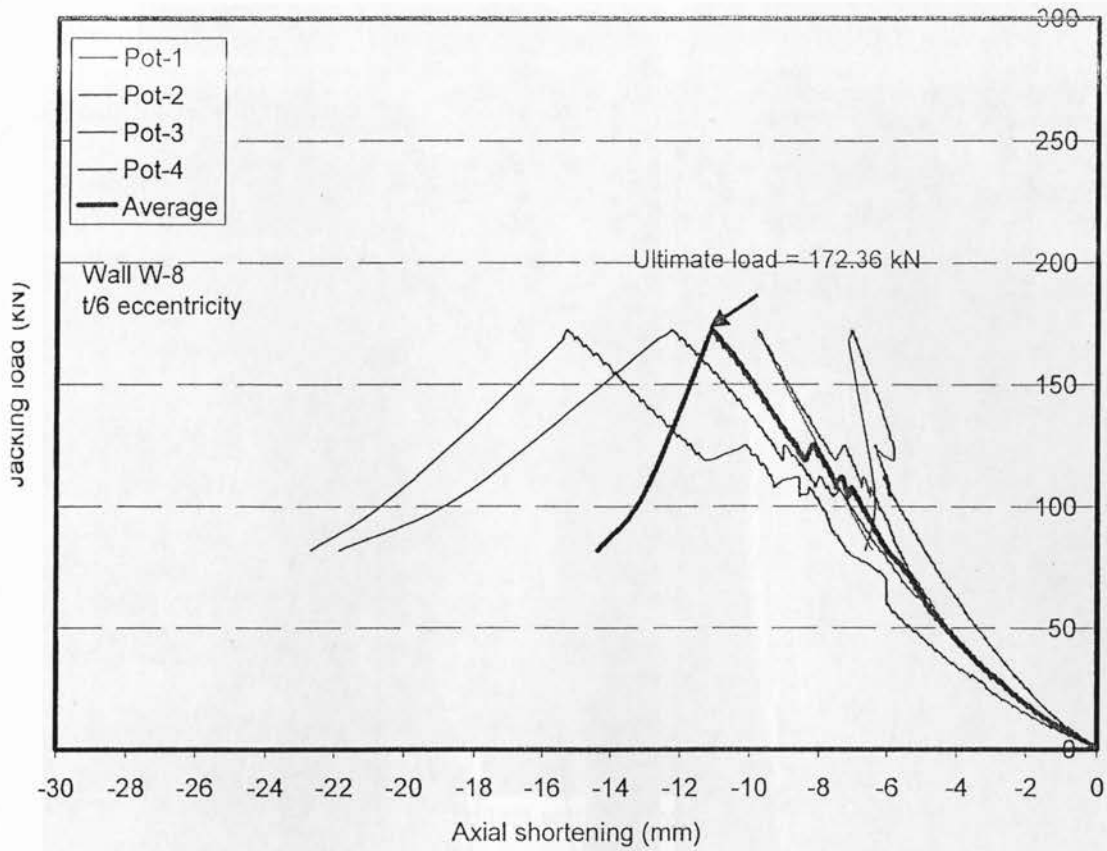


Figure 4.48. Axial load-axial shortening relationship for model W8

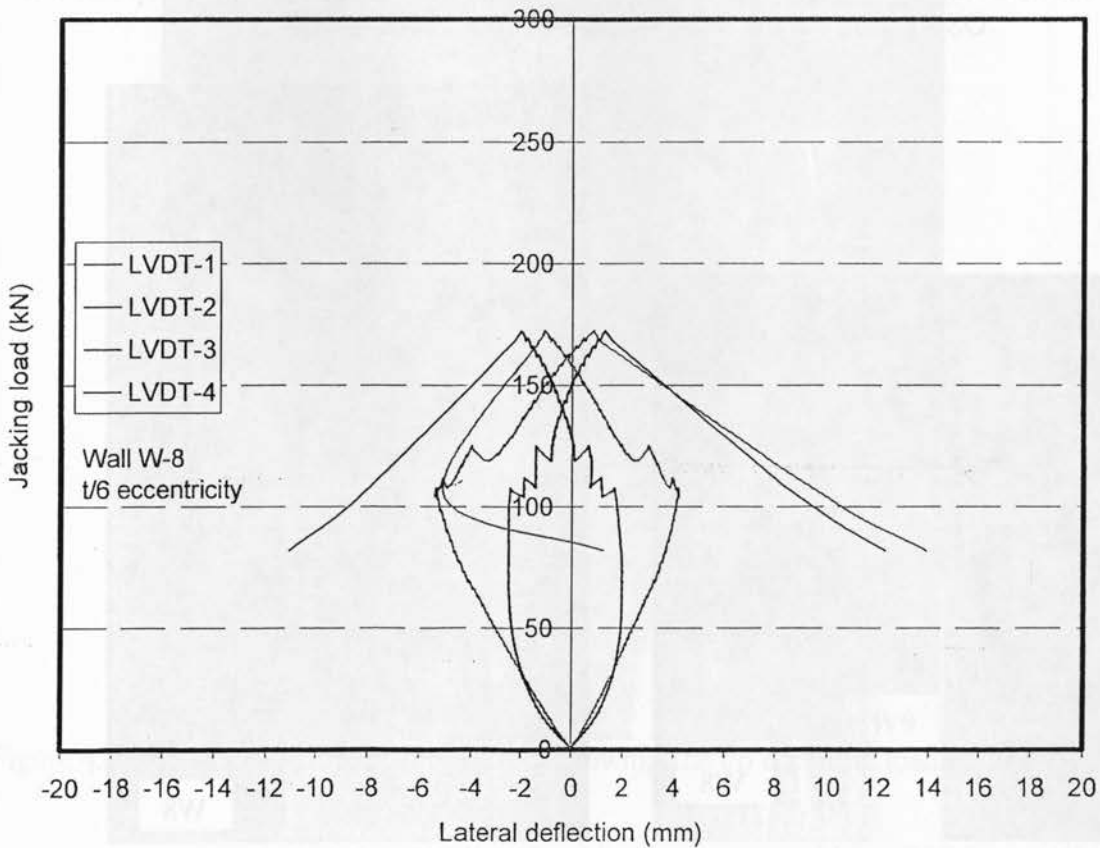


Figure 4.49. Axial load-lateral deflection relationship for model W8

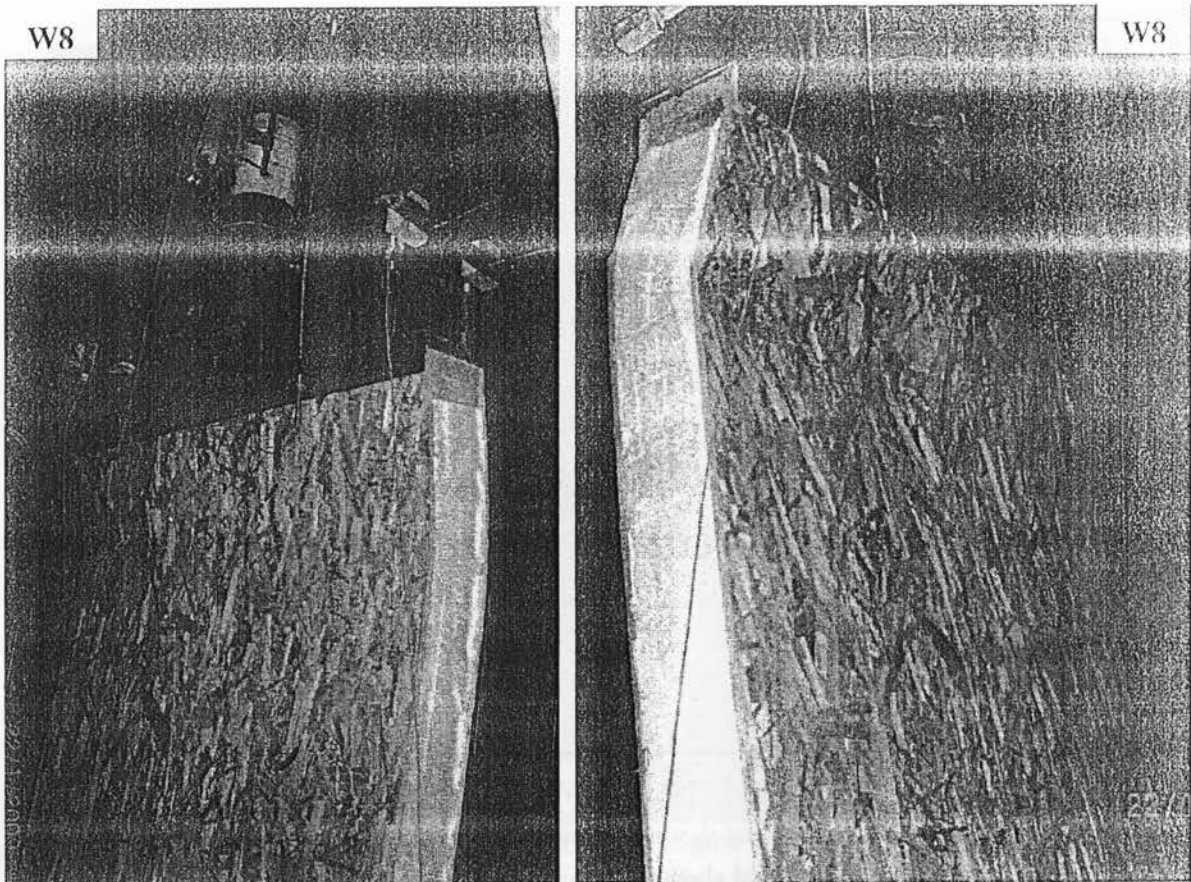


Figure 4.50. Views of the deformed shape of the wall W8 after OSB crushing near its top side and OSB fracture at the same location but on the south side



Figure 4.51. Views of OSB crushing near the top side of Wall W8 and OSB fracture at the same location but on the south side

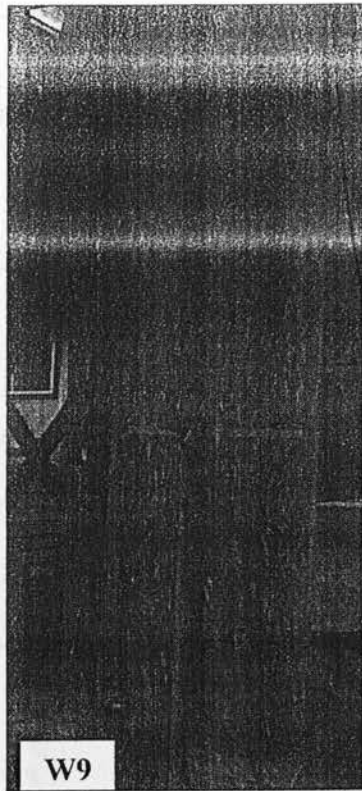


Figure 4.52. Views of the test setup for wall W9 before testing

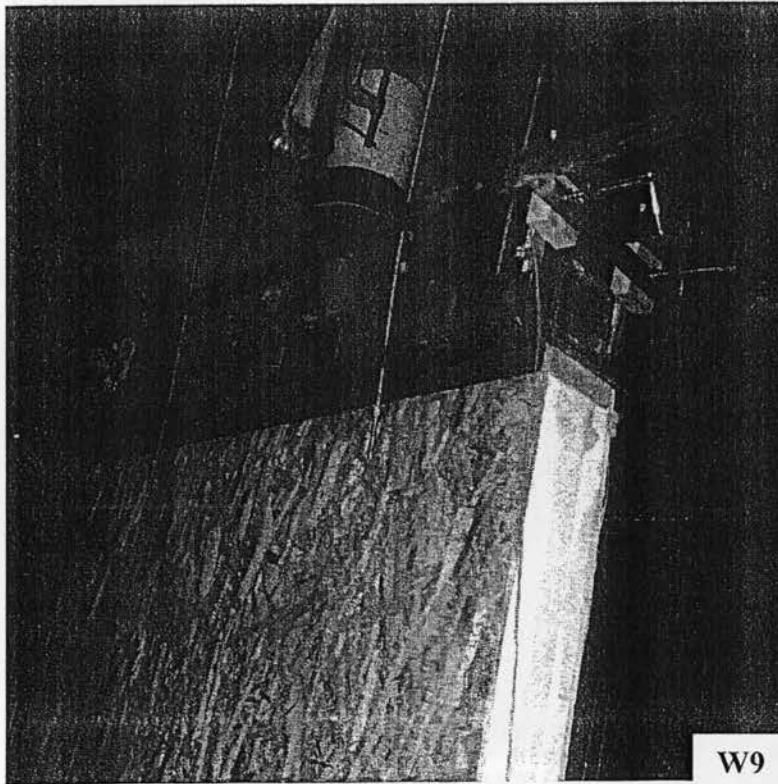


Figure 4.53. View of the top loading system showing the $t/6$ eccentric loading condition

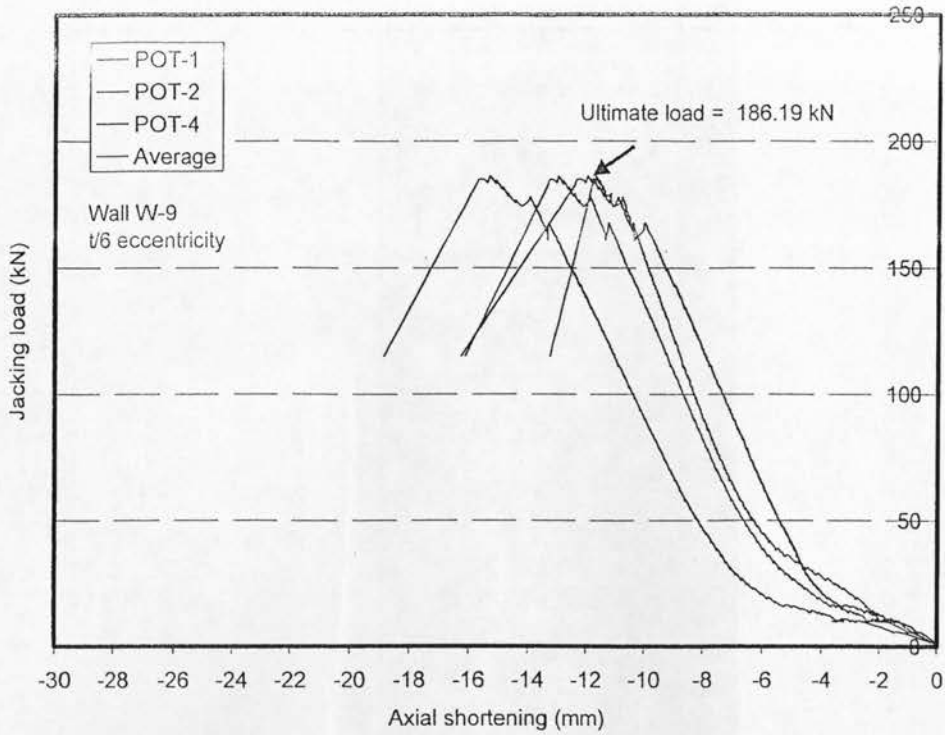


Figure 4.54. Axial load-axial shortening relationship for model W9

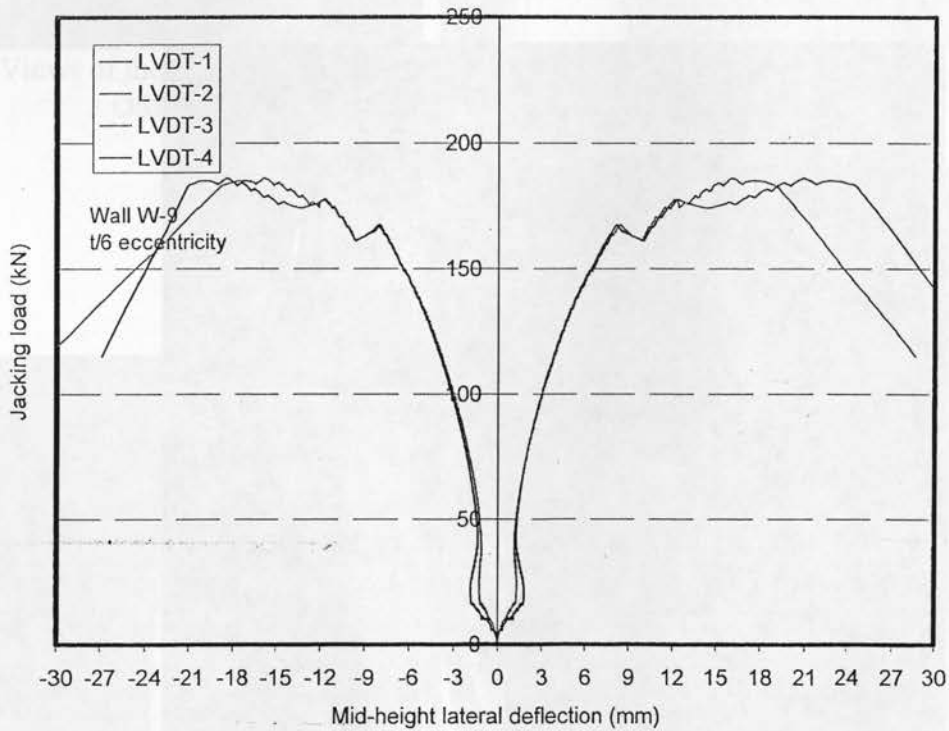


Figure 4.55. Axial load-lateral deflection relationship for model W9

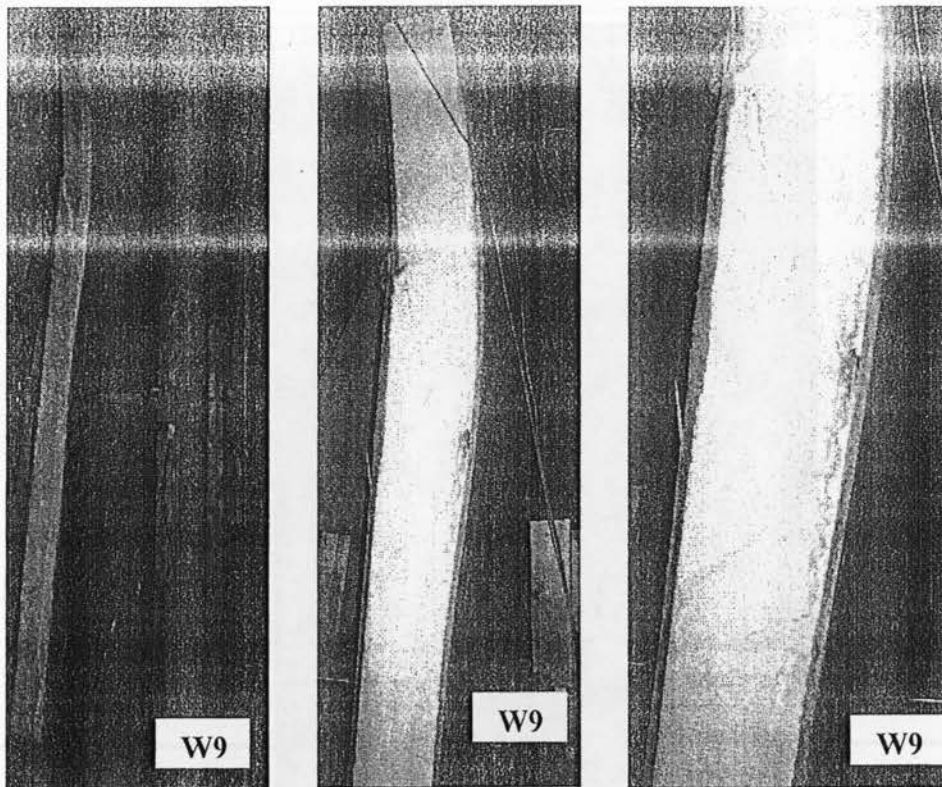


Figure 4.56. Views of the deformed shape of the east side of wall W9 showing OSB crushing near its top quarter point in addition to foam shear failure and OSB-foam delamination

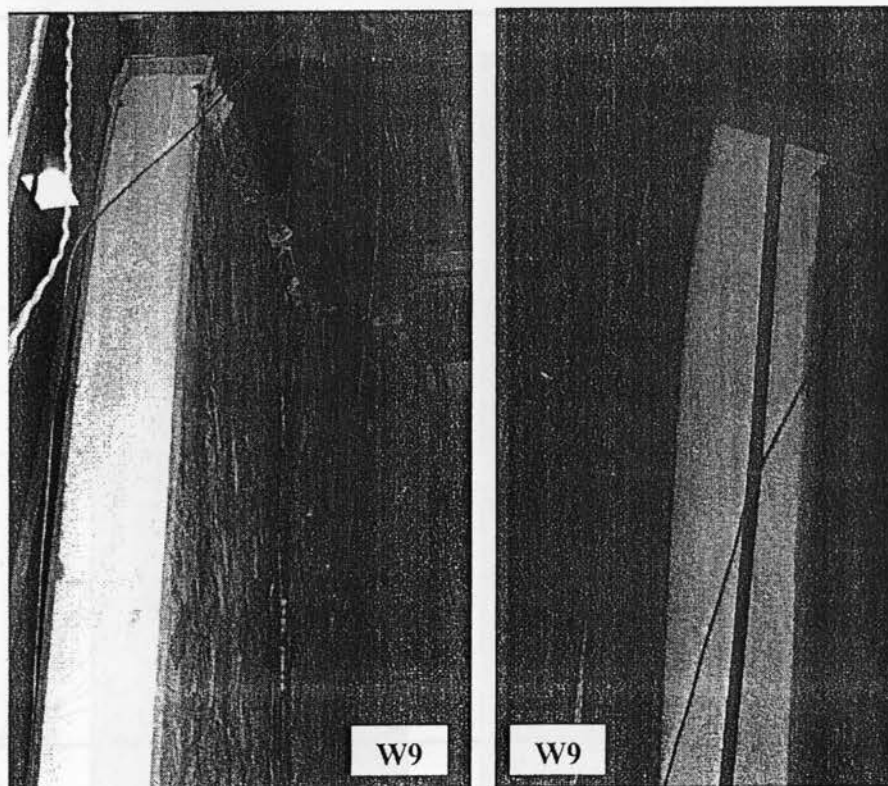


Figure 4.57. Views of OSB crushing near the top of the south side of Wall W9 in addition to OSB crushing near the quarter point of the south-east side

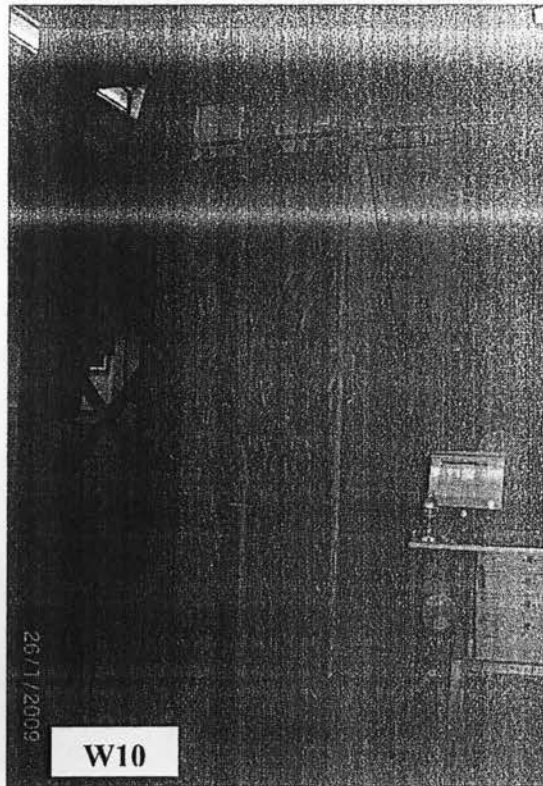


Figure 4.58. Views of the test setup for wall W10 before testing

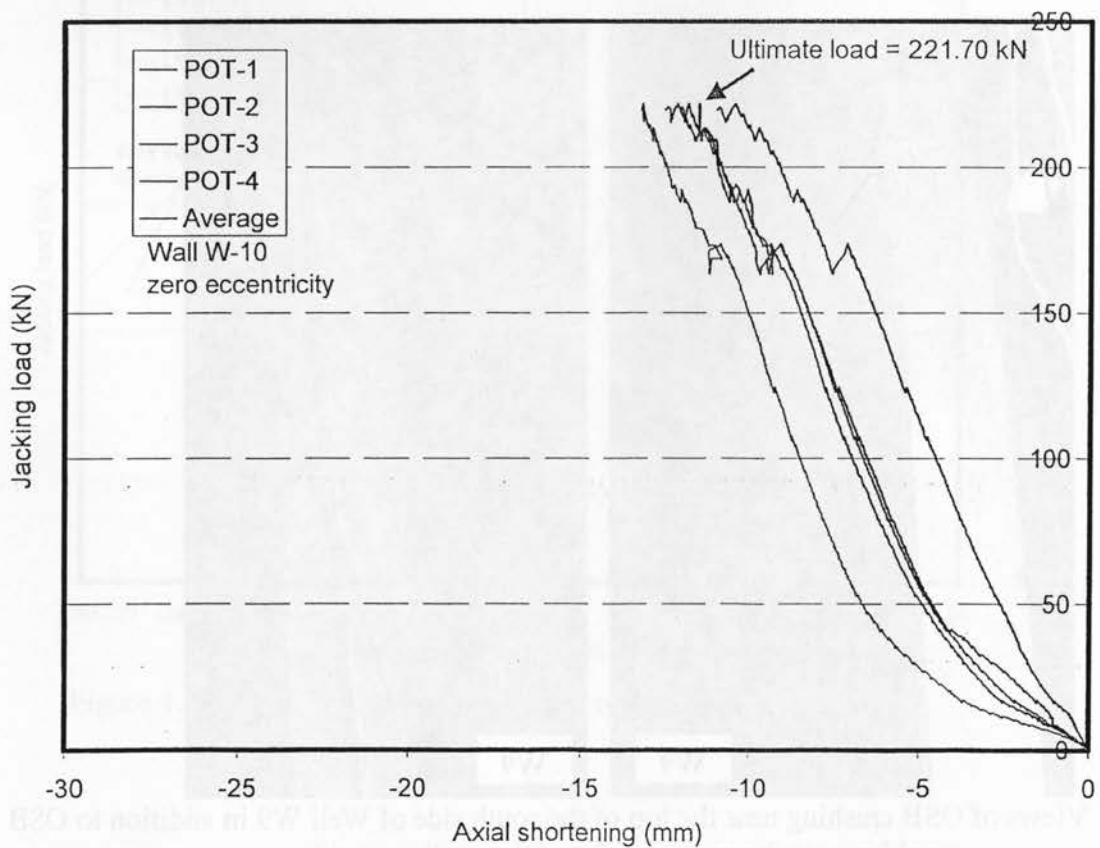


Figure 4.59. Axial load-axial shortening relationship for model W10

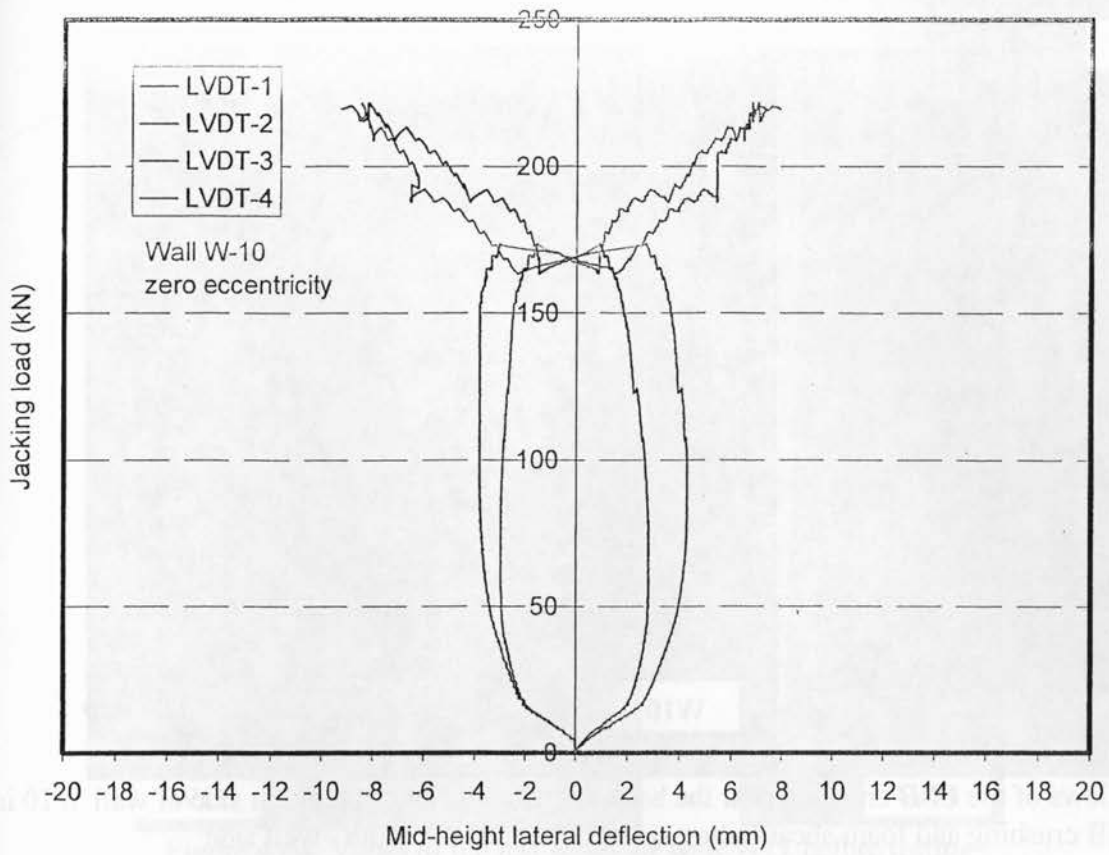


Figure 4.60. Axial load-lateral deflection relationship for model W10

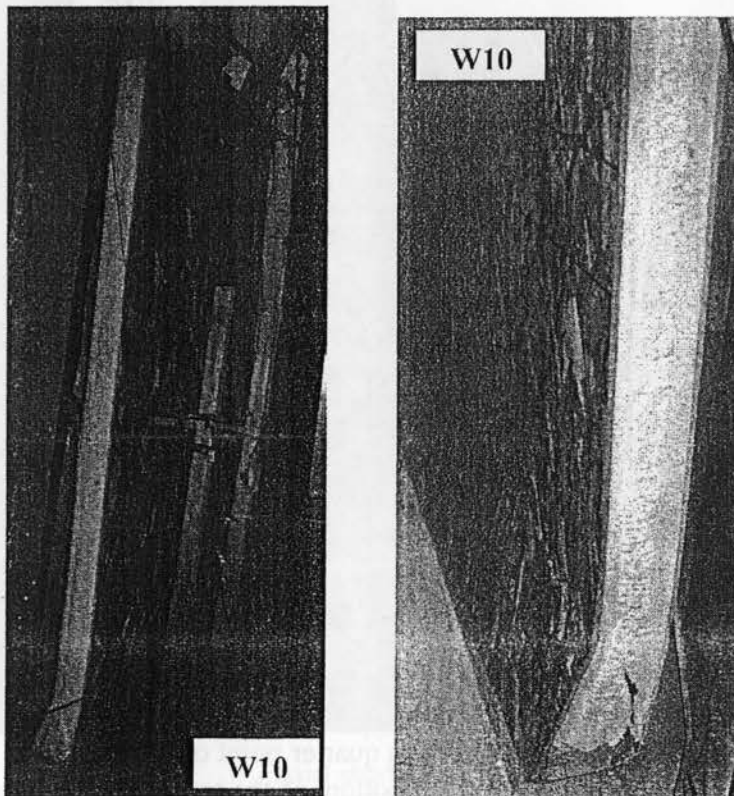


Figure 4.61. Views of the deformed shape of the west side of wall W10

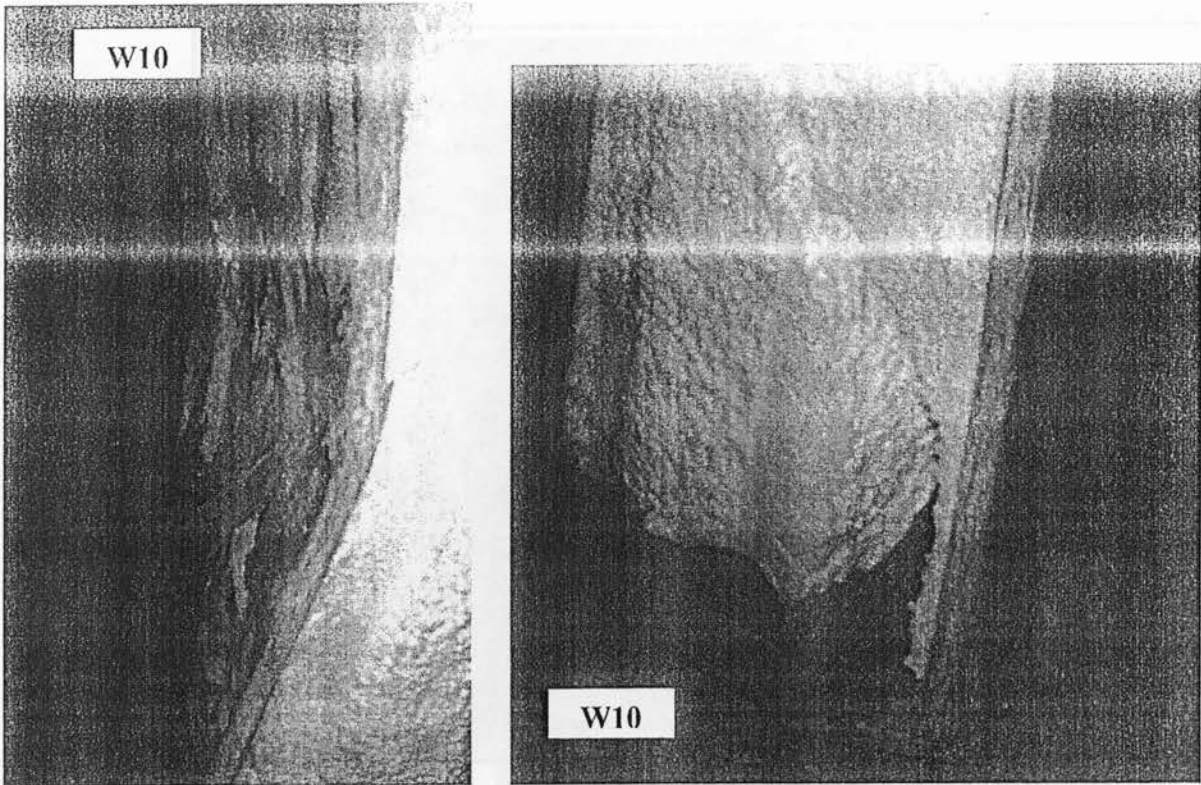


Figure 4.62. Views of the OSB crushing near the bottom quarter point of the north side of wall W10 in addition to OSB crushing and foam shear failure at the bottom of the south –west side

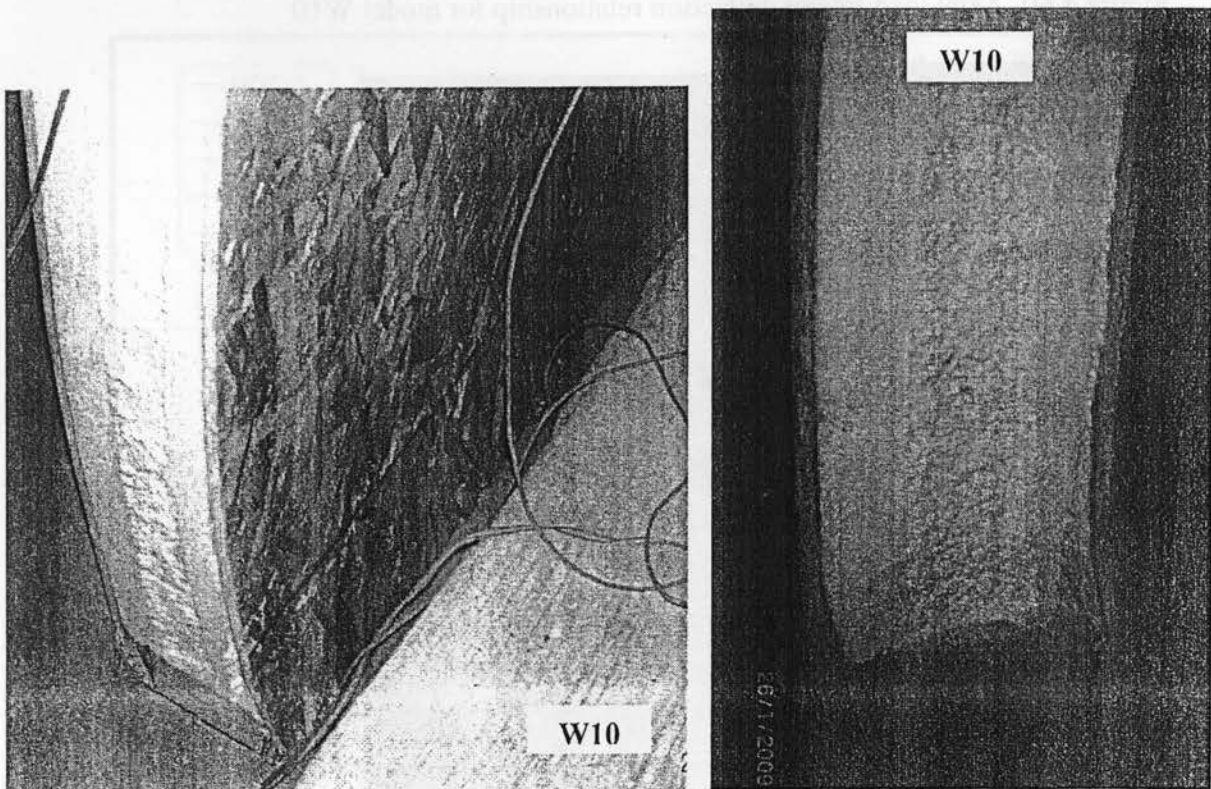


Figure 4.63. Views of the OSB crushing near the bottom quarter point of the north side of wall W10 in addition to OSB crushing and foam shear failure at the bottom of the south–east and north-east sides

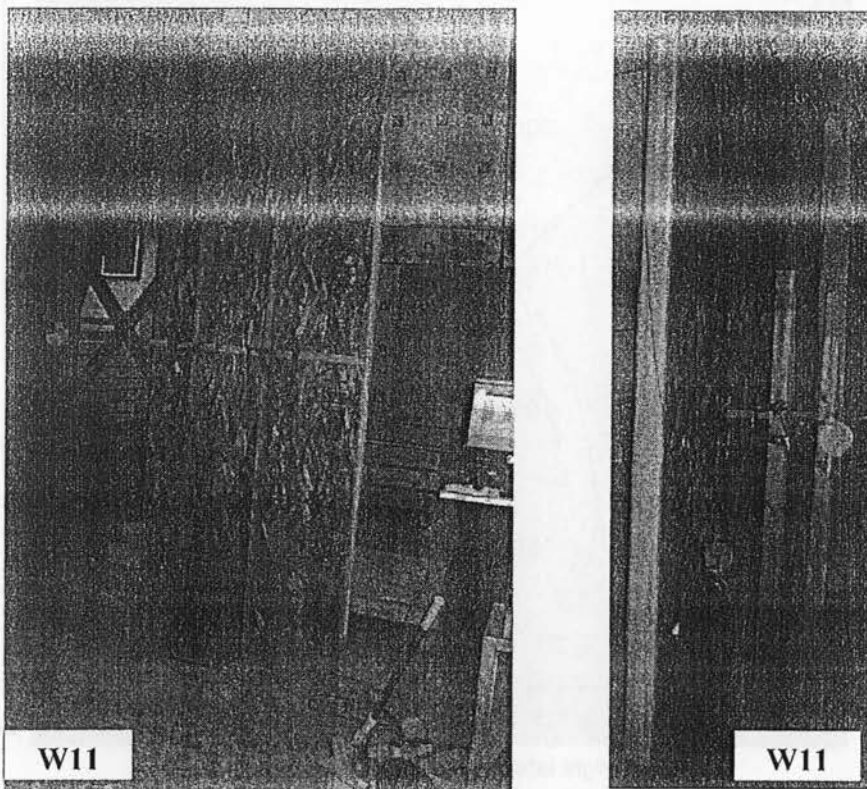


Figure 4.64. Views of the test setup for wall W11 before testing

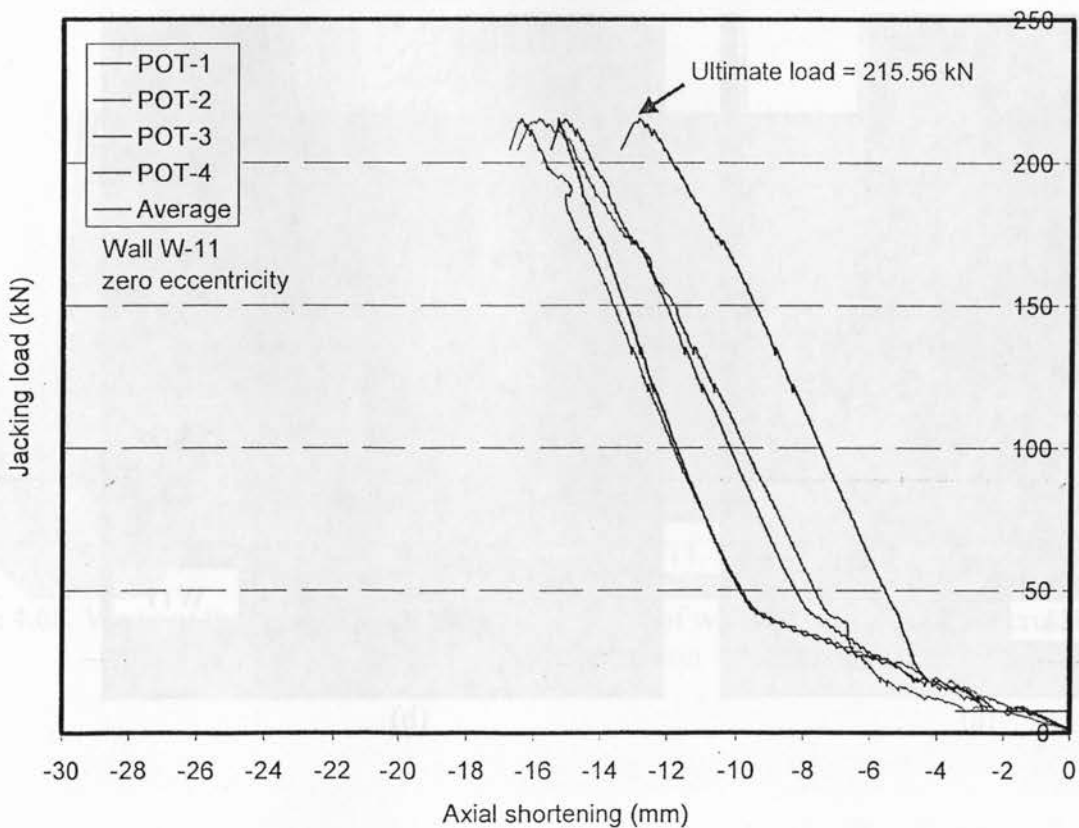


Figure 4.65. Axial load-axial shortening relationship for model W11

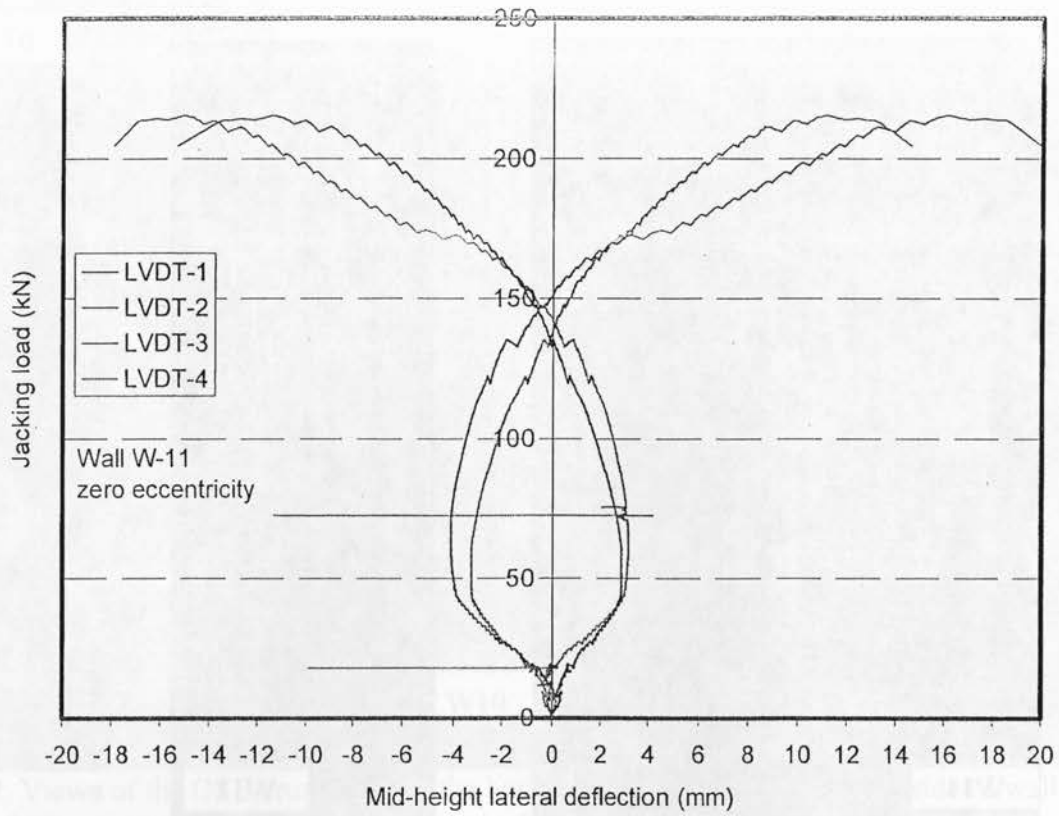
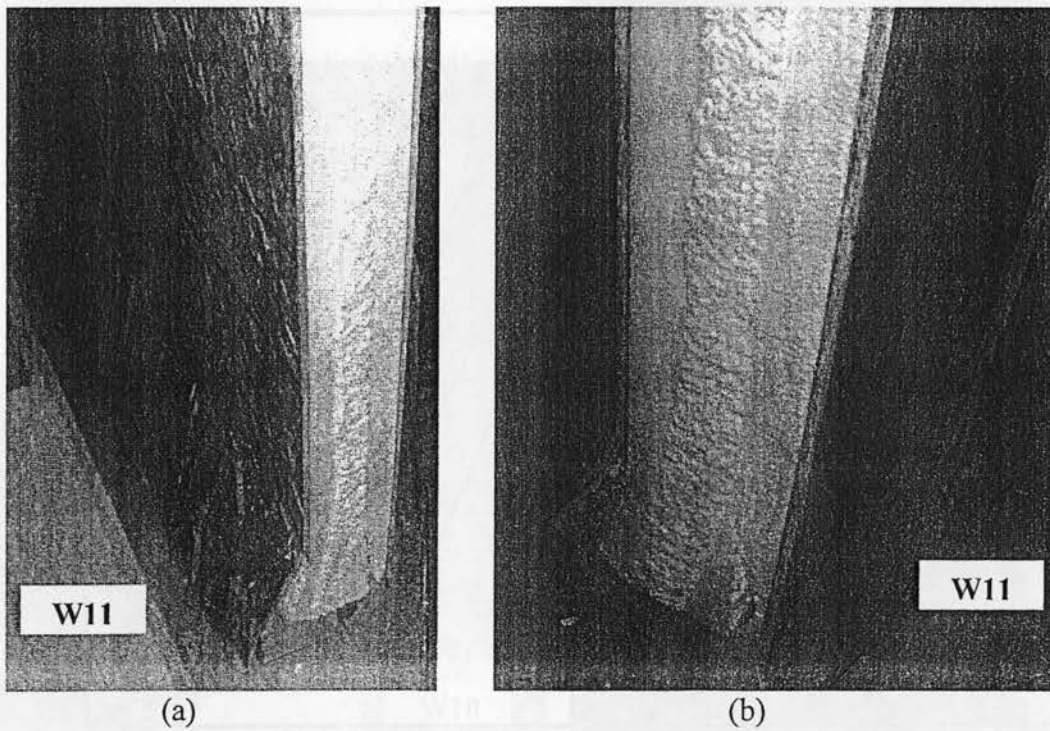
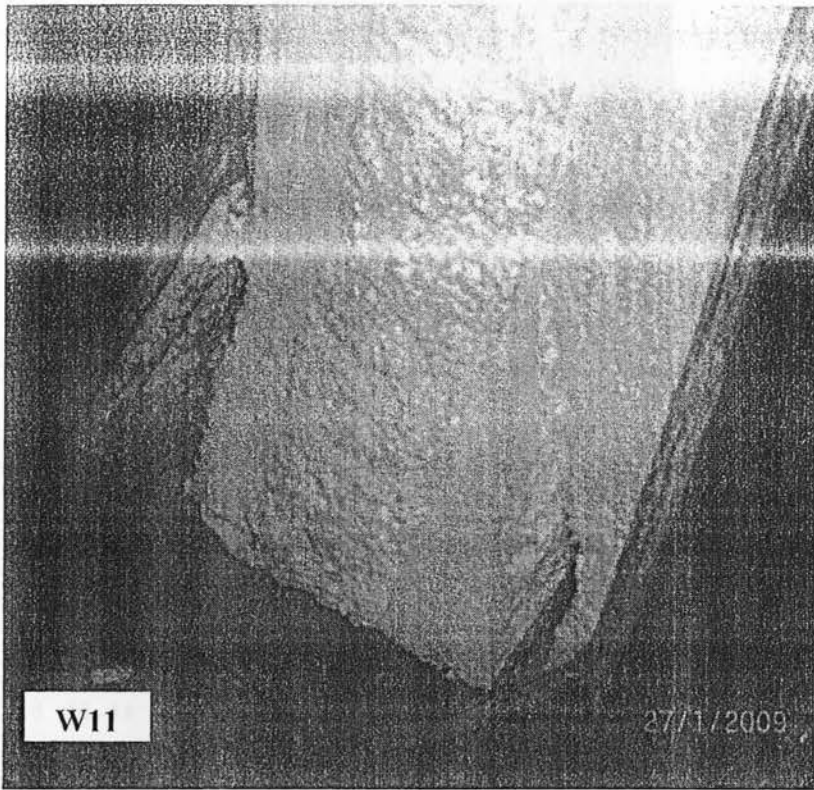


Figure 4.66. Axial load-lateral deflection relationship for model W11





(c)

Figure 4.67. Views of the deformed shape of the west side of wall W11 showing OSB crushing, foam shear failure and foam-OSB delamination

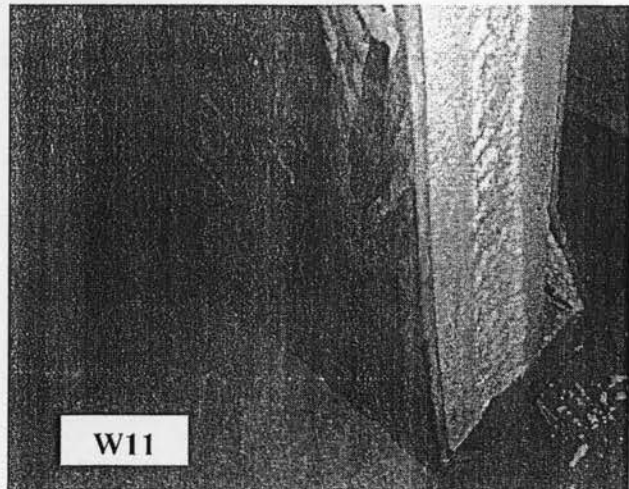
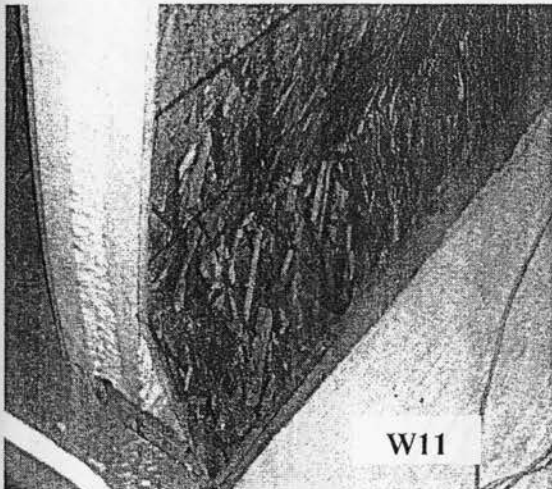


Figure 4.68. Views of the deformed shape of the east side of wall W11 showing OSB crushing and foam-OSB delamination



Figure 4.69. Views of the test setup for wall W12 before testing

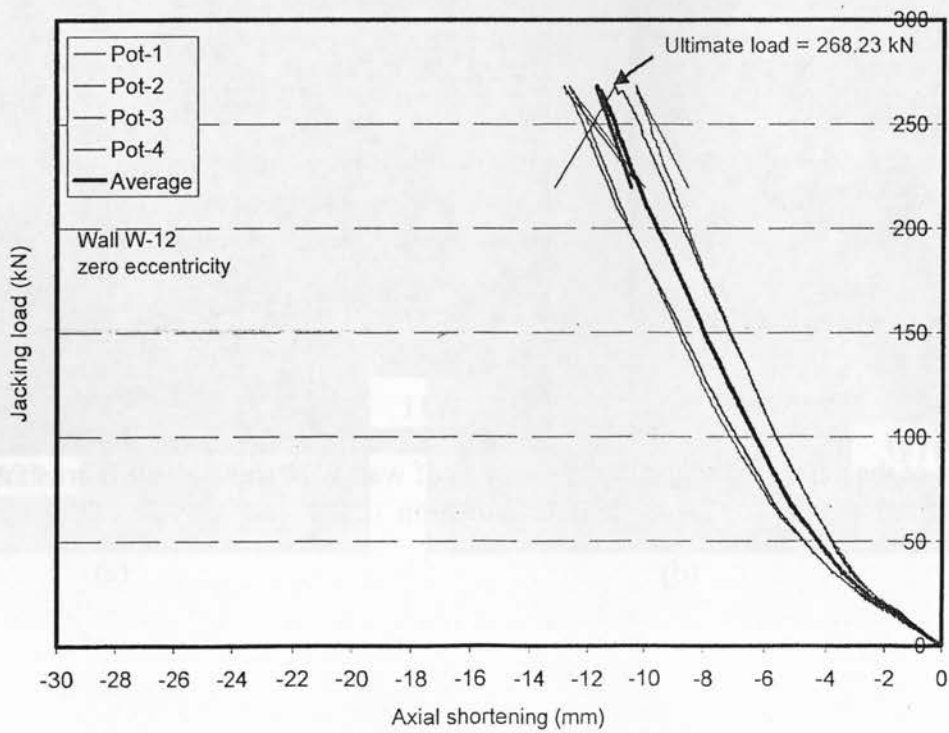


Figure 4.70. Axial load-axial shortening relationship for model W12

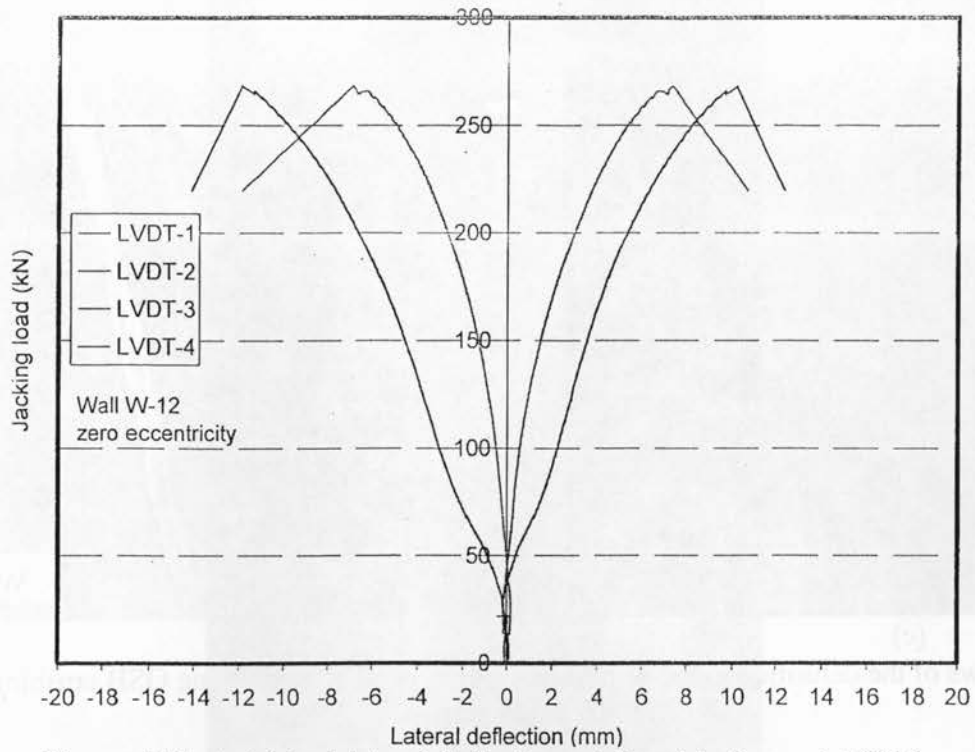
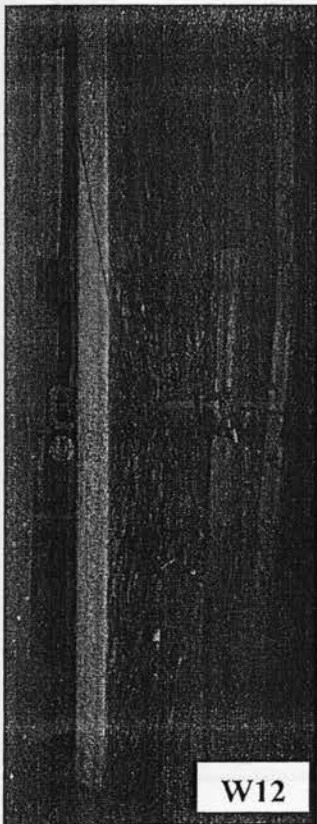
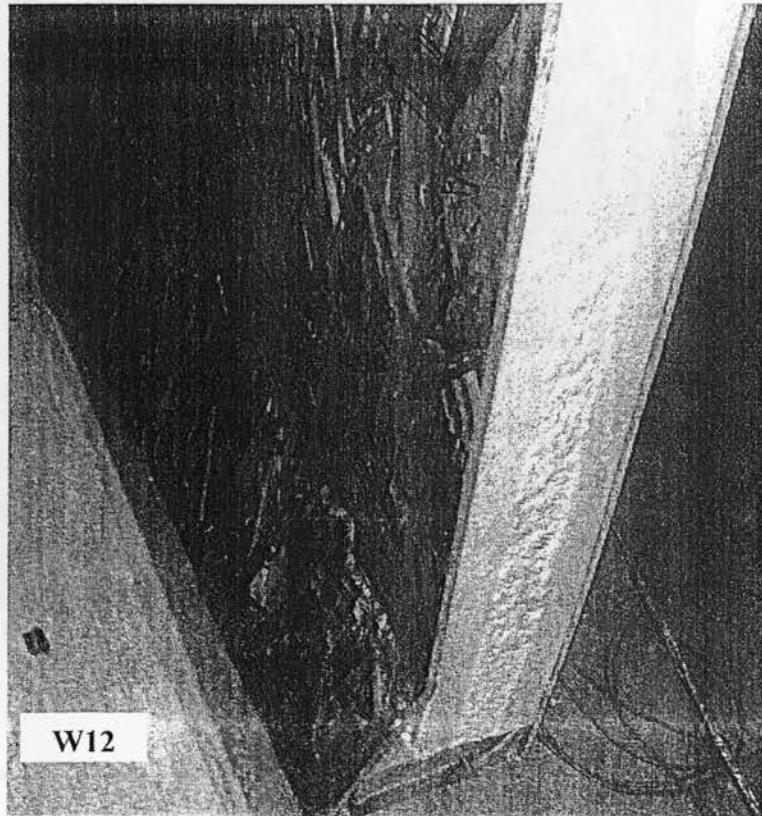


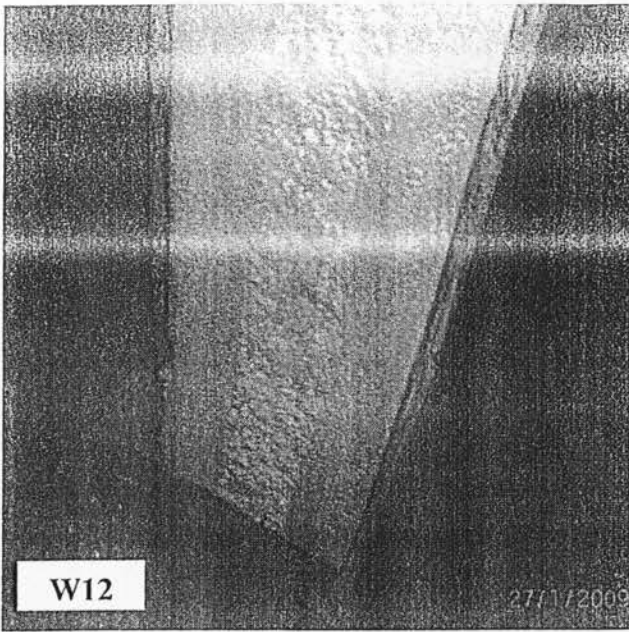
Figure 4.71. Axial load-lateral deflection relationship for model W12



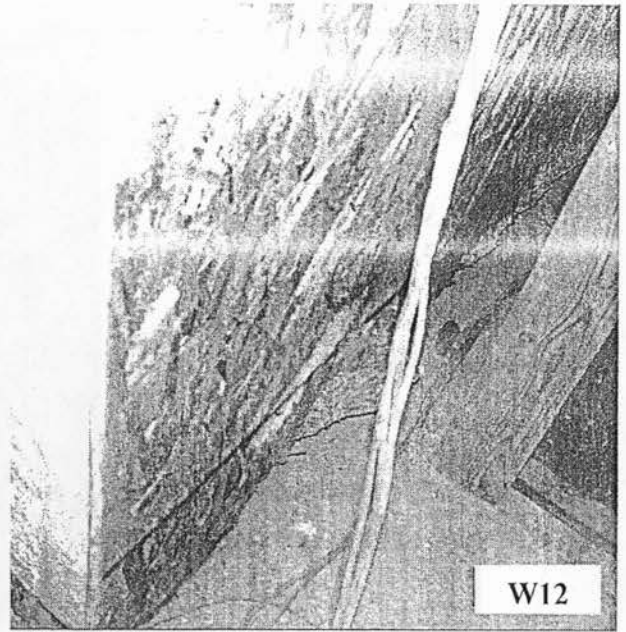
(a)



(b)



(c)



(d)

Figure 4.72 Views of the deformed shape of the west side of wall W12 showing OSB crushing and foam-OSB delamination

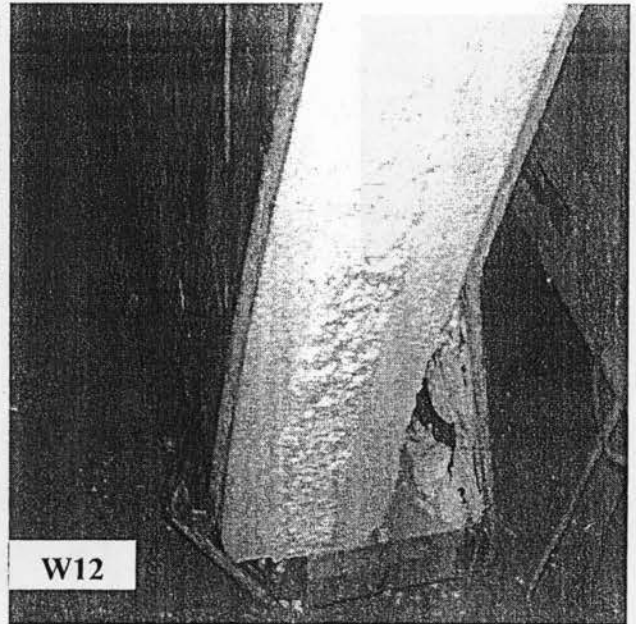
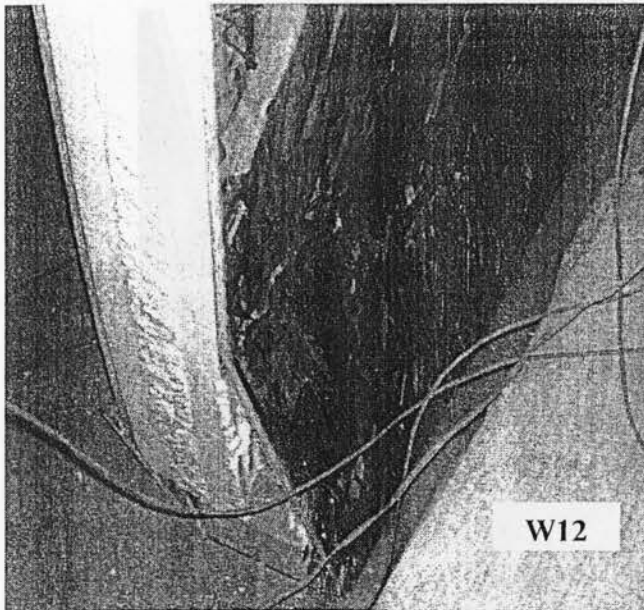


Figure 4.73. Views of the deformed shape of the east side of wall W12 showing OSB crushing and foam-OSB delamination

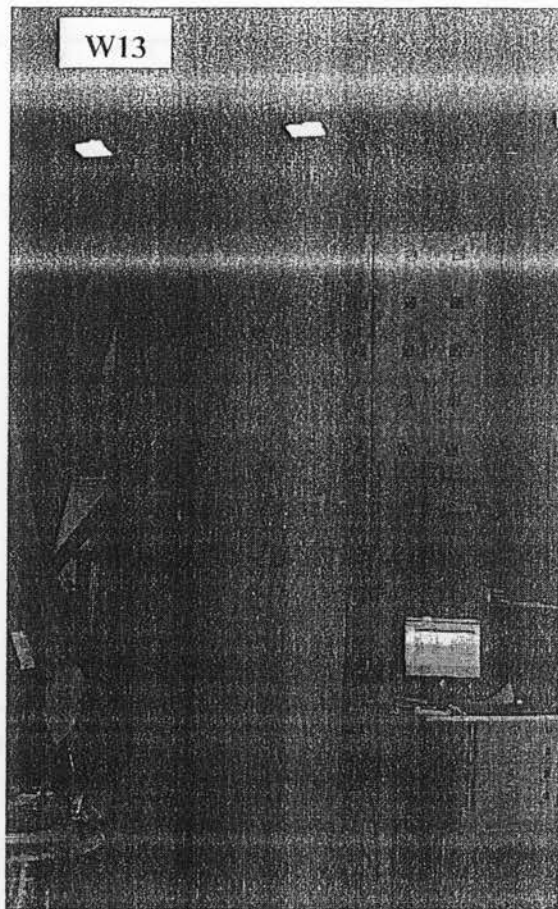


Figure 4.74. View of the test setup for wall W13 before testing

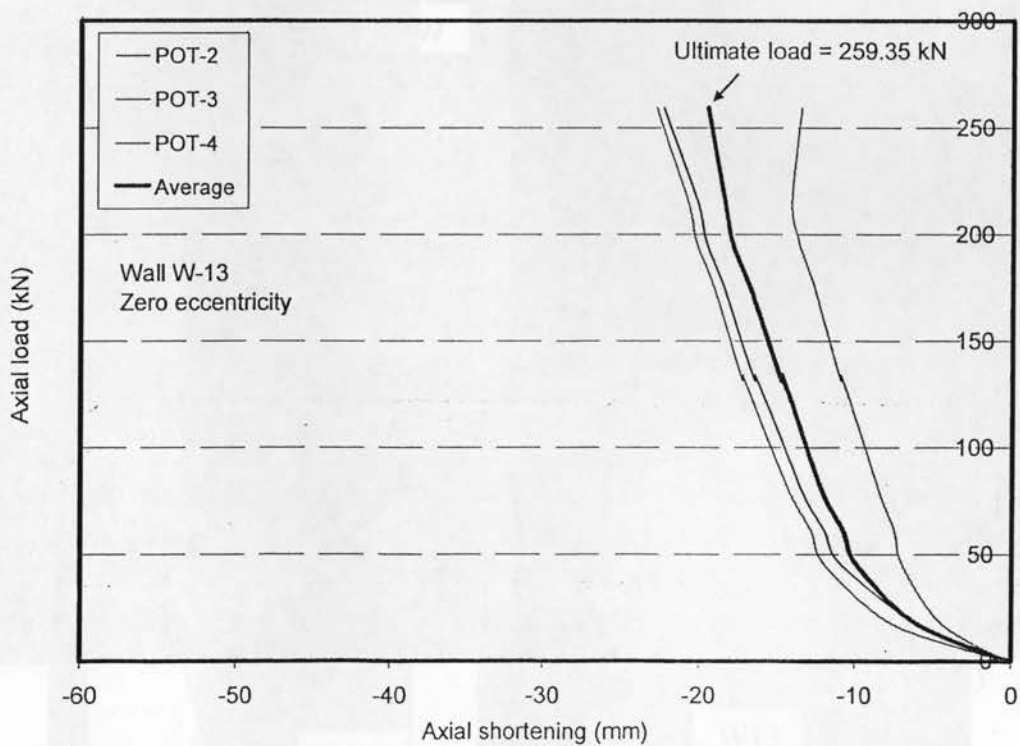


Figure 4.75. Axial load-axial shortening relationship for model W13

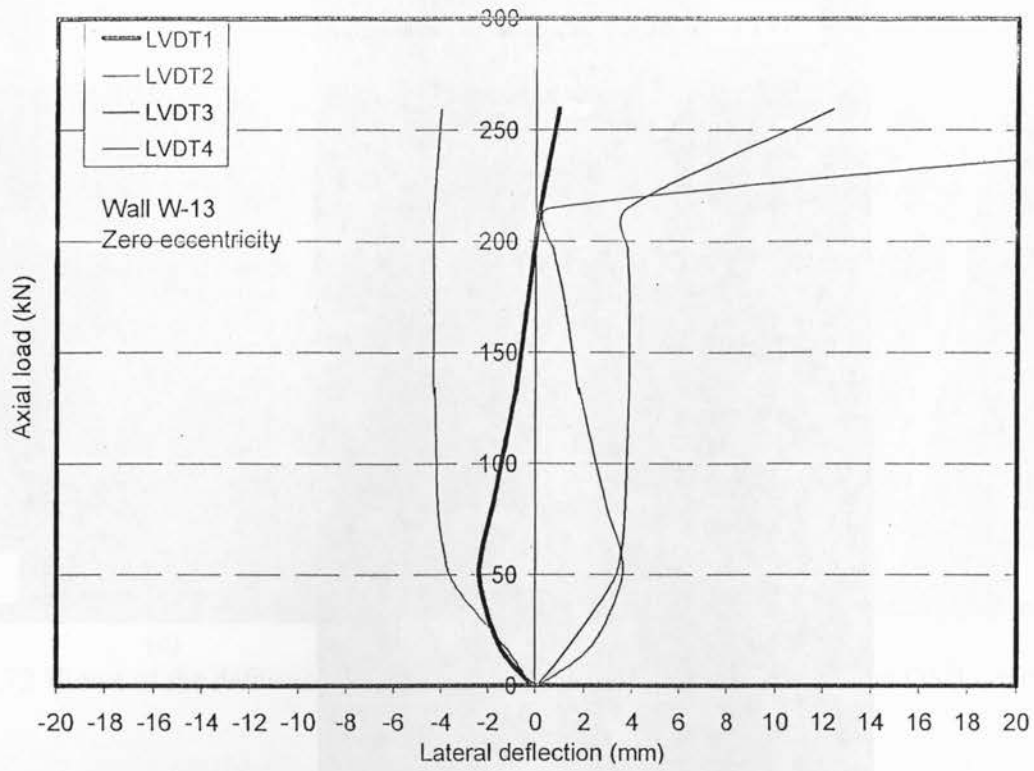
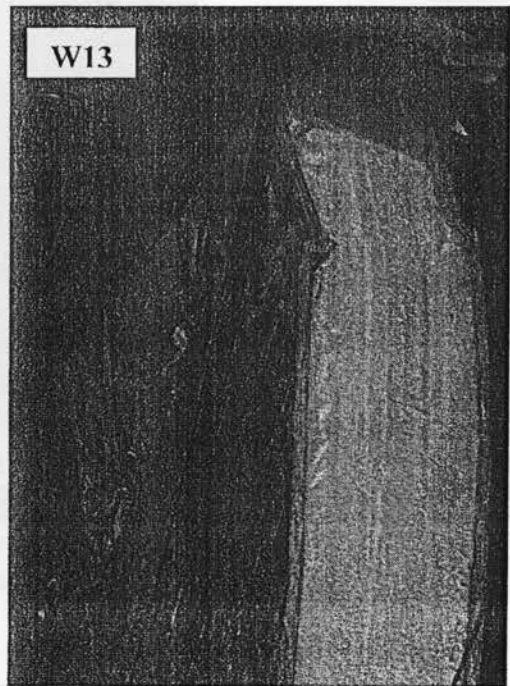


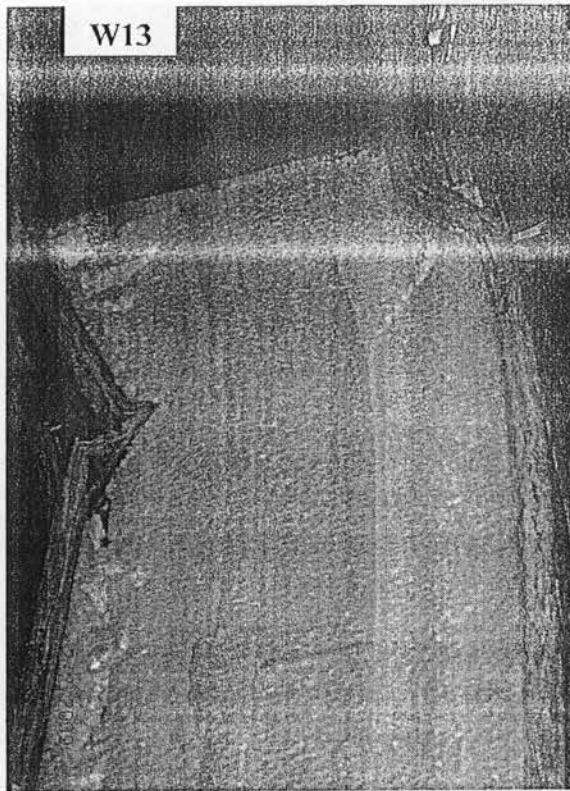
Figure 4.76. Axial load-lateral deflection relationship for model W13



(a)



(b)



(c)

Figure 4.77. View of the failure mode due to OSB crushing near its top end point in the south-west side of wall W13

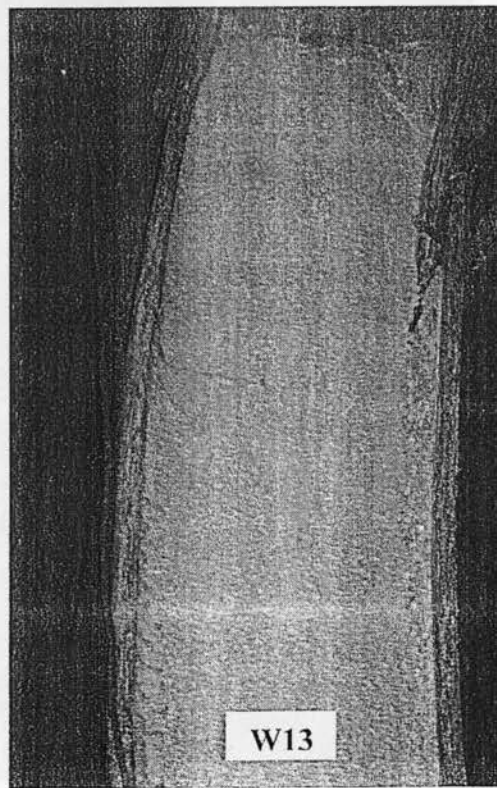


Figure 4.78. Signs of OSB crushing near the top of the wall in the east side

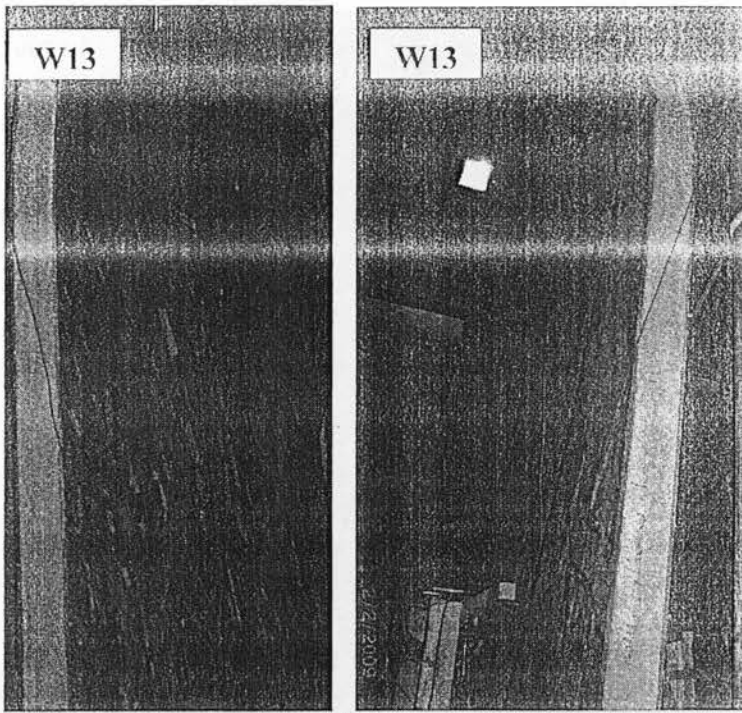


Figure 4.79. View of the deformed shape at failure of model W13 from the east and west sides

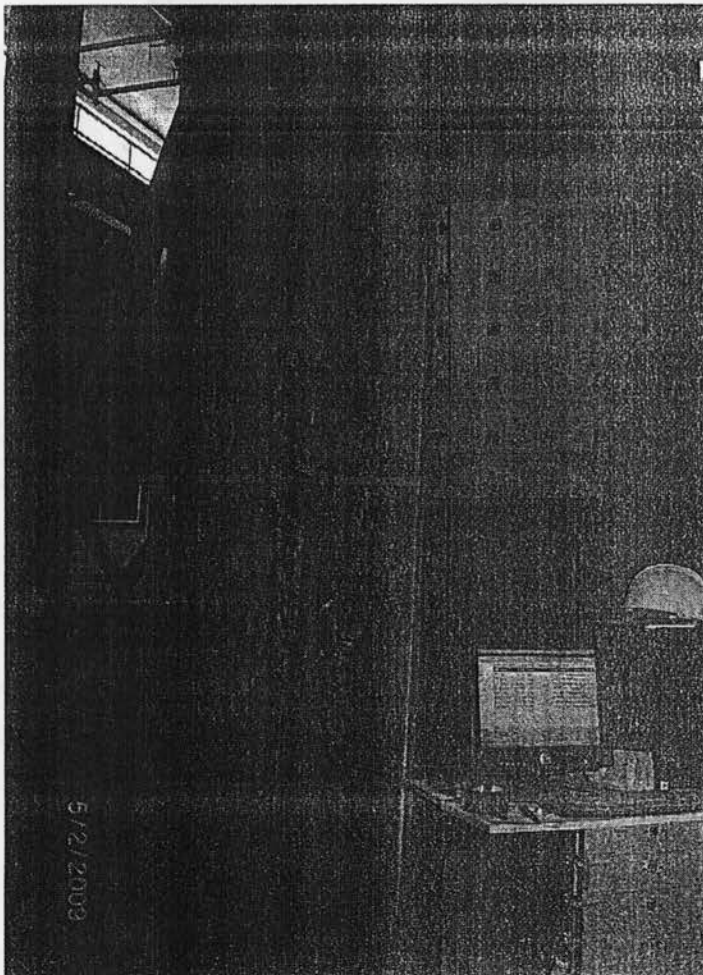


Figure 4.80. View of the test setup for wall W14 before testing

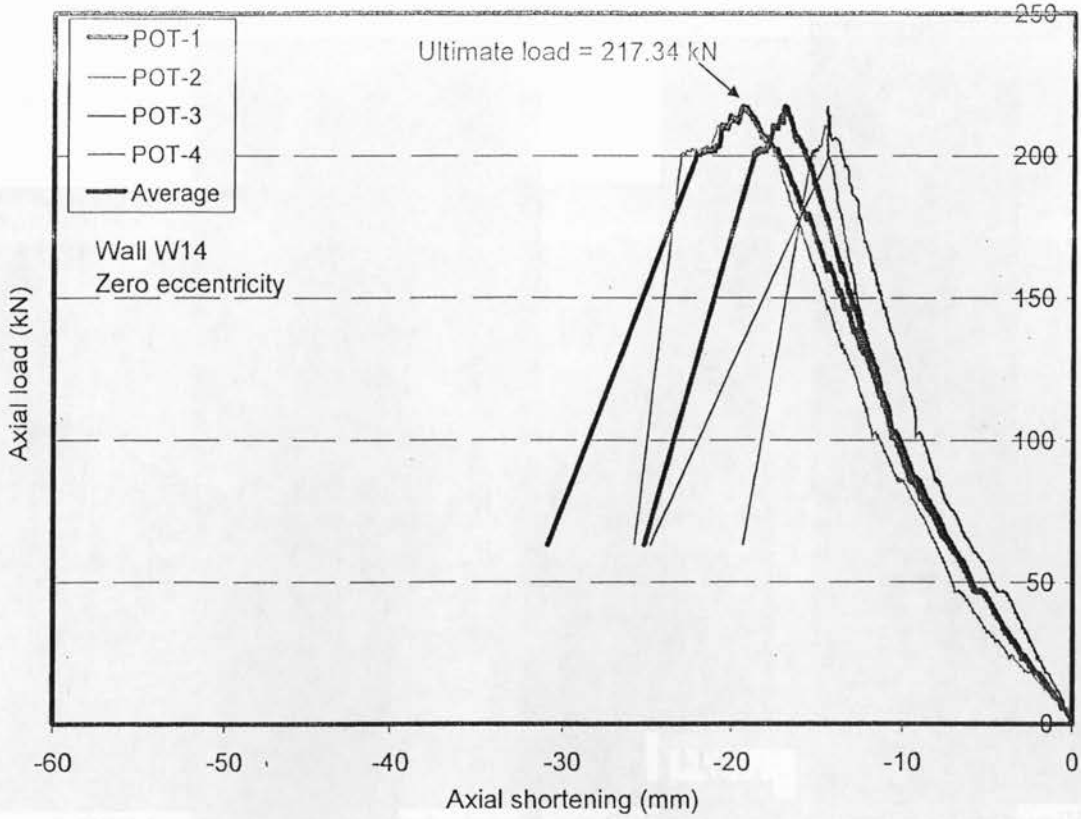


Figure 4.81. Axial load-axial shortening relationship for model W14

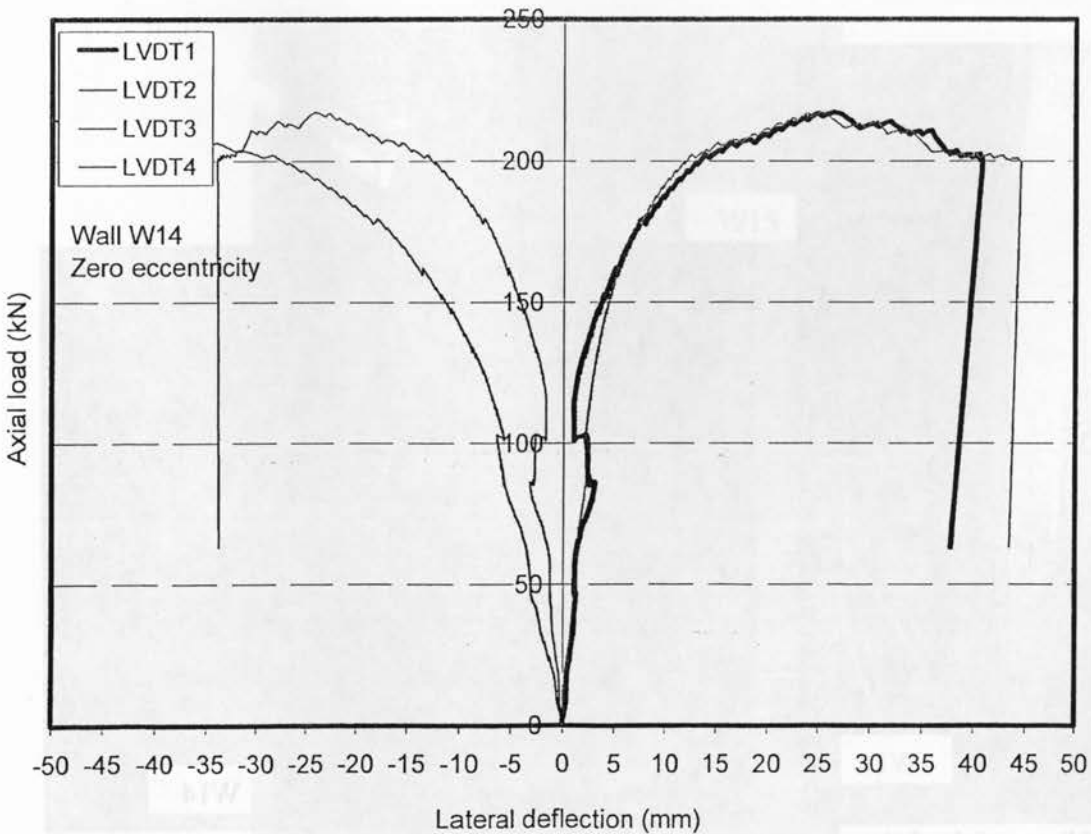


Figure 4.82. Axial load-lateral deflection relationship for model W14

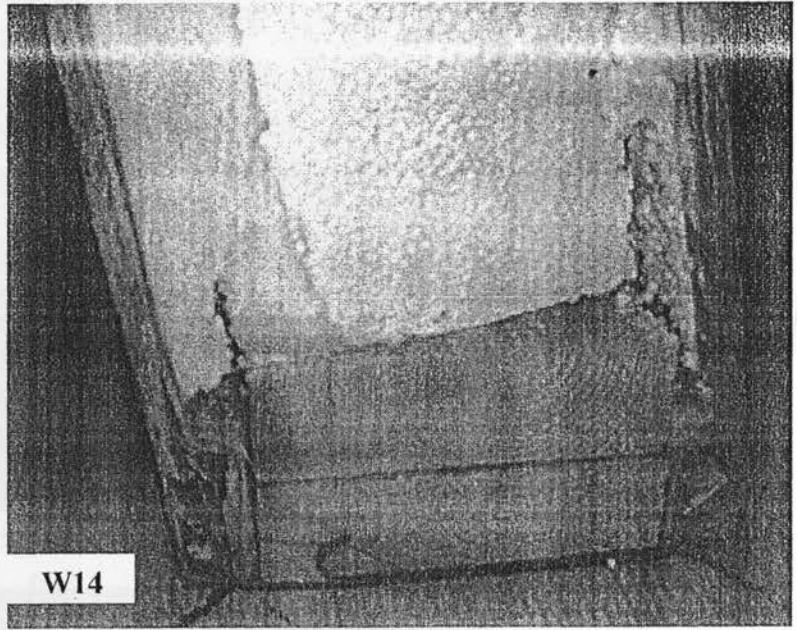
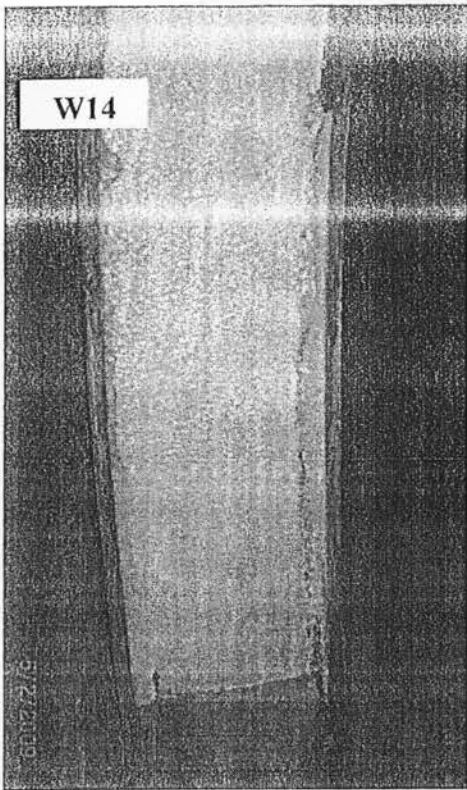


Figure 4.83. Views of the failure mode due to OSB crushing the bottom of the wall and OSB-foam splitting at the bottom of Wall W14

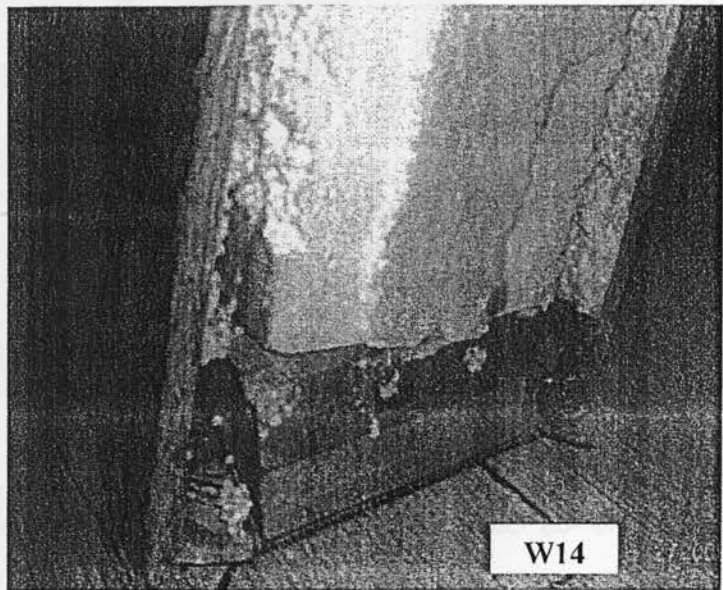
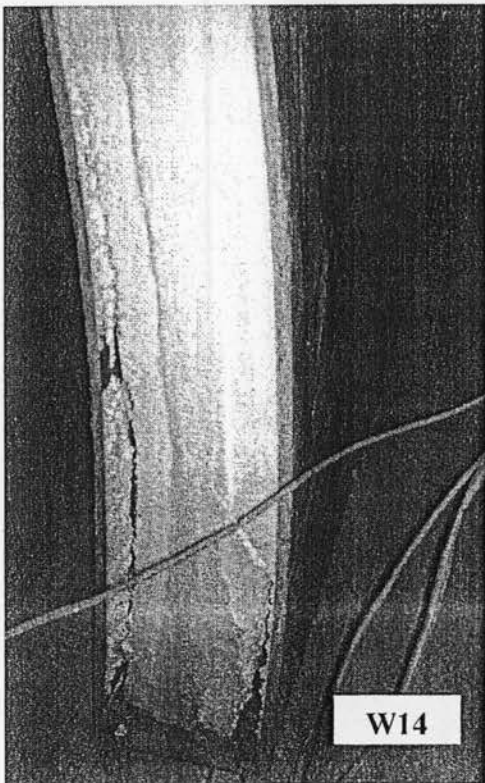


Figure 4.84. Views of the failure mode due to OSB crushing the bottom of the wall and OSB-foam splitting at the bottom of Wall W14

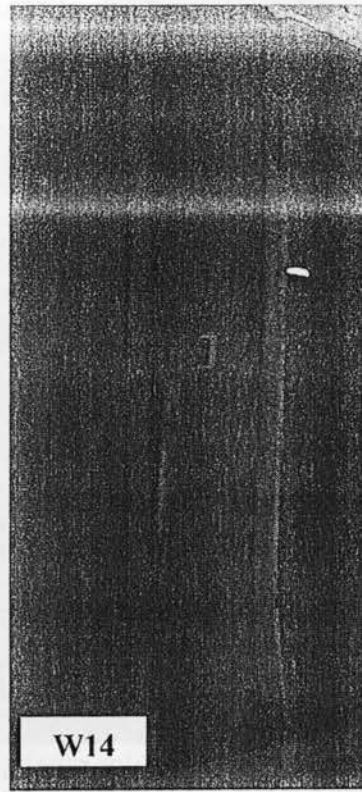
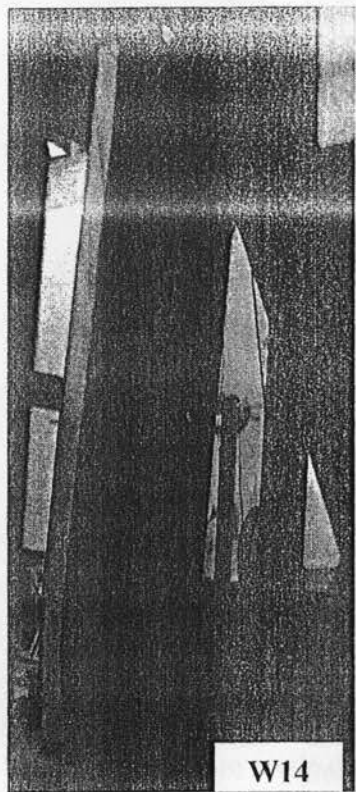


Figure 4.85. Views of wall W14 showing lateral deformation of the wall near the lower quarter point as a result of OSB crushing at this location

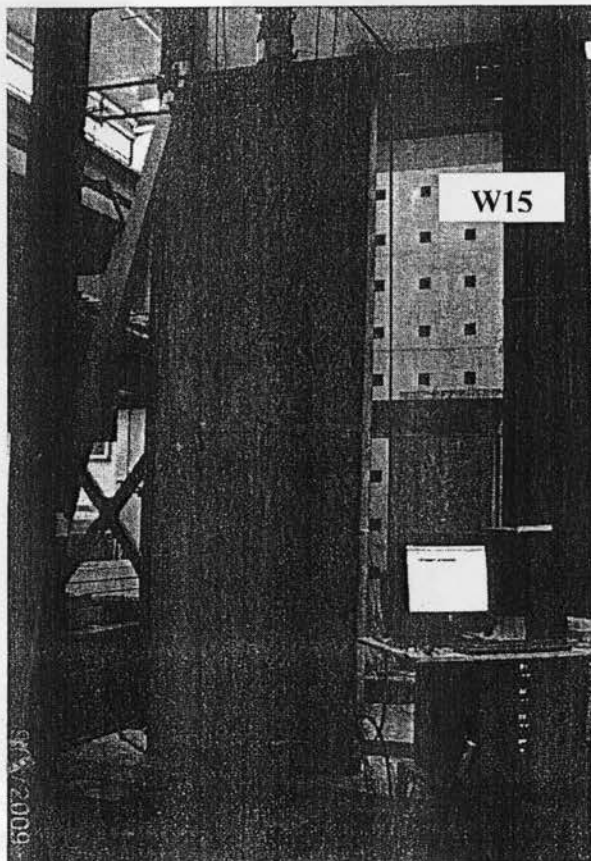


Figure 4.86. View of the test setup for wall W15 before testing

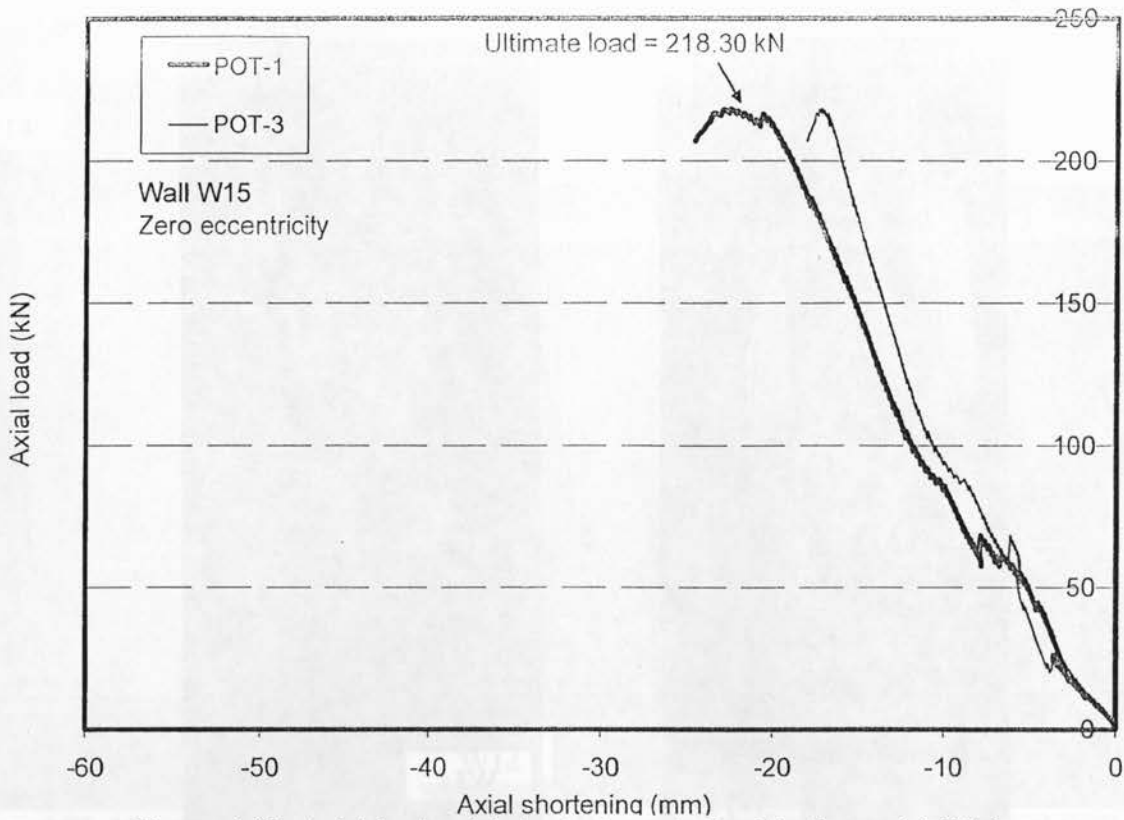


Figure 4.87. Axial load-axial shortening relationship for model W15

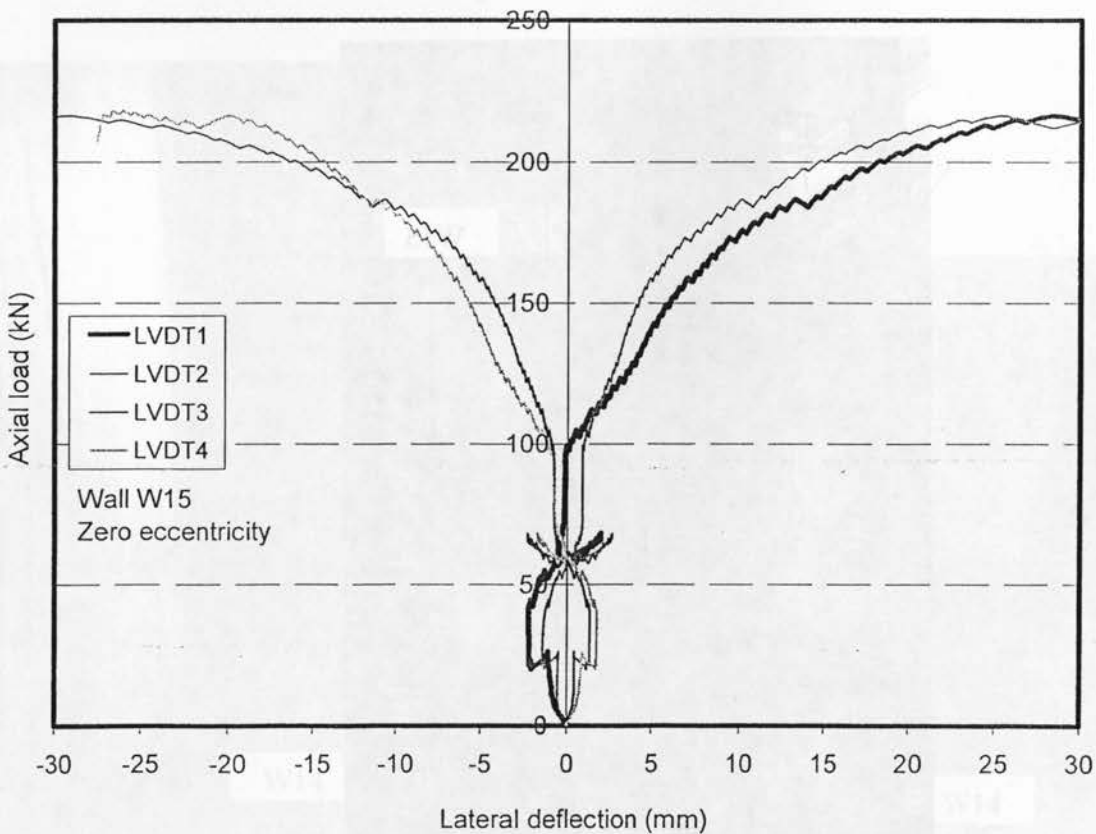


Figure 4.88. Axial load-lateral deflection relationship for model W15

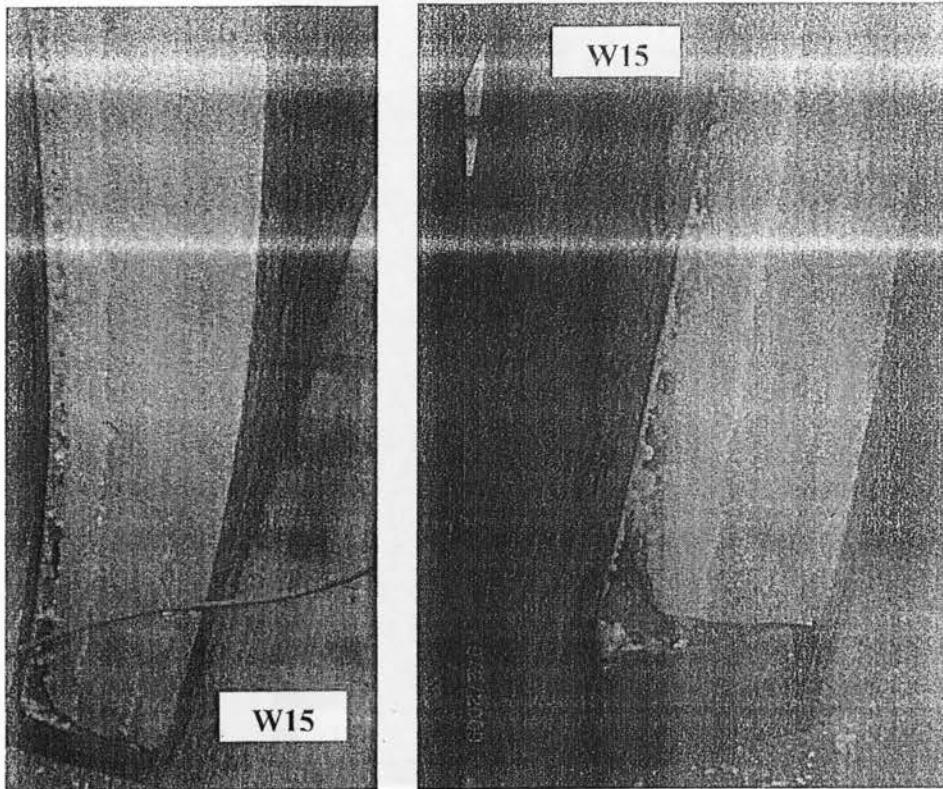


Figure 4.89. View of the failure mode due to OSB-foam splitting near its lower end point and OSB crushing in the south-east side of model W15

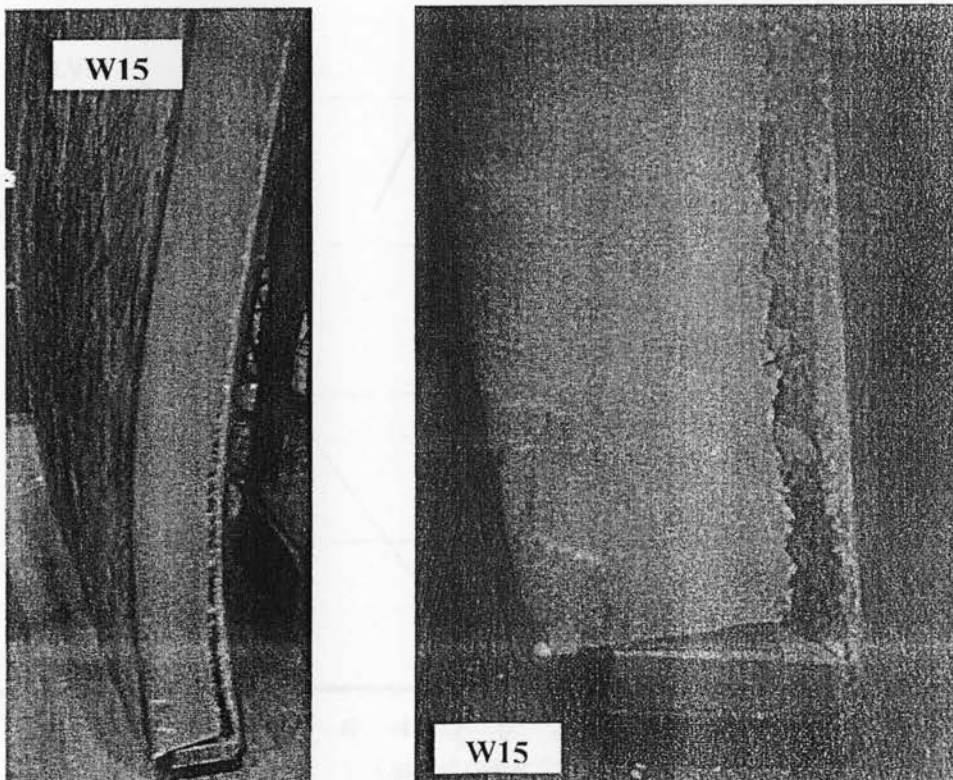


Figure 4.90. View of the failure mode due to OSB-foam splitting near its lower end point and OSB crushing in the south-west side of model W15

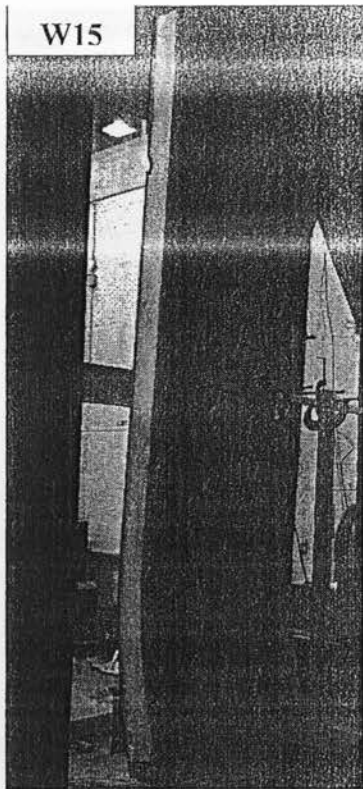


Figure 4.91. View of model W15 from the south-west corner showing lateral deformation of the wall near the lower end point as a result of OSB crushing at this location



Figure 4.92. View of the lateral movement of the wall near the lower end point as a result of OSB crushing at this location

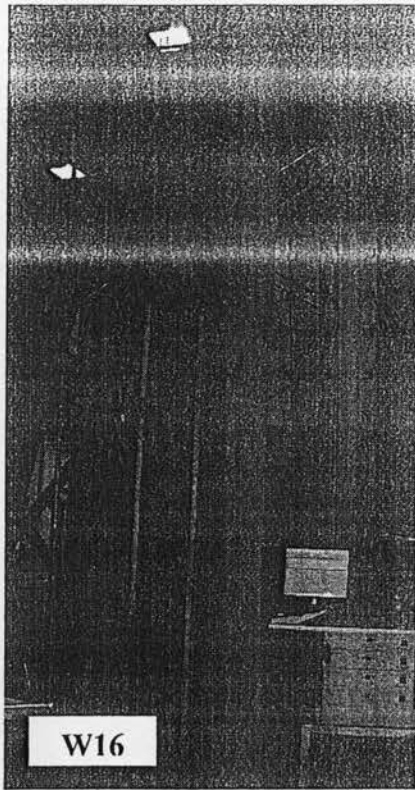


Figure 4.92. View of the test setup for wall W16 before testing

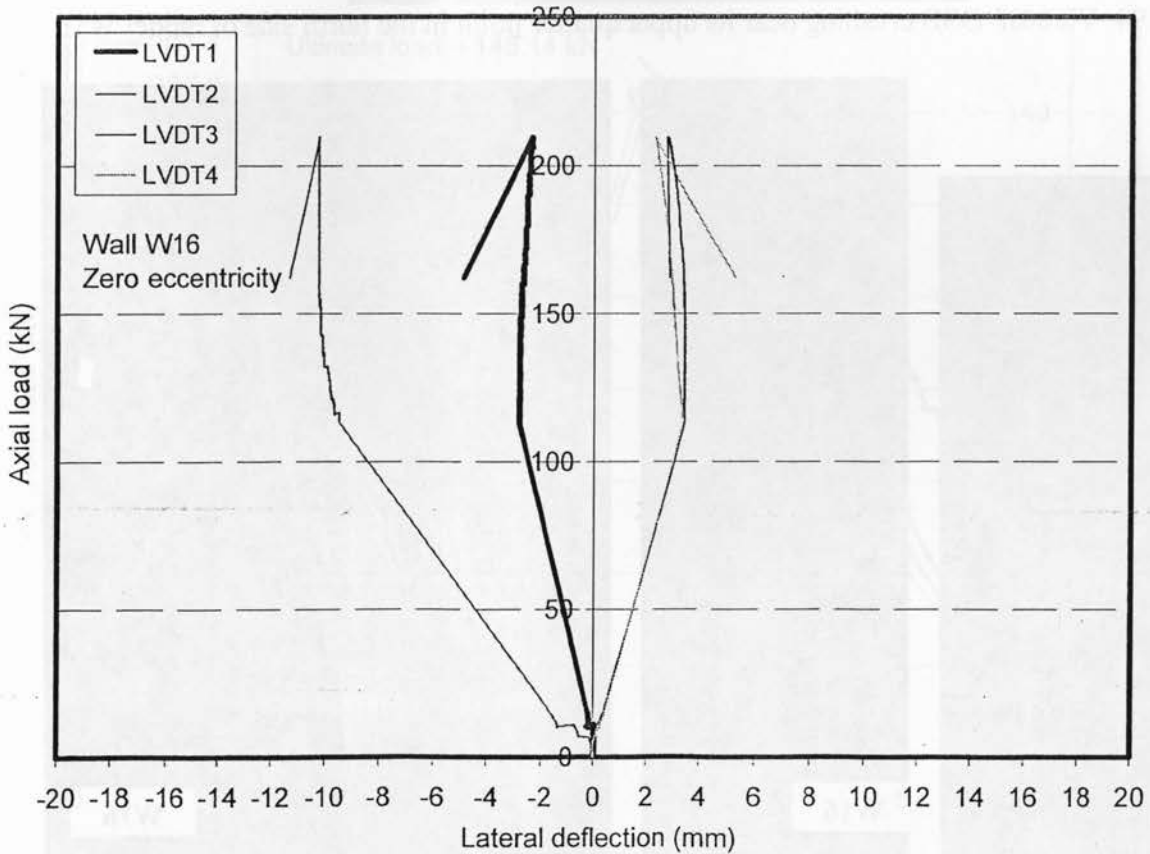


Figure 4.93. Axial load-lateral deflection relationship for model W16

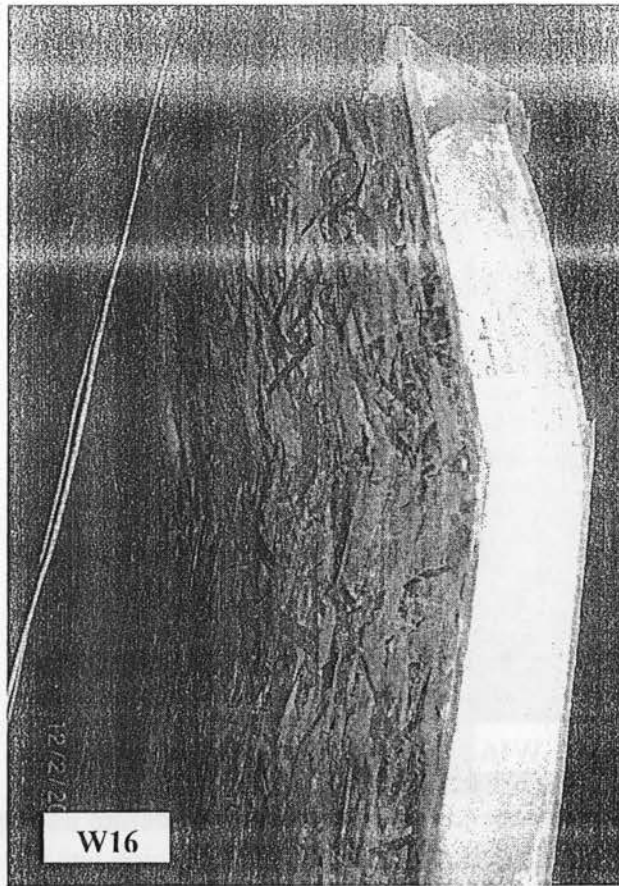


Figure 4.94. View of OSB crushing near its upper quarter point in the north side of model W16

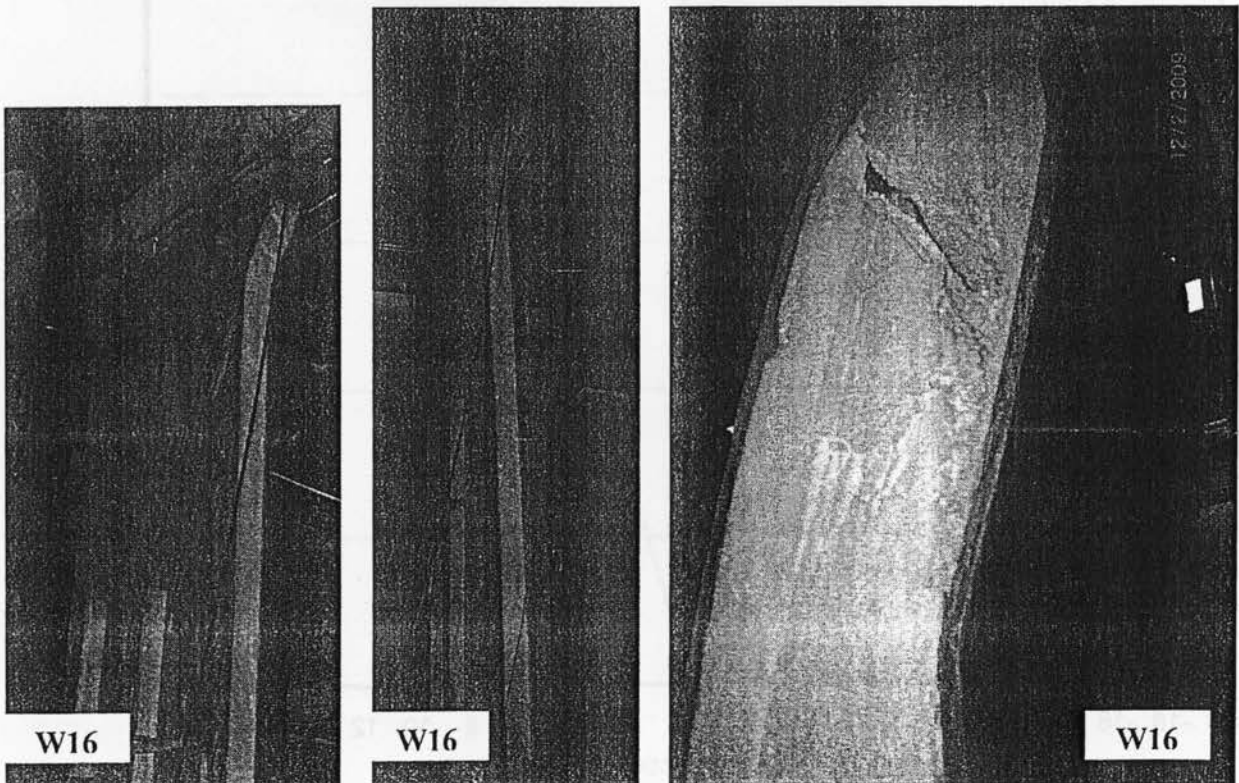


Figure 4.95. View of model W16 from the south-east corner showing lateral deformation of the wall near the top quarter point as a result of OSB crushing at this location

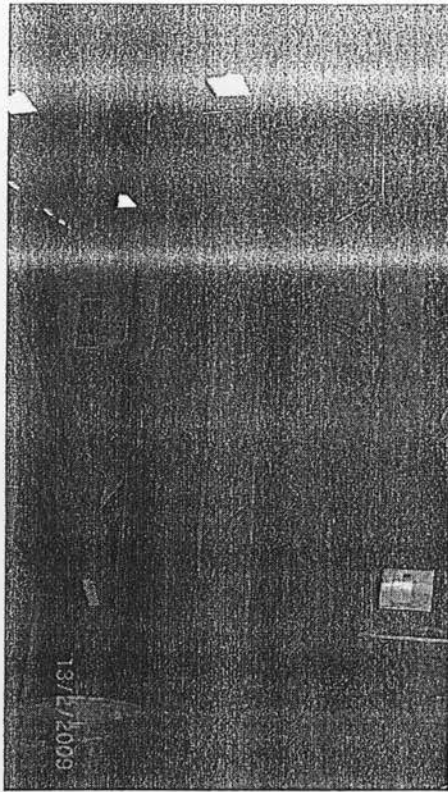


Figure 4.96. View of the test setup for wall W17 before testing

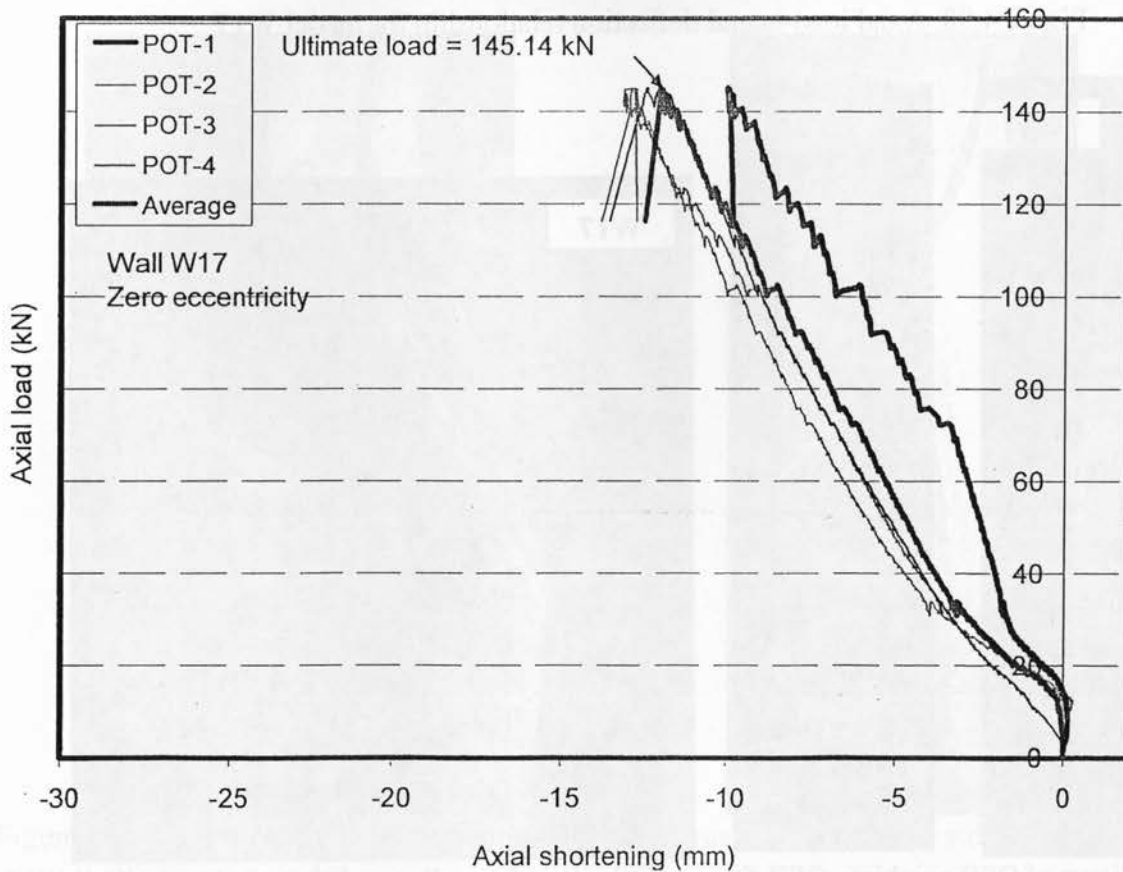


Figure 4.97. Axial load-axial shortening relationship for model W17

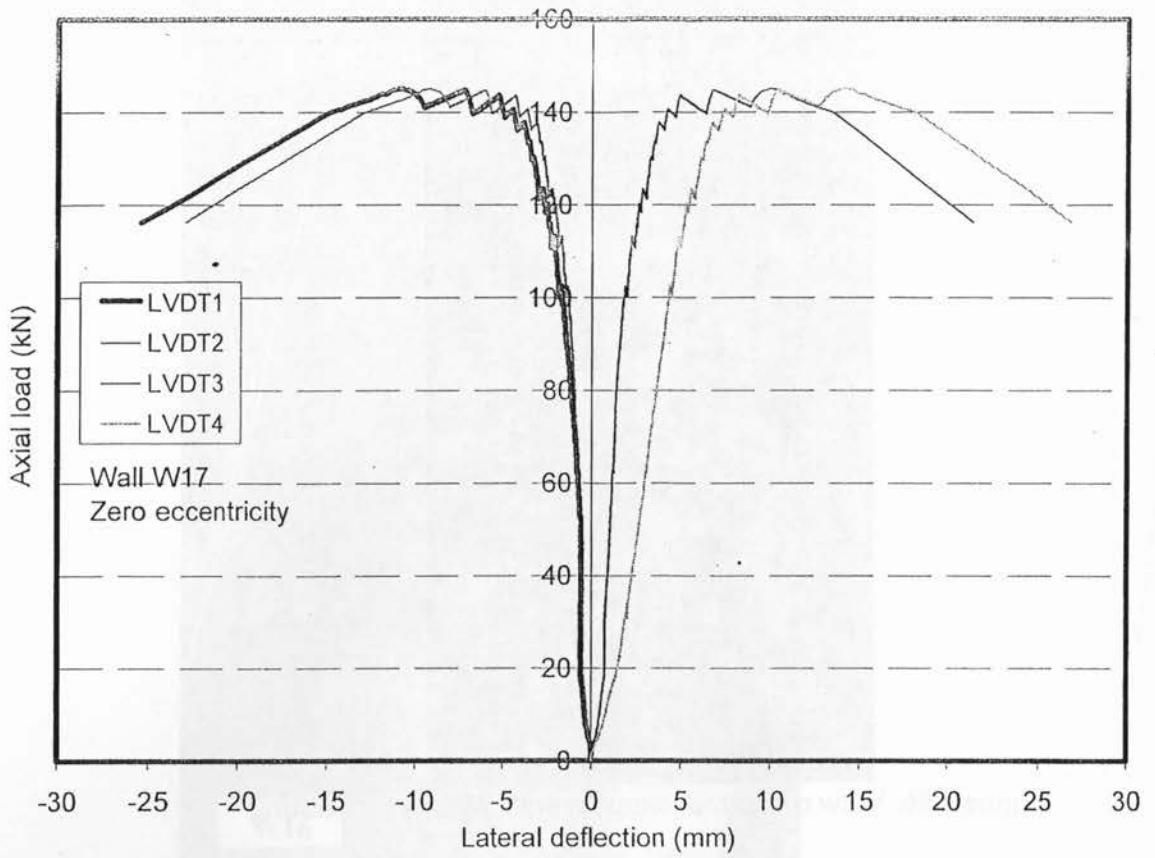


Figure 4.98. Axial load-lateral deflection relationship for model W17

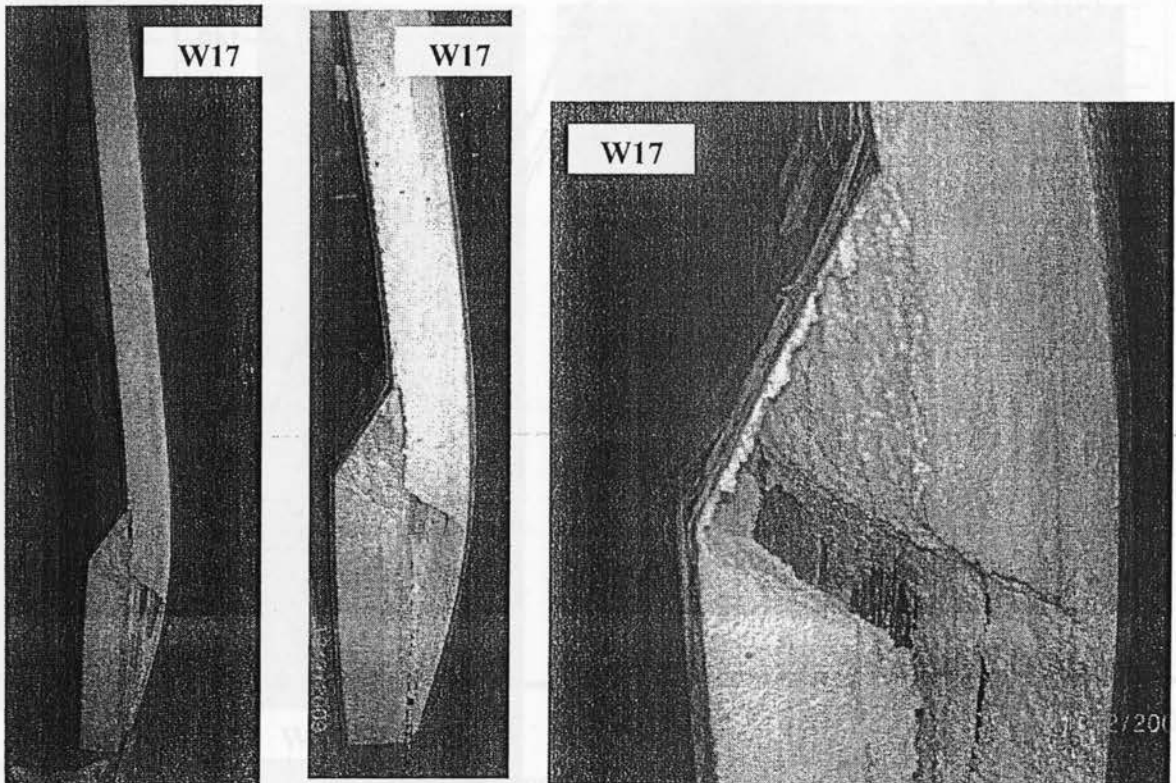


Figure 4.99. Views of OSB crushing, OSB-foam splitting and foam diagonal shear failure in Wall W17

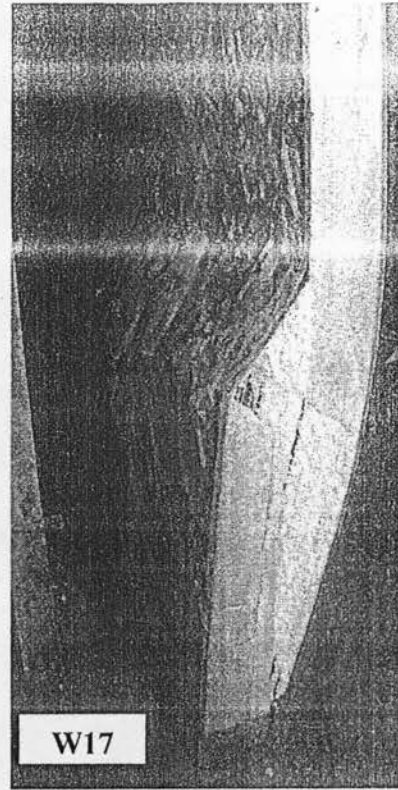
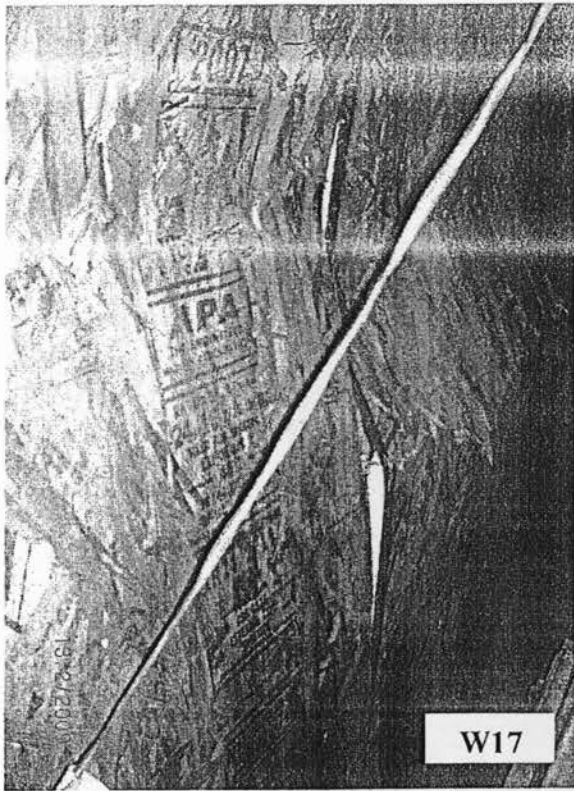


Figure 4.100. Others views of the failure pattern of wall W17

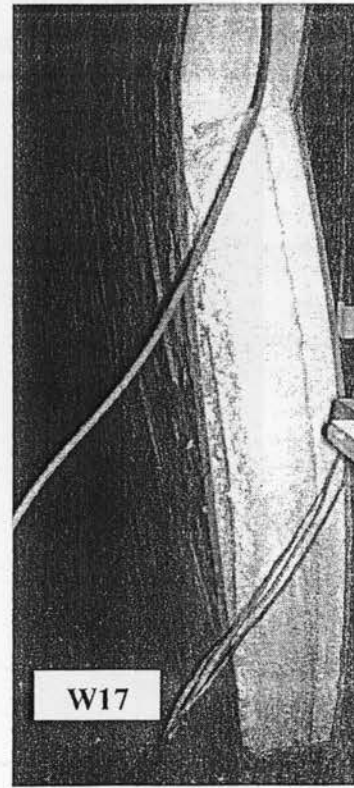
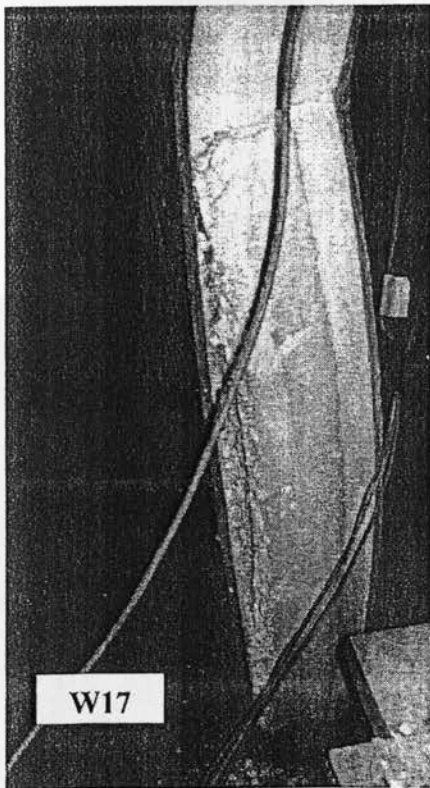


Figure 4.101. Views of OSB-foam splitting and OSB crushing at the other side of wall W17

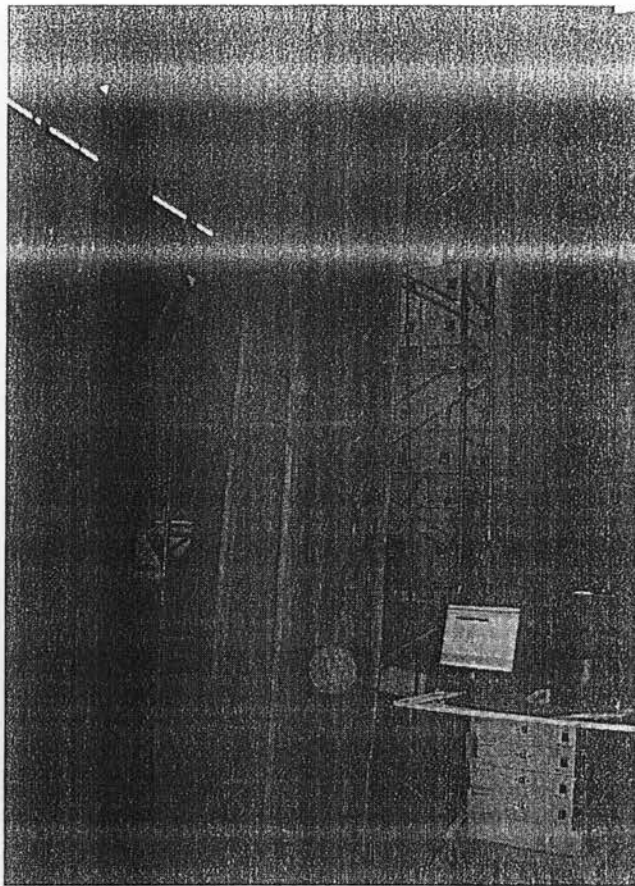


Figure 4.102. View of the test setup for wall W18 before testing

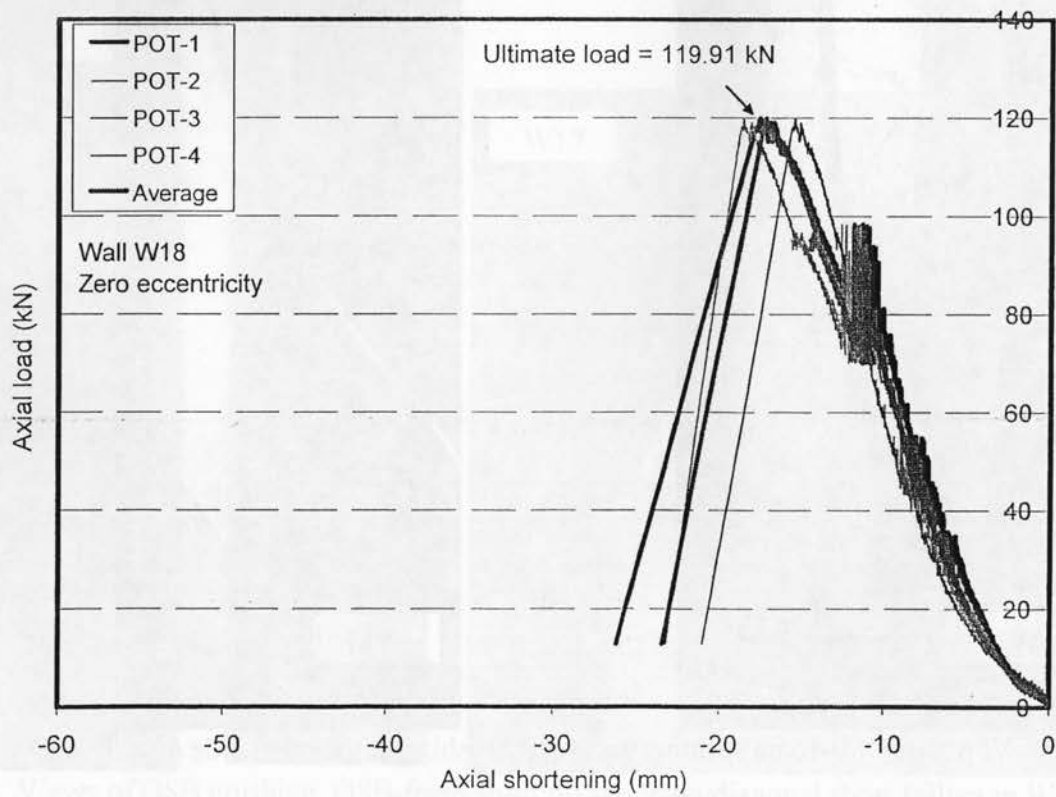


Figure 4.103. Axial load-axial shortening relationship for model W18

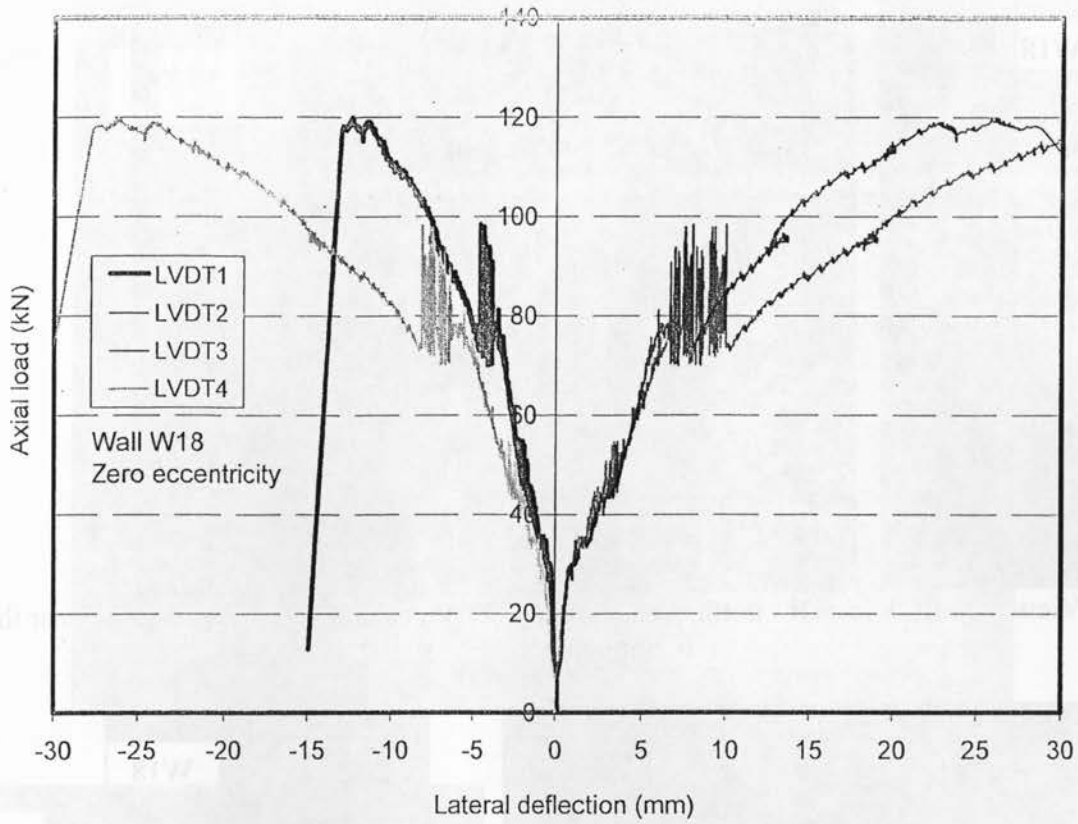


Figure 4.104. Axial load-lateral deflection relationship for model W18

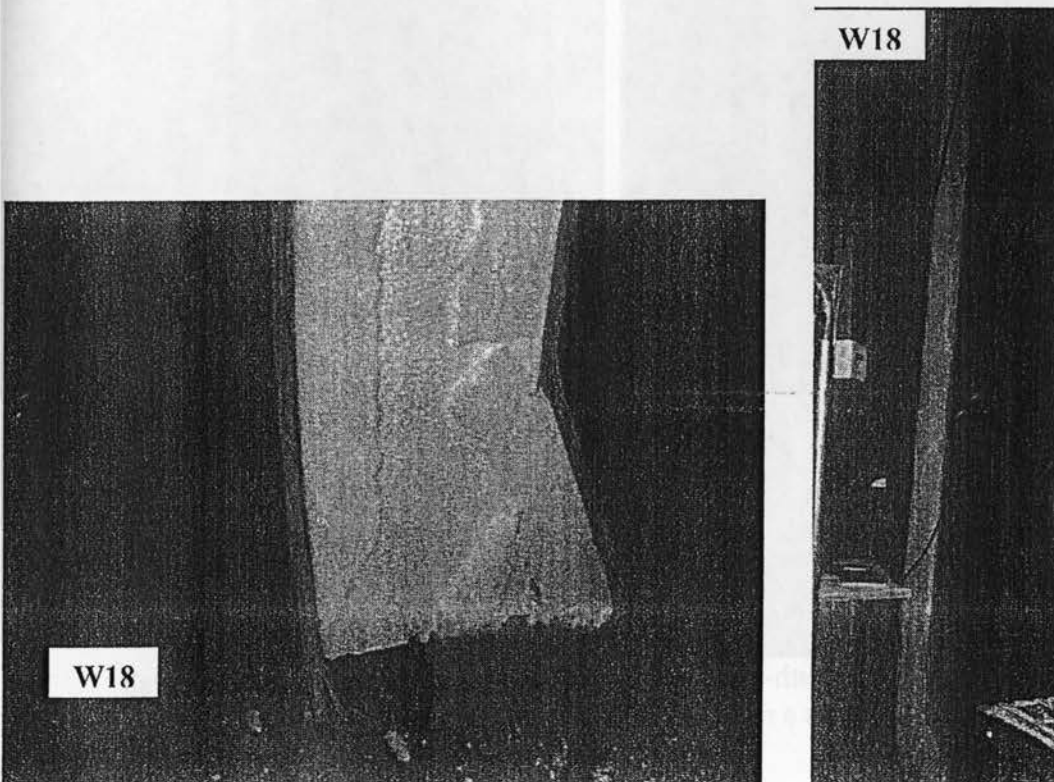


Figure 4.105. View of wall W18 at the north-east showing OSB crushing at and near the bottom end

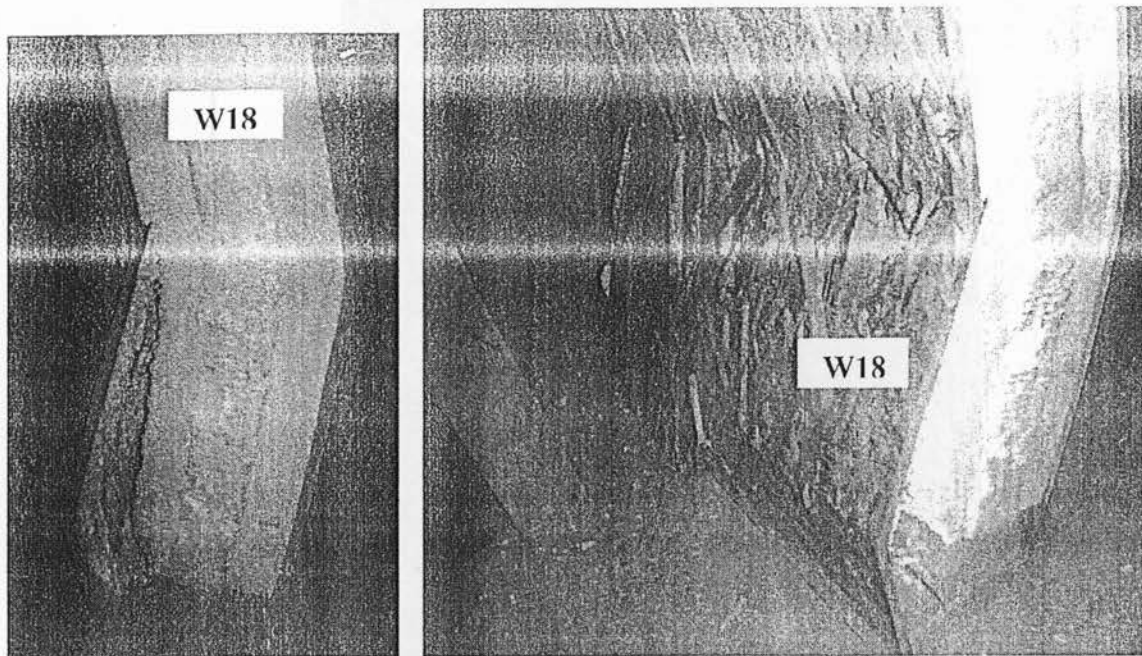


Figure 4.106. View of wall W18 at the north-west showing OSB crushing and foam splitting near the bottom end

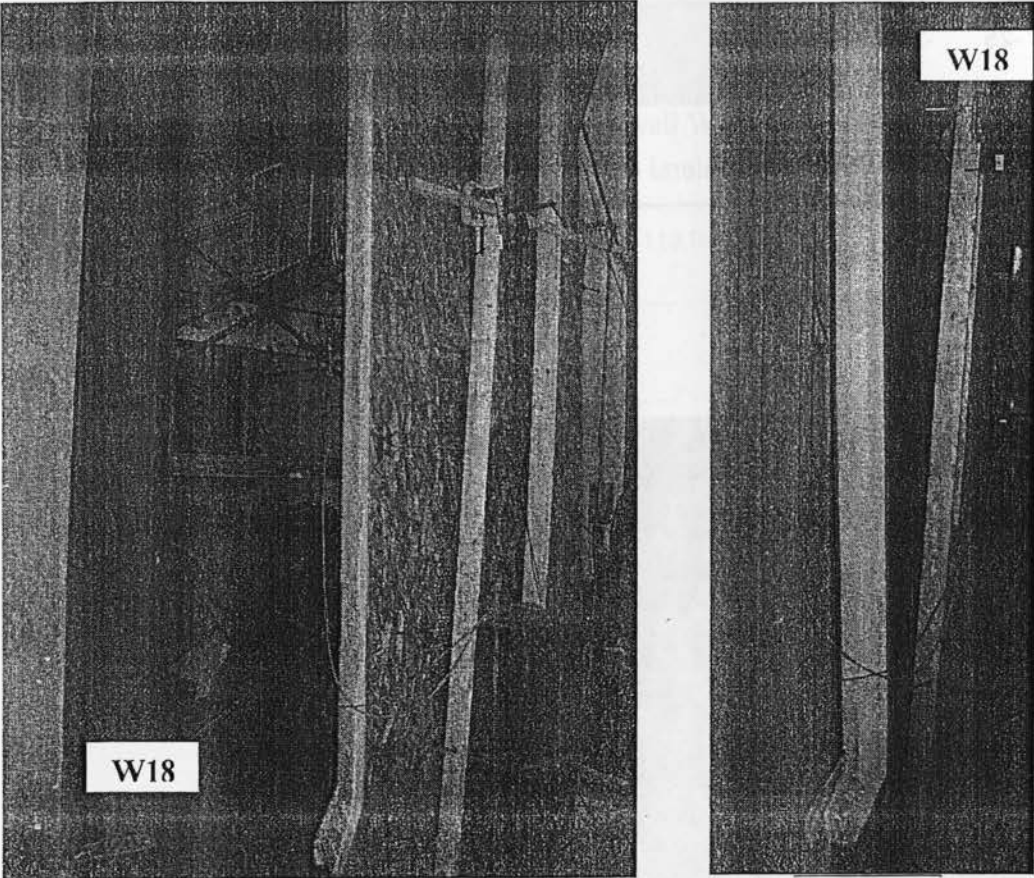
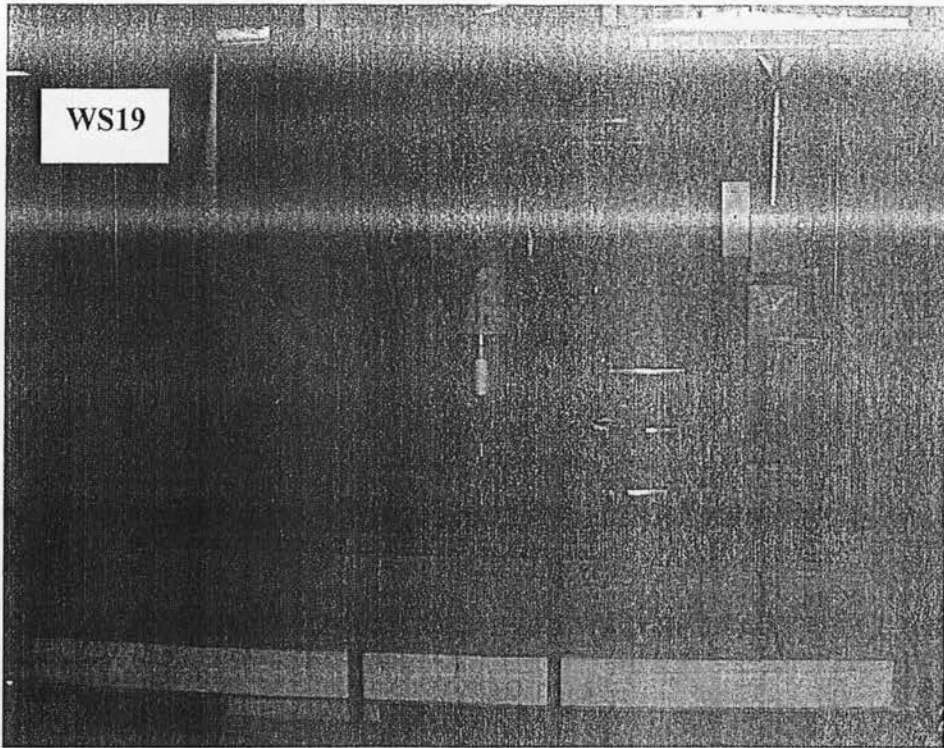
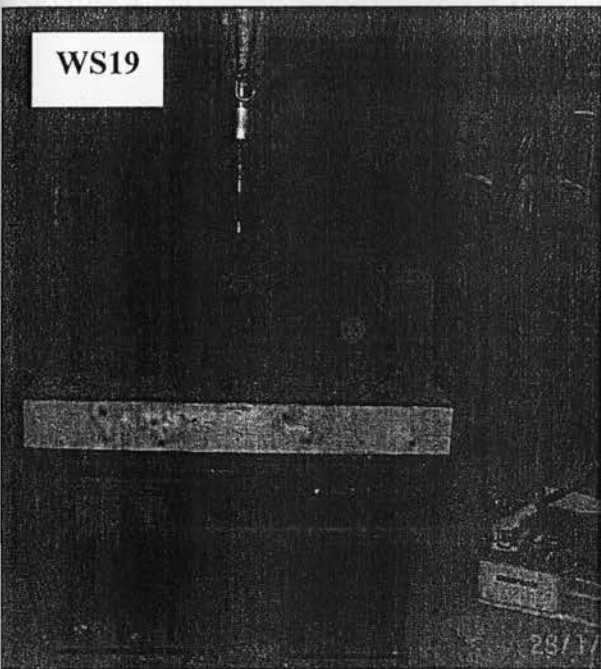


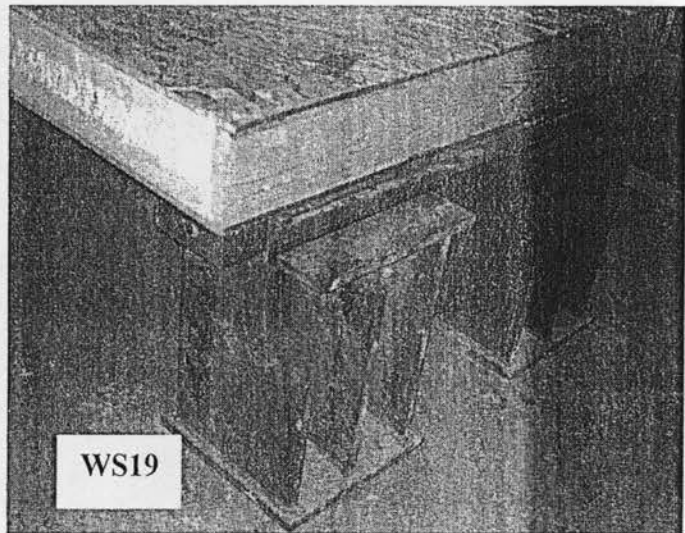
Figure 4.107. View of wall W18 from the south-east corner showing lateral deformation of the wall near the bottom quarter point as a result of OSB crushing at this location



(a)



(b)



(c)

Figure 4.108 Views of the test setup for model WS19 before testing

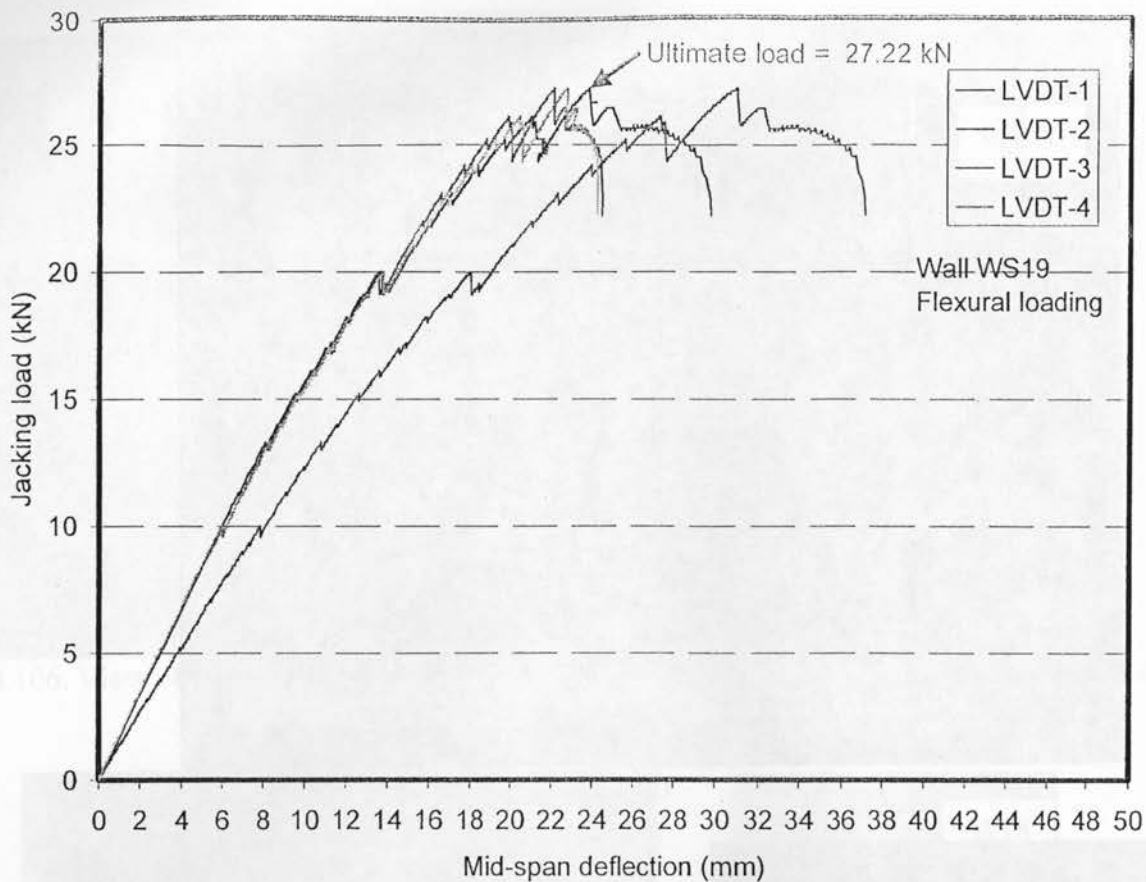


Figure 4.109. Jacking load-deflection relationship for model WS19

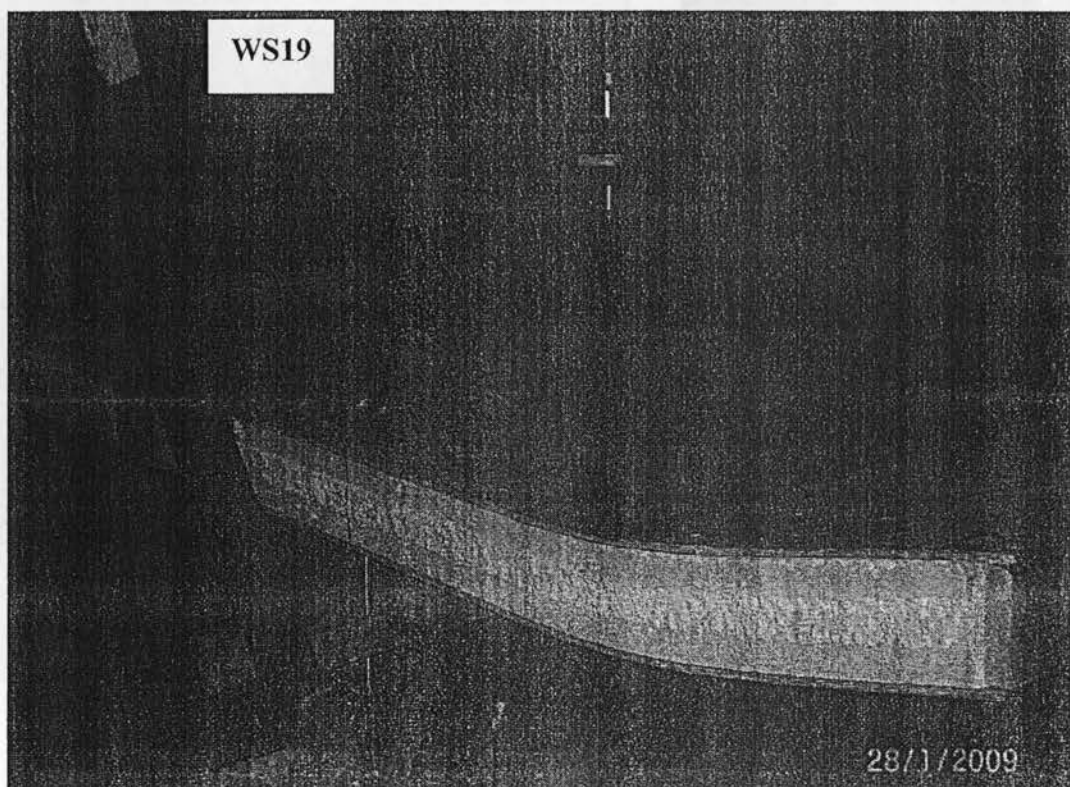


Figure 4.110. View of the deflected shape of model WS19 after failure

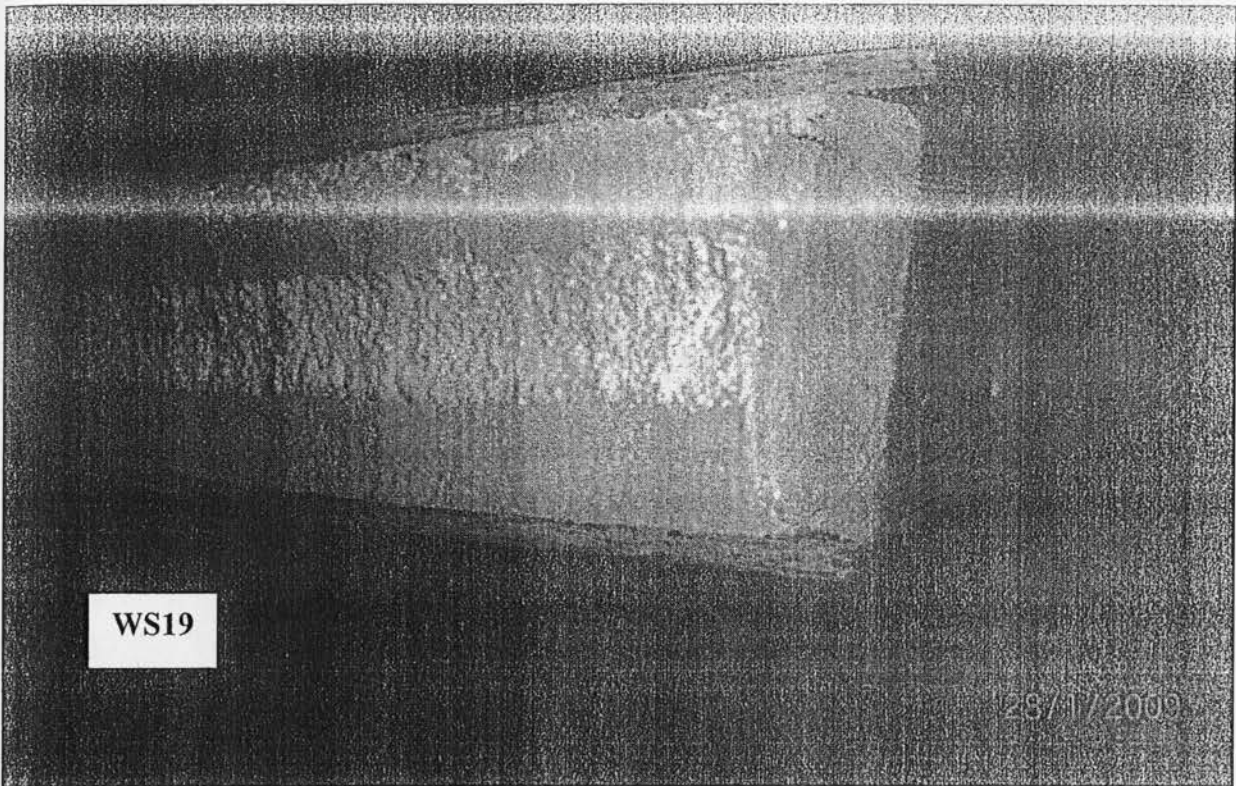


Figure 4.111. View of the horizontal shear failure at the interface between the foam and top OSB at one side of the support of model WS19

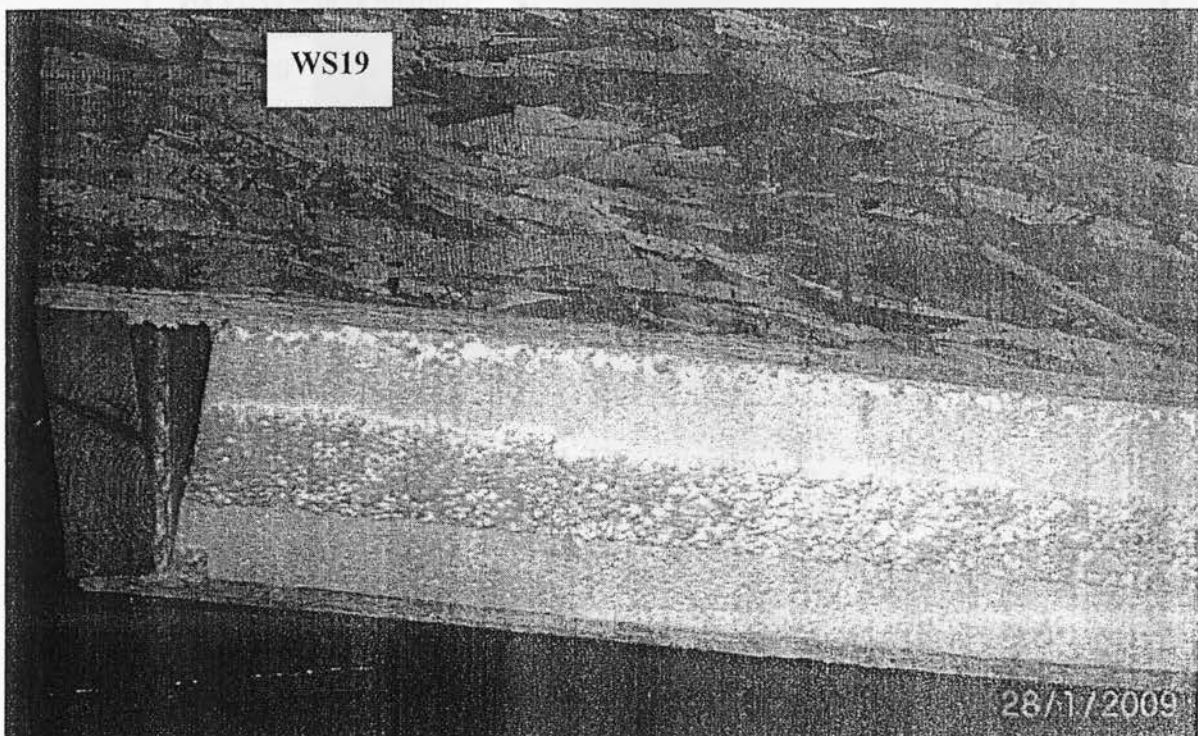


Figure 4.112. View of the horizontal shear failure at the interface between the foam and top OSB at the other side of the support of model WS19

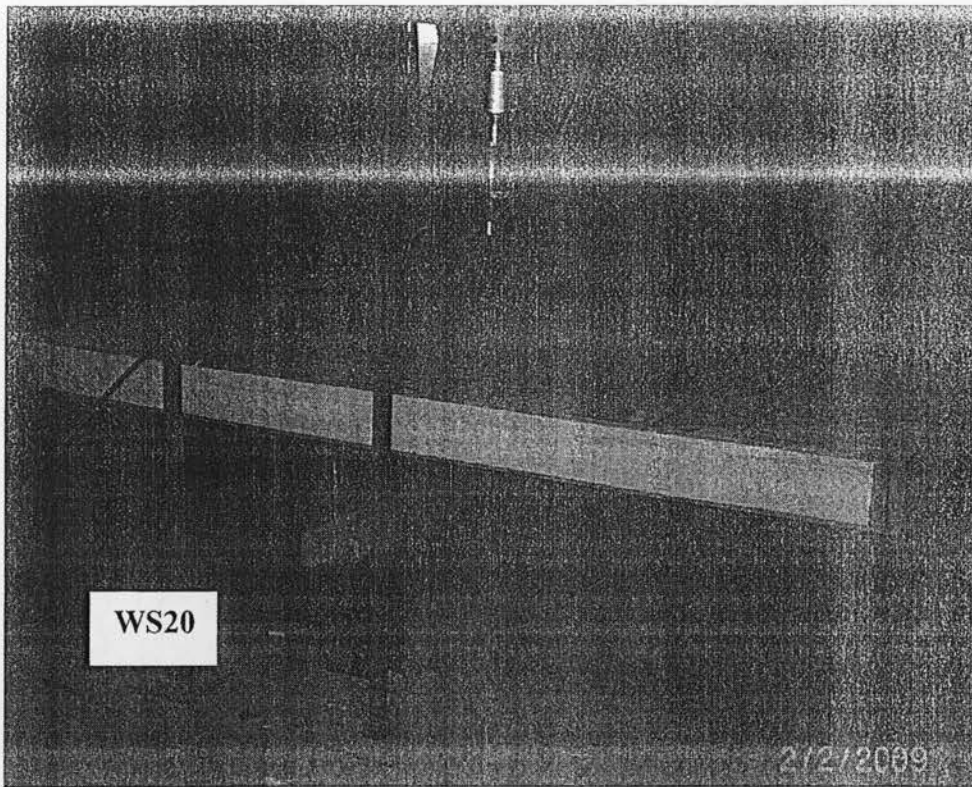


Figure 4.113. Views of the test setup for model WS20 before testing

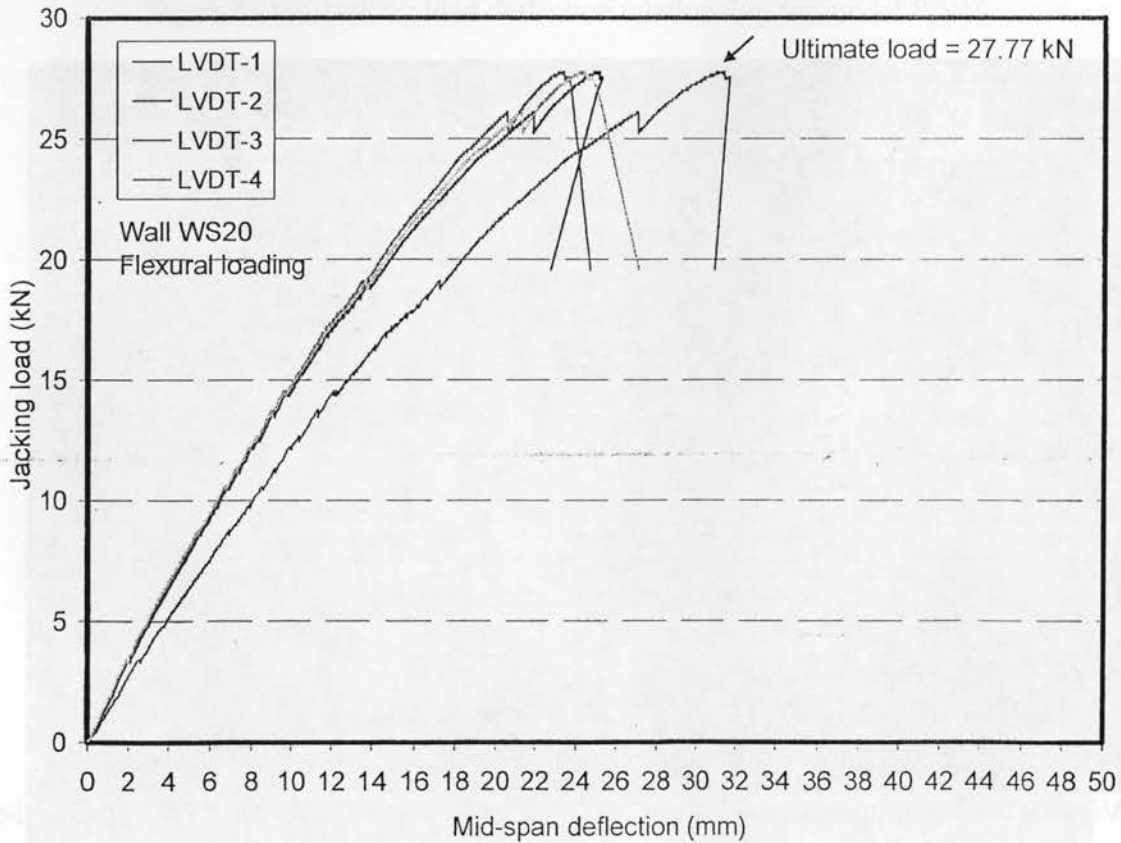


Figure 4.114. Jacking load-deflection relationship for model WS20

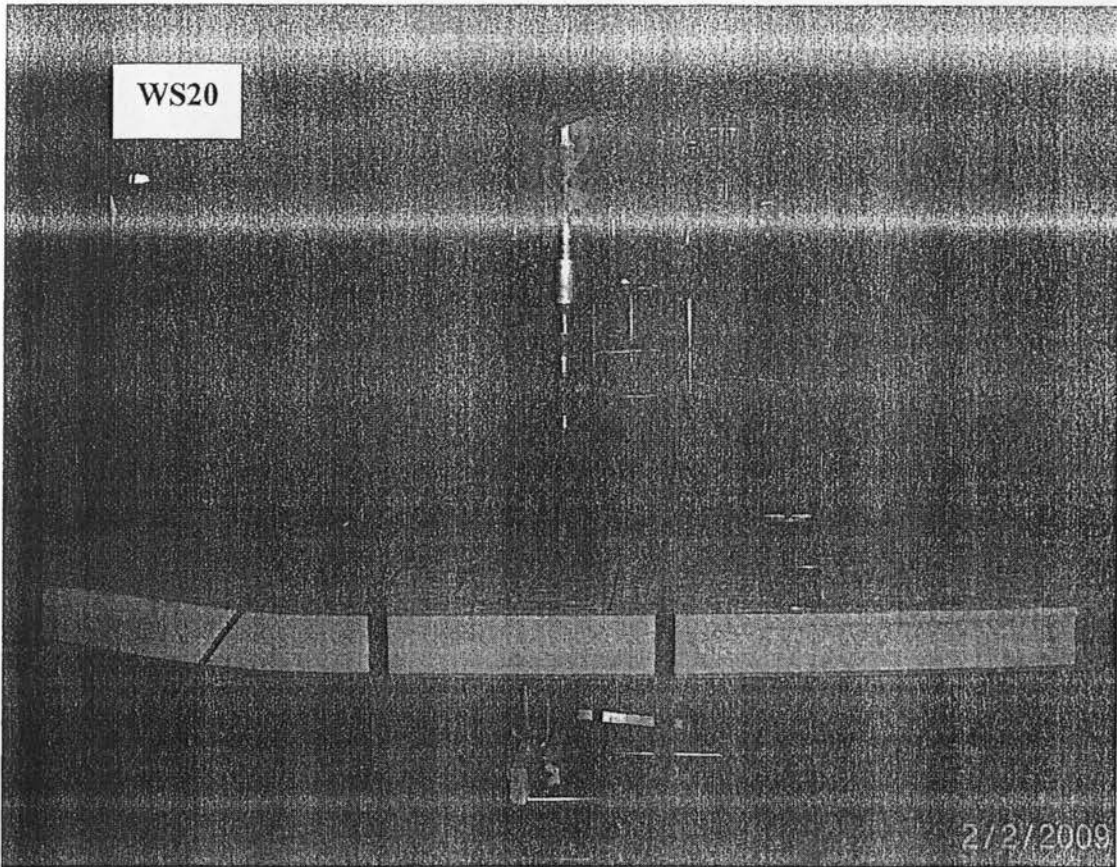


Figure 4.115. View of the deflected shape of model WS20 after failure

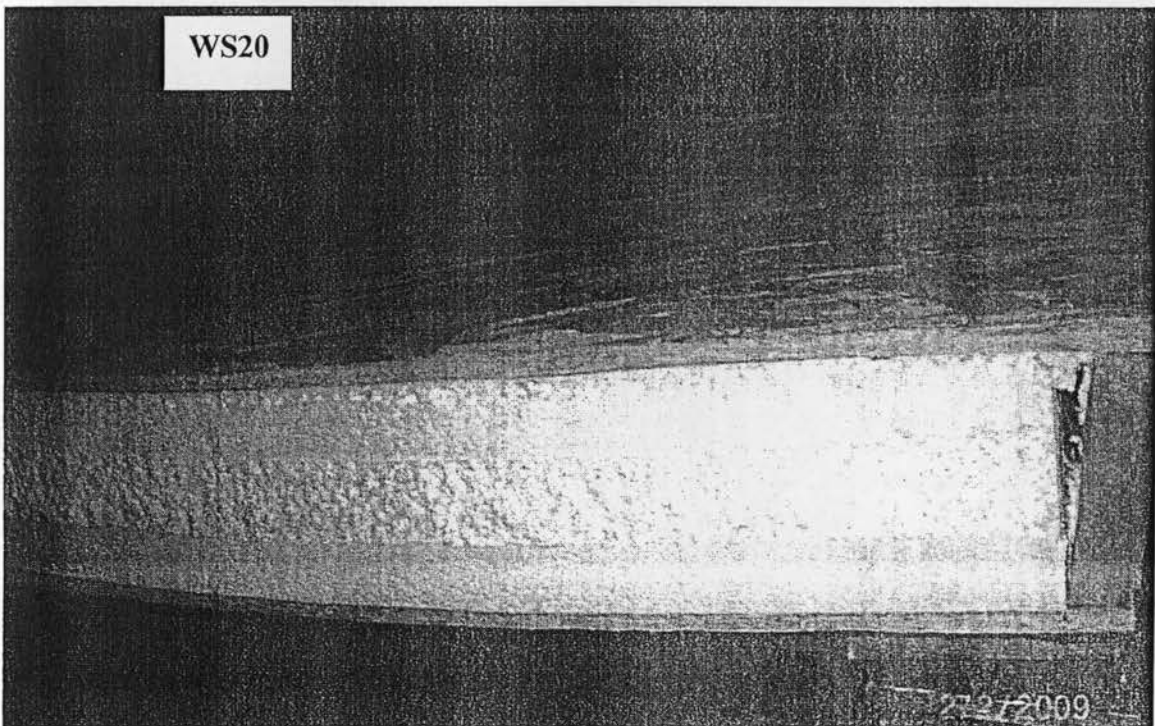


Figure 4.116. View of the horizontal shear failure at the interface between the foam and top OSB at one side of the support of model WS20

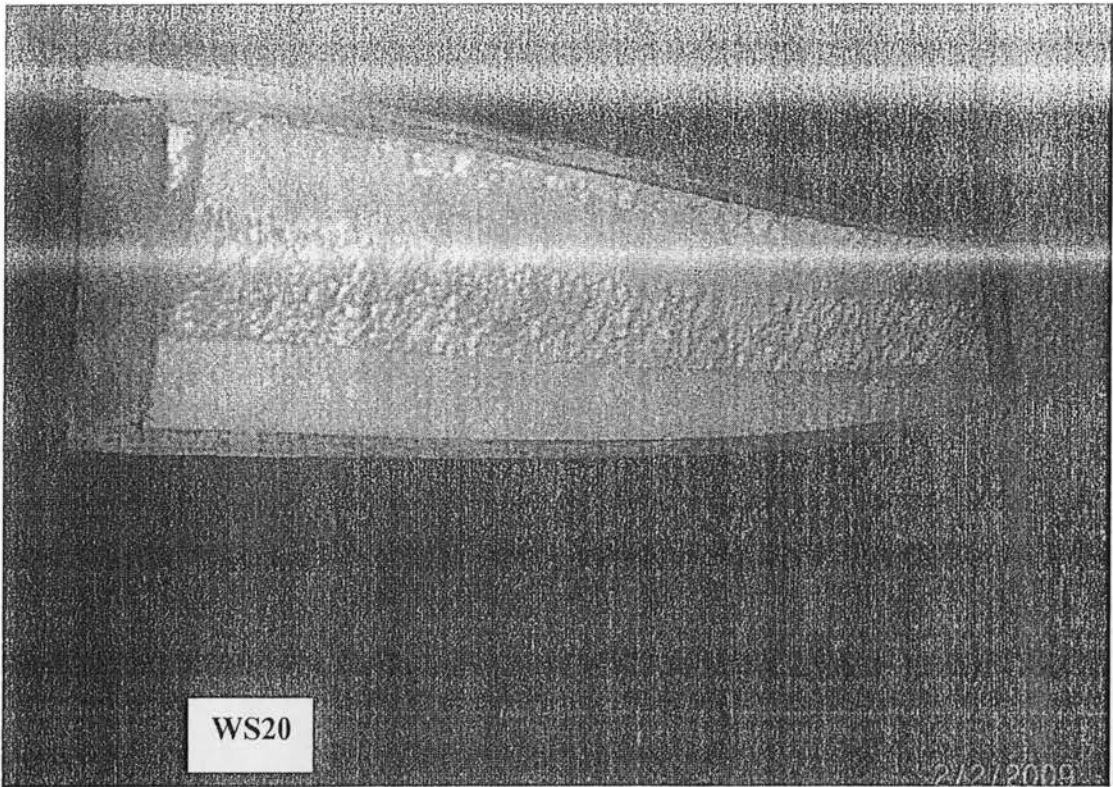


Figure 4.117. View of the horizontal shear failure at the interface between the foam and top OSB at the other side of the support of model WS20

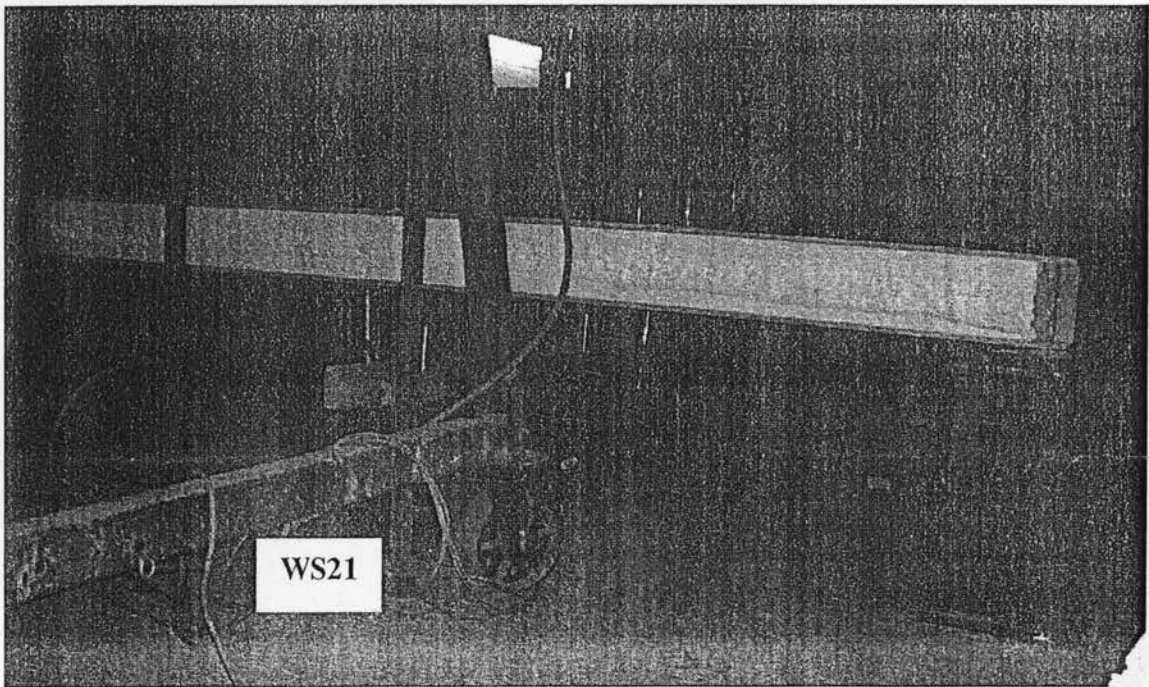


Figure 4.118. Views of the test setup for model WS21 before testing

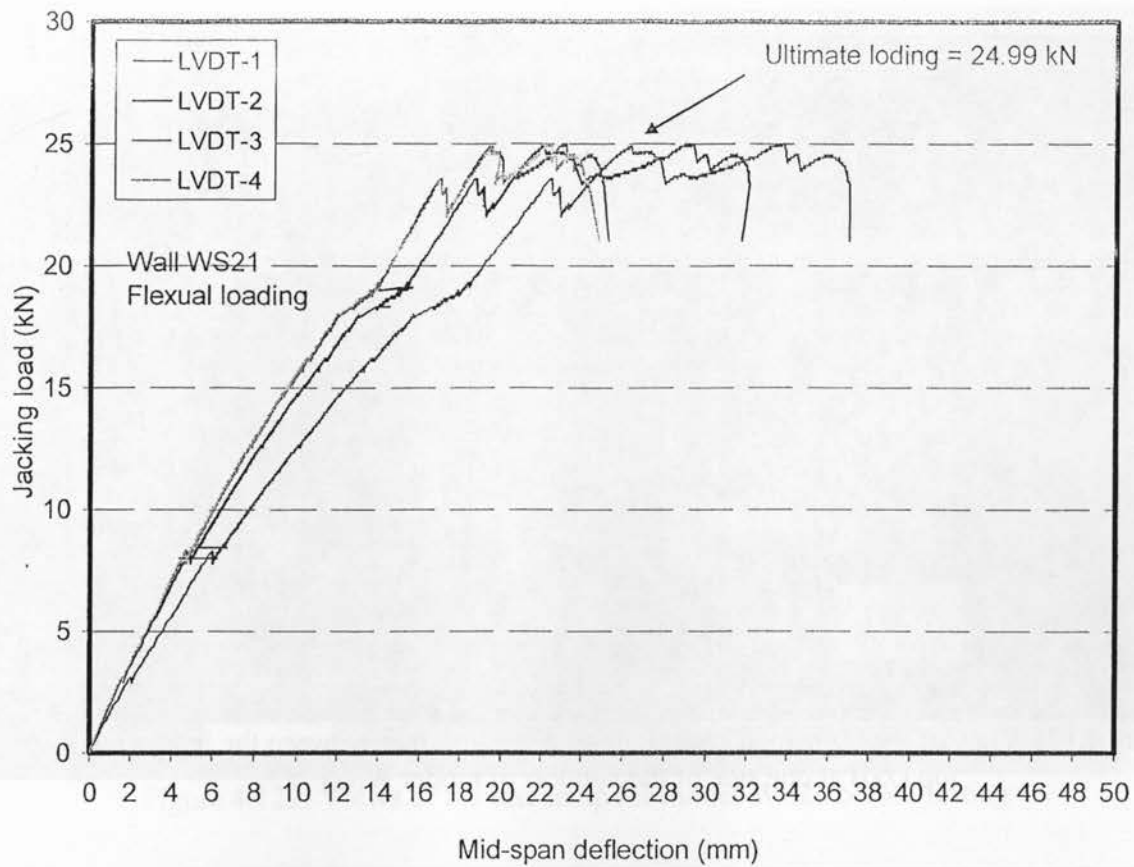


Figure 4.119. Jacking load-deflection relationship for model WS21

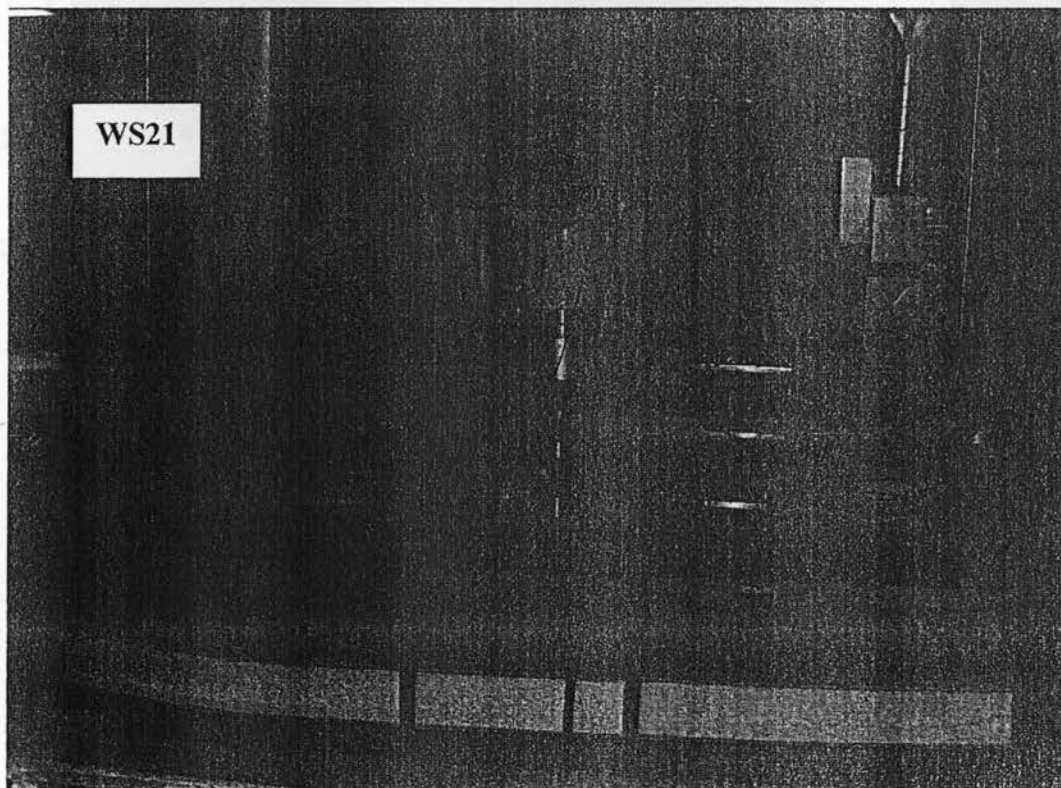


Figure 4.120. View of the deflected shape of model WS21 after failure

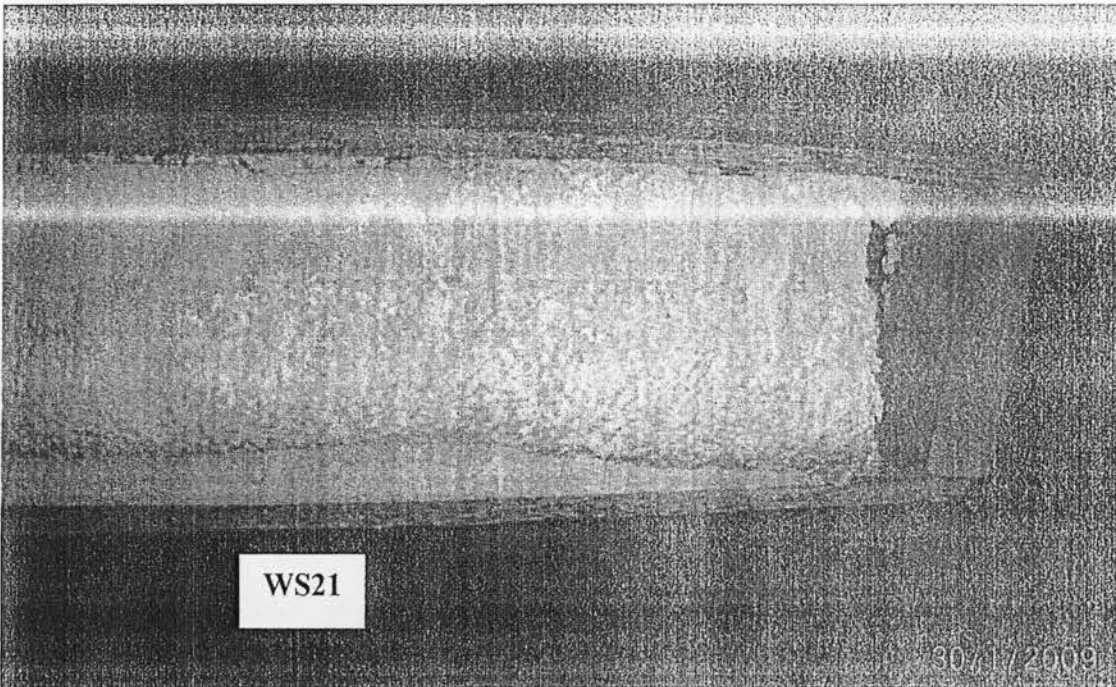


Figure 4.121. View of the horizontal shear failure at the interface between the foam and top OSB at one side of the support of model WS21

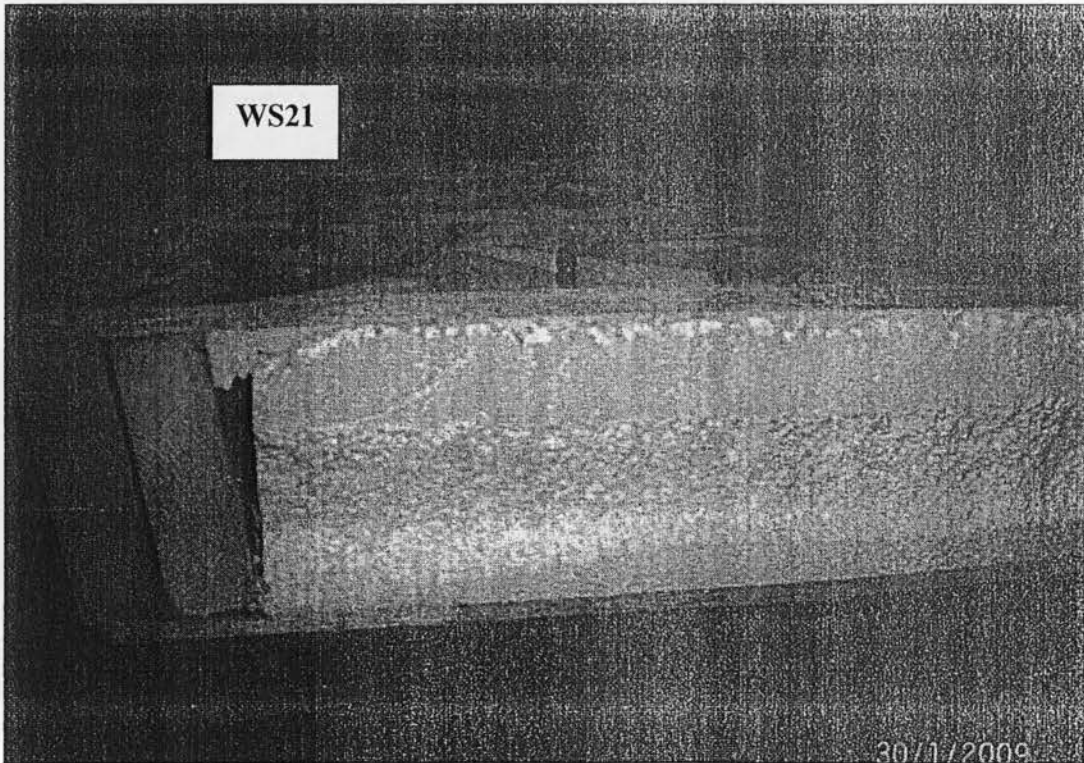


Figure 4.122. View of the horizontal shear failure at the interface between the foam and top OSB at the other side of the support of model WS21

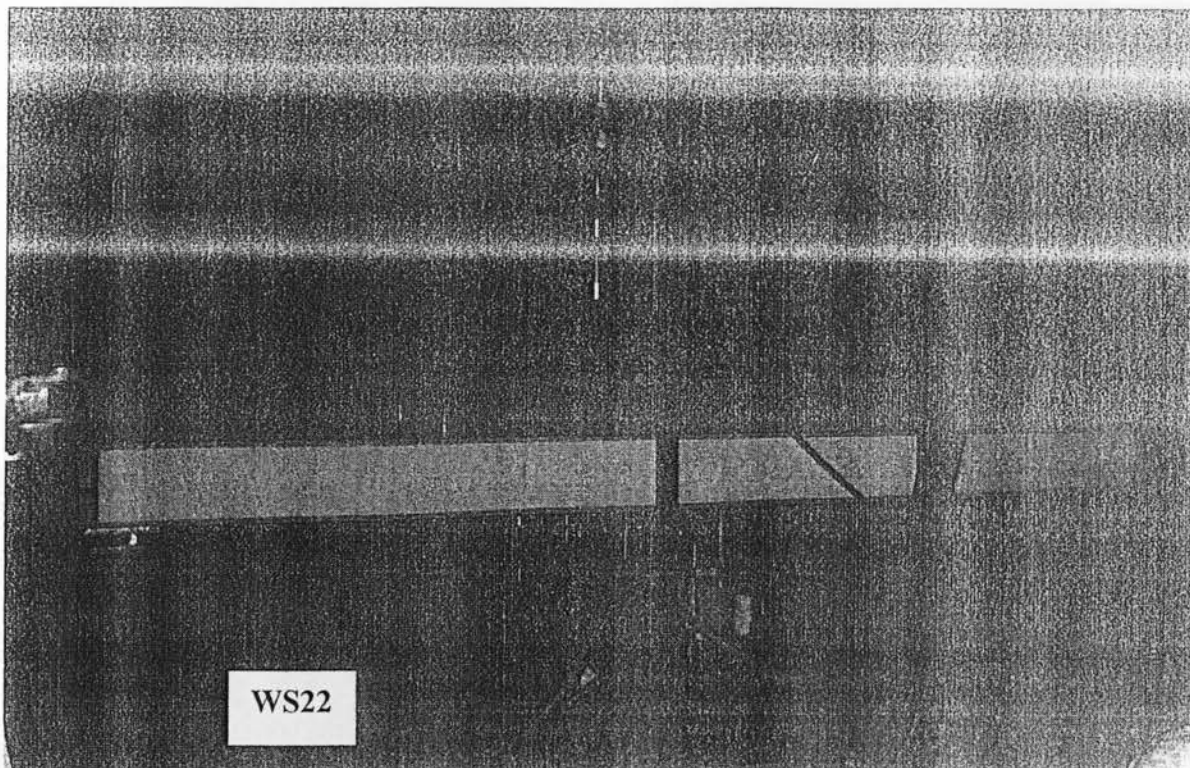


Figure 4.123. Views of the test setup for model WS22 before testing

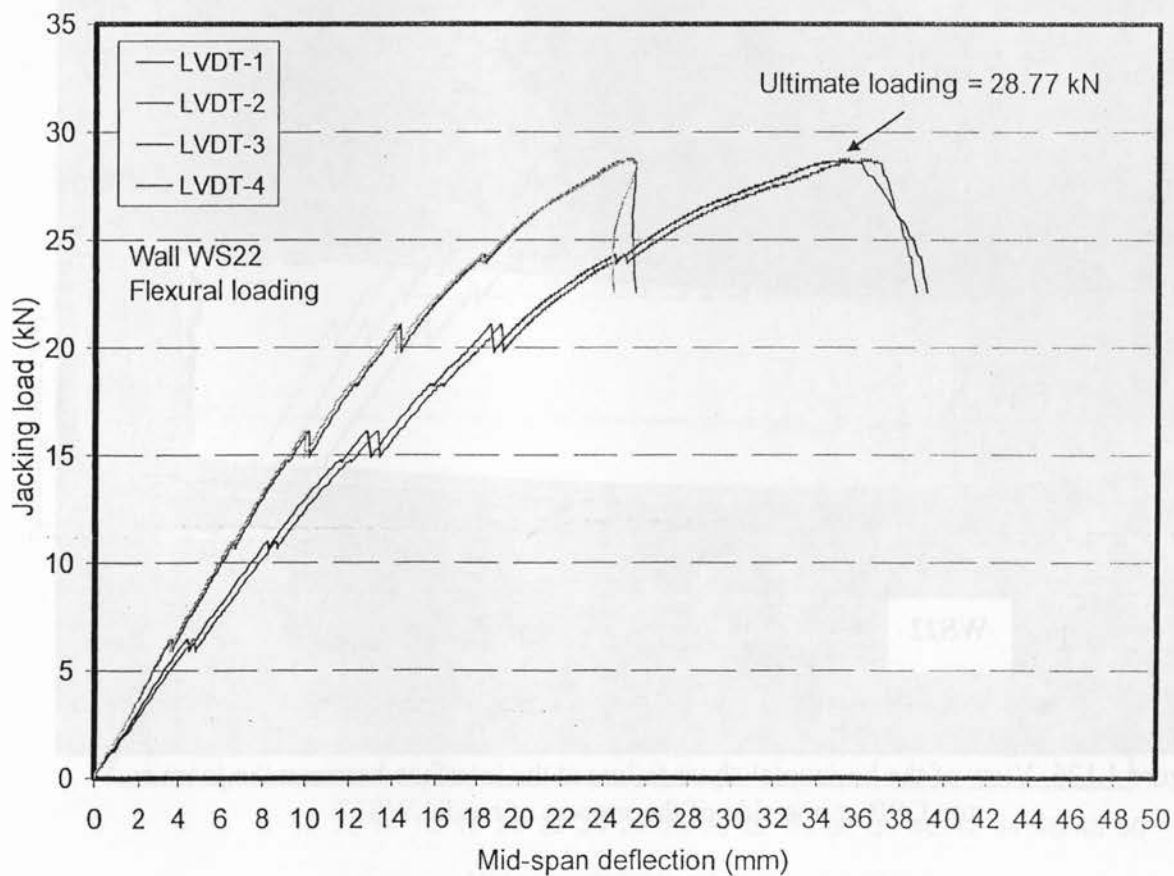


Figure 4.124. Jacking load-deflection relationship for model WS22

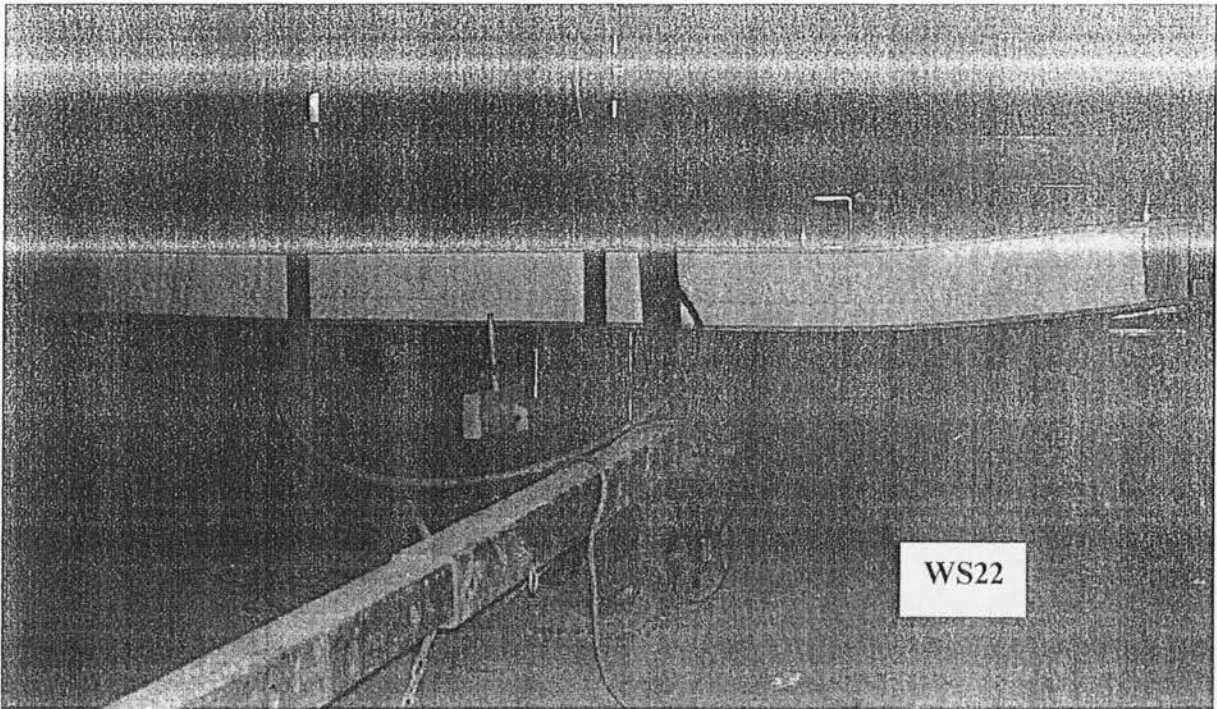


Figure 4.125. View of the deflected shape of model WS22 after failure

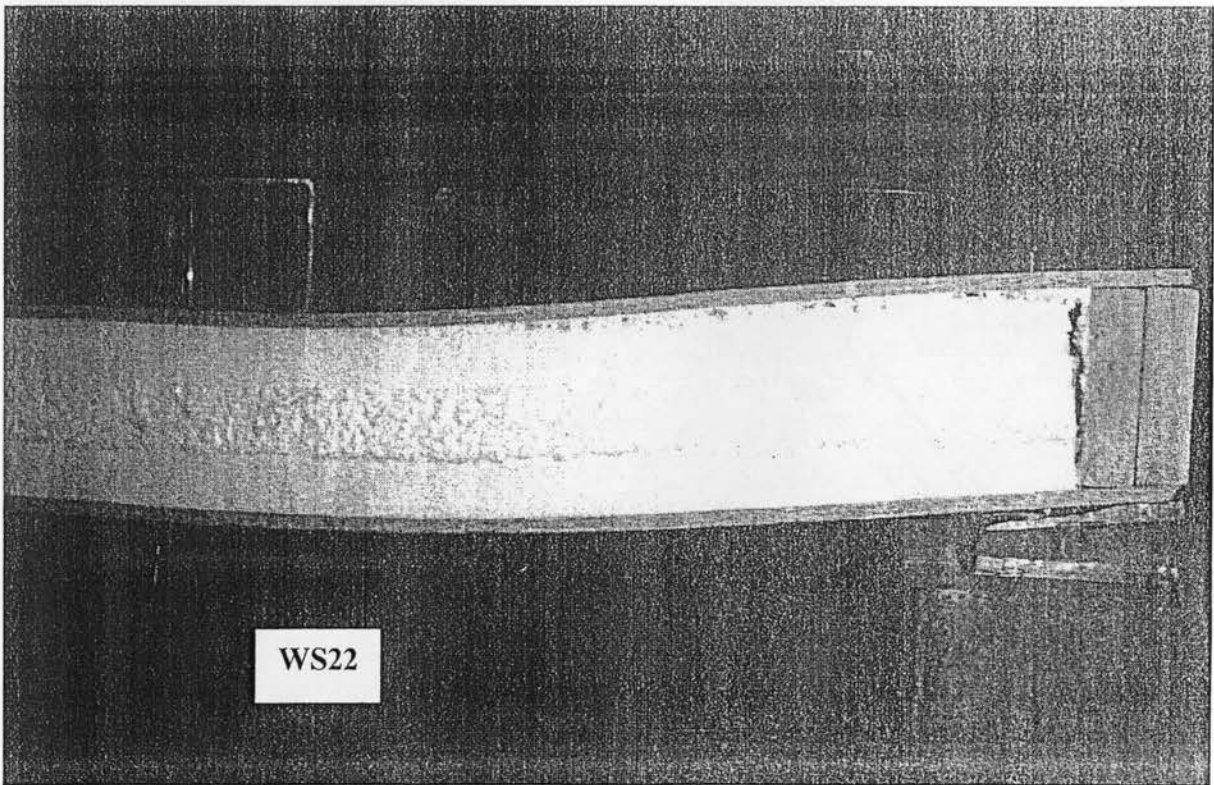


Figure 4.126. View of the horizontal shear failure at the interface between the foam and top OSB at one side of the support of model WS22

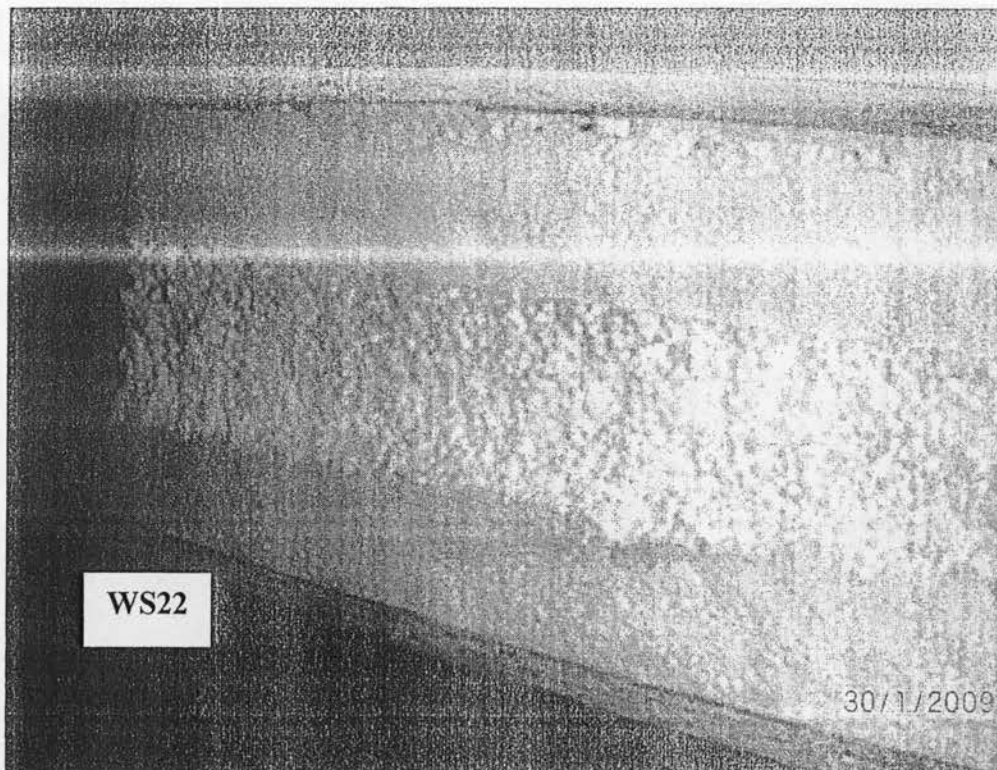


Figure 4.127 View of the horizontal shear failure at the interface between the foam and top OSB at the other side of the support of model WS22

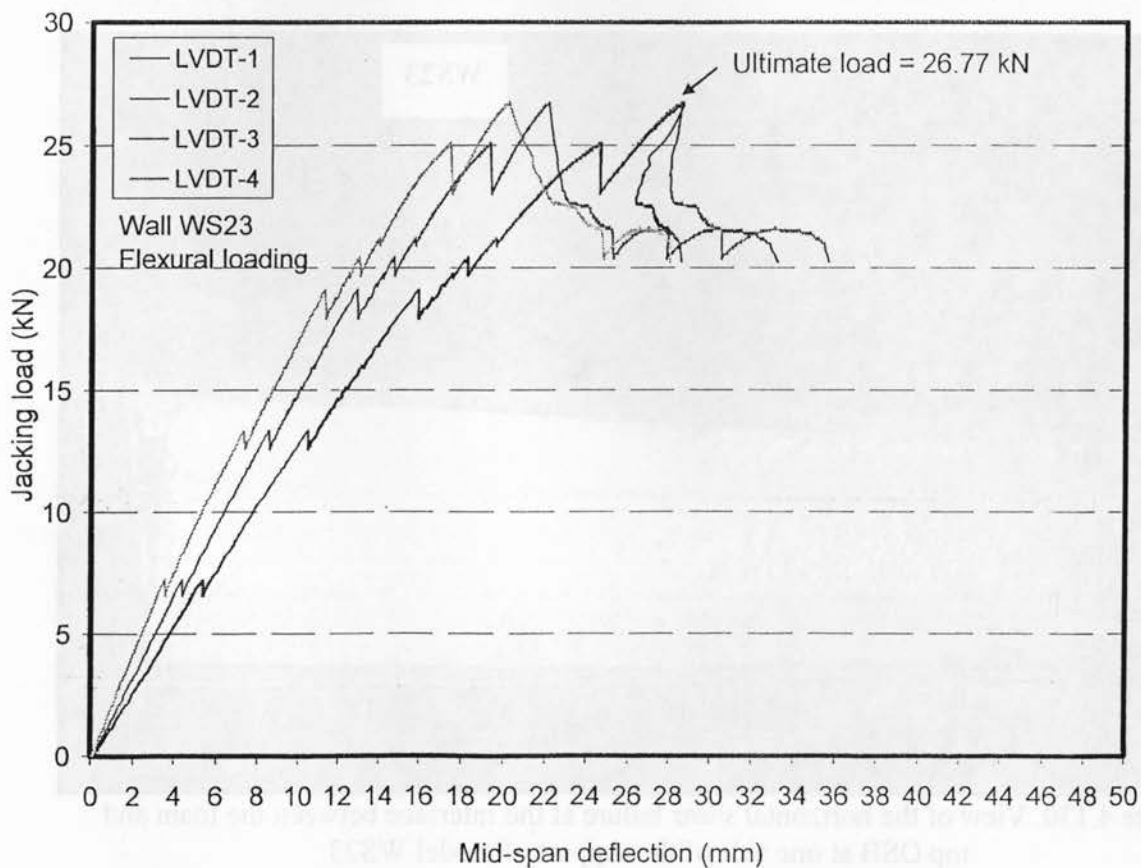


Figure 4.128. Jacking load-deflection relationship for model WS23

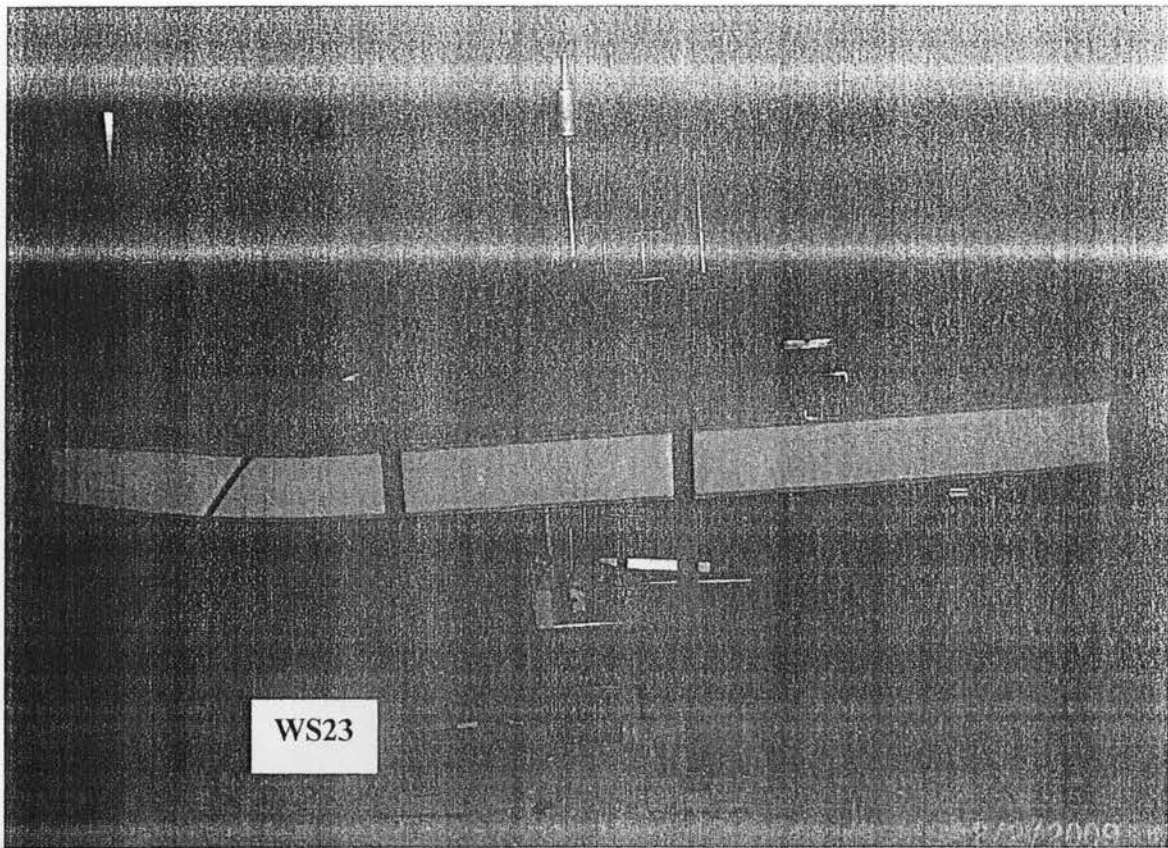


Figure 4.129. View of the deflected shape of model WS23 after failure

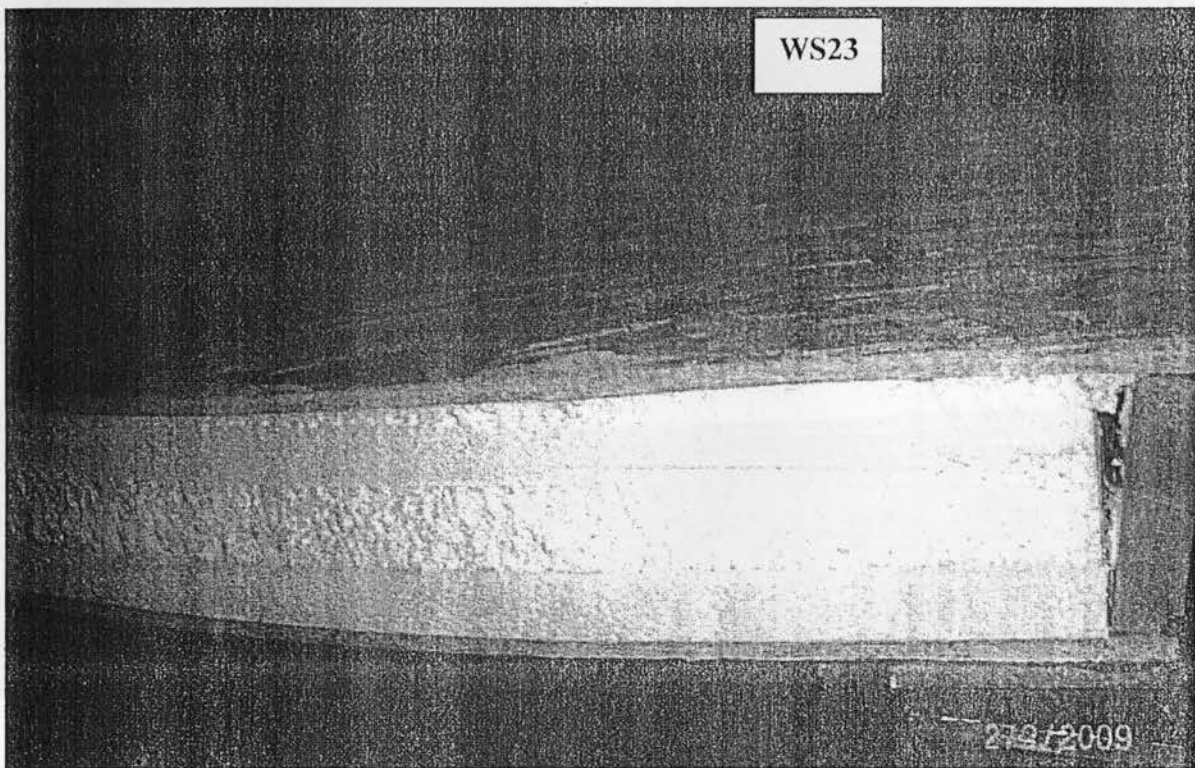


Figure 4.130. View of the horizontal shear failure at the interface between the foam and top OSB at one side of the support of model WS23

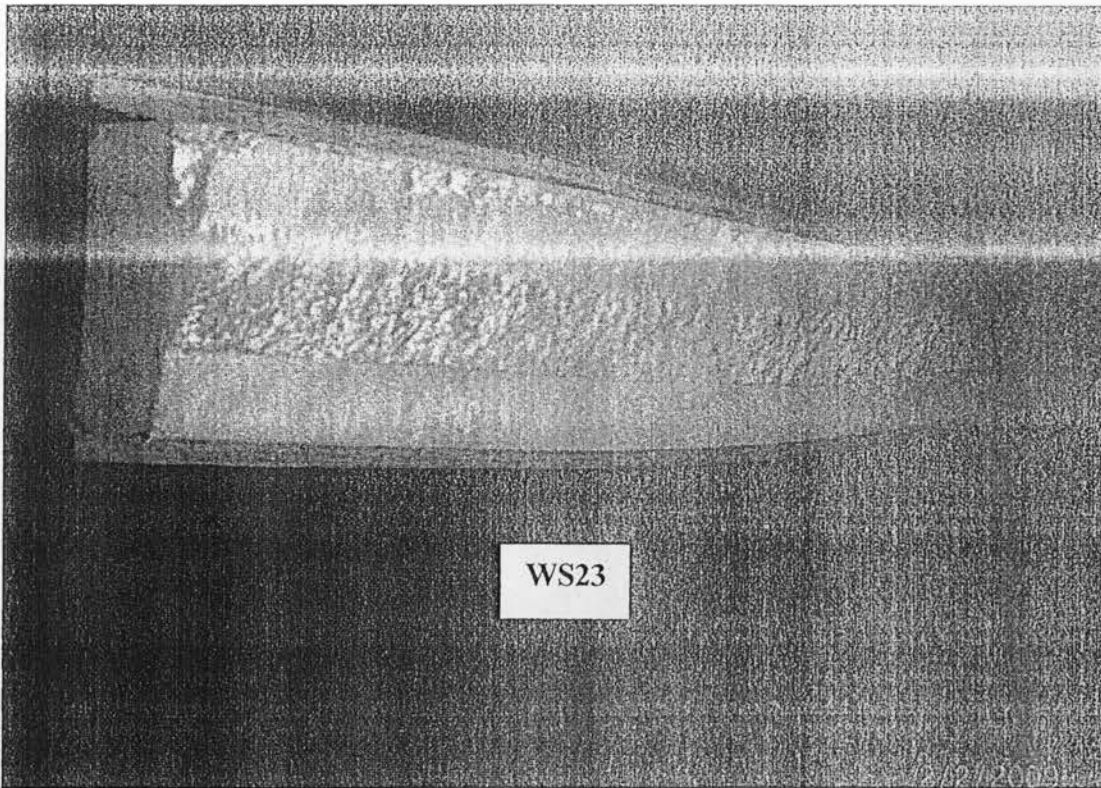


Figure 4.131. View of the horizontal shear failure at the interface between the foam and top OSB at the other side of the support of model WS23

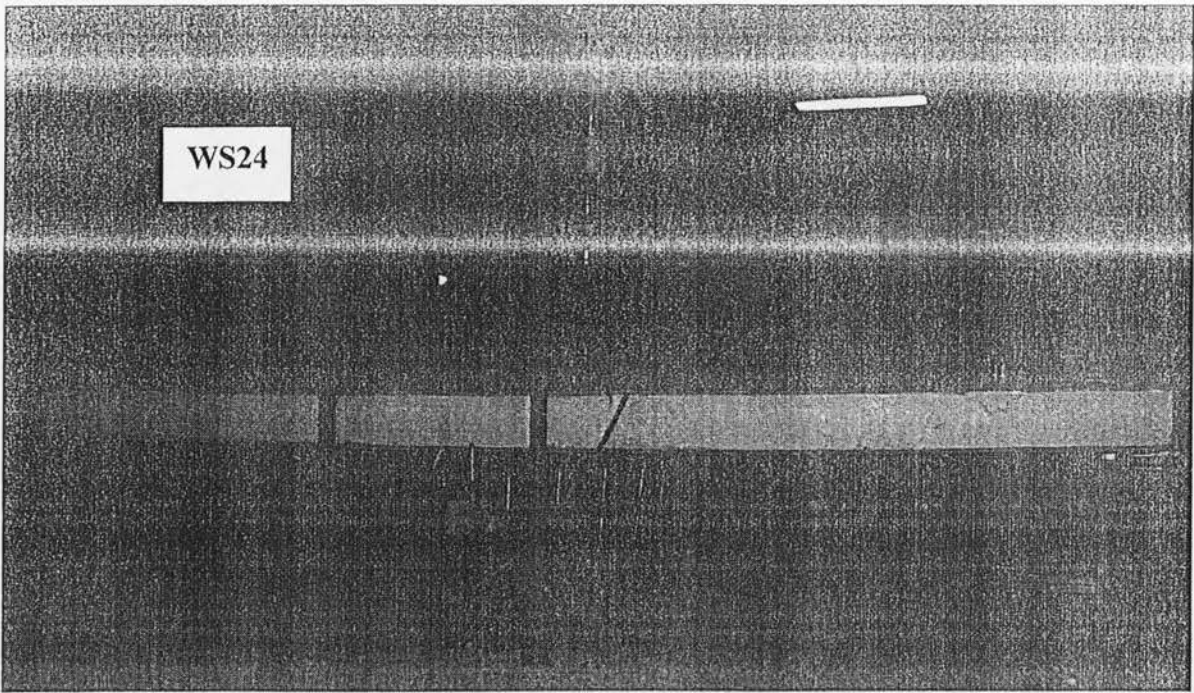


Figure 4.132. View of the setup of WS24 before testing

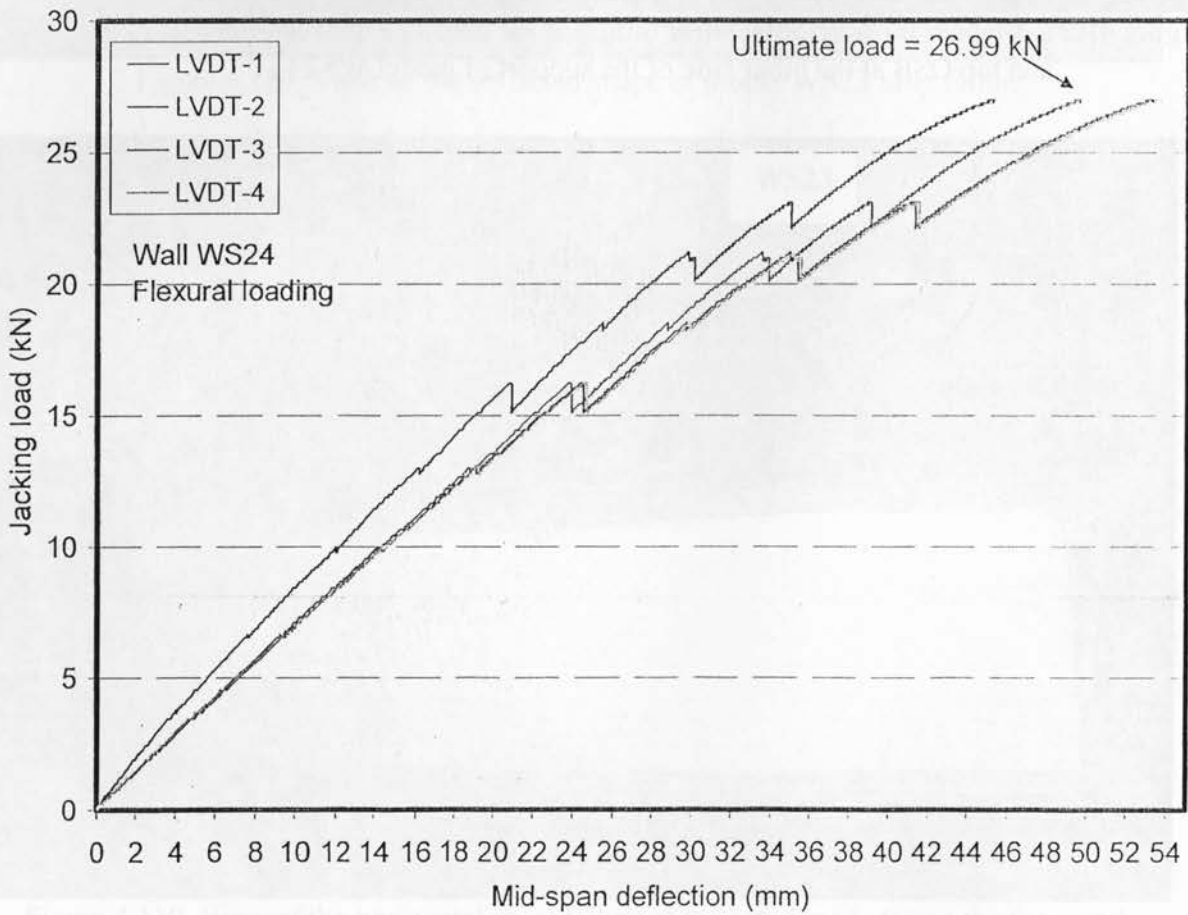


Figure 4.133. Jacking load-deflection relationship for model WS24

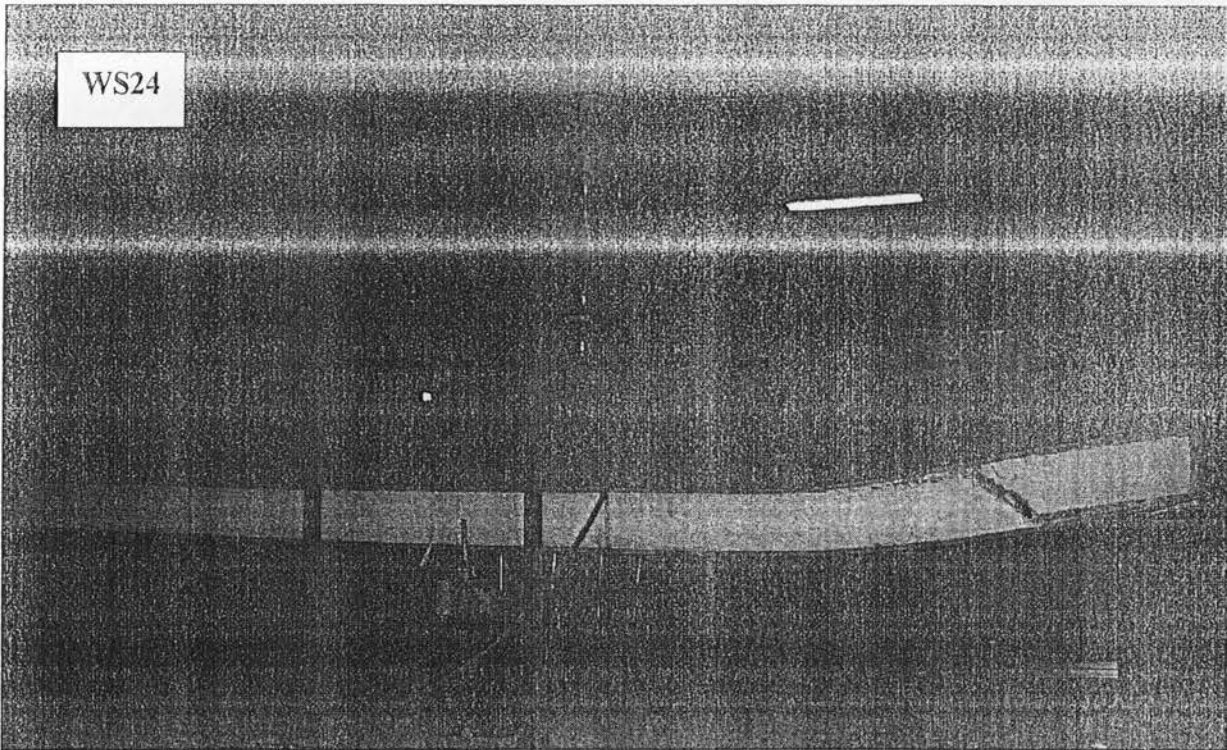


Figure 4.134. View of the deflected shape of model WS24 after failure

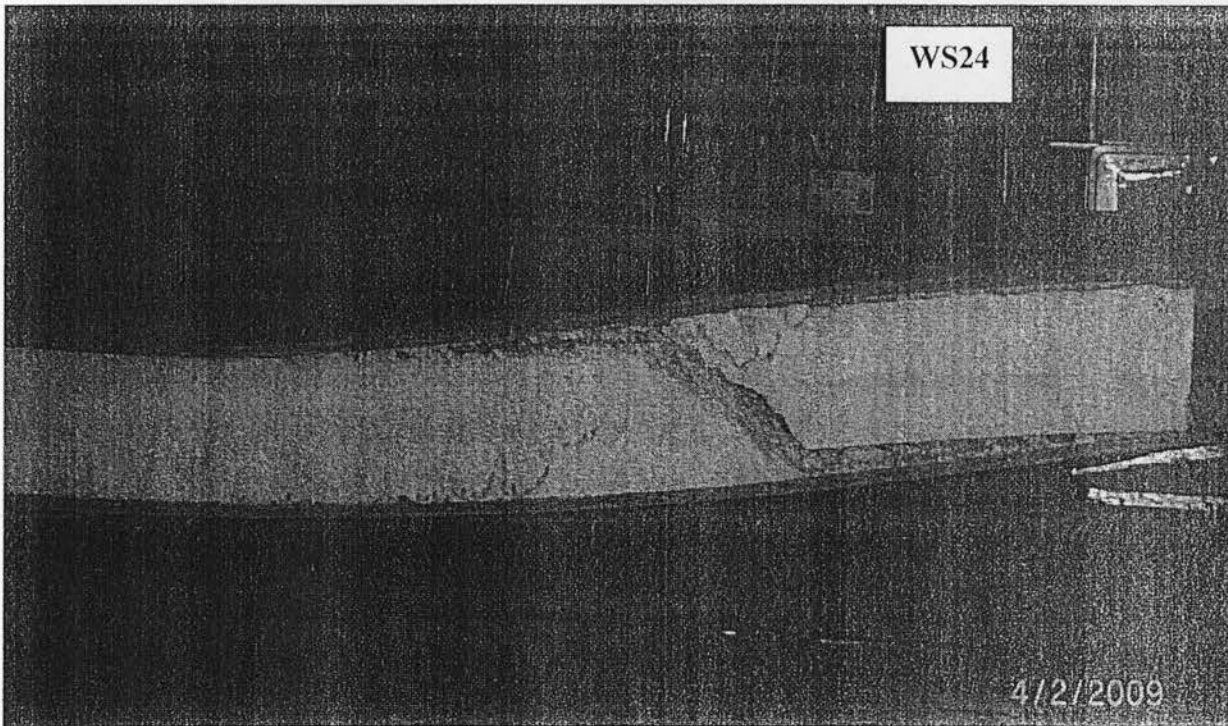


Figure 4.135. View of the diagonal shear failure at one side of the support of model WS24

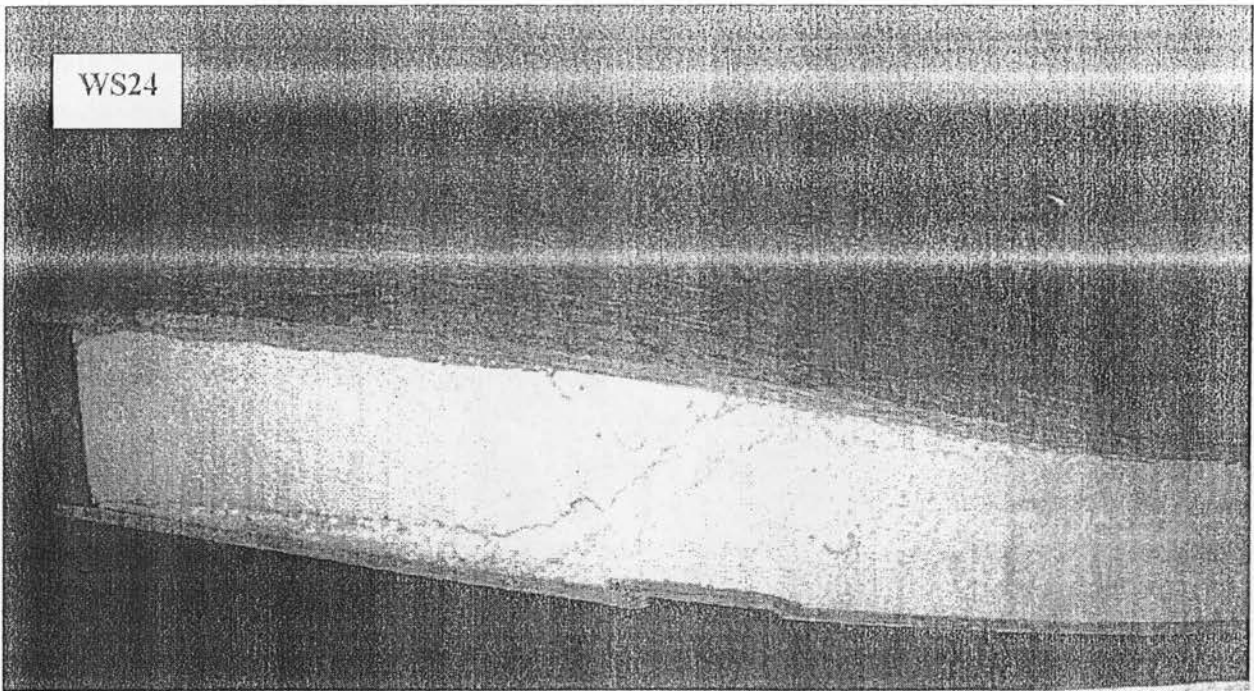


Figure 4.136. View of the diagonal shear failure at the other side of the support of model WS24

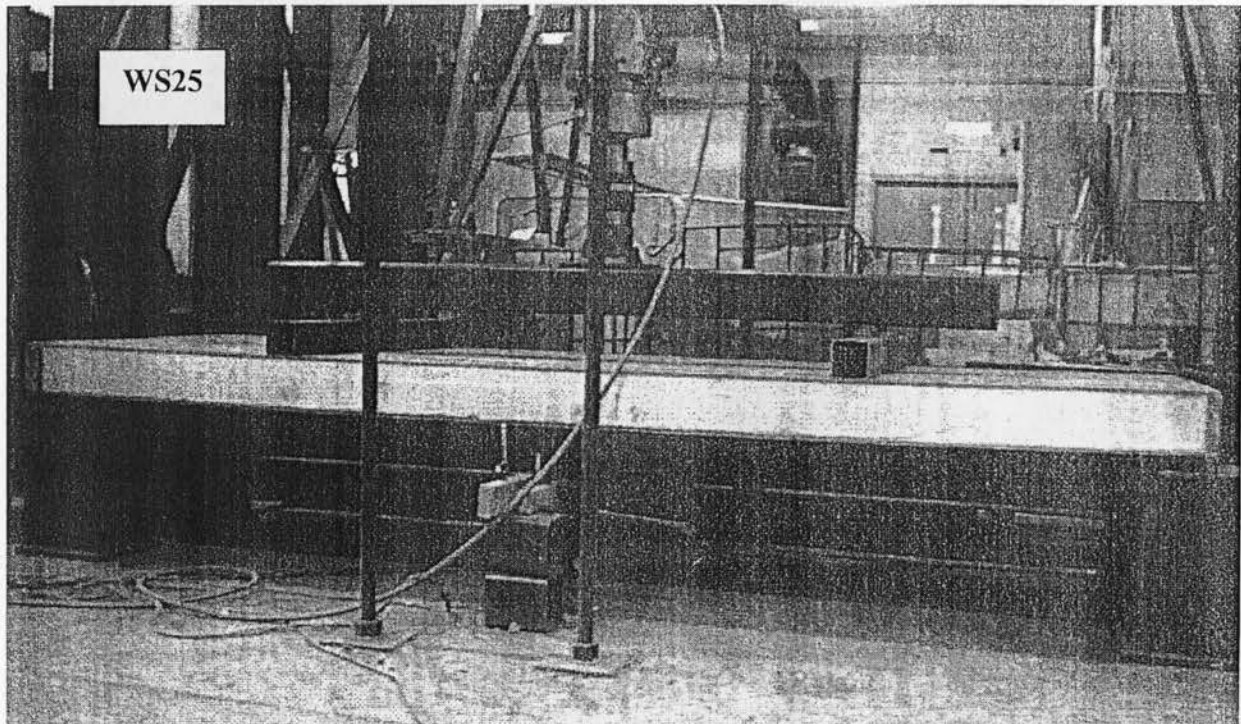


Figure 4.137. View of the setup of WS25 before testing

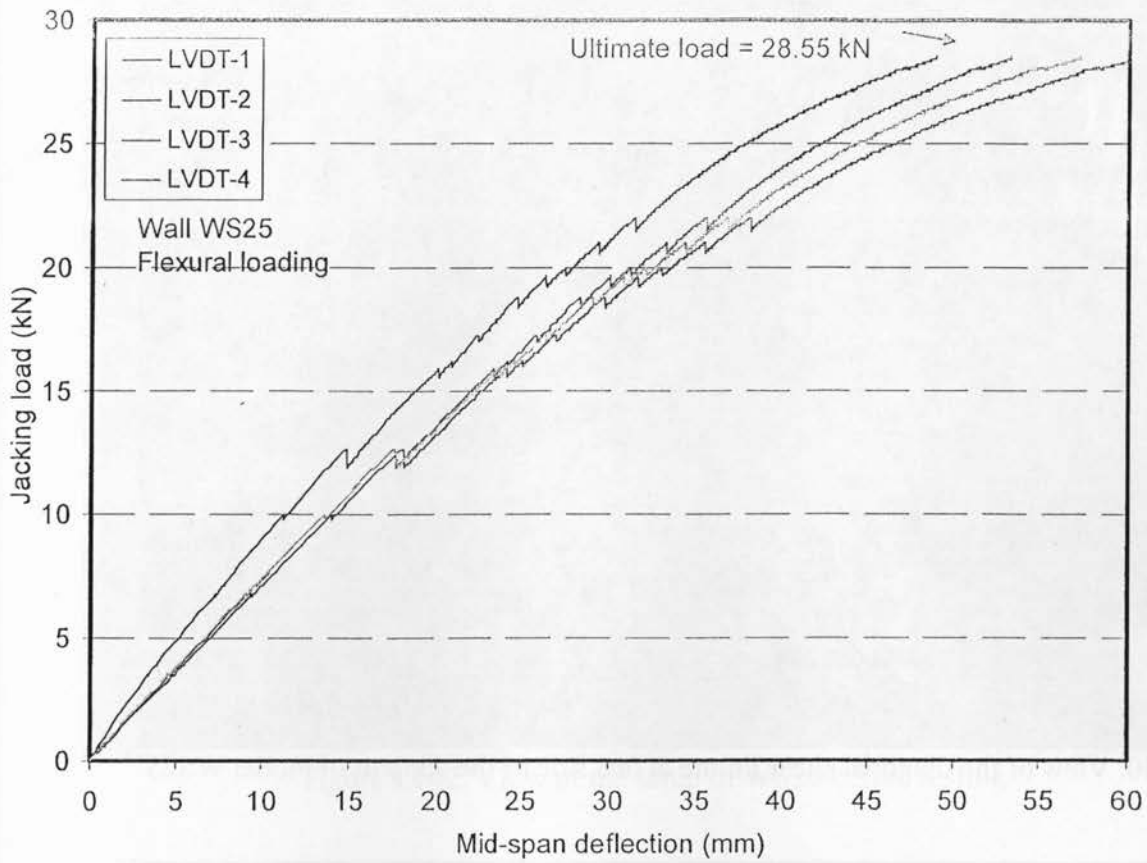


Figure 4.138. Jacking load-deflection relationship for model WS25

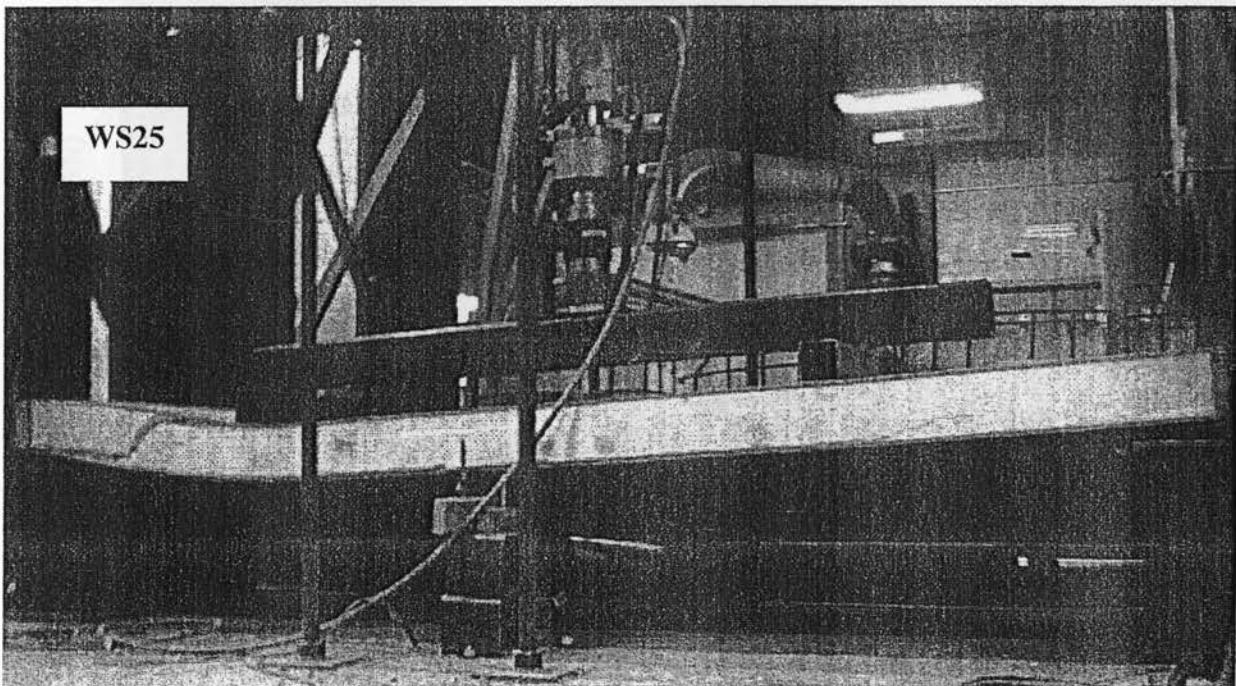


Figure 4.139. View of the deflected shape of model WS25 after failure

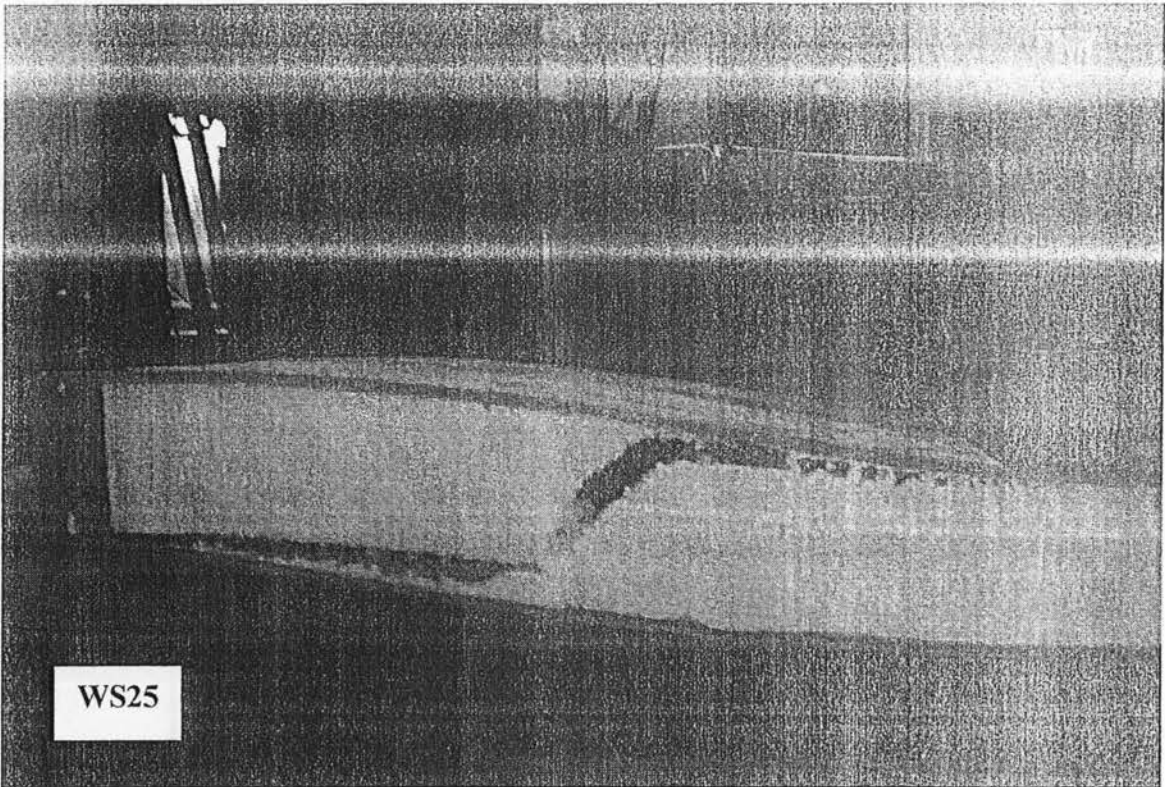


Figure 4.140. View of the diagonal shear failure at one side of the support of model WS25

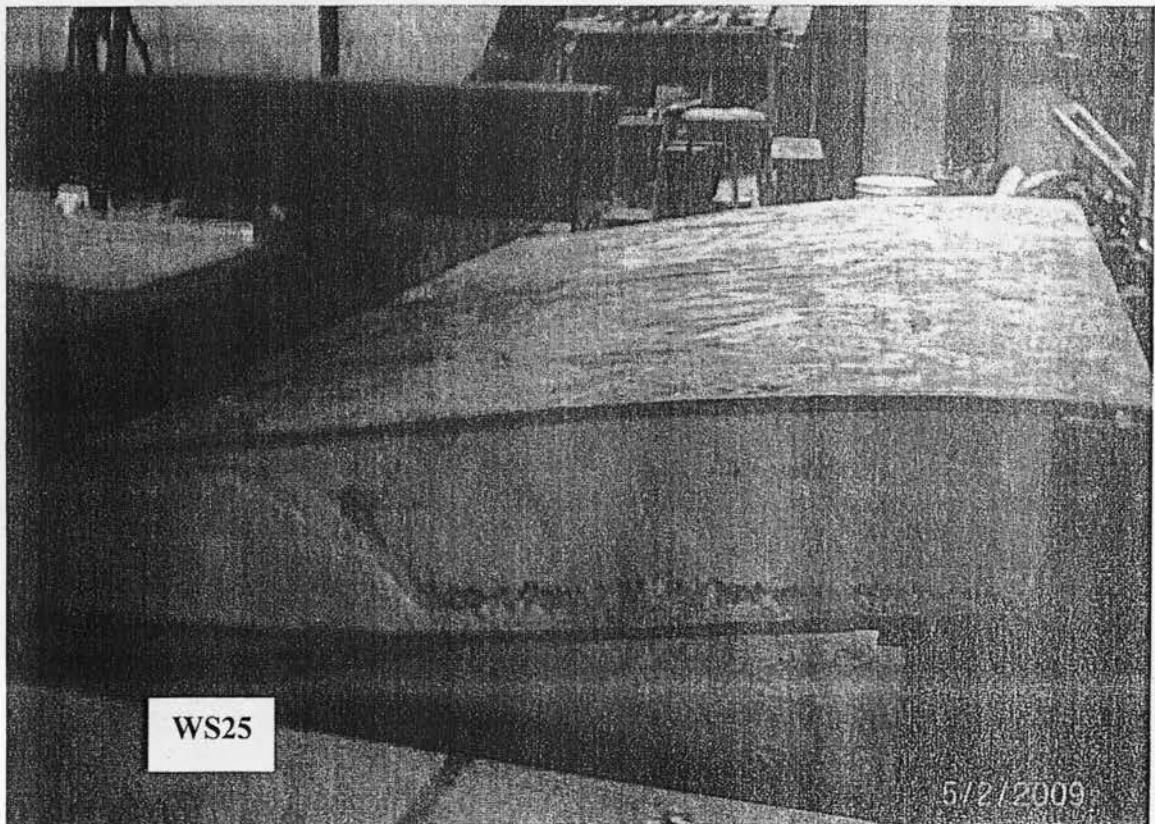


Figure 4.141. View of the diagonal shear failure at the other side of the support of model WS25

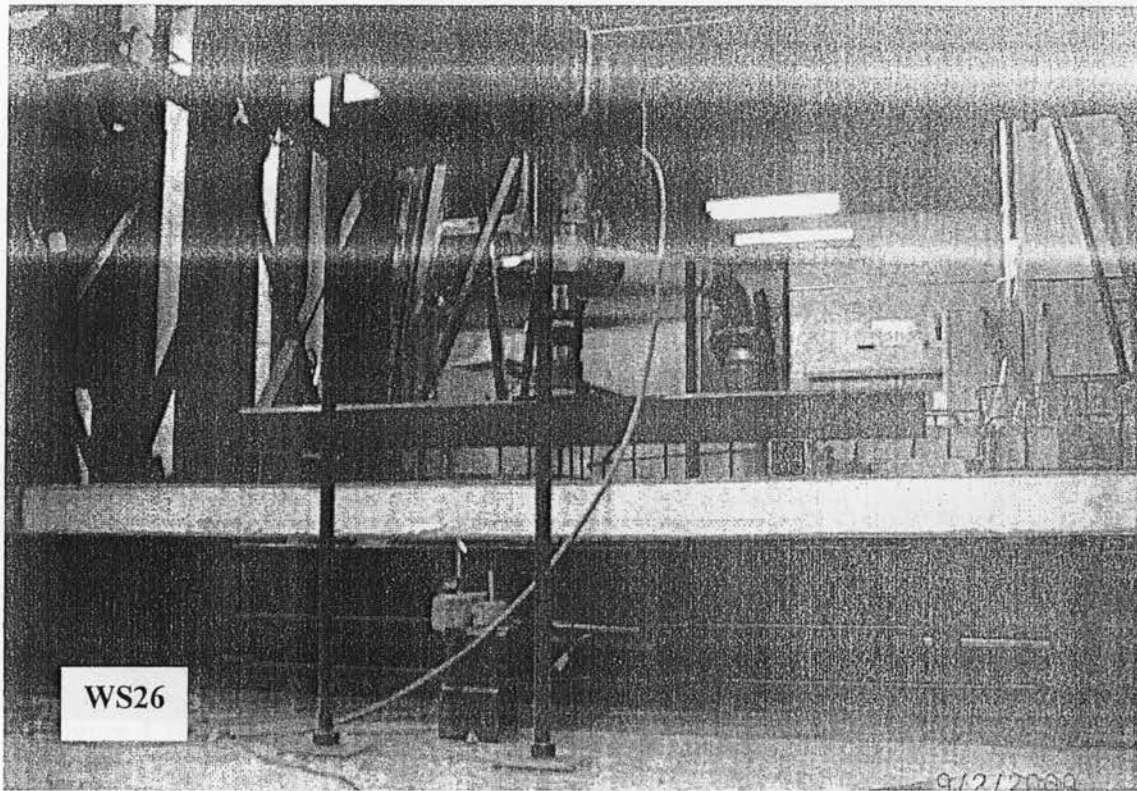


Figure 4.142. View of the setup of WS26 before testing

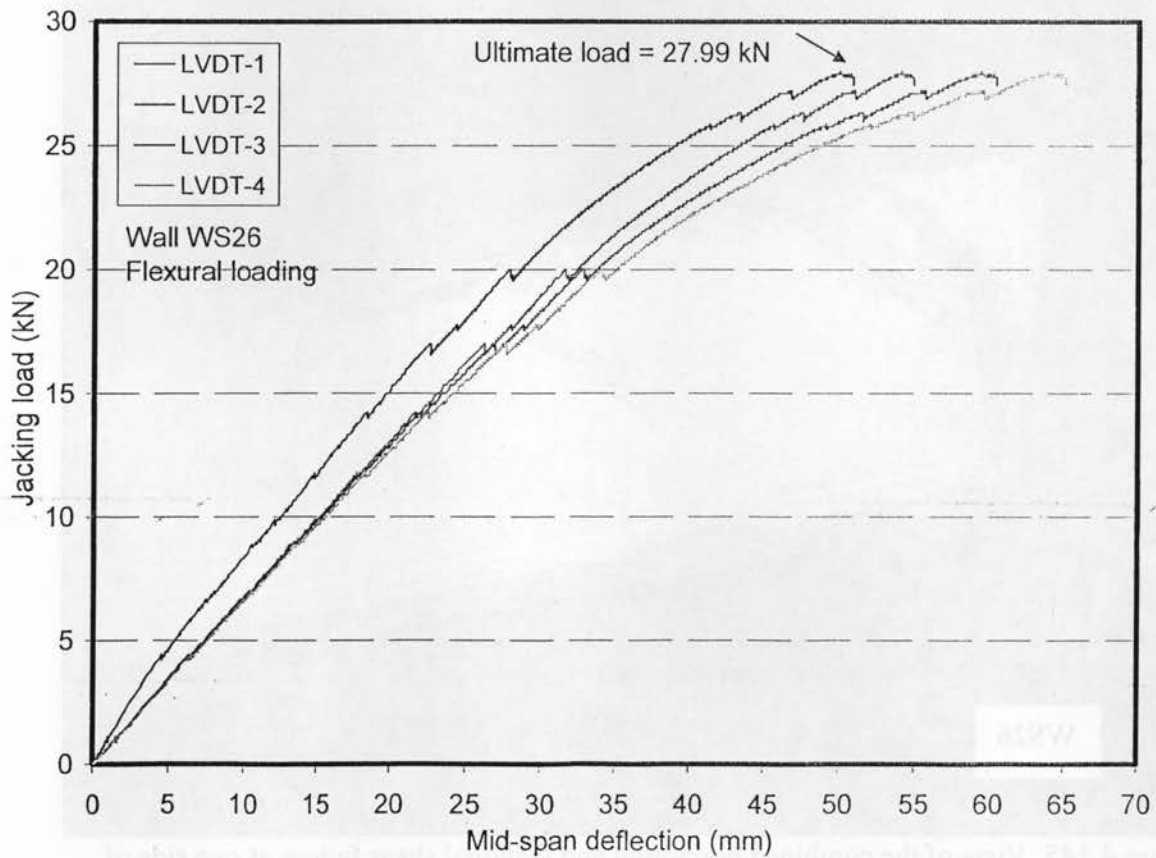


Figure 4.143. Jacking load-deflection relationship for model WS26

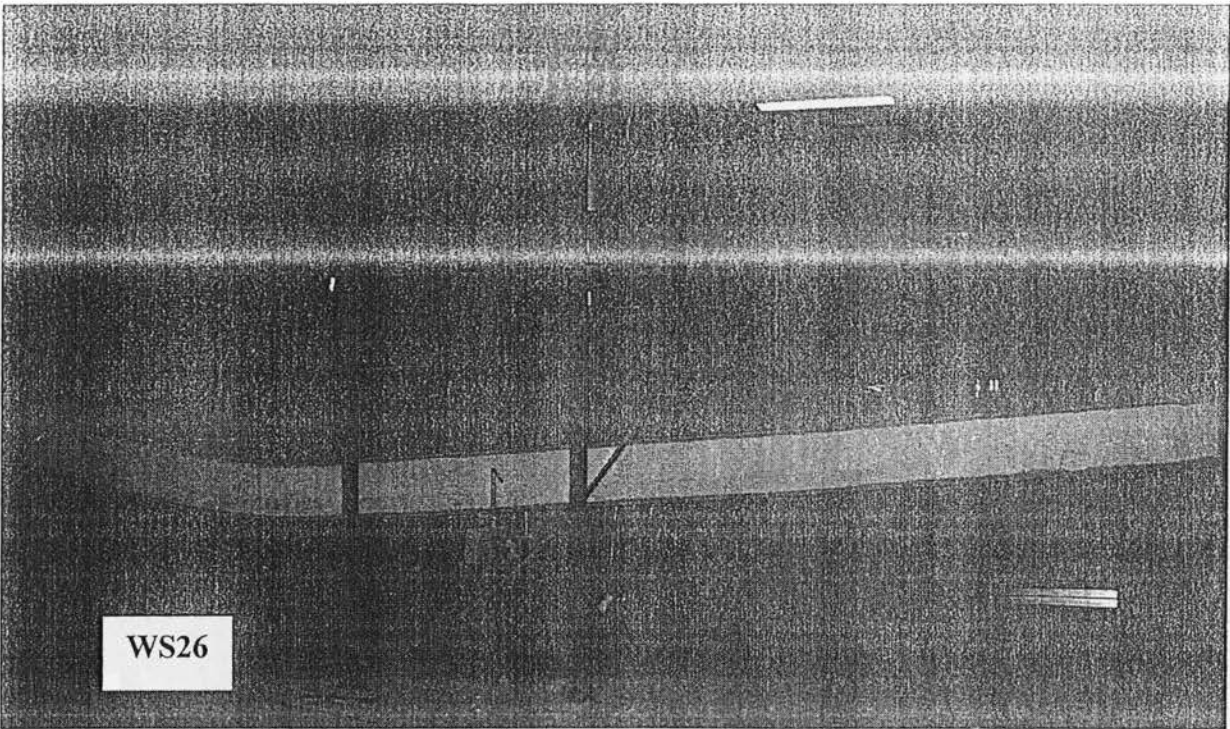


Figure 4.144. View of the deflected shape of model WS26 after failure

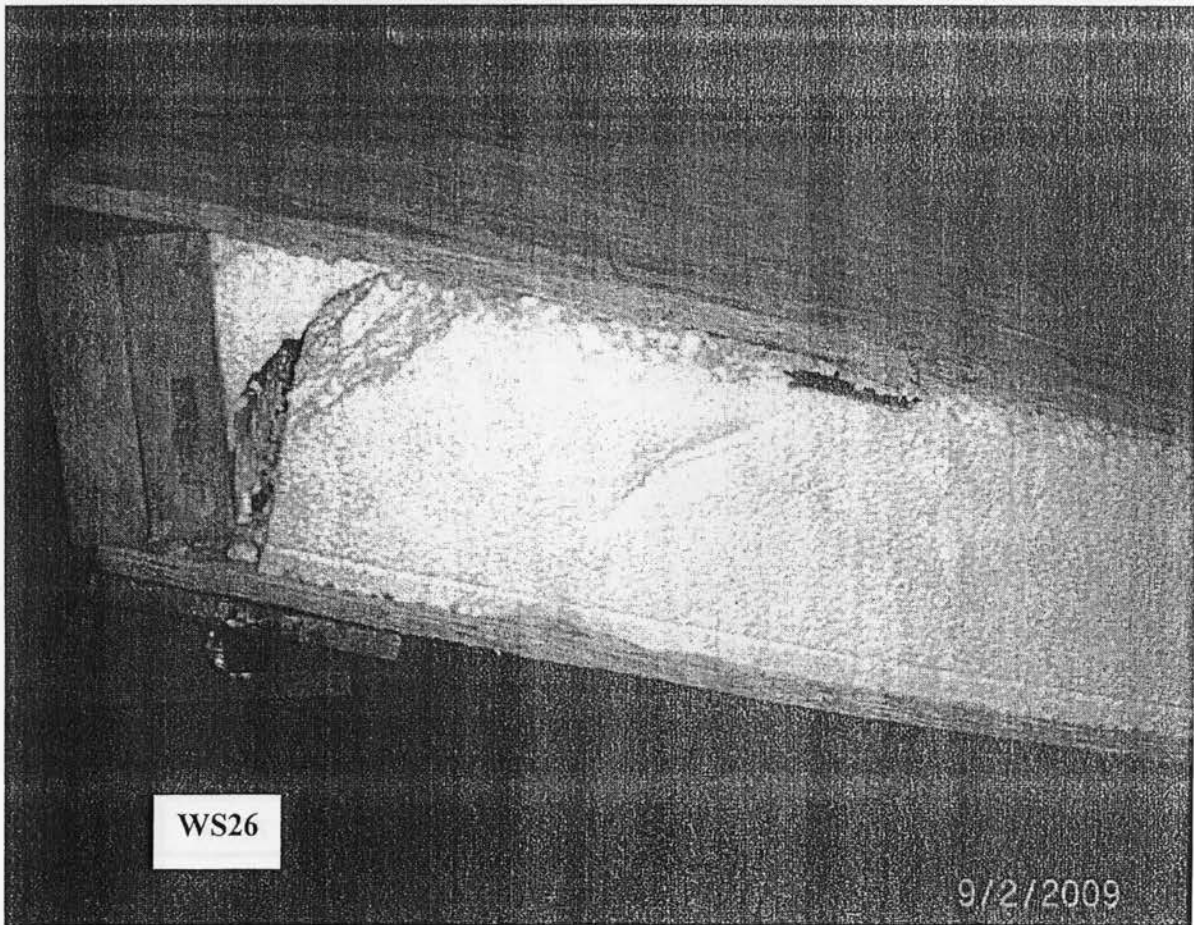


Figure 4.145. View of the combined horizontal and diagonal shear failure at one side of the support of model WS26

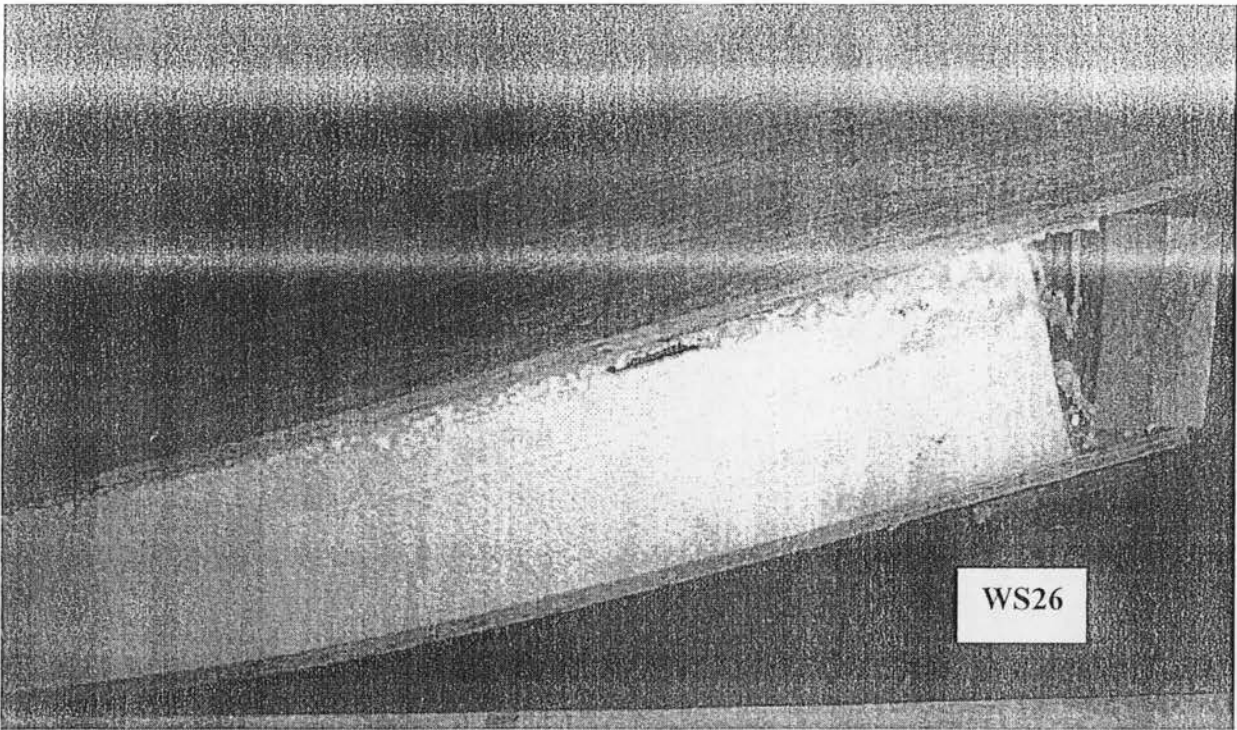


Figure 4.146. View of the horizontal shear failure at the other side of the support of model WS26



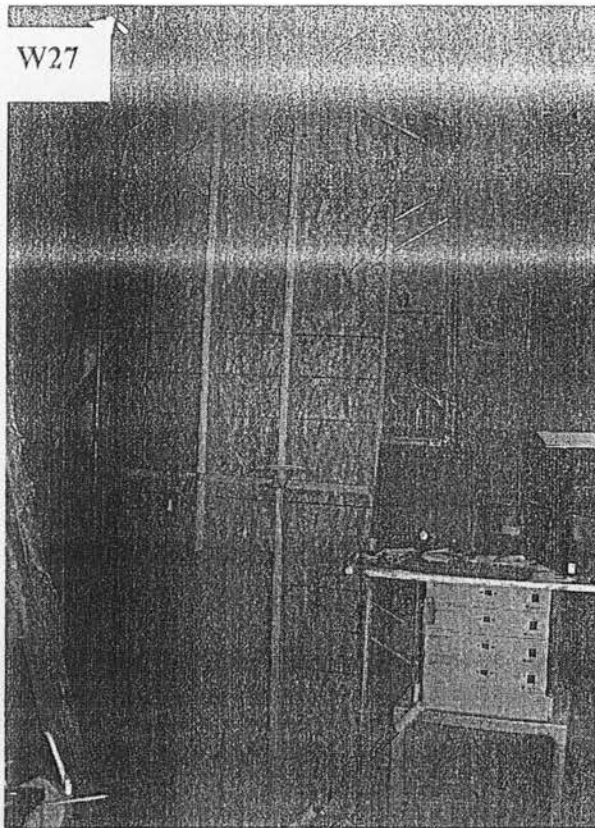


Figure 4.147. View of the test setup for wall W27 before testing

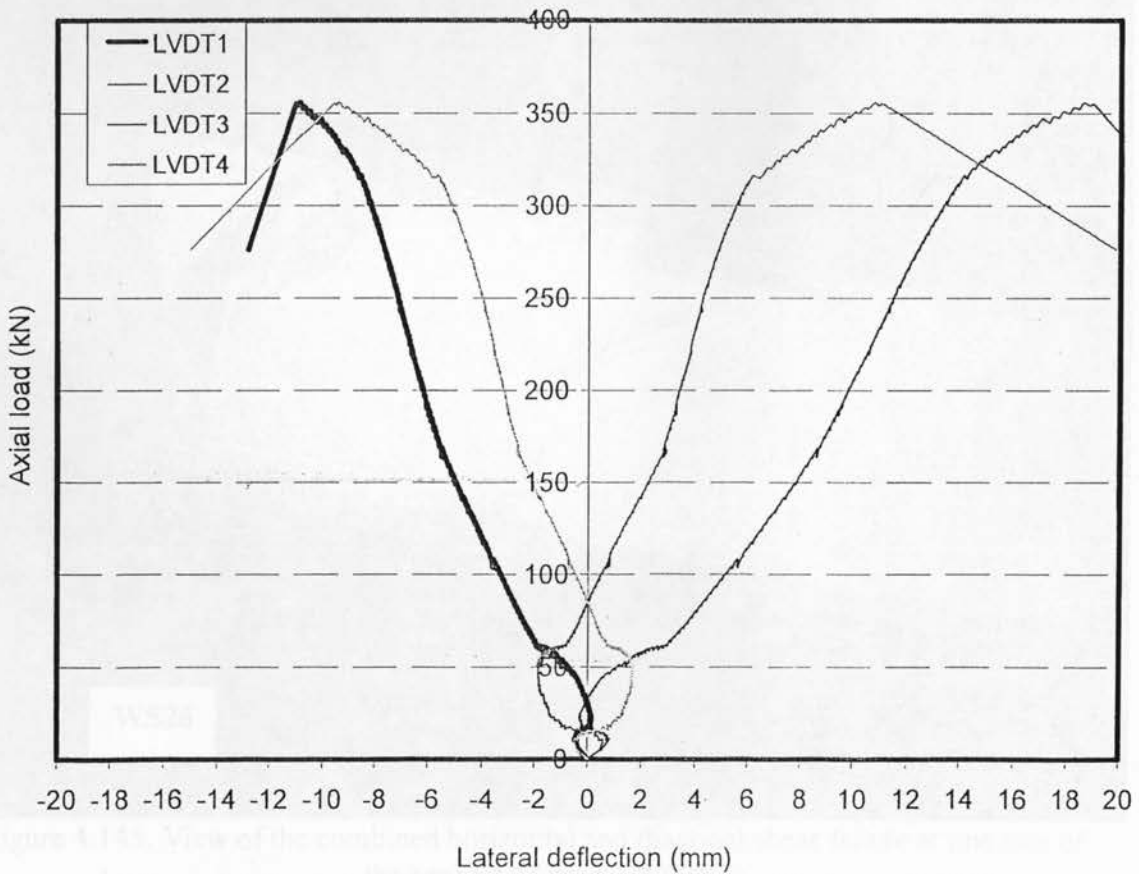


Figure 4.148. Axial load-lateral deflection relationship for model W27

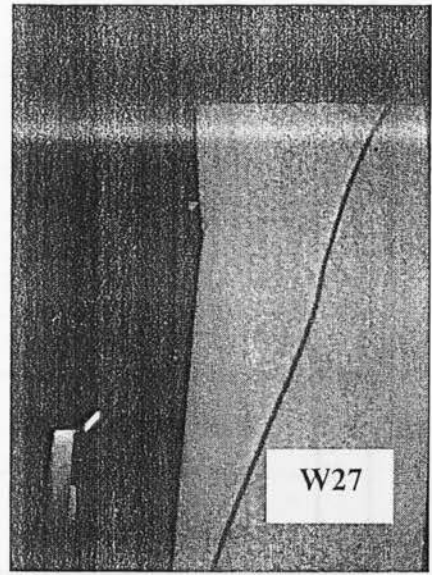
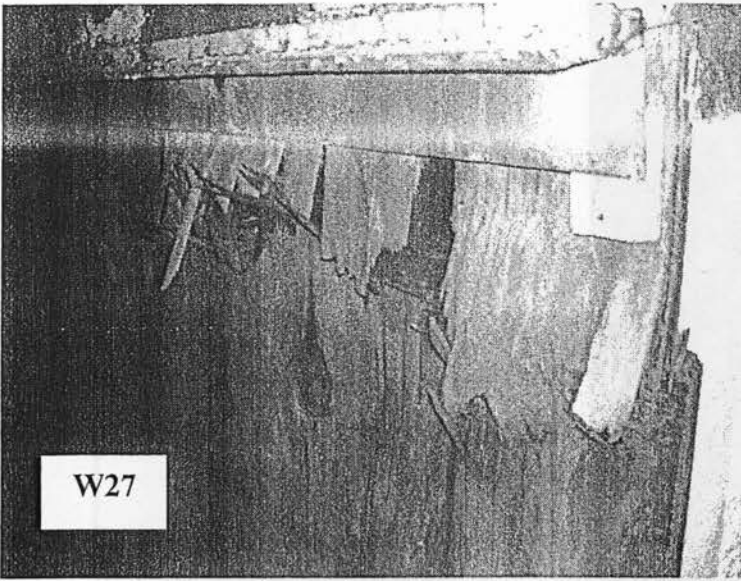


Figure 4.149. View of crushing of the pressure-treated facing at top of the north-west side of wall W27

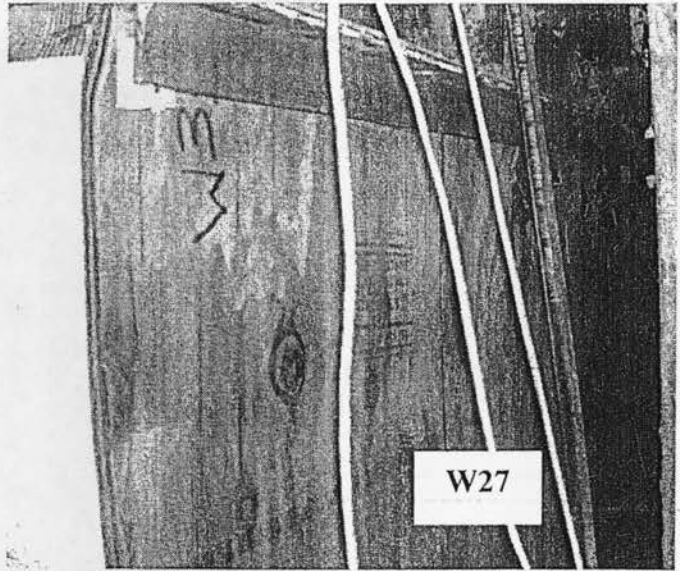
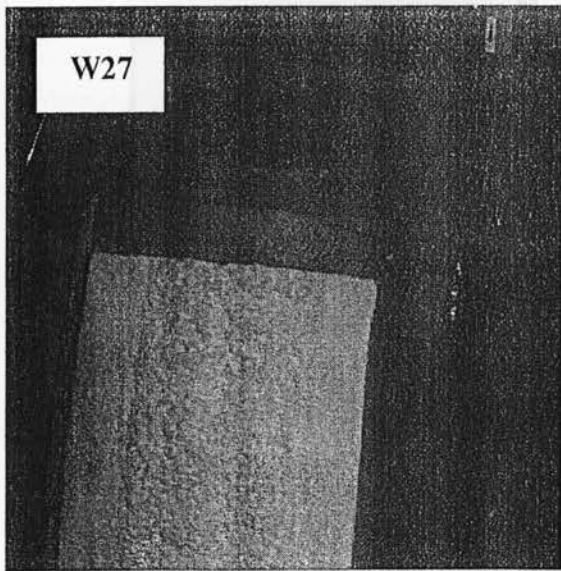


Figure 4.150. View of deformation of the pressure-treated facing at top of the north-east side of wall W27

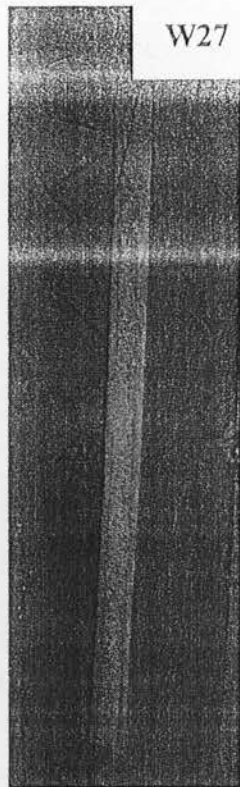


Figure 4.151. View of the lateral deformation of wall W27 after failure

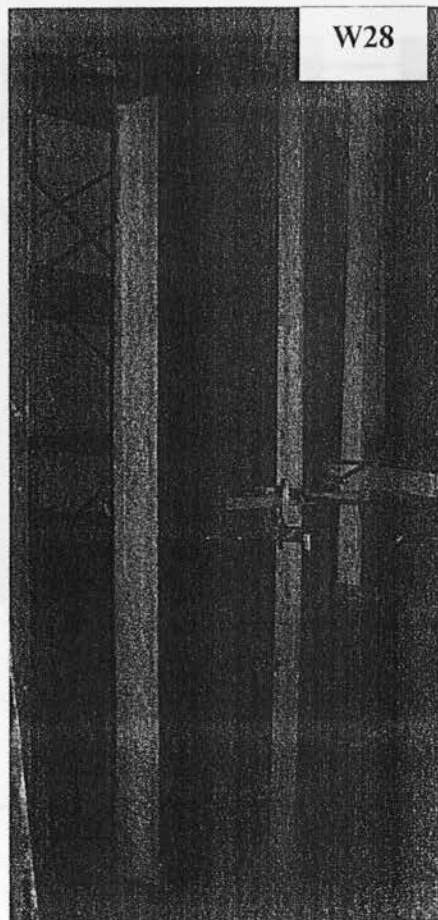


Figure 4.152. View of the test setup for wall W28 before testing

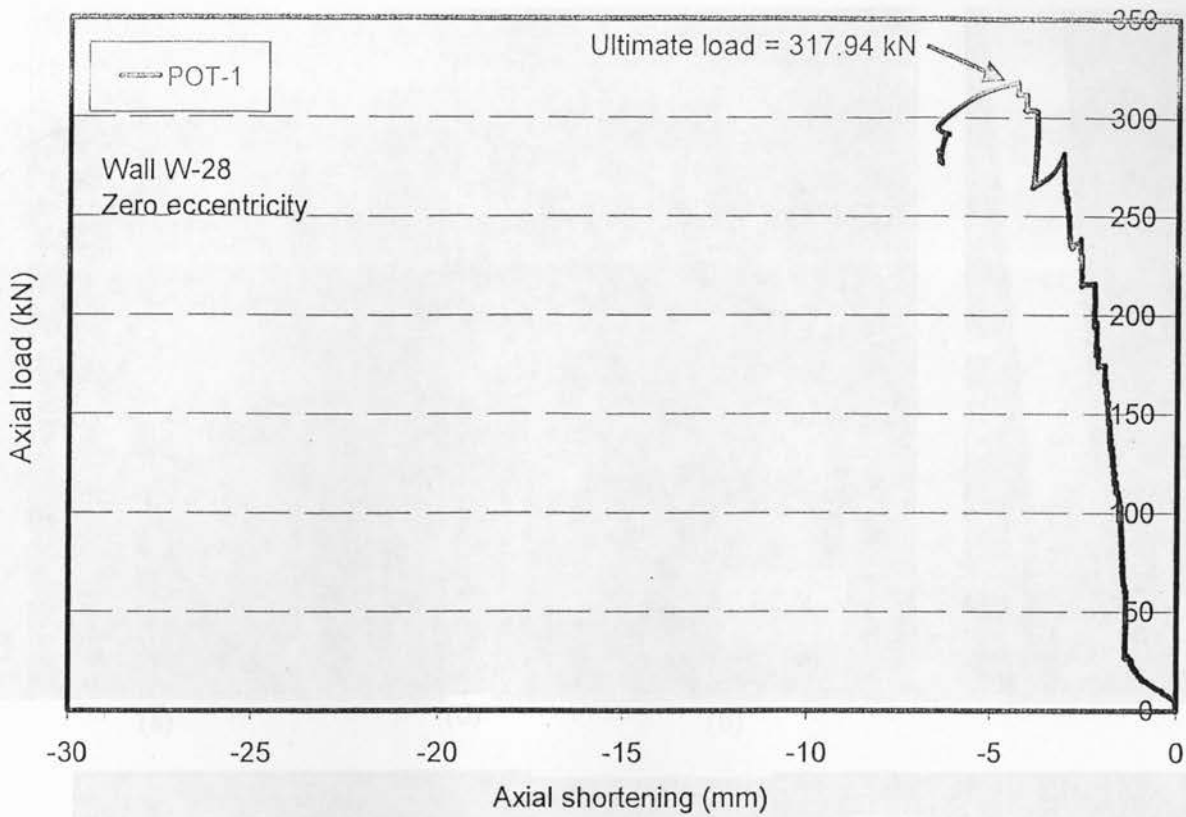


Figure 4.153. Axial load-axial shortening relationship for model W28

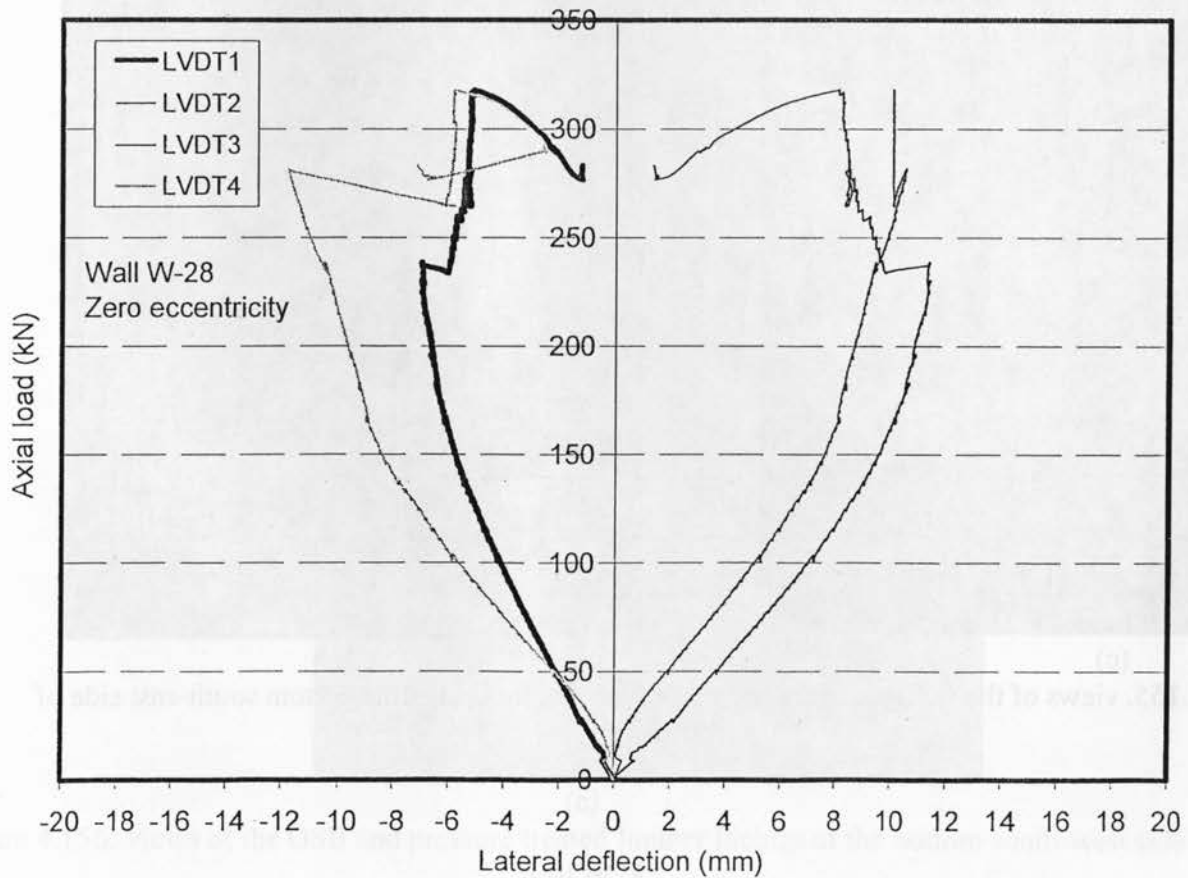
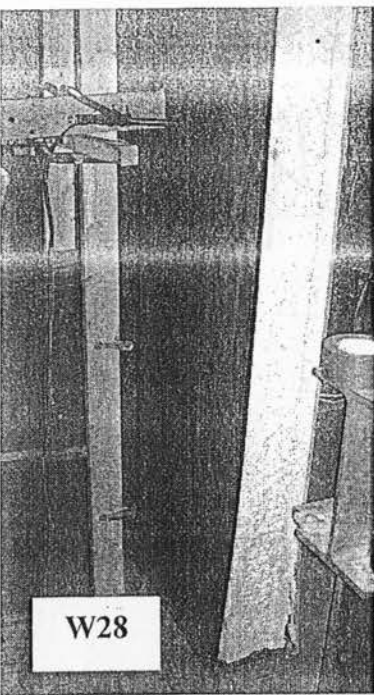
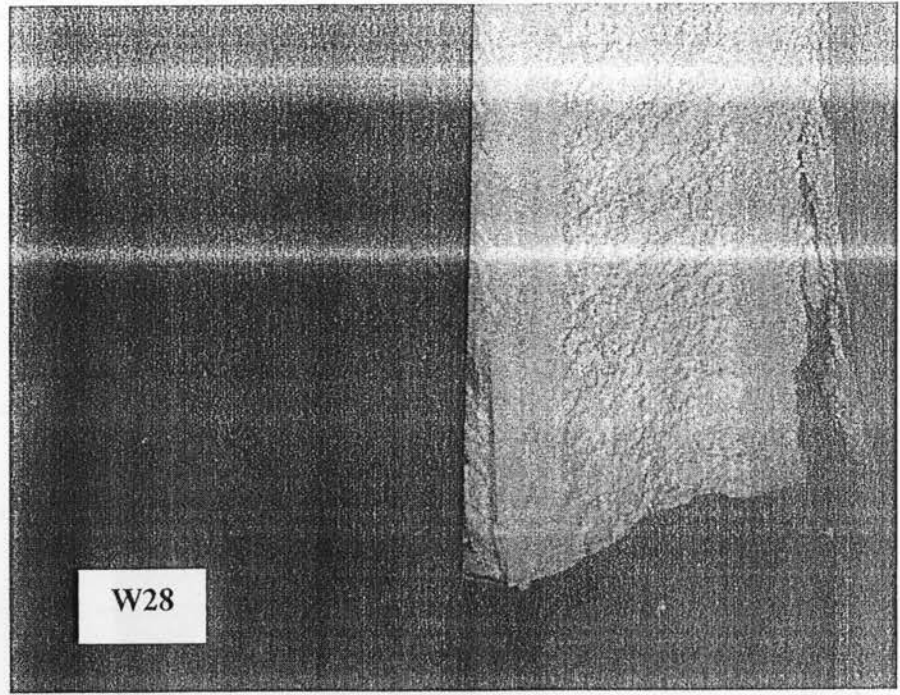


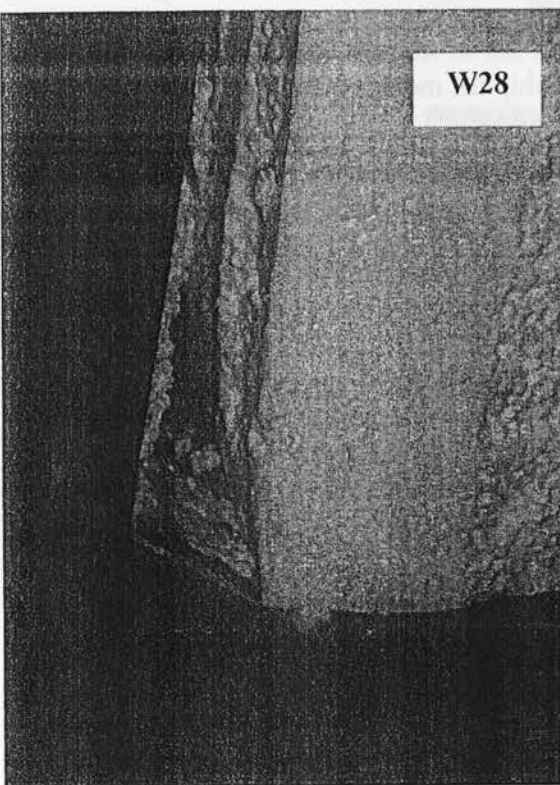
Figure 4.154. Axial load-lateral deflection relationship for model W28



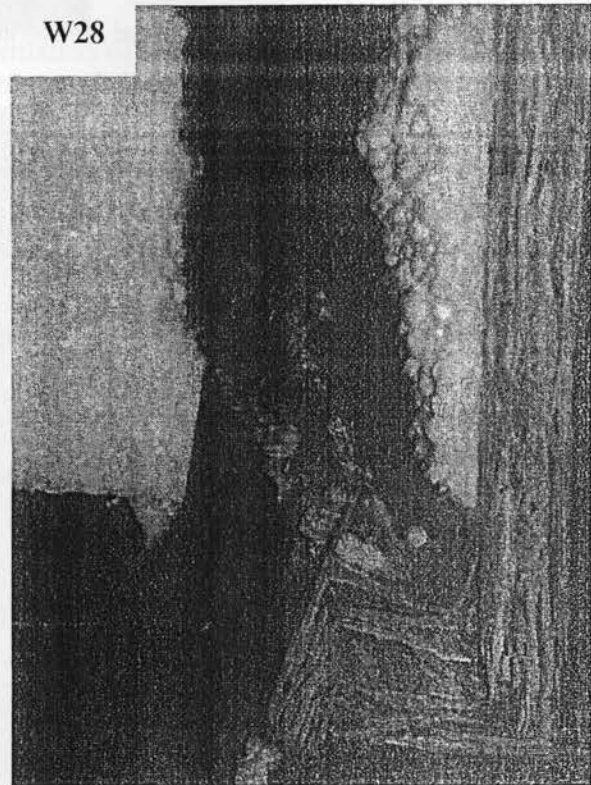
(a)



(b)

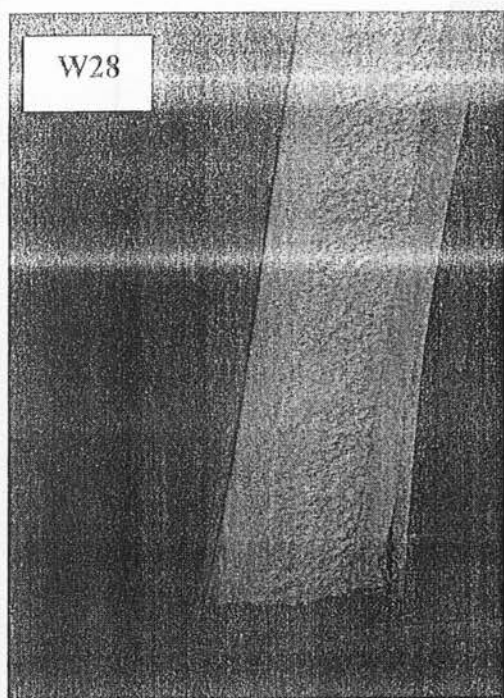


(c)

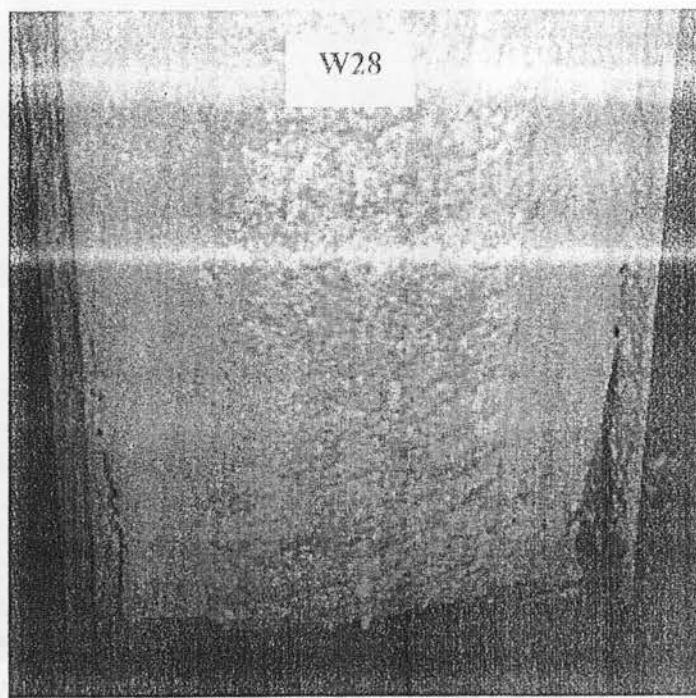


(d)

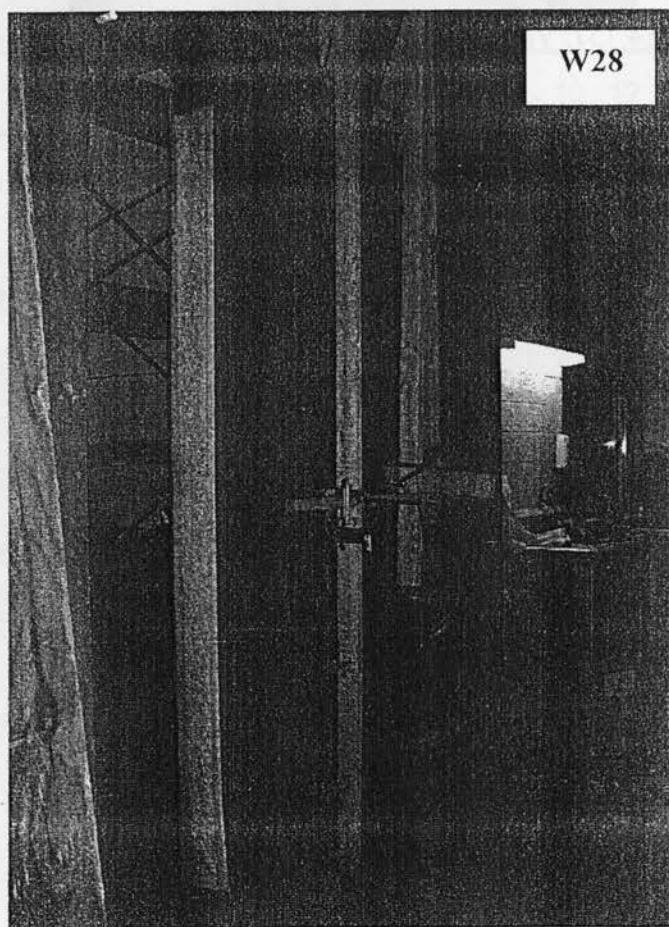
Figure 4.155. views of the OSB and pressure treated lumber facings at the bottom south-east side of wall W28



(a)



(b)



(c)

Figure 4.156. views of the OSB and pressure treated lumber facings at the bottom south-west side of wall W28

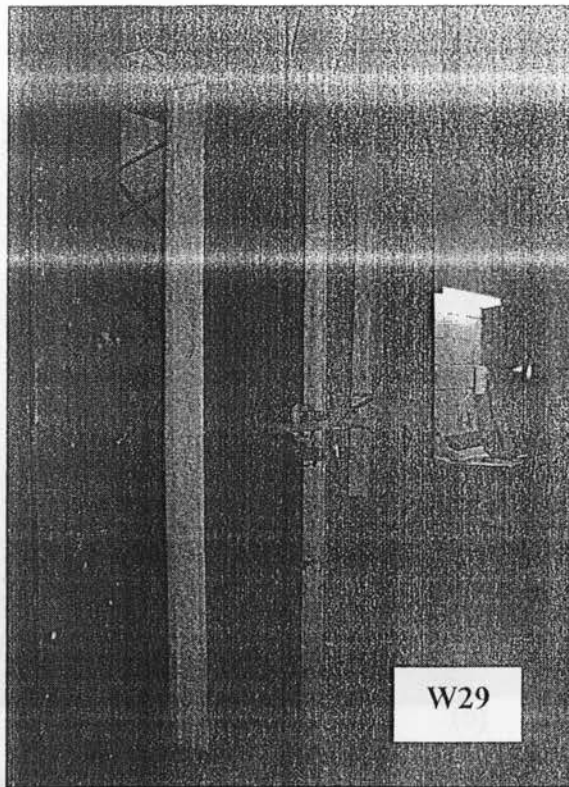


Figure.4.157. View of the setup of wall W-29 before testing

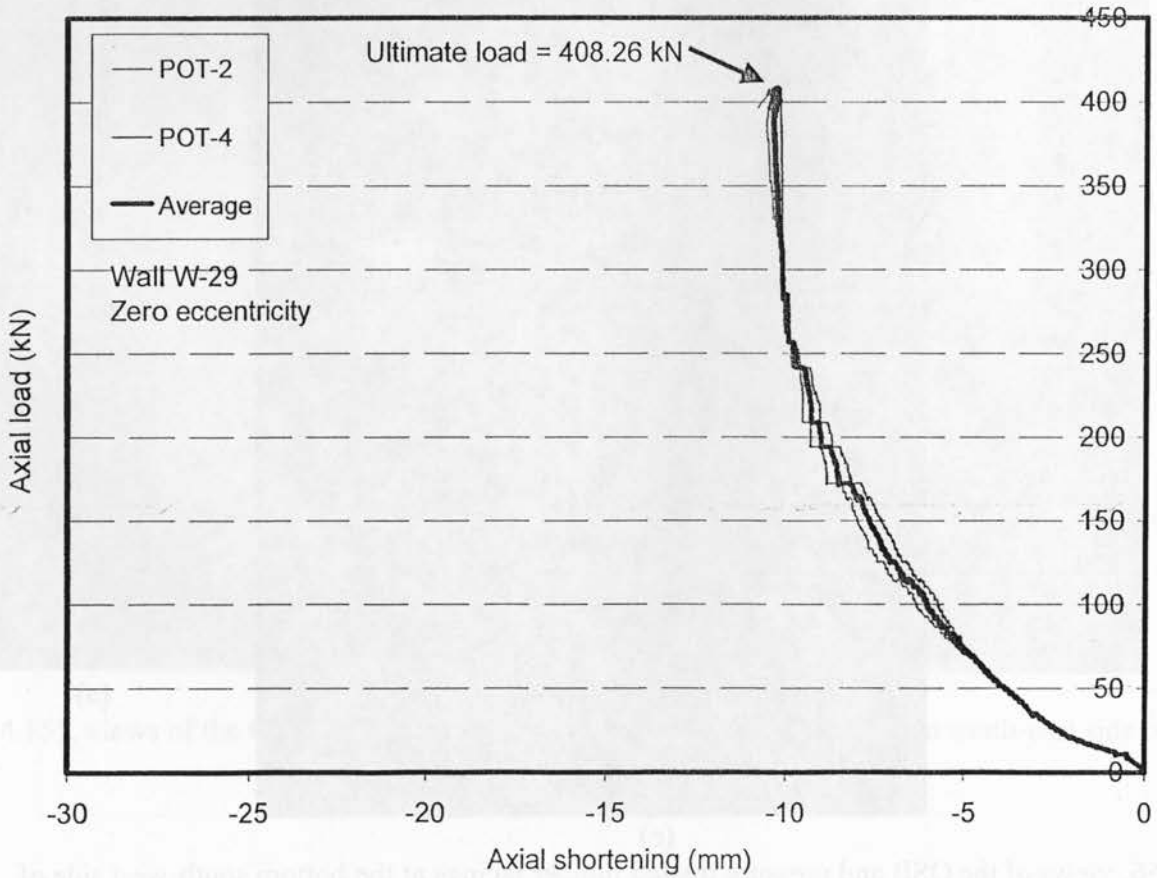


Figure 4.158. Axial load-axial shortening relationship for wall W-29

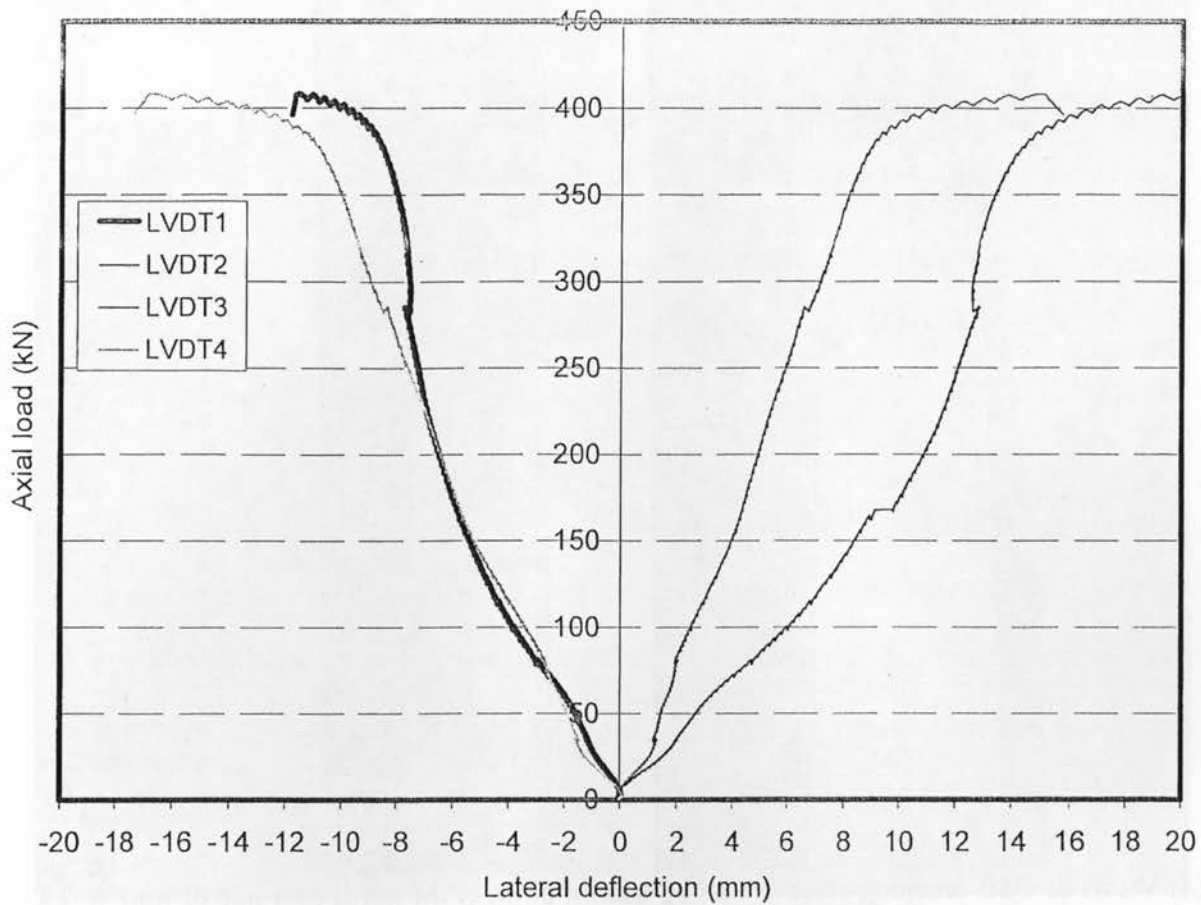


Figure 4.159. Axial load-lateral deflection relationship for wall W-29

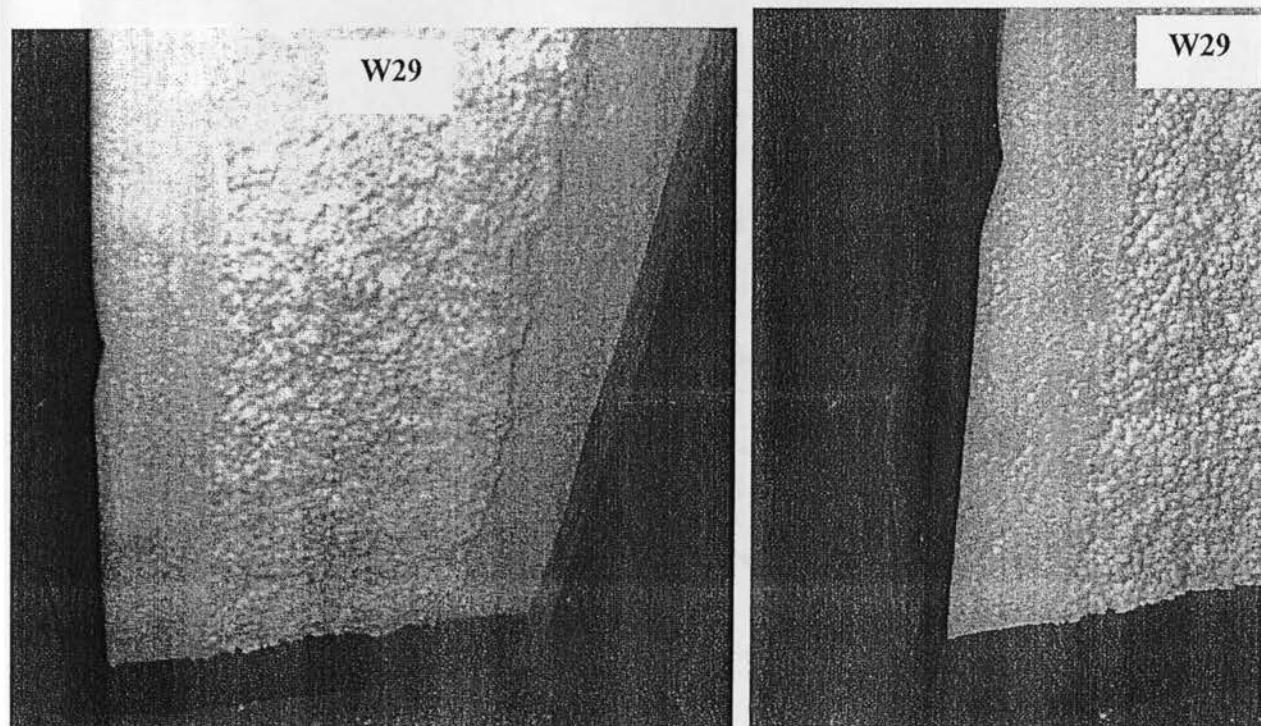


Figure 4.160. Splitting of Pressure treated lumber facing at the bottom south side of wall W-29

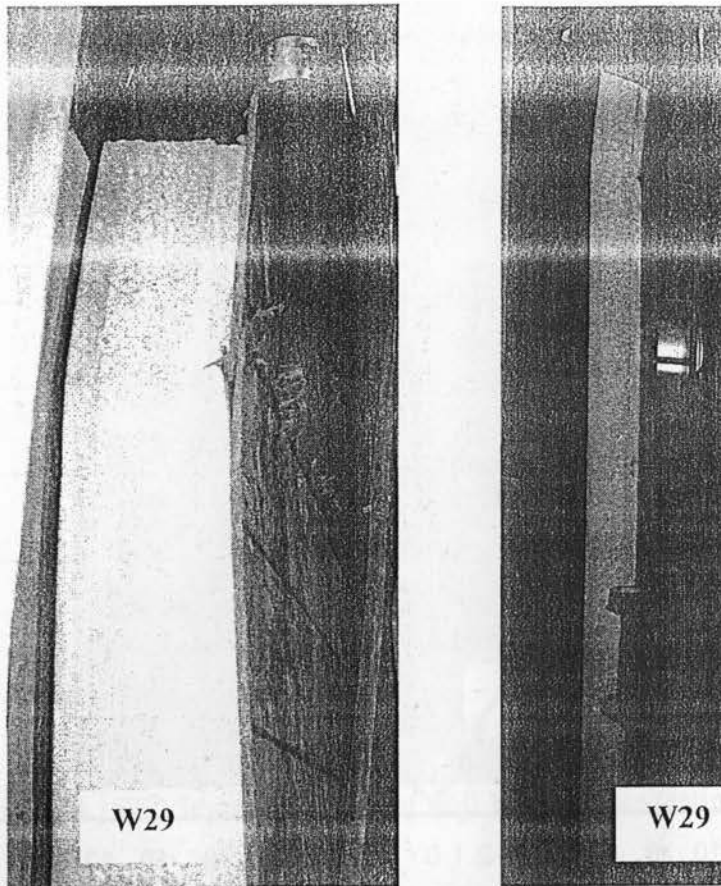


Figure 4.161. Views of OSB crushing close to the top quarter point of the north-east side of wall W-29

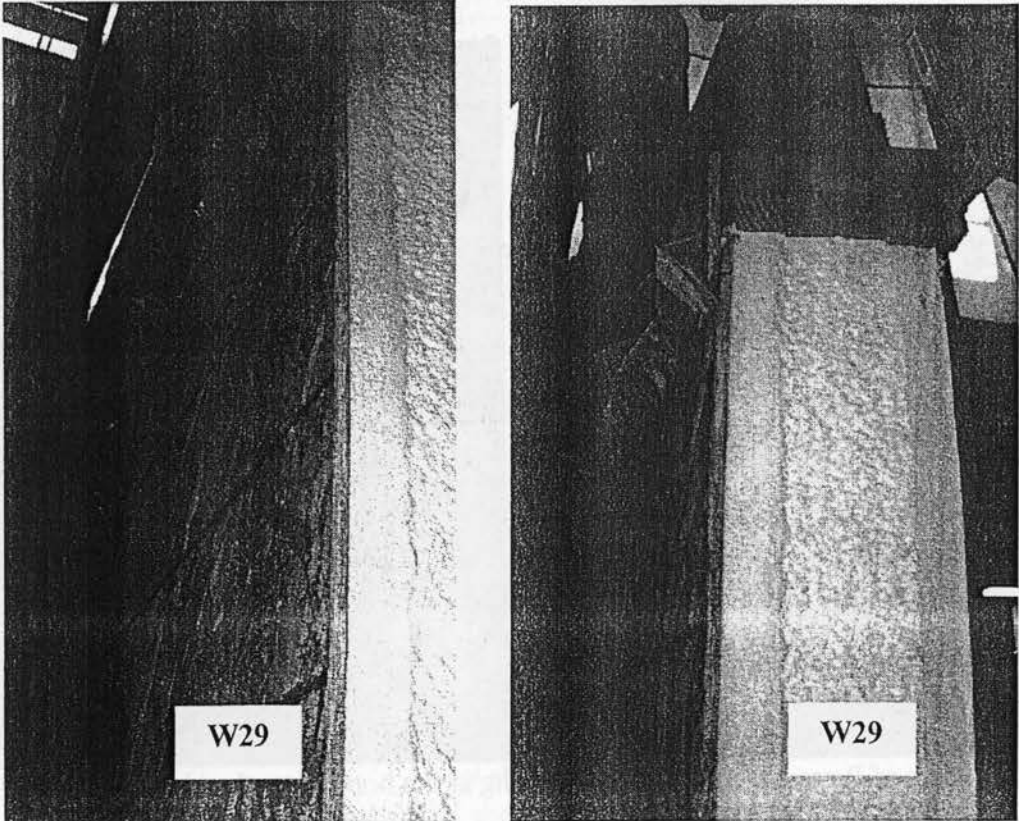


Figure 4.162. Views of OSB crushing at the top of the north-west side of wall W-29

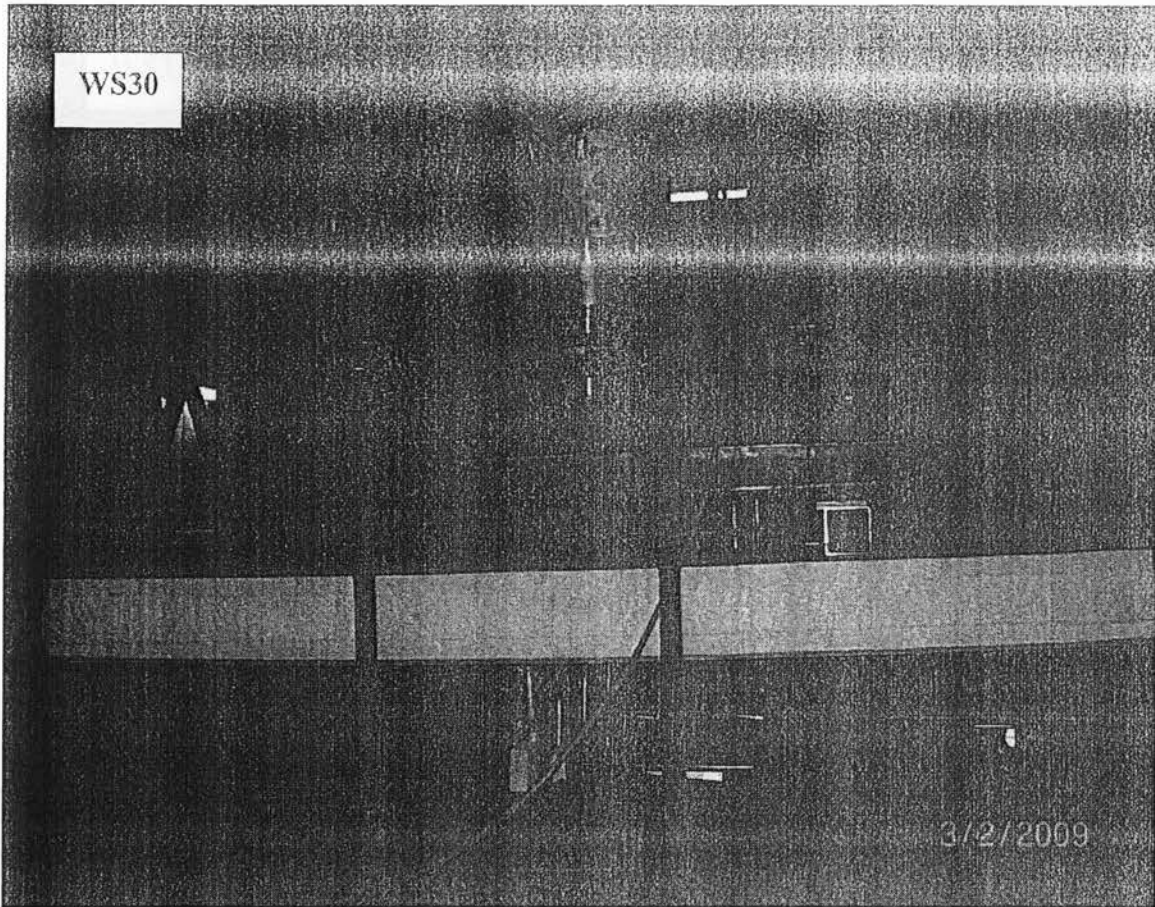


Figure 4.163. Views of the test setup for model WS30 before testing

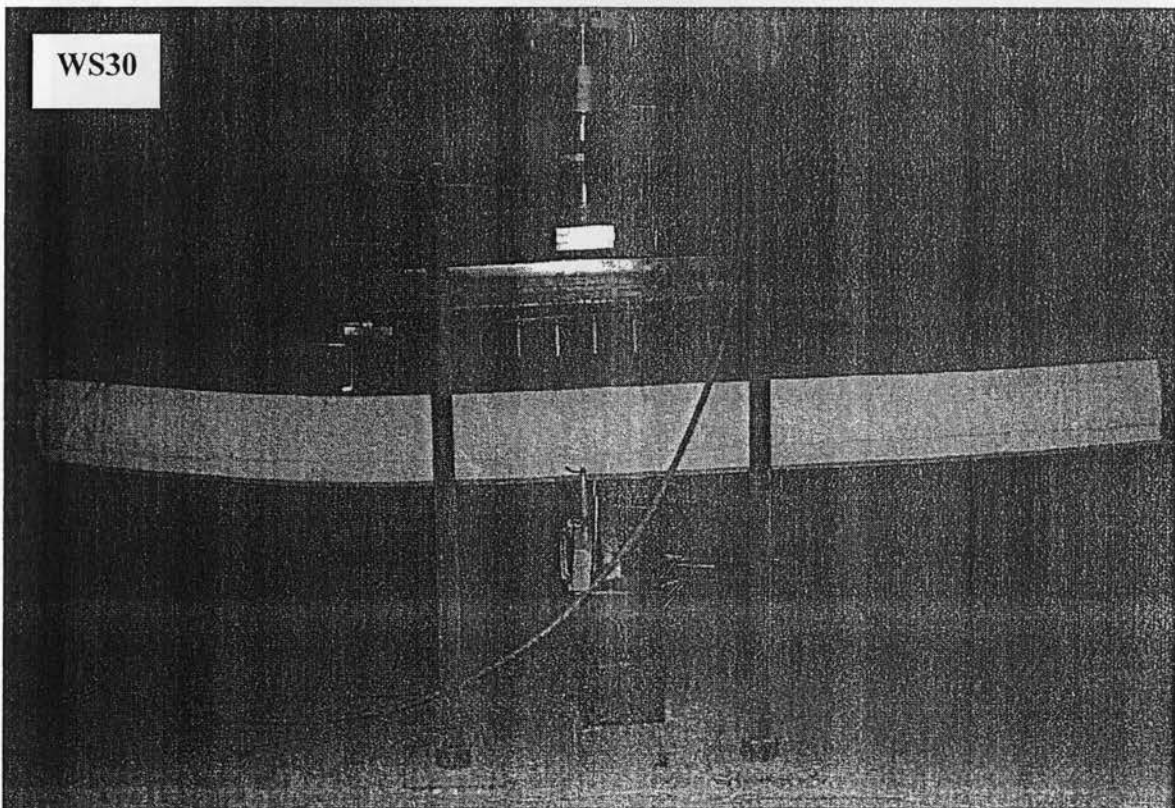


Figure 4.164. View of deformed shape of panel WS30 after failure

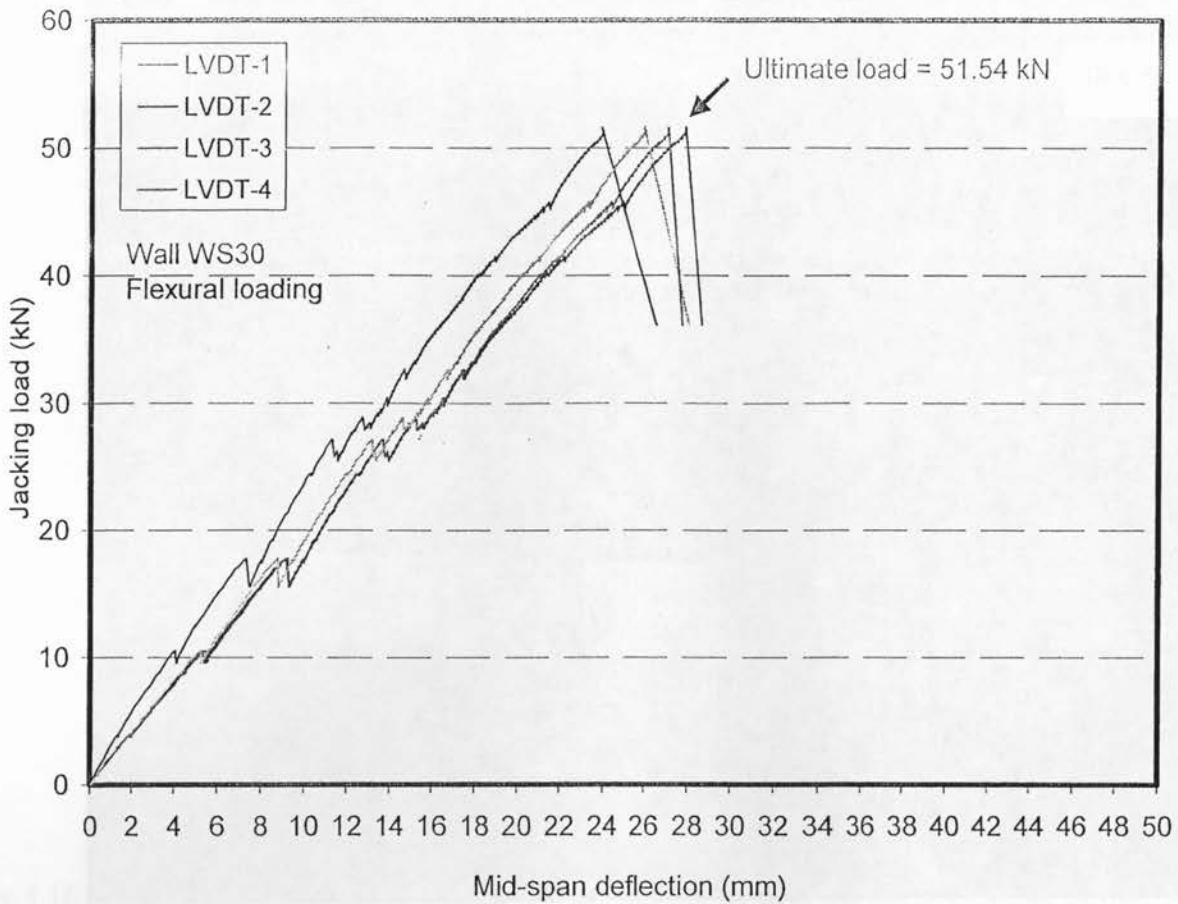


Figure 4.165. Jacking load-deflection relationship for model WS30

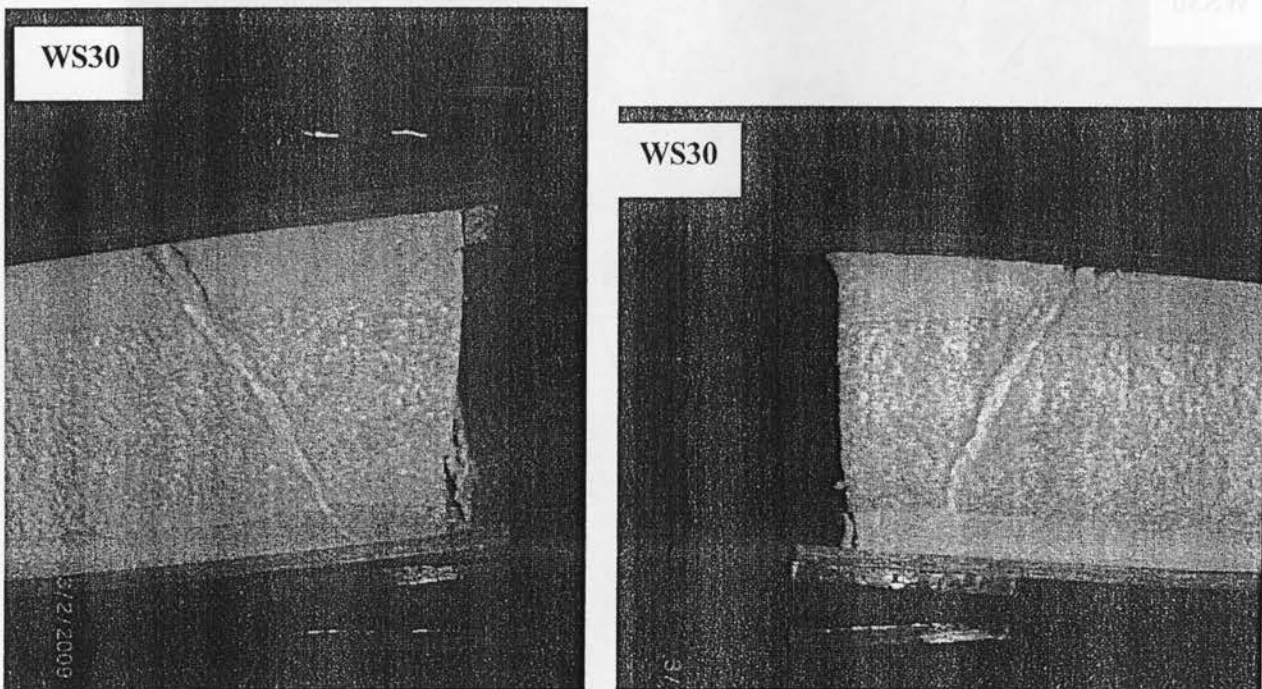


Figure 4.166. Views of the diagonal shear failure in the foam at the left and right free edges, respectively, of the right support of panel WS30

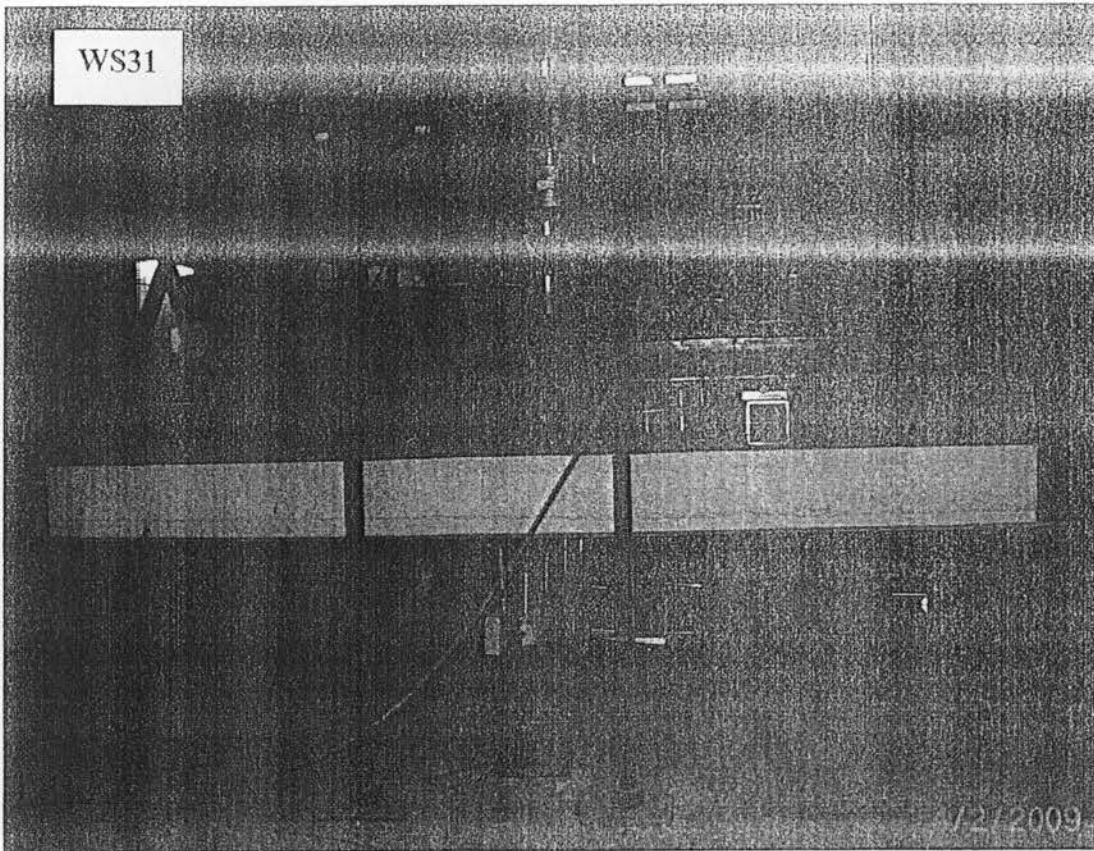


Figure 4.167. Views of the test setup for model WS31 before testing

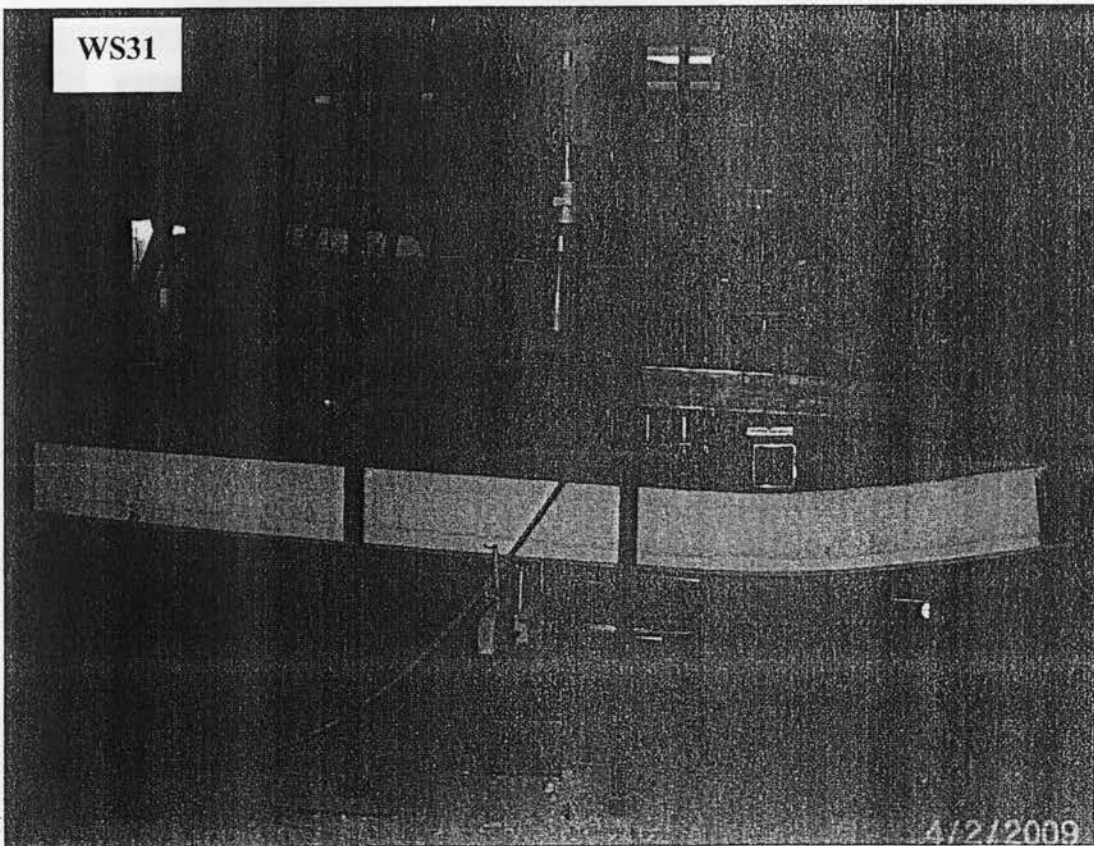


Figure 4.168. View of deformed shape of panel WS31 after failure

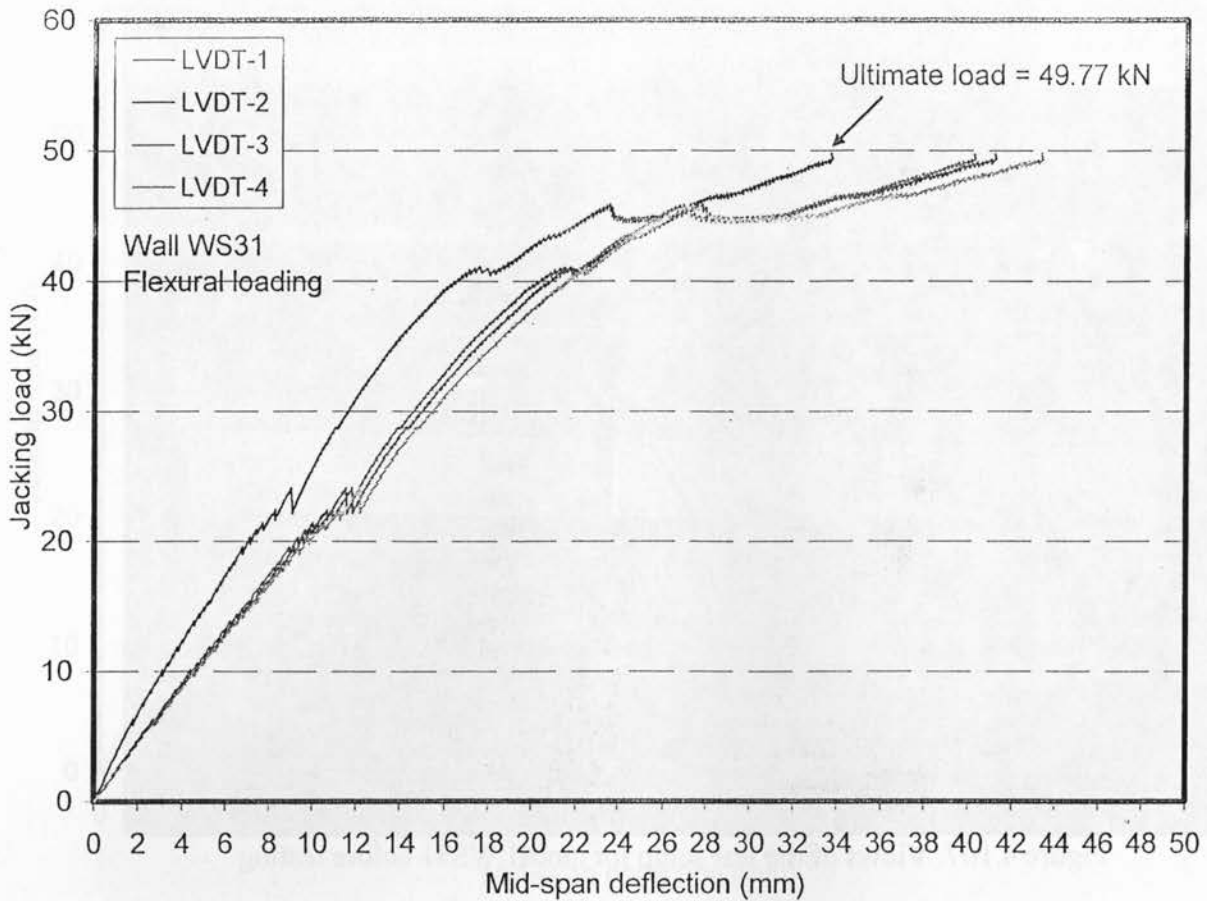


Figure 4.169. Jacking load-deflection relationship for model WS31

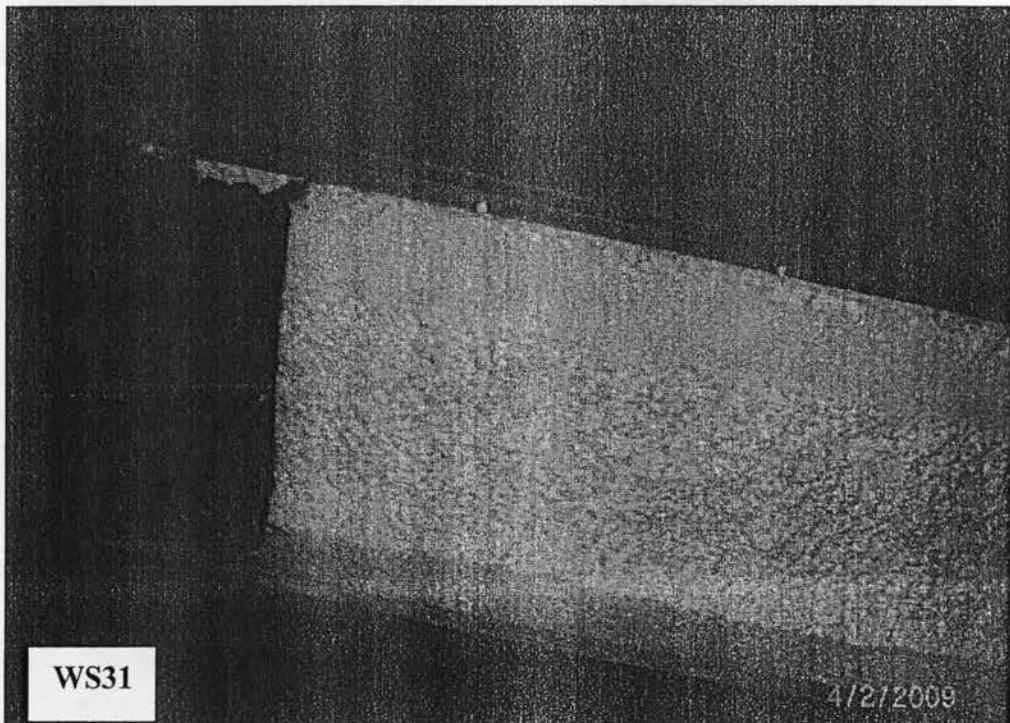


Figure 4.1.70. Views of the horizontal shear failure at the interface between the top facing and foam core the left free edge of the right support of panel WS31

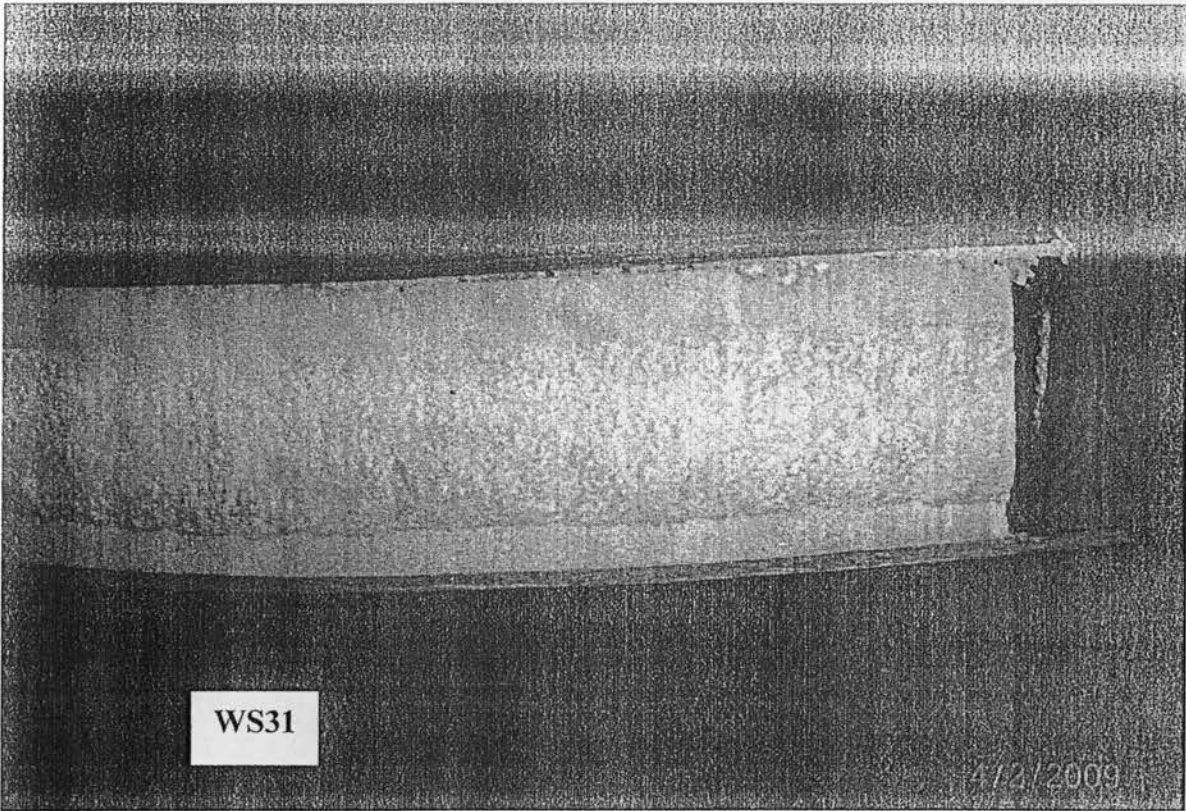


Figure 4.171. Views of the horizontal shear failure at the interface between the top facing and foam core the right free edge of the right support of panel WS31

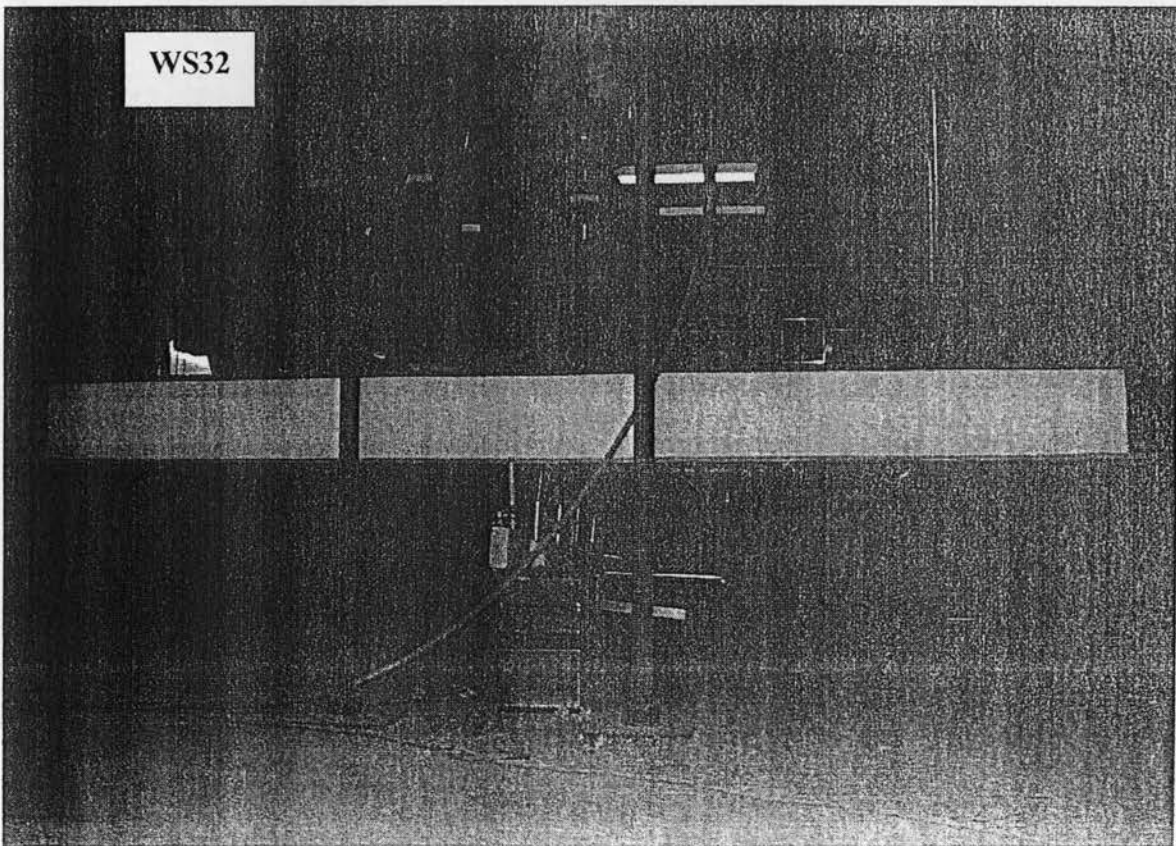


Figure 4.172. Views of the test setup for model WS32 before testing

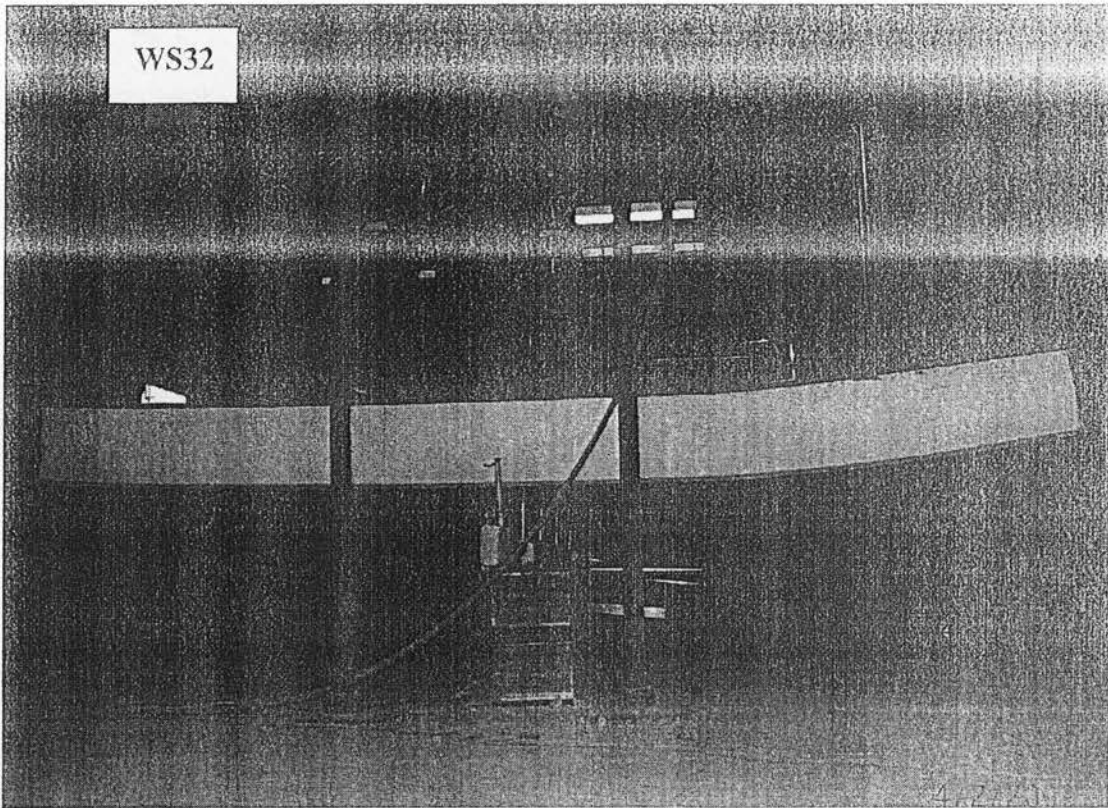


Figure 4.173. View of deformed shape of panel WS32 after failure

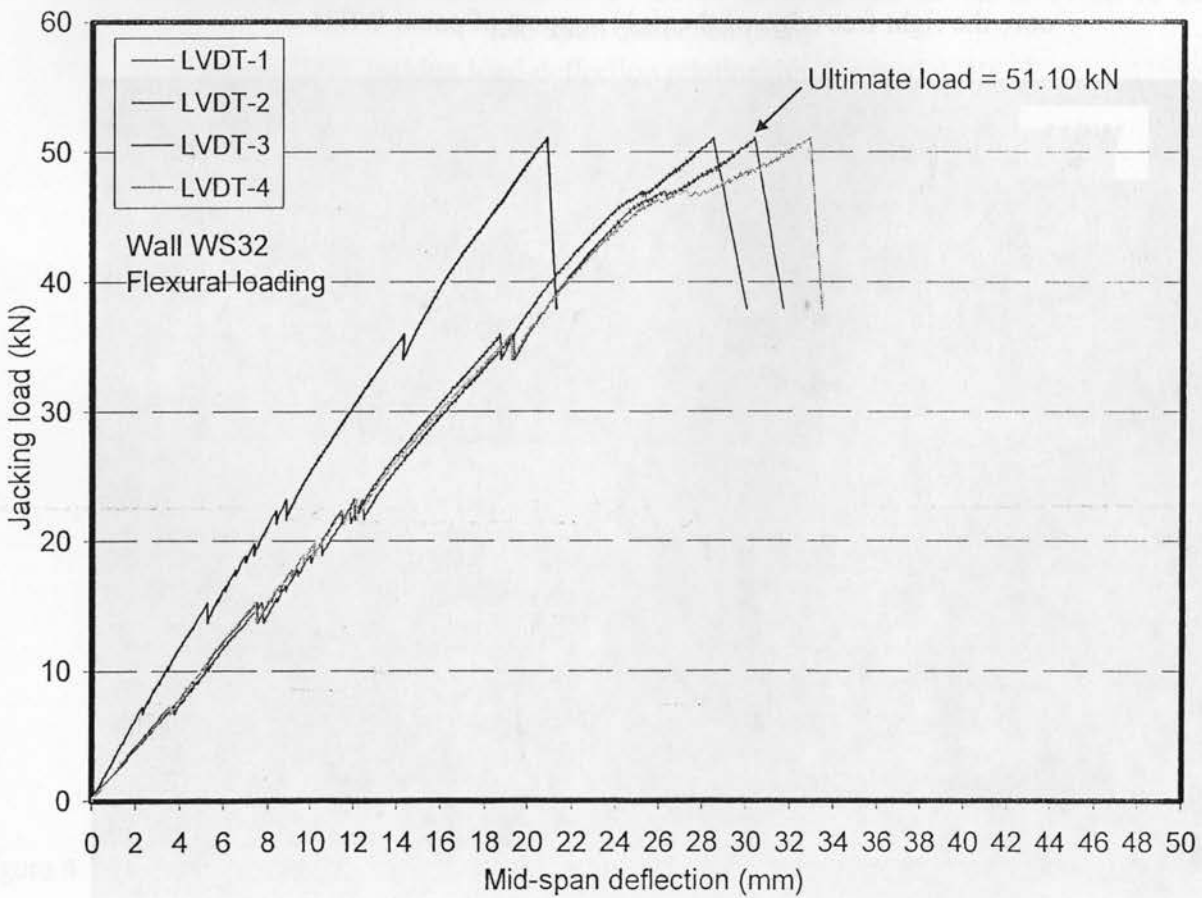


Figure 4.174. Jacking load-deflection relationship for model WS32

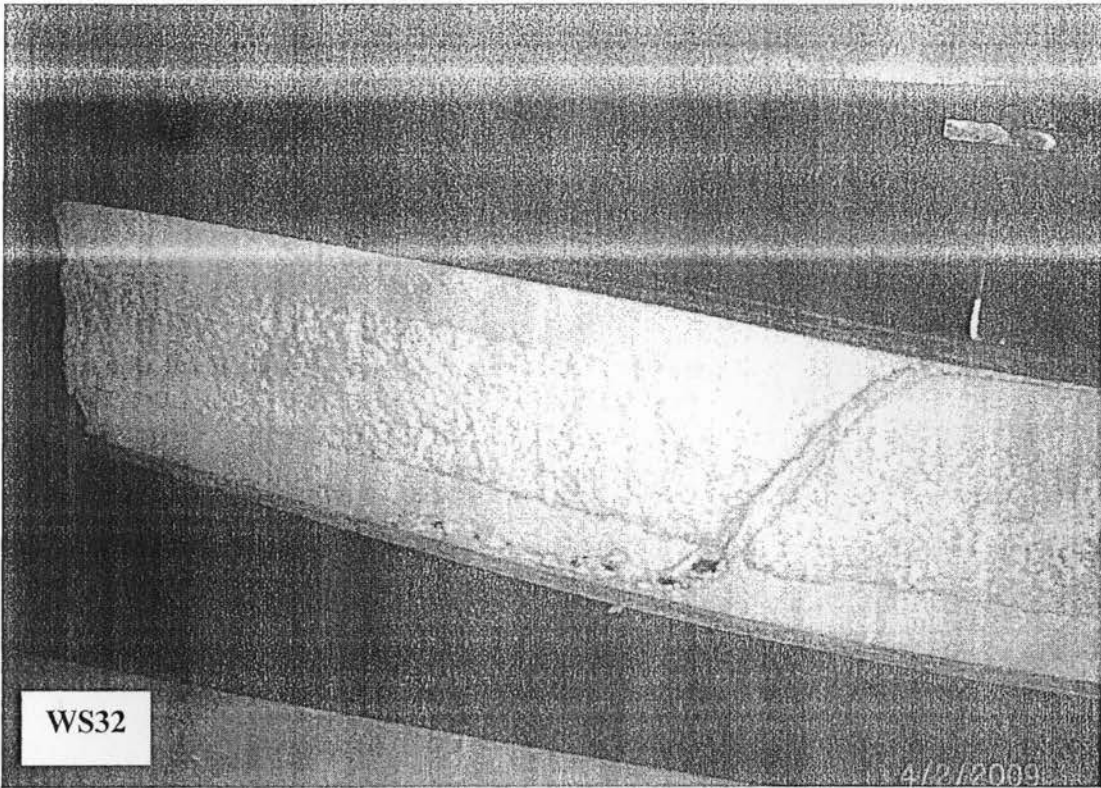


Figure 4.175. View of the combined diagonal and horizontal shear failure at the left free edge of the right support of panel WS32

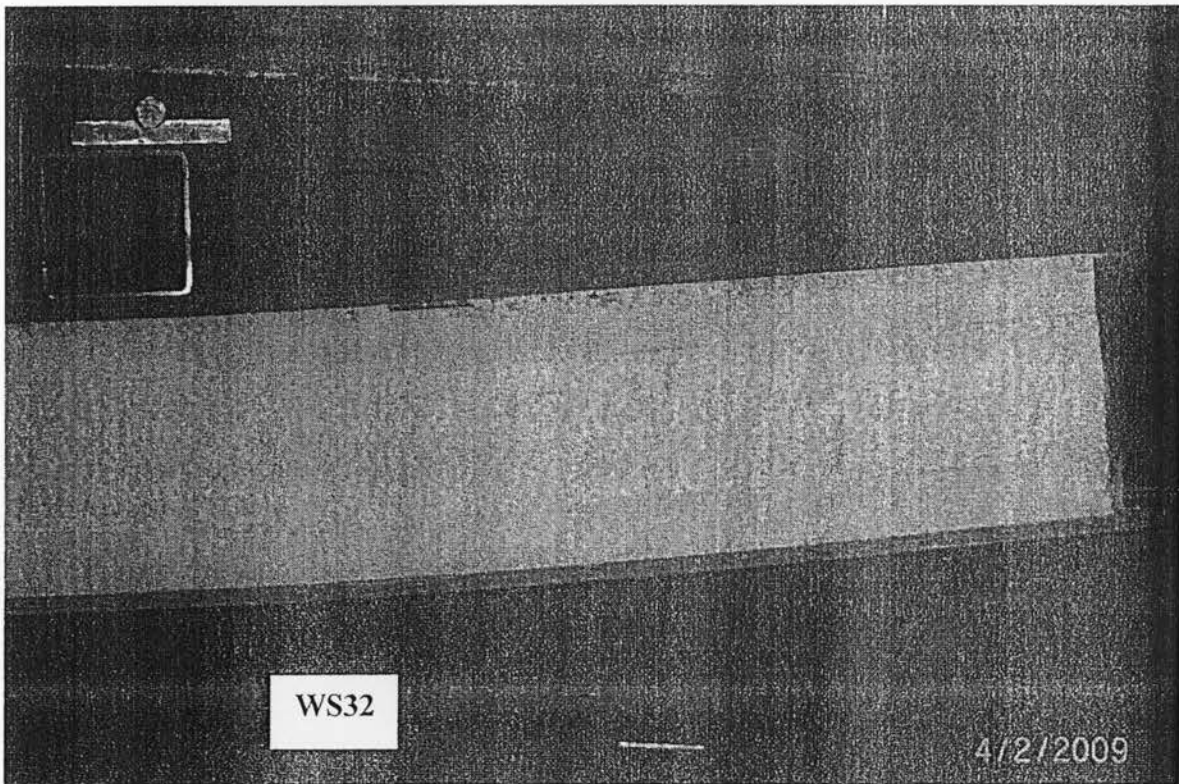


Figure 4.176. Views of the horizontal shear failure at the interface between the top facing and foam core at the right free edge of the right support of panel WS32